


# The Sustainable Engineering of Continuous Hydrothermal Synthesis

By
Pablo Caramazana González

Thesis submitted to the University of Nottingham for the degree of Doctor of Philosophy

**July 2017**

**Declaration**

I, Pablo Caramazana González, herby certify that this thesis has been composed by myself and that it is a record of my own work over the period from August 2013 to July 2016.

Except where specific reference is made to other sources or collaborators, the work presented in this thesis is the original work of the author. It has not been submitted, in whole or in part, for any other Degree.

Pablo Caramazana González

*To my family, who has been a vital support in my life,*

*especially to my grandmother and godfather,*

*who take care of us as they always did.*

# ABSTRACT

Nanomaterials are increasingly used in novel applications, devices and processes. As a result industrial scale production it is a growing area. Continuous-flow hydrothermal synthesis (CFHS) offers substantial advantages over conventional techniques that can manufacture nanomaterials, due to its potential scalability from laboratory to industrial plant, versatility to synthesize a large variety of nanomaterials and its simplicity. Also, increasing concern around the environmental impact of manufacturing processes has led to the development of more careful and sustainable strategies from industry. As such, CFHS represents a clear alternative by using water as solvent, with shorter reaction times and low manufacturing temperatures compared with other synthesis routes. This thesis assesses the life cycle environmental impact of CFHS at industrial scale for a wide range of nanomaterials. In general, the evaluation involves the production of the nanoparticles ("cradle-to-gate"), considering various operational parameters and conditions such as scale, precursor type, reaction temperature and operational configuration. The recent industrial plant built in Nottingham is used to provide essential data for the life cycle assessment (LCA). Chapter 4 specifically assesses the impact of scale-up of lithium iron phosphate (LFP) nanoparticles production from laboratory and pilot scale to the industrial plant. The influence of more concentrated precursor solutions and lower production yield is also evaluated in the case of industrial scale, allowing a wider comparison of alternative LFP production methods with CFHS. Chapter 5 combines practical experiments to model LCA of the industrial production. A set of experiments were carried out to produce titanium dioxide ($TiO_2$ or titania) nanoparticles in the laboratory, using different titanium precursors at a range of different reaction temperatures. The characteristics of each sample were used to

determine the relations between quality and yield at industrial scale as well as the environmental impact of each scenario. This chapter presents a detailed and useful basis for any future production of titania nanoparticles using CFHS. Chapter 6 and 7 evaluate the tribological performance of ten metal sulfides nanoparticles (nano-sulfides) as lubricant additives in water and pure mineral oil. To do this, silver sulfide was synthesized for the first time using CFHS (Chapter 6) alongside a range of other nano metal sulphides. The industrial production of five lubricants (formed by nanoparticles at 5wt% in mineral oil) was also evaluated in order to determine the life cycle impact of their production. This assessment quantified the impact of three synthesis configurations, two reaction temperatures and four metal salt precursors.

Overall, it has been proven that CHFS is able to produce a large variety of nanomaterials with different chemical compositions, including phosphates, metal oxides and metal sulfides, achived by varying the operational conditions such as temperature or precursor choice. The scale-up of this technique (carried out during the SHYMAN project) has led to a reduction of the overall environmental impact of production due to the optimization of the process and the higher productivity of the plant. Finally, CFHS has resulted in lower environmental impact than other existing and emerging techniques for the production of nanomaterials such as sol-gel, pyrolysis, plasma, Altair process or batch hydrothermal or solvothermal synthesis.

# ACKNOWLEDGEMENTS

I would to like to start thanking my supervisor Ed Lester, who offered me this magnificent opportunity four years ago. His supervision has enabled me to gain academic, industrial and professional experience, but above all Ed has always shared with me great ideas and advice to solve all kind of personal and professional problems. Sincere thanks are given to Jon McKechnie, who accepted to be supervisor in the key moment. Jon has offered terrific guidance and support, which have been vital to finishing this PhD.

I want to thank to Miquel Gimeno-Fabra for his immense help, support, patience and generosity in and out of the University, it was really a pleasure to discuss with him all type of problems and ideas. Also, it has been tremendous pleasure to work with Pete Dunne, his help in the laboratory and during the writing-up have been indispensable when carrying out experimental work and analysing tricky XRD patterns.

Thanks to Mirek Žilka, Marie Tichá and František Freiberg from Czech Technical University, who have spent a lot of time sharing valuable data, questions and answers during the SHYMAN project. Also, thanks to everyone at Prof Lester's Group and at Promethean Particles for their help. All of them have dedicated time and effort whilst providing very useful technical information.

I would like to acknowledge my friends from Nottingham and Spain, who have either visited me or have found time to keep in touch throughout these years.

Finally and most importantly, thanks to my family, who have always supported me from the distance, especially my parents, who have encouraged me to keep working every day, regardless of time or place, they are all part of this PhD.

# PUBLICATIONS AND PRESENTATIONS

1. Caramazana-González, P., Dunne, P.W., Gimeno-Fabra, M., Zilka, M., Ticha, M., Stieberova, B., Freiberg, F., McKechnie, J. and Lester, E.H., 2017. *"Assessing the life cycle environmental impacts of titania nanoparticle production by continuous flow solvo/hydrothermal syntheses"*, Green Chemistry, 19(6), pp. 1536-1547.

2. Stieberova, B., Zilka, M., Ticha, M., Freiberg, F., Caramazana-González, P., McKechnie, J. and Lester, E.H., 2017. *"Application of ZnO nanoparticles in Self-Cleaning Coating on a Metal Panel: An Assessment of Environmental Benefits"*, ACS Sustainable Chemistry & Engineering, 5(3), pp. 2493-2500.

3. SETAC Europe 22nd LCA Case Study Symposium, 20-22nd of September 2016, Montpelier (France). Presentation of *"Assessing the life cycle environmental impacts of titania nanoparticle production by continuous flow hydrothermal synthesis"*

4. Sustainable Hydrothermal Manufacturing of Nanomaterials summer school, 2014, Valladolid (Spain). Alvarez, A., Caramazana, P., Jimenez, C., Martinez, C., Starkey, C., 2014. *"Continuous hydrothermal synthesis of nanomaterials for tailored applications"*. Poster presentation, 1st place.

# TABLE OF CONTENTS

1. Chapter 1 – Introduction ..... 1

1.1. Opening ..... 2

1.2. Nanomaterials ..... 2

1.3. Life cycle assessment ..... 4

1.4. Continuous-flow hydrothermal synthesis ..... 5

1.5. Aims and motivation ..... 7

2. Chapter 2 – Background and literature review ..... 9

2.1. Sustainability ..... 10

2.1.1. Introduction ..... 10

2.1.2. Environmental impacts ..... 11

2.1.2.1. Ozone depletion layer ..... 12

2.1.2.2. Global warming ..... 13

2.1.2.3. Acidification potential ..... 14

2.1.2.4. Eutrophication ..... 15

2.1.3. Life cycle assessment ..... 15

2.2. Nanomaterials synthesis and processes ..... 17

2.2.1. Lithium iron phosphate ..... 17

2.2.1.1. Solid-state methods for the synthesis of lithium iron phosphate ..... 18

2.2.1.1.1. Solid-state synthesis of lithium iron phosphate ..... 18

2.2.1.1.2. Mechanochemical activation synthesis of lithium iron phosphate ..... 18

2.2.1.1.3. Carbothermal synthesis of lithium iron phosphate ..... 19

2.2.1.1.4. Microwave synthesis of lithium iron phosphate ..... 20

2.2.1.2. Solution methods for the synthesis of lithium iron phosphate ..... 20

2.2.1.2.1. Sol-gel synthesis of lithium iron phosphate ..... 20
2.2.1.2.2. Co-precipitation synthesis of lithium iron phosphate ..... 21
2.2.1.2.3. Spray pyrolysis synthesis of lithium iron phosphate ..... 21
2.2.1.2.4. Batch hydrothermal and solvothermal synthesis of lithium iron phosphate ..... 22
2.2.1.2.5. Continuous-flow hydrothermal synthesis of lithium iron phosphate ..... 22
2.2.2. Titanium dioxide ..... 23
2.2.2.1. Industrial processes for $TiO_2$ manufacture ..... 25
2.2.2.1.1. Industrial Sulfate process for the production of $TiO_2$ ..... 25
2.2.2.1.2. Industrial Chloride process for the production of $TiO_2$ ..... 27
2.2.2.2. Continuous-flow synthesis of $TiO_2$ nanoparticles ..... 28
2.2.2.2.1. Precursors of $TiO_2$ nanoparticles for solvo/hydrothermal syntheses ..... 29
2.2.3. Metal sulfides ..... 32
2.2.3.1. Solid-state methods for the production of metal sulfides nanoparticles ..... 32
2.2.3.1.1. Mechanochemical synthesis of metal sulfides ..... 32
2.2.3.2. Vapour phase methods for the synthesis of metal sulfides nanoparticles ..... 33
2.2.3.3. Solution methods for the production of metal sulfides nanoparticles ..... 33
2.2.3.3.1. Hot injection synthesis of metal sulfides ..... 33
2.2.3.3.2. Sol-gel synthesis of metal sulfides ..... 34
2.2.3.3.3. Co-precipitation synthesis of metal sulfides ..... 34
2.2.3.3.4. Batch hydrothermal and solvothermal synthesis of metal sulfides ..... 35
2.2.3.3.5. Continuous-flow hydrothermal synthesis of metal sulfides ..... 35
2.2.4. Concluding remarks for the production of nanomaterials ..... 36
3. Chapter 3 – Experimental ..... 37
3.1. Nozzle reactor ..... 38
3.1.1. Synthesis of titanium dioxide nanoparticles ..... 40
3.1.2. Synthesis of silver sulfide nanoparticles ..... 42
3.1.3. Synthesis of metal sulfide nanomaterials ..... 43
3.1.3.1. Standard configuration for metal sulphide production ..... 44
3.1.3.1.1. Method A ..... 44
3.1.3.1.2. Method B ..... 45
3.1.3.2. Extended residence time reaction with acid addition ..... 45

3.2. Characterisation ..... 48
3.2.1. X-ray diffractometry ..... 48
3.2.2. Transmission electron microscopy ..... 50
3.2.3. Thermogravimetric analysis ..... 51
3.2.4. Tribological analysis ..... 53
3.3. Environmental methodology ..... 56
3.3.1. Goal and scope ..... 57
3.3.2. Life cycle inventory ..... 57
3.3.3. Life cycle impact assessment ..... 58
3.3.4. Interpretation ..... 58
3.3.5. Environmental software ..... 58
3.3.5.1. SimaPro software ..... 59
3.3.5.2. CCaLC software ..... 59
4. Chapter 4 – Ex-ante life cycle assessment for the scale-up of a continuous flow hydrothermal synthesis of lithium iron phosphate nanoparticles. ..... 60
4.1. Introduction ..... 61
4.1.1. Processing parameters for the CFHS of LFP ..... 62
4.1.1.1. Temperature ..... 62
4.1.1.2. Precursor concentration ..... 63
4.1.1.3. Water and solutions flow rates ..... 64
4.1.1.4. Reactor design ..... 64
4.1.1.5. Carbon coating ..... 65
4.1.2. Prior LCA studies of LFP ..... 66
4.2. Life cycle assessment methods ..... 69
4.2.1. Laboratory scale ..... 71
4.2.2. Pilot scale ..... 74
4.2.3. Industrial scale ..... 76

4.2.3.1. Scale-up for the production of C-LFP nanoparticles ..... 76

4.3. Results and discussion ..... 81

4.3.1. Prior LCA studies ..... 88

4.4. Conclusions ..... 91

5. Chapter 5 - Assessing the life cycle environmental impacts of titania nanoparticle production by continuous flow solvo/hydrothermal syntheses ..... 94

5.1. Introduction ..... 95

5.1.1. $TiO_2$ production methods ..... 95

5.1.2. Spectrum of precursors used for $TiO_2$ synthesis ..... 97

5.1.3. Overview of $TiO_2$ LCA studies ..... 98

5.2. Life cycle assessment methods ..... 100

5.2.1. Scope and goal ..... 100

5.2.2. Precursor manufacturing ..... 101

5.2.3. Laboratory synthesis of titania nanoparticles ..... 109

5.2.4. Scale-up for the production of titania nanoparticles by CFHS ..... 110

5.3. Results and discussion ..... 112

5.3.1. Phase and crystallinity ..... 112

5.3.2. Size ..... 117

5.3.3. Yield ..... 120

5.3.4. Cumulative energy demand and global warming potential ..... 122

5.4. Conclusions ..... 129

6. Chapter 6 – Synthesis, friction performance and environmental assessment of silver sulfide nanoparticles as lubricant additive by continuous flow hydrothermal synthesis ..... 131

6.1. Introduction ..... 132

6.2. Methodology .....134
6.2.1. Laboratory synthesis of $Ag_2S$ nanoparticles and tribological tests ..... 134
6.2.2. Life cycle assessment methods ..... 135
6.2.2.1. Precursor manufacturing ..... 136
6.2.2.2. Scale-up for the production of lubricant with $Ag_2S$ nanoparticles..... 137
6.3. Results and discussion .....141
6.3.1. Characterization ..... 141
6.3.2. Tribological tests of lubricants formed with $Ag_2S$ nanoparticles ..... 144
6.3.3. Greenhouse emissions..... 146
6.4. Conclusions .....150
7. Chapter 7 – The sustainability and tribological performance of various nano-sulfides produced using continuous-flow hydrothermal synthesis .....152
7.1. Introduction .....153
7.2. Methodology .....155
7.2.1. Laboratory synthesis and tribological tests ..... 155
7.2.2. Life cycle assessment methods ..... 157
7.2.2.1. Precursor manufacturing ..... 157
7.2.2.2. Scale-up for the production of lubricants with nano-sulfide additives ..... 159
7.3. Results and discussion .....163
7.3.1. Tribological tests of nano-sulfides as lubricant additives ..... 163
7.3.1.1. Water-based tests ..... 163
7.3.1.2. Mineral oil-based tests ..... 168
7.3.2. Greenhouse emissions..... 174
7.4. Conclusions .....181
8. Chapter 8 - Conclusions and future work .....183

8.1. General conclusions .....183

8.2. Future work .....186

8.2.1. Lithium iron phosphate nanoparticles..... 186

8.2.2. Titanium dioxide nanoparticles..... 187

8.2.3. Metal sulfide nanoparticles..... 188

References .....190

Appendix .....205

# LIST OF FIGURES

Figure 1.1: Schematic illustration of surface area, volume and ratio surface:volume of large particle and small nanoparticles. 3

Figure 1.2: Basic diagram to describe a generic life cycle assessment. 5

Figure 1.3: Diagram phase of water for solid, liquid, gas and supercritical conditions, where ● Triple point ($T_{tr}$=0.01 °C; $P_{tr}$=6.11 mbar); ▼ Melting point ($T_m$=0 °C; $P_m$=1.013 bar); ■ Normal boiling point ($T_b$=99.61 °C; $P_b$=1 bar), and ▲ Critical point (Tc=374°C Pc=221 bar) (Marcus, 2012). 6

Figure 2.1: Schematic drawn of the apparatus used for the continuous-flow hydrothermal synthesis of LFP (Xu et al., 2008). 23

Figure 2.2. Schematic flowchart for $TiO_2$ production, sulfate process. 26

Figure 2.3. Schedule for $TiO_2$ production, chloride process. 28

Figure 2.4: Schematic flowchart for the production of different titanium precursors used for the synthesis of nano-$TiO_2$. TiOS: titanium oxysulfate, $TiCl_4$: titanium tetrachloride, TIPO: titanium isopropoxide, PTOOD: potassium titanium oxide oxalate and TiBALD: titanium bis(ammonium lactato) dihydroxide. 31

Figure 3.1: Schematic flow diagram of the continuous-flow hydrothermal synthesis (top) and a scheme of the inside Nozzle reactor (down) (Lester et al., 2006). 39

Figure 3.2: Sketch of the reactor section with the inlets of supercritical water (top) and metal salt solution (bottom), as well as the reaction or mixing point (right) (Sierra-Pallares et al., 2016). 40

Figure 3.3: Configuration for the synthesis of the $TiO_2$ with different precursors. 42

Figure 3.4: Schematic configuration for the synthesis of silver sulfide nanoparticles. 43

Figure 3.5: Standard configuration method A for the synthesis of the nano-sulfide materials. 44

Figure 3.6: Standard configuration method B for the synthesis of the nano-sulfides materials. 45

Figure 3.7: Extended residence time with acid addition configuration for the synthesis of the $MoS_2$ nanoparticles. 46

Figure 3.8: Illustration of the diffraction of X-rays by crystal planes (Klugg and Alexander, 1974). 48

Figure 3.9: Illustration of the Transmission electron microscope (Pennycook and Nellist, 2011). 51

Figure 3.10: Schematic diagram of the Thermogravimetric Analyser. 52

Figure 3.11: Photo and schematic diagram of a Tribometer. 54

Figure 3.12: Schematic diagram of the Life Cycle Assessment methodology (Baumann and Tillman, 2004). 57

Figure 4.1: Flowchart of the CFHS of LFP nanoparticles at laboratory scale. 73

Figure 4.2: Flowchart of the CFHS of LFP nanoparticles at pilot scale. 75

Figure 4.3: Flowchart of the CFHS of LFP nanoparticles at industrial scale. 79

Figure 4.4: Total GHG emissions to produce 1 kg of C-LFP nanoparticles at five different scenarios. 81

Figure 4.5: Percentages of GHG emission to produce 1 kg of C-LFP nanoparticles at five different scenarios. 85

Figure 4.6: Theoretical total GHG emissions to produce 1 kg of C-LFP nanoparticles according to different publications with lack of information. [a] Liang et al. (2017) total GHG emissions for raw materials (excluded processing) 89

Figure 5.1: Scheme for the production of titanium oxysulfate, which includes the steps of digestion reduction and separation of products. 102

Figure 5.2: Scheme for the production of titanium tetrachloride, including the chlorination process and the stages of separation. 103

Figure 5.3: Scheme for the production of titanium isopropoxide according to the literature with the stages of mixing and separation. 105

Figure 5.4: Scheme for the production of titanium bis(ammonium lactato) dihydroxide, which includes the inlets of lactic acid and ammonia, the precipitation with 2-propanol and the separation stages. 106

Figure 5.5: Scheme for the production of potassium titanium oxide oxalate dehydrate, which includes all production and separation stages. 108

Figure 5.6: Simplified schematic of the counter-current continuous-flow hydrothermal reactor. 109

Figure 5.7: Scheme for the large-scale continuous-flow production of titania nanoparticles. 112

Figure 5.8: Powder X-ray diffraction patterns of products obtained at varying reaction temperatures from five different precursors: (a) titanium oxysulfate, (b) titanium tetrachloride, (c) titanium isopropoxide, (d) titanium bis(ammonium lactato) dihydroxide and (e) potassium titanium oxide oxalate; and (f) the corresponding calculated crystallite diameters. 113

Figure 5.9: Representative TEM images of all samples acquired. 116

Figure 5.10: TEM images and corresponding size distributions (n = 200) of samples prepared at 400 °C from (a) titanium oxysulfate, (b) titanium tetrachloride, (c) titanium isopropoxide, (d) titanium bis(ammonium lactato) dihydroxide and (e) potassium titanium oxide oxalate. Scale bars represent 50 nm. 117

Figure 5.11: Size distribution histograms of all samples where possible. 119

Figure 5.12: Thermogravimetric traces of products obtained at varying reaction temperatures from five different precursors: (a) titanium oxysulfate, (b) titanium tetrachloride, (c) titanium isopropoxide, (d) titanium bis(ammonium lactato) dihydroxide and (e) potassium titanium oxide oxalate; and (f) the % conversion for each synthesis. 121

Figure 5.13: The cumulative energy demand (CED) to produce 1 kg of titania nanoparticles at each synthesis temperature from: (a) titanium oxysulfate (b) titanium tetrachloride, (c) titanium isopropoxide, (d)

titanium bis(ammonium lactato) dihydroxide and (e) potassium titanium oxide oxalate. 124

Figure 5.14: The global warming potential (GWP) to produce 1 kg of titania nanoparticles at each synthesis temperature from: (a) titanium oxysulfate (b) titanium tetrachloride, (c) titanium isopropoxide, (d) titanium bis(ammonium lactato) dihydroxide and (e) potassium titanium oxide oxalate. 126

Figure 6.1: Flowchart of the lubricant production with $Ag_2S$ nanoparticles synthesised by continuous-flow hydrothermal synthesis. 140

Figure 6.2: Powder X-ray diffraction patterns of products obtained at varying reaction temperatures for the synthesis of $Ag_2S$ nanoparticles. 142

Figure 6.3: TEM images of $Ag_2S$ nanoparticles samples prepared at different temperatures; 300 °C (a-b); 350 °C (c-d) and 400 °C (e-g) and EDX spectrum (h) of $Ag_2S$ nanoparticles at 400 °C. 143

Figure 6.4: Coefficient friction tests of (a) water, (b) water-based suspension 5 wt% $Ag_2S$ nanoparticles, (c) mineral oil and (d) mineral oil-based suspension 5 wt% $Ag_2S$ nanoparticles. 145

Figure 6.5: Average and standard deviation of coefficient friction for all of the samples studied. 146

Figure 6.6: Percentage of greenhouse emissions for production of 1 kg of lubricant with 5 wt% $Ag_2S$. 149

Figure 7.1: Flowchart of the lubricant production with sulfides nanoparticles synthesised by continuous-flow hydrothermal synthesis. 161

Figure 7.2: Coefficient of friction tests of (a) pure water and (b) pure mineral oil lubricant. 163

Figure 7.3: Coefficient of friction tests of water suspensions with nano-sulfides at 5 wt% as additive. (a) FeS 400A, (b) FeS 400B, (c) CdS400A, (d) CdS 400B, (e) ZnS 300B, (f) ZnS 400B, (g) PbS 300B, (h) CuS 300B, (i) $Ag_2S$ 400B and (j) $MoS_2$. 166

Figure 7.4: Coefficient of friction tests of water suspensions with nano-sulfides at 1 wt% as additive. (a) PbS 300B and (b) $MoS_2$. 167

Figure 7.5: Coefficient of friction tests of mineral oil lubricant with nano-sulfides at 5 wt% as additive. (a) FeS 400A, (b) FeS 400B, (c) CdS 400A, (d) CdS 400B, (e) ZnS 300B, (f) ZnS 400B, (g) PbS 300B, (h) CuS 300B, (i) $Ag_2S$ 400B and (j) $MoS_2$. 170

Figure 7.6: Coefficient of friction tests and average of mineral oil lubricant with different content of nano-sulfides as additive. (a) PbS 300B - 2 wt%, (b) PbS 300B - 7 wt%, (c) CuS 300B - 2 wt%, (d) CuS 300B - 2 wt%, (e) $MoS_2$ - 2 wt%, (f) $MoS_2$ - 7 wt%, (g) PbS 300B, (h) CuS 300B and (i) $MoS_2$. 171

Figure 7.7: Percentage of greenhouse emissions to produce 1 kg of lubricant with 5 wt% sulfides nanoparticles. 176

Figure 7.8: Total GHG emissions to produce 1 kg of different nano-sulfides. 179

Figure A.1: Aspen HYSYS simulation of laboratory synthesis of LFP nanoparticles. 205

Figure A.2: Aspen HYSYS simulation of pilot scale for the production of LFP nanoparticles. 208

Figure A.3: Aspen HYSYS simulation of the evaporation stage for the industrial production. 211

Figure A.4: Aspen HYSYS simulation of the calcination stage. 211

Figure A.5: Aspen HYSYS simulation of the titanium oxysulfate production. 213

Figure A.6: Aspen HYSYS simulation of the titanium tetrachloride production. 215

Figure A.7: Aspen HYSYS simulation of distillation of benzene and isopropanol. 217

Figure A.8: Aspen HYSYS simulation of distillation of isopropanol and water. 218

Figure A.9: Aspen HYSYS simulation of distillation of ethanol and water. 219

Figure A.10: Aspen HYSYS simulation of the evaporation stage for the industrial production of nano-sulfides. 220

# LIST OF TABLES

Table 2.1. Physical Properties of brookite, anatase and rutile. 24

Table 2.2. Feedstocks of $TiO_2$ industries. 25

Table 2.3. Comparative of the titanium precursors used for the CFHS and CFSS synthesis of nano-$TiO_2$. 31

Table 3.1. Details of the nano-sulfide materials synthesised using different operational conditions and configurations. 47

Table 3.2. Details of the nano-sulfide materials used as additives with water as lubricant. 55

Table 3.3. Details of the nano-sulfide materials used as additives with mineral oil as lubricant. 55

Table 4.1. Summary of LCAs studies with LFP cathode material. 68

Table 4.2. Scenarios considered in this study. 69

Table 4.3. Summary of the processing parameters analysis for the optimum operational conditions at industrial scale production of C-LFP nanoparticles. 78

Table 4.4. Material and energy inputs and outputs to produce 1 kg of C-LFP by a CFHS at different scales and parameters. 80

Table 4.5. Summary of greenhouse gases emissions to produce 1 kg of C-LFP by a CFHS at five different scenarios. 84

Table 4.6. Production information for each different scenario. 86

Table 5.1. Material and energy inputs required for the production of 1 kg of a 15% titanium oxysulfate solution. 102

Table 5.2. Material and energy inputs required to produce 1 kg of titanium tetrachloride. 104

Table 5.3. Material and energy inputs required to produce 1 kg of titanium isopropoxide. 105

Table 5.4. Material and energy inputs required to produce 1 kg of bis(ammonium lactato) dihydroxide. 107

Table 5.5. Material and energy inputs required to produce 1 kg of potassium titanium oxide oxalate dehydrate. 108

Table 5.6. Summary of the properties of products obtained from the lab-scale continuous flow synthesis of titania nanoparticles. An. = anatase, B. = brookite, Am. = amorphous. 115

Table 5.7. Cumulative energy demand values in MJ $kg^{-1}$ $TiO_2$ for all of the precursors and temperatures at industrial-scale production. Temp. = Temperature, Pre. = Precursor, IPA = Isopropanol, IPA dis. = Isopropanol distillation, $H_2O_2$ = Hydrogen Peroxide, Pack. = Packaging, Trans. = Transport, DIW = Deionised Water, Elec. = Electricity, H&C = Heating and Cooling, CP = Cleaning process, PP = Postprocessing, Wash = Washing, Neu. = Neutralization and WWT = Water waste treatment. 127

Table 5.8. Global warming potential values in kg $CO_2$-eq per kg $TiO_2$ for all of the precursors and temperatures at industrial-scale production. Temp. = Temperature, Pre. = Precursor, IPA = Isopropanol, IPA dis. = Isopropanol distillation, $H_2O_2$ = Hydrogen Peroxide, Pack. = Packaging, Trans. = Transport, DIW = Deionised Water, Elec. = Electricity, H&C = Heating and Cooling, CP = Cleaning process, PP = Postprocessing, Wash = Washing, Neu. = Neutralization and WWT = Water waste treatment. 128

Table 6.1. Summary of the operational conditions for the laboratory and industrial production. 138

Table 6.2. Material and energy inputs and outputs to produce 1 kg of lubricant with 5 wt% of $Ag_2S$ nanoparticles. 139

Table 6.3. Summary of greenhouse gases emissions to produce 1 kg of lubricant with 5 wt% of $Ag_2S$ nanoparticles. 147

Table 6.4. Summary of greenhouse gases emissions to produce 1 kg of $Ag_2S$ nanoparticles. 150

Table 7.1. Details of the nano-sulfides synthesis at laboratory scale conditions. 156

Table 7.2. Scenarios for the industrial production of nano-sulfides considered in this Thesis. 160

Table 7.3. Material and energy inputs and outputs to produce 1 kg of lubricant with 5 wt% of nanoparticles. 162

Table 7.4. Details of the Nano-sulfides materials used as additives with water as lubricant. 167

Table 7.6. Summary of greenhouse gases emissions to produce 1 kg of lubricant with 5 wt% sulfides nanoparticles. 175

Table 7.7. Summary of greenhouse gases emissions to produce 1 kg of sulfide nanoparticles. 180

Table A.1. Inputs and outputs of the Aspen HYSYS simulation for the production of LFP nanoparticles by continuous-flow hydrothermal synthesis at laboratory scale. 206

Table A.2. Life cycle inventory and greenhouse gas emissions for the synthesis of 1 kg of LFP nanoparticles at laboratory scale. 207

Table A.3. Inputs and outputs of the Aspen HYSYS simulation for the production of LFP nanoparticles by continuous-flow hydrothermal synthesis at laboratory scale. 209

Table A.4. Life cycle inventory and greenhouse gas emissions for the synthesis of 1 kg of LFP nanoparticles at pilot scale. 210

Table A.5. Life cycle inventory and total greenhouse gas emissions to dry 1 kg of LFP nanoparticles for the industrial scale of the continuous-flow hydrothermal synthesis. 212

Table A.6. Life cycle inventory and total greenhouse gas emissions to calcine 1 kg of C-LFP for the laboratory, pilot and industrial scale of the continuous-flow hydrothermal synthesis. 212

Table A.7. Inputs and outputs for the production of 1 kg of TiOS precursor (15 %wt.) in Aspen HYSYS simulation. 214

Table A.8. Inputs and outputs for the production of 1 kg of TiCl4 precursor in Aspen HYSYS simulation. 216

Table A.9. Information about the distillation of benzene and isopropanol in Aspen HYSYS simulation. 217

Table A.10. Information about the distillation of isopropanol and water in Aspen HYSYS simulation. 218

Table A.11. Information about the distillation of ethanol and water in Aspen HYSYS simulation. 219

Table A.12. Life cycle inventory and total greenhouse gas emissions to dry 1 kg of nano-sulfides for the industrial scale of the continuous-flow hydrothermal synthesis. 221

# 1. Chapter 1 – Introduction

This Chapter represents a general introduction for the topics of nanomaterials, life cycle assessment (LCA) and continuous-flow hydrothermal synthesis (CFHS). Firstly, the concept of sustainability in the context of chemical engineering is presented alongside the environmental challenge of achieving sustainable processes and products. The basics of nanomaterials are then defined as well as the variety of advantages they present as a result of their size. The concept of LCA is described in the context of its use as environmental assessment methodology in this thesis. CHFS is also introduced as a potential method for the production of nanomaterials with its specific benefits of scalability, versatility and potential reduction of the environmental impacts with respect to other nanomaterial production methods. Finally, the aims and motivation of the present work are briefly described.

# Chapter 1

## 1.1. Opening

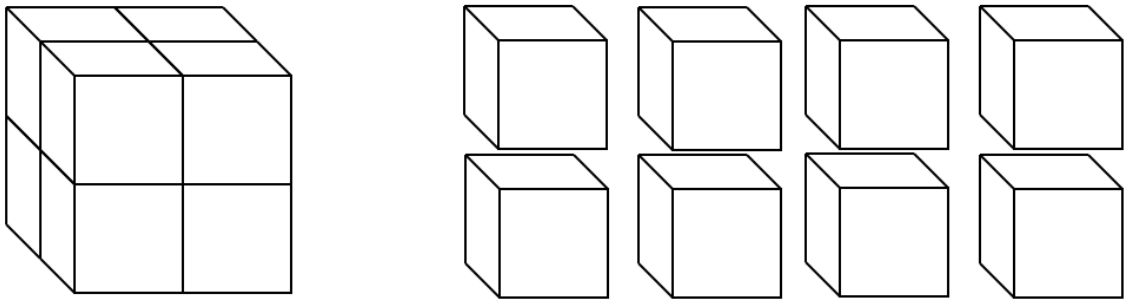
Brundtland Commission (Brundtland, 1987) defined sustainable development as *"development that meets the needs of the present without compromising the ability of future generations to meet their own needs"*. Nowadays, engineers face the environmental challenge of developing emergent technologies and products without compromising the environment. This drive is led by the ever-increasing concern about major environmental issues such as climate change, resource depletion and pollution. New policies, both public and private, environmental management and design strategies have appeared in the last years, focusing on more sustainable processes and products capable of assuring the future of the next generations and preserving the environment.

According to Professor Cathala (Cathala, 1951), *"Chemical engineering is a science that will teach (...) how to conceive, calculate, draw, build and operate the equipment by which any kind of chemical reaction may be carried out on an industrial scale"*. Historically, chemical engineers have been responsible for these tasks in different industries, in fields such as energy, petrochemical, pharmaceutical, environmental and fast moving market for consumer goods. All of these industries produce goods that are used daily by mankind. Chemical engineers do not just operate and sustain existing processes but also innovate, design and optimise new processes and have done so for economic and environmental reasons.

## 1.2. Nanomaterials

Nanomaterials are crystalline structures with 50% of the material with at least one dimension less than 100 nanometres (Franks, 1987). The size and shape of these nanomaterials have led to their use in new applications in medicine (Barreto et al.,

2011, Pankhurst et al., 2003), the environment (Li et al., 2008, Liu, 2006) and new technologies (Chen et al., 2005, Wu et al., 2010). Nanoparticles present unique properties that macro or micro-materials are not able to reach due mainly to their large size. For instance nanoparticles have a significantly higher surface area than micron sized powders, with up to 95% of atoms being present on the higner number of surface thus creating the highest surface:volume ratio. Figure 1.1 represents a schematic illustration. The total volume of the smaller particles corresponds with the same volume of the larger particle. However, the area of the "big particle" is clearly lower, thus its division in smaller nanoparticles leads the creation of new areas, therefore the surface and the ratio surface:volume increases considerably. Non-porous particles do not exceed 1 $m^2$ $g^{-1}$ until they are finer than 1000 nanometres.



$$Surface = 2 \times 2 \times 6 = 24$$
$$Volume = 2 \times 2 \times 2 = 8$$
$$\frac{Surface}{Volume} = 3$$

$$Surface = 1 \times 1 \times 6 \times 8 = 48$$
$$Volume = 1 \times 1 \times 1 \times 8 = 8$$
$$\frac{Surface}{Volume} = 6$$

Figure 1.1: Schematic illustration of surface area, volume and ratio surface:volume of large particle and small nanoparticles.

These changes improve properties such as optical (Zhu et al., 2008), electrical conductivity (Gaberscek et al., 2007, Yamada et al., 2001), the friction between surfaces (Dai et al., 2016) or catalytic activity (Tichá et al., 2016) . Many applications that use nanoparticles describe the improvement in performance with

respect to the bulk particles. For example, the discharge capacity of lithium iron phosphate (LFP) cathode material increased with the reduction of size (Gaberscek et al., 2007) or the enhanced photocatalytic degradation rate of organic contaminants by titanium dioxide ($TiO_2$) nanosheets instead of commercial titanium dioxide particles (Zhou et al., 2011).

## 1.3. Life cycle assessment

Due to the increasing demand for quality nanomaterials in potential applications, new synthesis routes have been of significant interest to engineers and scientists for many years. In short, there has been considerable effort to find competitive and sustainable industrial production routes (Edelstein and Cammaratra, 1998, Cao, 2004, Kralisch et al., 2015). Many of these techniques are described in detail in Chapter 2, which covers the synthesis of the nanomaterials treated in the present thesis (LFP, $TiO_2$ and metal sulfides nanoparticles). Many nanoparticle synthesis publications describe their own techniques as "green" (Bar et al., 2009, Raveendran et al., 2003, Vigneshwaran et al., 2006), generally by virtue of using low temperatures, or the use of "green solvents" or the use of microorganisms and bacteria. However, in principle, such a label should only really be given to a technology after a proper assessment of its environmental impact. Life cycle assessment (LCA) is a systematic, scientific and well-accepted environmental technique, which can be used for performing environmental assessment. LCA was introduced in the 90's by the Society Environmental Toxicology and Chemistry (SETAC) to understand the consequences of the production, the use and the end-of-life of a product, including all of the steps and needs of a product life (cradle-to-grave). The potential to make the assessment narrower (cradle-to-gate) and wider

(cradle-to-cradle) are also possible. The methodology of the LCA is expanded upon Chapter 3, however (in short) it involves the assessment of whole life of the product, including raw materials extraction, production, use, recycling and disposal (Figure 1.2). LCA establishes system boundaries to define all inputs and outputs of the system such as energy consumption or contaminant emissions; so a comprehensive evaluation is carried out analysing the whole lifetime of the product. The information obtained from the LCA is used as feedback to prevent future impacts, to reduce emissions of the production and to optimize the process, among other advantages.

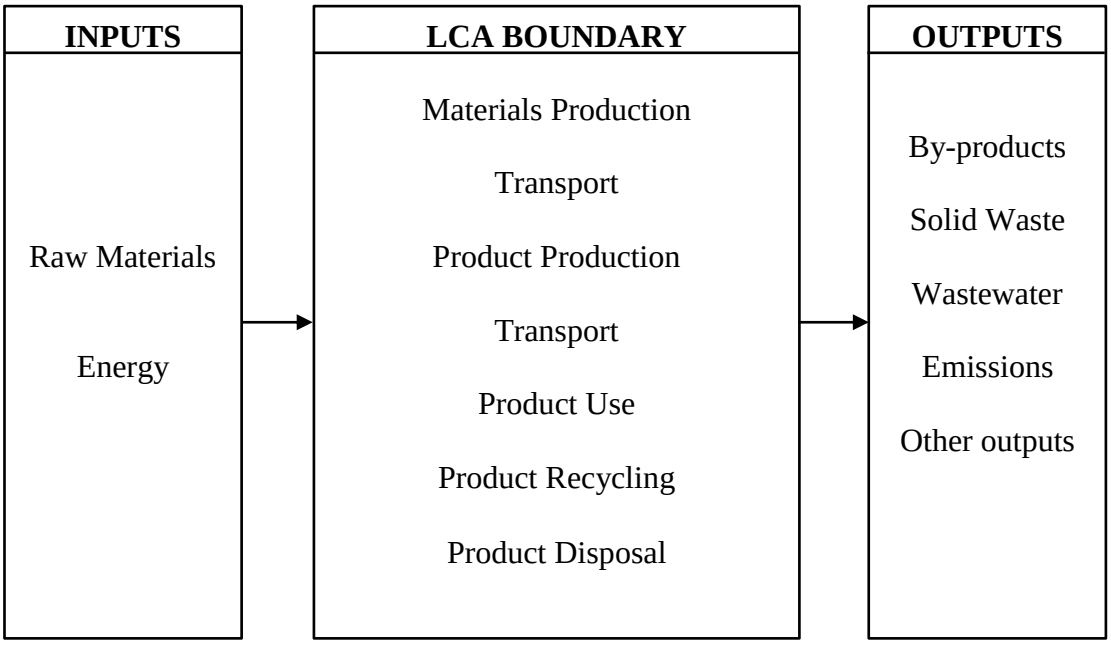



Figure 1.2: Basic diagram to describe a generic life cycle assessment.

## 1.4. Continuous-flow hydrothermal synthesis

Continuous-flow hydrothermal synthesis (CFHS) was initially carried out by Adschiri et al. (1992a) to synthesise metal oxide nanoparticles rapidly in a continuous system with the use of water as solvent. This synthesis route uses the properties of supercritical water (SCW) to synthesise nanomaterials with different sizes and morphologies (Dunne et al., 2015a, Munn et al., 2015). A supercritical fluid

occurs when its temperature and pressure are above the critical point, in the case of water this is 374 °C and 221 bar (Marcus, 2012) (Figure 1.3). SCW possesses properties of liquid and gas phase, being effectively a mixture of both. For instance, the density is approximately 317 kg $m^{-3}$ and dielectric constant 5.44 around the critical point (Marcus, 2012). This drastic decrease permits the dissolution and ionization of electrolytes as well as the miscibility with non-polar compounds.

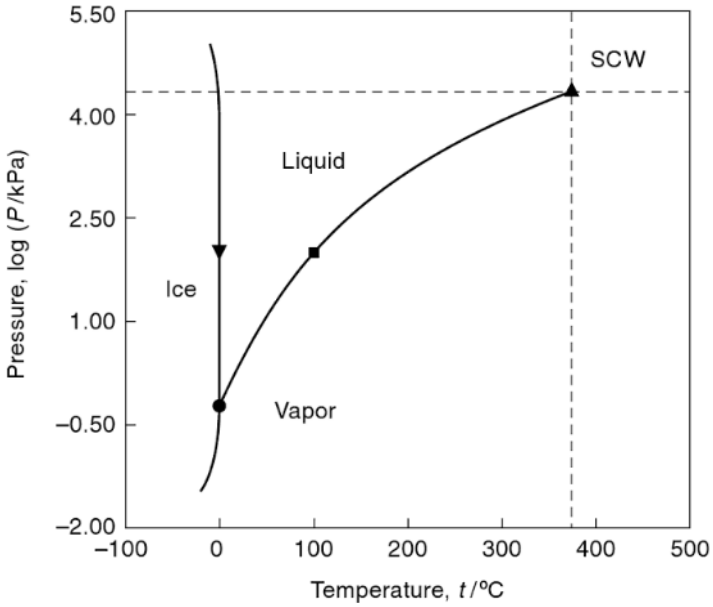



Figure 1.3: Diagram phase of water for solid, liquid, gas and supercritical conditions, where ● Triple point ($T_{tr}$=0.01 °C; $P_{tr}$=6.11 mbar); ▼ Melting point ($T_m$=0 °C; $P_m$=1.013 bar); ■ Normal boiling point ($T_b$=99.61 °C; $P_b$=1 bar), and ▲ Critical point (Tc=374°C Pc=221 bar) (Marcus, 2012).

Adschiri et al. (1992a) took advantage of the properties of SCW to synthesise nanomaterials. Under supercritical conditions there is an increase of the dissociation constant of water, therefore the concentration of ions $H^+$ and $OH^-$ increases (Adschiri et al., 1992a). When the metal salt is mixed with the SCW, the metal ions are hydrolysed (Reaction 1.1), followed by a dehydration of the metal hydroxide (Reaction 1.2) to precipitate metal oxide nanoparticles.

$$ML_x + xOH^- \rightarrow M(OH)_x + xL^- \quad (1.1)$$

$$M(OH)_x \rightarrow MO_{\frac{x}{2}} + \frac{x}{2}H_2O \quad (1.2)$$

This rapid and facile synthesis has been widely developed since the Adschiri group first published their work. The exhaustive study of new reactors, reagents, solvents and operational conditions and configurations have offered a large variety of nanomaterials and the possibility to scale-up the process to industrial production (Dunne et al., 2015a, SHYMAN-project, 2015).

## 1.5. Aims and motivation

Recently the awareness has increased about the environmental impact of all anthropogenic activities on nature. Environmental issues like climate change present a global challenge for engineers and scientists, who have started to research and develop new materials, products and processes that create a lower environment burden. In addition, new policies have already been adopted to limit air emissions, raising awareness of efficiency and recycling. Even the behaviour of consumers has changed in recent years to insist on more environmentally-friendly products from the industries that create them. The present thesis is an assessment of the potential for CFHS to not only comply but also become a leader in the sustainable manufacture of nanomaterials. CFHS offers many advantages as an alternative for the industrial production of nanomaterials. The technology is relatively simple but flexible – i.e. it can produce a large variety of nanoparticles with different size and morphology - and uses an inexpensive and non-toxic solvent (water). In this thesis, LCA methodology is used to assess the benefits of the scale-up production of the novel LFP cathode nanomaterial; the environmental impacts of the $TiO_2$ nanoparticles synthesis across a broad set of temperatures and precursors; and the frictional performance of various

metal sulfide nanomaterials alongside their net environmental impact. Therefore it could be concluded that the present work has the following objectives:

1. To demonstrate the advantages of nanoparticle synthesis by the scale-up from laboratory to industrial scale.
2. To evaluate environmental impacts of CFHS industrial production for a variety of nanomaterials.
3. To determine the most favourable operational conditions for the industrial production of LFP and $TiO_2$ nanoparticles.
4. To describe the first successful continuous hydrothermal synthesis of silver sulfide nanoparticles and its application as lubricant additive in water and mineral oil.
5. To compare the frictional performance of a wide range of metal sulfides nanomaterials in water and mineral oil lubricant and directly correlate the performance advantages of each alongside the LCA of each.

# 2. Chapter 2 – Background and literature review

In this chapter, the concepts of sustainability, life cycle assessment (LCA) and the most common environmental impacts are described in order to explain the methodology used to carry out an environmental evaluation of an emergent technology. The chapter also contains a literature review for the main synthesis methods (both laboratory and industrial scale) for lithium iron phosphate (LFP), titanium dioxide ($TiO_2$) and metal sulphides. The differences between each process and product is established as well as the pros and cons of each. Specifically, this section describes the most important methods to synthesise LFP and metal sulfides nanoparticles as well as their limitations; the industrial production of micron sized $TiO_2$ by traditional processes; the potential of the continuous-flow hydrothermal synthesis (CFHS) to produce all these materials.

# Chapter 2

## 2.1. Sustainability

### 2.1.1. Introduction

Although the concept of 'sustainability' officially appeared in the 80s, previous events such as the United Nations Conference on Human Environment celebrated in Stockholm (1972) already talked about environmental issues (Wallace, 2005). Environmental disasters were not the only cause of the rise in sustainability approaches; political and social concerns had also started to appear from the end of the 60's. Some of the most important environmental disasters are described briefly in the following list:

- The book Silent Spring was published by Rachel Carson in 1962 describing the negative effects of the abusive use of pesticides.
- Santa Barbara oil spill in 1969 was the largest spill to that point with 80.000 to 100.000 barrels lost into the sea.
- OPEC oil crisis in 1973 consisted in an oil embargo, provoking a significant impact over the world economy, as well as a political change in energy dependency.
- Seveso dioxin disaster in Italy in 1976 resulted in the emission of high amounts of tetra-chlorodibenzo-p-dioxin, affecting to population of the area.
- Bhopal explosion and release of methyl isocyanate gas in 1984 affected more than 600.000 people and caused the death of at least 4.000.
- Chernobyl nuclear power station explosion in 1986 released radioactive material that contained to 100.000 $km^2$, producing the death to 31

people, an exclusion zone of 30 km and several consequences that still remain today.

The first U.N. Conference on the Human environment (1972) took place in Stockholm, where 113 industrialised countries attended to address the problems of environmental degradation and international scale pollution. As a result of this conference, the Stockholm Declaration and Action Plan can be considered like the first international agreement in sustainability. After this meeting, many international meetings continued to focus on environmental challenges and issues. The Brundtland Commission in 1987 published the report of 'Our Common Future', including more than 75 studies on environment and development issues, as well as 15 public hearings. In 1992, the Earth Summit in Rio de Janeiro, where 100 countries and 30,000 people attended to a conference about the environment. In Rio, a comprehensive version of international attitudes and behaviours was approved, including 27 universal sustainable development principles. The Kyoto Protocol (1997) was an international treaty with objective of reducing the emissions of greenhouse gases ($CO_2$, $CH_4$ and $N_2O$) by 5% in respect to 1990, between 2008 and 2012.

### 2.1.2. Environmental impacts

Since the industrial revolution, the levels of greenhouse gases (GHG) in the atmosphere have increased. The main cause of this increase is anthropogenic activity, which releases these contaminants into the atmosphere (Wuebbles and Edmonds, 1991). The emission of contaminant substances is related to environmental problems like the global warming or climate change, as well as low air quality. Some of the

most salient environmental impacts and their problems are listed in the following subsections.

#### 2.1.2.1. Ozone depletion layer

The ozone depletion consists in the destruction of the molecular ozone at the second layer of the atmosphere, commonly called Stratosphere. The stratospheric ozone (good ozone) is the second layer of the atmosphere (From 20 to 50 km height). The "good ozone" is the responsible of the protection from the ultraviolet radiation. It is able to absorb solar radiation, which can cause long-term skin cancer to humans. High concentrations of chlorofluorocarbons (CFCs) are able to destroy it, which in turn increases the risk to health. CFCs are dissociated by solar energy into atoms, one of them being chlorine atom. The ozone depletion layer is a cyclical problem because the same chlorine atom can break more than one ozone molecule (Reactions 2.1 and 2.2).

$$Cl + O_3 \rightarrow ClO + O_2 \quad (2.1)$$

$$ClO + O \rightarrow Cl + O_2 \quad (2.2)$$

Generally the CFCs have been typically used as refrigerants and solvents. Their production started in the 1930s, but it decreased drastically after the 1980s due to signing of the Montreal Protocol in 1987, which was an international arrangement to reduce the use of CFCs. On the other hand, tropospheric ozone (bad ozone) is produced by the reaction between nitrogen oxide emissions ($NO_x$) and hydrocarbons at the troposphere (ground-level). Ozone ($O_3$) is an oxidant substance, which on the Earth's surface is highly dangerous, with potential effects on the respiratory system, such as lung irritation (Allen and Shonnard, 2012).

### 2.1.2.2. Global warming

As mentioned previously, the emission of greenhouse gases (GHG) into the atmosphere creates a layer above the Earth's surface. During the daytime, the Earth receives sunlight, which is filtered by the atmosphere. The radiation that passes the atmosphere is adsorbed by the Earth's surface (infrared radiation) and later is emitted from the ground floor. The problem occurs when the greenhouse layer does not permit the output of infrared radiation and it is reflected again to the Earth's surface. The consequence is an increase in temperature and consequently this fact affects climate, polar ice cap, sea-level, humans and environment (Allen and Shonnard, 2012).

The principal greenhouse gases and their anthropogenic sources are:

- Carbon Dioxide ($CO_2$), it is an emission from fossil fuel combustion and the high deforestation of rainforest produced by human activity.
- Nitrous Oxide ($NO_2$) is emitted by low temperature combustion and deforestation.
- Methane ($CH_4$) is usually produced by agricultural and livestock activities.
- Chlorofluorocarbons CFCs are used as refrigerants, solvents and aerosols.
- Tropospheric ozone ($O_3$) is a product of the photochemical reaction between nitrous oxides and volatile organic compounds produced by industrial combustions.

Global Warming Potential (GWP) is a relative measure which is used to determinate the climatic impact produced by GHG. It measures the radiation absorbed by the gas comparing with the same quantity of an emission of $CO_2$ in a relative period of time.

For example, the 100 year GWP of $CH_4$, is equivalent to 25, thus one kilogram of $CH_4$ traps 25 times more heat than 1 kilogram of $CO_2$ over a 100 year period. The relationship between $CO_2$ and the others gases:

- $CO_2$ → 1 GWP/100 years
- $NO_2$ → 298 GWP/100 years
- $CH_4$ → 25 GWP/100 years
- CFCs (CFC-11) → 4750 GWP/100 years
- $O_3$ → 2000 GWP/100 years

The Intergovernmental Panel on Climate Change (IPCC) is the international organization that assesses the effect on climate change. In 1988, the World Meteorological Organization (WMO) and the United Nations Environment Programme (UNEP) founded the IPCC with the objective of providing information about potential environmental, social and economic impacts which are caused by the climate change. IPCC is a group of scientists, who voluntarily evaluate and analyse the data related to climate change. Since its formation, IPCC has written and published five assessments analysing the information and evidence of climate change in 1990, 1995, 2001, 2007 and 2014.

#### 2.1.2.3. Acidification potential

In general, the acidification of the enviroment is generated by combustion in automobiles, factories, etc., as well as, metal smelting. It is an emission produced by the sulfur present in solid and liquid fossil fuels like coal, which has the highest quantity of sulfur in any fossil fuel. Also $NO_X$ emissions are integrated in this environmental impact. These substances can be transported across the atmosphere

long distances (from country to country) and ultimately be deposited as aqueous phase due to the reactions with water.

$$H_2O + SO_2 \rightarrow H_2SO_4 \quad (2.3)$$

$$H_2O + NO_X \rightarrow HNO_3 \quad (2.4)$$

The precipitation of these acids is responsible of what is commonly known as "acid rain", which changes the pH of ground and water, and is able to impact on the health of the people, ecosystems and buildings. Some examples include respiratory problems, skin irritation, acidification of rivers and corrosion of monuments (Allen and Shonnard, 2012).

#### 2.1.2.4. Eutrophication

This environmental impact begins with the introduction of nitrates and phosphates into a hydrological ecosystem, such as a lake or river, increasing the nutrient levels which leads to algal blooms. The sudden proliferation of algae reduces drastically the oxygen level in the water, which then has a negative effect on the flora and fauna in the surrounding ecosystem. Eutrophication can effectively lead to anoxic conditions where the oxygen in the water falls to 0 mg/L

### 2.1.3. Life cycle assessment

LCA is a method which studies a product from its origin (cradle) to its end-of-life (grave) with the objective of evaluating the environmental impacts from a sustainability point of view. It must take into account all the stages of a product life and the necessary sources for its production, use, recycling and end of life.

LCA started at the end of the 60s, when some companies and independent initiatives wished to identify the high cost points of a production and more sustainable processes and products. For instance, a study carried out by Midwest Research

Institute in United States (1969 - 1970) for Coca Cola about the environmental consequences of their packaging manufacture and alternatives to beverage cans as plastic or glass bottles. The study included all energy consumption, raw material and environmental impacts in the packing production, concluding with the implementation of plastic bottles for their drinks (Baumann and Tillman, 2004).

During the 1970s the number of studies increased, mainly with a focus on the problems of availability of raw materials, energy and fuel, catalysed by the crisis with OPEC in 1973. In the 1980s, the approach caught the attention of the general public. At this point, 'Green parties' were founded and some governments and state organisations began to conduct their own LCA reports (Baumann and Tillman, 2004). Finally, during the early 90s the Society for Environmental Toxicology and Chemistry arranged a forum where the scientists debated LCA methodology. After the forum, many workshops and conference were organised to develop and work together about LCA reports. In 1993, the Code of Practice was published. The last step was the standardization of the code by the International Organization for Standardization, which presented the following LCA standards:

- In 1997, ISO 14040 Life Cycle Assessment – Principles and Frameworks.
- In 1998, ISO 14041 Life Cycle Assessment – Goal and scope definition and inventory analysis.
- In 2000, ISO 14042 Life Cycle Assessment – Life cycle impact assessment.
- In 2000, ISO 14043 Life Cycle Assessment – Life cycle interpretation.
- In 2002, ISO/TS 14048 Life Cycle Assessment – Data documentation format.

## Chapter 2

The methodology of the LCA is widely defined in Chapter 3, describing the necessary steps for the completion of an LCA. Recently, a few LCA studies have been published to evaluate emergent techniques for synthesis of nanomaterials (Tsang et al., 2016, Pini et al., 2015, Pourzahedi and Eckelman, 2015, Grubb and Bakshi, 2011, Deorsola et al., 2012, Bobba et al., 2016), applications or products which include nanoparticles (Zackrisson et al., 2010, Majeau-Bettez et al., 2011, Liang et al., 2017, Yu et al., 2014, Stieberova et al., 2017, Akram et al., 2014) and processes for producing micron sized materials in order to compare with new synthesis routes (Middlemas et al., 2015, Reck and Richards, 1999). All of them are described and compared with the results of the present thesis in Chapters 4-7.

## 2.2. Nanomaterials synthesis and processes

Nanomaterials can be synthesised using different techniques, this section describes the most typical laboratory synthesis and industrial production of the materials used in this thesis.

### 2.2.1. Lithium iron phosphate

Lithium iron phosphate (LFP or $LiFePO_4$) has drawn recently attention for applications like batteries in electric vehicles and new technologies (Huang et al., 2009, Horiba, 2014, Howell, 2008, Yuan et al., 2011). This material has been presented as an excellent cathode candidate (Padhi et al., 1997b) and it has gained interest due to commercialization of lithium ion batteries (LIBs) by companies like Sony since the 90's (Nazri and Pistoia, 2008). LFP is a non-toxic and low cost material with high capacity (170 mAh $g^{-1}$), thermal stability and long life-time (Padhi et al., 1997b, Padhi et al., 1997a, Kang and Ceder, 2009, Cheruvally, 2008).

Although LFP can be found in nature (triphylite), the impurities of the mineral make it unusable in batteries. Over the last two decades many techniques have been developed to synthesise LFP that are competitive at large-scale production (Wu et al., 2011, Jugović and Uskoković, 2009, Toprakci et al., 2010, Franger et al., 2003).

#### 2.2.1.1. Solid-state methods for the synthesis of lithium iron phosphate

##### 2.2.1.1.1. Solid-state synthesis of lithium iron phosphate

It is one of the most conventional techniques for the production of ceramics and nanoparticles. Firstly, the stoichiometric amount of salts are mixed and ball milled, subsequently by a heat-treatment to remove impurities and residual gases (300-400 °C) (Wu et al., 2011). Between the most common precursors are $Li_2CO_3$, $LiOH{\cdot}H_2O$, $FeC_2O_4{\cdot}2H_2O$ and $NH_4H_2PO_4$ (Padhi et al., 1997b, Hong et al., 2012, Koltypin et al., 2007). Later, a calcination stage is carried out to crystallise LFP, the temperature increases up to 400-800 °C for 10-24 hours (Jugović and Uskoković, 2009). Gases like argon, hydrogen or nitrogen are used to create an inert or reductive atmosphere during the synthesis. After calcination stage, the product is cooled down before grinding and sieving. The addition of carbon sources such as glucose, sucrose or polyvinyl alcohol is commonly used to improve the electrochemical properties of the LFP product (Hong et al., 2011a). Solid-state processing is able to produce high quantities of LFP with particle sizes of 30 nm to 1000 nm (Wu et al., 2011).

##### 2.2.1.1.2. Mechanochemical activation synthesis of lithium iron phosphate

Mechanochemical method uses a high-energy ball-milling vessel at high speed revolution to improve the reactivity of initial precursor mixture (3-24 h) (Toprakci et al., 2010). The use of this technique reduces considerable the size of the LFP

particles down to nano-size. As a result, the surface area increases, improving the electronic conductivity (Jugović and Uskoković, 2009, Franger et al., 2003). The use of inert gases (Ar, $H_2$ or $N_2$) and high temperatures (500-900 °C) in the calcination stage are similar to solid-state method, but with shorter period of time (1-10 h) (Toprakci et al., 2010, Wu et al., 2011). Smaller and more homogeneous nanoparticles improve the electrochemical properties, but the speed and the temperature have to be controlled to avoid the decomposition of precursors that could affect negatively the product quality (Zhang, 2011).

#### 2.2.1.1.3. Carbothermal synthesis of lithium iron phosphate

The carbothermal reduction (CTR) was developed to reduce the price of the LFP synthesis using cheaper and more abundant precursors such as $Fe_2O_3$, $FePO_4$ or $Fe(NO_3)_3$, $Fe^{3+}$ instead of $Fe^{2+}$ reagents (Barker et al., 2003, Zhang, 2011). Also, CTR does not require any pre-heat step, reducing significantly the time and the energy in comparison with solid-state and mechanochemical activation (Jugović and Uskoković, 2009). The reducing agent used can be carbon black, graphite or other organic carbon sources. The precursor and the reducing agent have to be well-mixed to keep all of them in contact during 2-4 h in a ball-milling. After, the sintering step is carried out to produce the LFP nanoparticles, the temperature can range from 550 °C to 850 °C in a period of 8-10 h in an inert atmosphere (Toprakci et al., 2010). The oxidation of the carbon permits the reduction the $Fe^{3+}$ to $Fe^{2+}$ and depending on the temperature CO or $CO_2$ are produced. Finally, the product is cooled down, before to be grinded and sieved. This technique requires an exhaustive control or the parameters (Temperature, precursors and reducing agent) to get a product with good properties and high quality.

#### 2.2.1.1.4. Microwave synthesis of lithium iron phosphate

The use of microwaves to synthesise LFP permits a rapid and uniform heating of the precursors (Wu et al., 2011). This leads to a faster reaction at lower temperatures requiring only minutes at power inputs as low as 300 W to 1000 W (Toprakci et al., 2010). Initial experiments were carried out with inert gas in a conventional microwave (Higuchi et al., 2003), but more developed techniques do not report the need the inert gases (Murugan et al., 2008). It is necessary to use precursor or additives that can absorb microwave energy (receptors), such as iron powder, activated carbon or carbon black (Jugović and Uskoković, 2009). Generally, LFP nanoparticles produced by microwave solid-state have good quality, but excessive reaction time or power input can considerably impact on the electrochemical properties by decomposing the reagents. Microwaves can be combined with other techniques such as hydrothermal and solvothermal synthesis (Murugan et al., 2008).

### 2.2.1.2. Solution methods for the synthesis of lithium iron phosphate

#### 2.2.1.2.1. Sol-gel synthesis of lithium iron phosphate

Sol-gel involves three steps; first is the formation of a sol that consists of a suspension of particles. The precursors are mixed, stirred (12-24 h) and heated-up (60-80 °C) (Toprakci et al., 2010). This synthesis uses a wide variety of precursors, surfactants and solvents such as water, methanol or ethanol (Fan et al., 2016, Choi and Kumta, 2007). The second step is the gelation to form a gel that results in a rigid network with pores where the colloidal particles are allocated. Then the gel is dried (≈80 °C) producing a xerogel. Finally the xerogel is treated at high temperature (>600 °C) in a calcination process in an inert or vacuum atmosphere (Wang and Sun, 2012). Many parameters such as solvent choice, temperature, time and pH affect

significantly to morphology and quality of the final product. In general, LFP nanoparticles synthesised by the sol-gel method are uniform and with high purity due to the control of process (Hench and West, 1990, Wang and Sun, 2012). Also, the low reaction temperature lowers the cost of production, but the complexity of this method hinders the scale-up to industrial production.

#### 2.2.1.2.2. Co-precipitation synthesis of lithium iron phosphate

Precursor salts are mixed in solution of water and miscible additives like ethylene glycol to elevate the boiling temperature (>100 °C) (Ni et al., 2005, Delacourt et al., 2006). Stirring and a slightly basic pH are set to precipitate nanoparticles (Arnold et al., 2003). Later the suspension is filtered, washed and dried under nitrogen atmosphere. Finally, a calcination process is carried out to enhance the crystallinity of product at elevated temperature (500-800 °C) and inert atmosphere (Arnold et al., 2003, Liu and Cao, 2010). Low reaction temperature is one of the principal advantages, as well as the phase purity, well-crystallized and homogenous nanoparticles.

#### 2.2.1.2.3. Spray pyrolysis synthesis of lithium iron phosphate

This technique involves the solution of the stoichiometric amounts of precursors in water to generate a suspension that is sprayed in a reactor at high temperature (400-800 °C) (Jang and Taniguchi, 2017). The spray is generated by pumping the solution and the use of carrier gas. After, the collected dried powders are calcined at high temperature (>500 °C) (Konarova and Taniguchi, 2010, Konarova and Taniguchi, 2009). The size, uniformity and low agglomeration of particles synthesised by this method are its principal characteristics (Taniguchi, 2005).

#### 2.2.1.2.4. Batch hydrothermal and solvothermal synthesis of lithium iron phosphate

Batch hydrothermal synthesis of LFP nanoparticles was initially carried out by Yang et al. (2001), using an aqueous solution of $FeSO_4$, $H_3PO_4$ and LiOH in excess at 120 °C for 5 h in an autoclave reactor. A vast number of additives and conditions have been studied to improve the electrochemical properties of LFP nanoparticles synthesised by these methods (Chen et al., 2008, Toprakci et al., 2010, Devaraju and Honma, 2012). In general, the temperature reaction is above of 175 °C to obtain small, uniform and high purity LFP nanoparticles, while the time could range between 5-10 h (Jugović and Uskoković, 2009). The molar ratio (Fe:P:Li) is 1:1:3 to maintain a neutral or slightly basic pH, that is beneficial for the reaction (Lee and Teja, 2006). After the reaction the suspension of nanoparticles is filtered and dried. In many studies, a carbon coating and calcination process have been carried out to improve the capacity and $Li^+$ diffusion of the LFP nanoparticles (Bodoardo et al., 2009). In a similar way, the solvothermal method can synthesise LFP nanoparticles. The main difference is the change of water solvent by organic solvents like polyethylene glycol or dimethyl formamide, improving the control of the reaction and the quality product (Yang et al., 2010, Devaraju and Honma, 2012). Both solvothermal and hydrothermal techniques work with lower temperatures and times than solid-state techniques, as well as a higher quality product in terms of crystallinity, homogeneity and size distribution.

#### 2.2.1.2.5. Continuous-flow hydrothermal synthesis of lithium iron phosphate

Unlike previous techniques, LFP nanoparticles can be continuously synthesised as it is shown in Figure 2.1 (Xu et al., 2008). In general, a superheated water stream is

mixed with a cold precursor solution stream in a reactor. The high dissociation constant and low polarity of the supercritical water leads to the nucleation of nanoparticles. Then the suspension is cooled down and depressurised before it is dried. In many occasions, a calcination stage is carried out with a carbon source such as fructose or glucose to form carbon coating (Murugan et al., 2008). Continuous hydrothermal synthesis allows an easier control of process parameters like temperature or flow, as well as the morphology of the nanoparticles than batch techniques (Dunne et al., 2015a, Lester and Azzopardi, 2004, Lester et al., 2006). By this, the nanoparticles synthesised are characterised by high crystallinity, homogeneity, small size and narrow distribution.

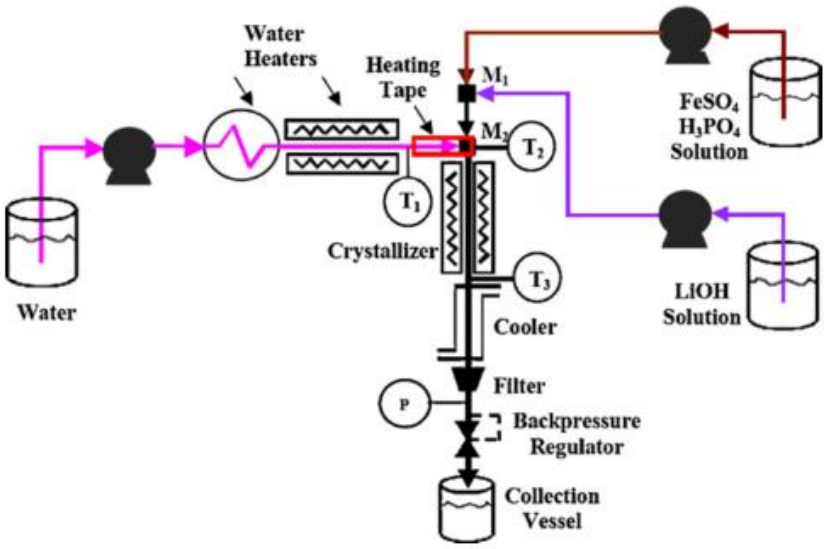



Figure 2.1: Schematic drawn of the apparatus used for the continuous-flow hydrothermal synthesis of LFP (Xu et al., 2008).

### 2.2.2. Titanium dioxide

Titanium dioxide ($TiO_2$) was first reported by William Gregor in 1791, who analysed black grains of sand from Cornwall's beaches (Weeks, 1933). Unlike the typical silica sand, the black grains could be attracted by a magnet. Mr Gregor researched

the dissolution of these grains with different chemicals such as hydrochloric acid, soda and sulfuric acid, to finally discover a white powder, $TiO_2$ (Trengove, 1972). This element is the ninth most plentiful in the surface of the Earth, easily encountered in three polymorph structures as oxide form; anatase, rutile and brookite. Table 2.1 describes some their properties (Chen and Mao, 2007, Sepeur, 2008).

Table 2.1. Physical Properties of brookite, anatase and rutile.

| | Brookite | Anatase | Rutile |
|---|---|---|---|
| Crystal Structure | Orthorhombic | Tetragonal | Tetragonal |
| Melting Point (°C) | Transformation to anatase | Transformation to rutile | ≈ 1825 |
| Density ($kg/m^3$) | 4133 | 3890 | 4260 |
| Colour | Brown/Yellowish Brown | Brown/Pale Yellow | Blood red/Brownish |
| Hardness | 5.5-6 | 5.5-6 | 6.5-7 |
| Refractive Index | 2.63 | 2.52 | 2.72 |

In general, anatase and rutile are extensively used and manufactured at an industrial scale, due to their properties like high chemical and thermal stability (Cargnello et al., 2014), refractive index, non-toxicity, catalytic and photocatalytic activity and high hardness (Thompson and Group, 1977, Büchner, 1989, Chen and Mao, 2007). All of these properties facility their use in medical implants (Macwan et al., 2011), pigments industry (Grubb and Bakshi, 2011), wastewater treatment (Carp et al., 2004, Gaya and Abdullah, 2008) and technological applications (Diebold, 2003).

### 2.2.2.1. Industrial processes for $TiO_2$ manufacture

The two processes that have been traditionally used for the industrial production are sulfate and chloride (Reck and Richards, 1999). Feedstocks for these processes can come from natural resources or by-products of other minerals manufacturing. Table 2.2 details the variety of raw materials, their titanium content and the process within are used (Büchner, 1989, Thompson and Group, 1977, Force, 1991).

Table 2.2. Feedstocks of $TiO_2$ industries.

| Raw Material | Source | Titanium content (%) | Process | Comments |
|---|---|---|---|---|
| Ilmenite | Mineral ore | 43-61 | Sulfate | Formula $FeTiO_3$ FeO 34-49 wt% |
| Rutile Deposits | Mineral ore | 90-98 | Chloride | Highest Ti content Low resources |
| Anatase Deposits | Mineral ore | 30-90 | Sulfate-chloride | High resources |
| Titaniferous Slag | By-product | 70-85 | Sulfate-chloride | Ilmenite is treated to produce iron, slag is a by-product |
| Synthetic rutile | Product | 85-90 | Chloride | Produced from Ilmenite, due to higher price of natural rutile |

#### 2.2.2.1.1. Industrial Sulfate process for the production of $TiO_2$

In general, this process uses ilmenite or slag (titaniferous slag) as raw materials. Rutile cannot easily be dissolved in sulfuric acid. Ilmenite or slag is digested in an exothermic reaction (Reaction 2.5), which uses between 1.5 and 1.7 excess of acid (lower excess with ilmenite), being the yield of 95% approximately (Thompson, 1995).

$$FeTiO_3 + 2H_2SO_4 \rightarrow TiOSO_4 + FeSO_4 + H_2O \quad (2.5)$$

When ilmenite is used as raw material, it is necessary to add scrap iron to reduce any ferric iron to ferrous. After digestion, the solution passes different separation methods to remove iron, impurities and unreacted mineral. These methods are filtration, sedimentation and flocculation. Cold water (10 °C) is added to precipitate and remove the $FeSO_4 \cdot 7H_2O$. Next stage consists in a hydrolysis with steam and $TiO_2$ seed crystals to precipitate the titanium dioxide (Reaction 2.6 and 2.7).

$$TiOSO_4 + (n+1)H_2O \rightarrow TiO_2nH_2O + H_2SO_4 \quad (2.6)$$

$$TiO_2nH_2O \rightarrow TiO_2 + nH_2O \quad (2.7)$$

Further production stages are carried out to wash and increase the purity of the product before of calcination. Calcination step varies on the type of product desired, but generally the temperatures are between 800 and 1000 °C and the time ranges between 18-24 h.

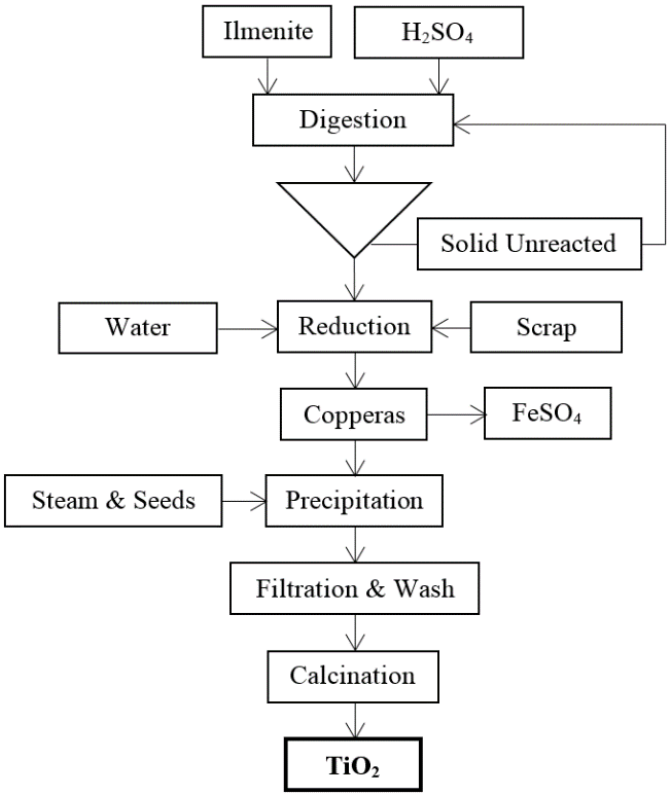



Figure 2.2. Schematic flowchart for $TiO_2$ production, sulfate process.

#### 2.2.2.1.2. Industrial Chloride process for the production of $TiO_2$

The Chloride process uses rutile (mineral or synthetic) as raw material or slag with high purity of $TiO_2$ (Reck and Richards, 1999). Firstly, the ore is mixed with carbon (coke) in a bed-fluid reactor and the chlorine is injected, the reaction is exothermic, so that the temperature is maintained around 950 °C.

$$2TiO_2 + 4Cl_2 + 3C \rightarrow 2TiCl_4 + 2CO + CO_2 \quad (2.8)$$

Some of the metallic impurities like iron become chlorinated ($Fe + 3Cl \rightarrow FeCl_3$), but others, which do not react, can be removed from the system as solids. A set of coolers condensate impurities and metallic components to be removed from the main stream. Next step consists in a distillation to obtain high purity $TiCl_4$. After distillation $TiCl_4$ is oxidised in a reactor with oxygen at high temperature. In general, the inlet is preheated and enriched with air to react from 1000 °C to 1700 °C in the reactor chamber (Reaction 2.9) (Büchner, 1989).

$$TiCl_4 + O_2 \rightarrow TiO_2 + 2Cl_2 \quad (2.9)$$

Depending on the raw material and purity of mineral, the process could produce by-products (metallic compounds). Figure 2.3 shows a schematic representation of the stages followed in this synthesis route.

The main advantages of sulfate process are the use of low cost raw materials and high amount of resources. However, the low content of titanium in in their feedstocks generates large amount of waste and high demand of sulfuric acid. By contrast, chloride is a continuous process which uses more pure minerals, generating less waste. These benefits also carry out a more expensive price of raw materials and capital investment.

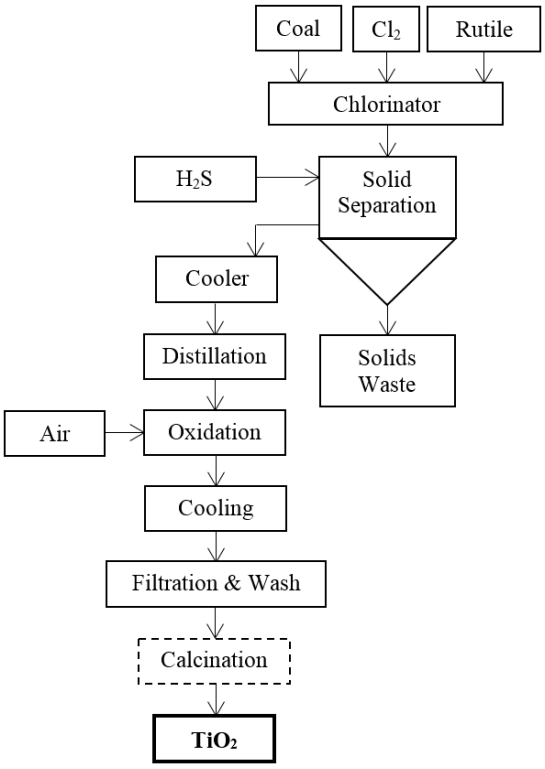



Figure 2.3. Schedule for $TiO_2$ production, chloride process.

### 2.2.2.2. Continuous-flow synthesis of $TiO_2$ nanoparticles

Emergent applications are demanding smaller particle size than the micron-sized $TiO_2$ produced by sulfate and chloride processes. Therefore in the last years, continuous-flow hydrothermal and solvothermal syntheses (CFHS and CFSS) have been widely studied as potential alternatives to produce industrially $TiO_2$ nanoparticles (<100 nm) (Toft et al., 2009, Zhang et al., 2009, Kawasaki et al., 2009, Malinger et al., 2011, Makwana et al., 2016). The product is similar in the publications; anatase phase $TiO_2$ nanoparticles (nano-$TiO_2$) with size between the 4 and 18 nm. However differences can be found in the operational conditions, temperature and precursor choice. Reaction temperature is generally 400 °C in the majority of the publications, but lower reaction temperatures (120-220 °C) can also produce nano-$TiO_2$ (Malinger et al., 2011). The most significant parameter is the selection of precursor (organic and inorganic reagents), which also affects to the

solvent choice (water or organic solvent). For instance, organic precursor titanium tetraisopropoxide (TiPO or TIPO) uses commonly isopropanol (IPA) as a solvent (Toft et al., 2009). By contrast, an inorganic precursor like titanium sulfate ($Ti(SO_4)_2$) can be easily dissolved in water (Makwana et al., 2016). There is a large variety of precursors for the CFHS and CFSS of nano-$TiO_2$.

#### 2.2.2.2.1. Precursors of $TiO_2$ nanoparticles for solvo/hydrothermal syntheses

- Titanium halide precursors

These are mainly titanium tetrachloride ($TiCl_4$) and titanium tetrafluoride ($TiF_4$). Halides can be easily hydrolysed to produce $TiO_2$. The main disadvantage of these precursors is the use of highly hazardous chemicals. Halides are a very reactive components, so it must be treated carefully, thus they are able to produce HF, HCl and $Cl_2$ easily with water and oxygen. Even the reaction of $TiCl_4$ with water is extremely exothermic (explosive).

- Titanium sulfate precursors

Titanium sulfate ($Ti(SO_4)_2$) and oxysulfate ($TiOSO_4$ or TiOS) are produced as by-product of the sulfate process. Their solubility in water is the main advantage of these precursors, as well as their lower price and greater availability in the market than other titanium precursors for hydrothermal synthesis (Dambournet et al., 2009).

- Alkoxides precursors

It is an organic component with $Ti(OR)_4$ structure. These compounds are very used to synthesis of $TiO_2$ in sol-gel method (Kakihana et al., 2010), although they can be also used in solvothermal synthesis with the use of an organic solvent (Toft et al., 2009, Pighini et al., 2007). In general, alkoxides produce nano-$TiO_2$ in water (via

sol-gel) following, hydrolysis and condensation. (Niederberger and Garnweitner, 2006):

In hydrolysis, the molecule of water reacts with the alkoxide group to release of alcohol (ROH):

$$\equiv M - OR + H_2O \rightarrow \equiv M - OH + ROH \quad (2.10)$$

In condensation, the hydroxylated molecules react between them to releases water:

$$\equiv M - OH + HO - M \equiv \rightarrow \equiv M - O - M \equiv + H_2O \quad (2.11)$$

Also, the condensation releases more alcohol species by the reaction between hydroxide and alkoxide bond:

$$\equiv M - OH + RO - M \equiv \rightarrow \equiv M - O - M \equiv + ROH \quad (2.12)$$

It is important to take into account that the reactions (2.10 – 2.12) are used by sol-gel method because titanium alkoxide species are very sensitive to water. These precursors are unstable in an aqueous solution, rapidly producing a water-insoluble precipitate mixture (Kakihana et al., 2010).

- Water-Soluble Titanium complex precursors

This group has got many different complex compounds, which are synthesised by diluting the titanium compounds in ammonia ($NH_3$) or hydrogen peroxide ($H_2O_2$). This forms an oxo-hydroxy complex that is modified by the addition of an acid such as citric, lactic, oxalic, etc. (Cargnello et al., 2014). The main advantage of these complex elements is their high stability and dissolution in water (Kessler, 2013).

Figure 2.4 represents a flowchart for the production of the five precursors used for the synthesis of nano-$TiO_2$ in Chapter 5. Also, Table 2.3 shows the pros and cons of these reagents.

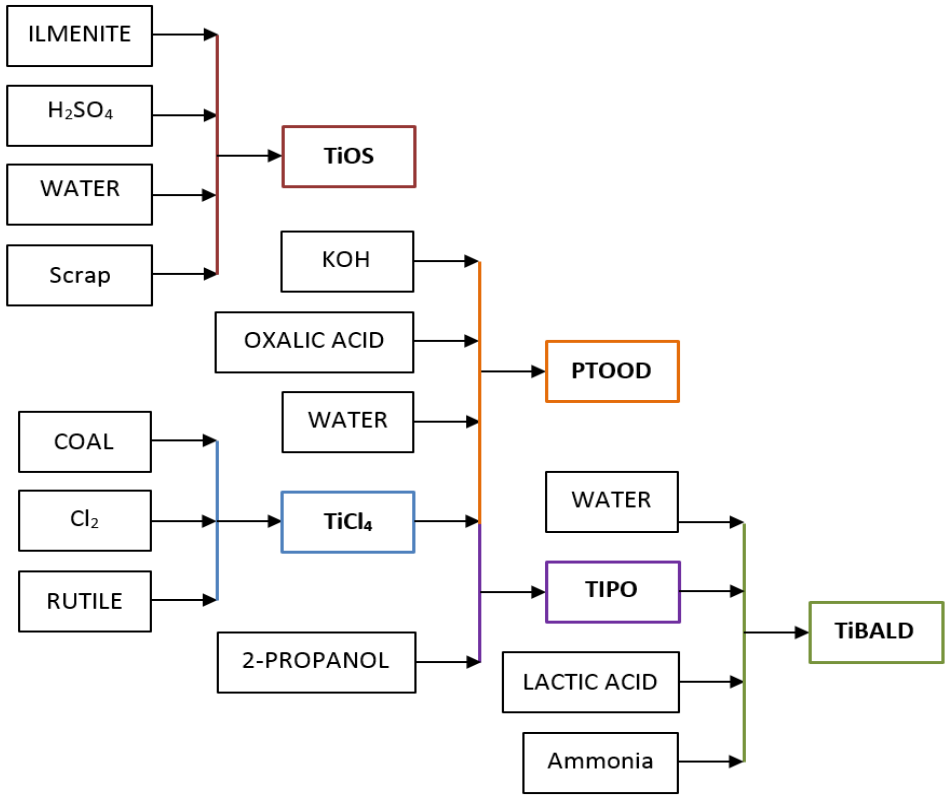



Figure 2.4: Schematic flowchart for the production of different titanium precursors used for the synthesis of nano-$TiO_2$. TiOS: titanium oxysulfate, $TiCl_4$: titanium tetrachloride, TIPO: titanium isopropoxide, PTOOD: potassium titanium oxide oxalate and TiBALD: titanium bis(ammonium lactato) dihydroxide.

Table 2.3. Comparative of the titanium precursors used for the CFHS and CFSS synthesis of nano-$TiO_2$.

| Precursor | Group | Advantages | Disadvantages |
|---|---|---|---|
| Titanium tetrachloride | Halides | Low price<br>Easy market availability | Explosive<br>Exothermic reaction with water |
| Titanium oxysulfate | Sulfates | Use in water<br>Medium price<br>Easy market availability | Difficult to dissolve as solid product |
| Titanium isopropoxide | Alkoxide | Low risk<br>Medium price | Hydrophobic |
| Titanium bis(ammonium lactato) | Water soluble titanium complex | Use in water<br>Low risk | Expensive<br>Complex production |
| Potassium titanium oxide oxalate | | | |

### 2.2.3. Metal sulfides

Many metal sulfides occur as mineral ores in nature, such as pyrite ($FeS_2$), sphalerite (ZnS), molybdenite ($MoS_2$) and galena (PbS), which are used as metal and sulfur sources by the industry (Greenwood and Earnshaw, 2012). In addition, these ores contain traces of other less common mineral sulfides like covellite (CuS), hawleyite (CdS) or argentite ($Ag_2S$), which are resources for the production of non-ferrous metals (Greenwood and Earnshaw, 2012, Weber et al., 2013). Metal sulfides have been mainly studied for electronic applications such as batteries (Greenwood and Earnshaw, 2012, Sun et al., 2014), semiconductors (Vaughan and Craig, 1978, Trindade et al., 2001), photovoltaic cells (Trindade et al., 2001) and sensors (Tian et al., 2014, Sagade and Sharma, 2008) due to their electrical and magnetic properties; but also they have demonstrated their potential in catalysis (Vaughan, 2006, Kalpana and Selvaraj, 2016), lubricants (Zhao et al., 2016, Kalin et al., 2012) and antimicrobial applications (Kumari et al., 2014). In the last years, the synthesis of metal sulfides nanoparticles (nano-sulfides) has attracted interest for technical applications that require higher quality product (Smaller size, higher crystallinity and homogeneity) than typical micro-size metal sulfides. Consequently, there is a major effort in developing these new synthesis routes. Many of them are similar to the previous mentioned by LFP synthesis methods, but others like hot injection are briefly described in this section.

#### 2.2.3.1. Solid-state methods for the production of metal sulfides nanoparticles

##### 2.2.3.1.1. Mechanochemical synthesis of metal sulfides

Mechanochemical has been used to synthesise several metal sulfides nanoparticles such as ZnS, CdS and PbS (Tsuzuki and McCormick, 1999, Baláž et al., 2003,

Suryanarayana, 2001, Tsuzuki and McCormick, 2004). The precursors are solid salts like chloride, nitrate or acetate compounds. These reagents are mixed with sulfur source in a high-speed ball milling over a specific period of time. In order to generate smaller size and narrower distribution the period of time can vary from minutes to hours, as well as, the grinding rate (Tsuzuki and McCormick, 1999). The continuous milling effect fractures, deforms and welds the reactants. The use of inert gases (Ar, $H_2$ or $N_2$) is also common used to avoid oxidation of metal precursor (Baláž et al., 2003).

#### 2.2.3.2. Vapour phase methods for the synthesis of metal sulfides nanoparticles

These techniques involve gas phase reaction (Feldman et al., 1996), spray pyrolysis (Ramaiah, 1999) and chemical vapour deposition (CVD) (Li et al., 2004), which have gained interest because of their relatively low Opex costs and simple production. However, the Capex costs are high (Wegner et al., 2011), the reactions are carried out at high temperatures (700-1000 °C) and the toxicity of some reactants hinder their implementation as an industrial process. The synthesis is carried out by the mixing of precursor solutions and sulfur source in a chamber at high temperature in an inert atmosphere (Argon or nitrogen gases). In the case of CVD the product is deposited onto a substrate before it can be collected.

#### 2.2.3.3. Solution methods for the production of metal sulfides nanoparticles

##### 2.2.3.3.1. Hot injection synthesis of metal sulfides

This technique is commonly used for the production of metal sulphide based quantum dots (Mews et al., 1994, Joo et al., 2003) and small nanocrystals (Du et al., 2012, Zhang et al., 2010), due to their excellent control over the morphology and

composition. In general, firstly the metal precursor and a chelating agent like oleylamine are dissolved in solvent and heated up under stirring. After a while, the sulfur source ($H_2S$ or sulfur solution) is injected into the reactor. Temperature is maintained around the boiling point for a period. So, nucleation and growth can be controlled and therefore the growth rate of nanomaterial. The main drawbacks of this method are the cost of precursors and agents, as well as the several stages of production.

#### 2.2.3.3.2. Sol-gel synthesis of metal sulfides

Sol-gel has been studied for the synthesis of ZnS nanorods (Senthilkumaar and Selvi, 2008) and CdS, PbS and ZnS films (Tang and Cameron, 1996, Reisfeld, 2002). As previously described in LFP synthesis, their main advantages are the low reaction temperature and control of the operational conditions (pH, precursor concentration, reaction time), which results in a controlled size distribution and homogeneity of product. However, the use of sintering stage is frequently required to increase the purity and crystallinity of the nanomaterial (Reisfeld, 2002).

#### 2.2.3.3.3. Co-precipitation synthesis of metal sulfides

Co-precipitation is not commonly used to produce metal sulfides, due to their low solubility and lack of control over nanoparticle formation (Lewis, 2010). Nevertheless, some researchers have studied the synthesis of nano-sulfides by this technique (Shen et al., 2003, Xu et al., 2004, Ni et al., 2001, Hassan and Ali, 2008). In general, sulfide solutions are prepared with water, glycol or ethanol at low temperature. Later, a sulfur source like carbon disulfide ($CS_2$) is added to precipitate the nano-sulfides. Basic pH can be required to precipitate the nanoparticles by the

addition of ammonia (Xu et al., 2004). Finally the suspension is filtered, washed and dried to collect the nanoparticles.

#### 2.2.3.3.4. Batch hydrothermal and solvothermal synthesis of metal sulfides

Both methods permit a wide range of operational conditions, solvents, precursor and procedures, being of one the most common routes for the synthesis of nano-sulfides (Hu et al., 2014, Zhuang et al., 2008, Deng et al., 2006, Ni et al., 2007, Wang et al., 2006, Xia et al., 2008, Wen et al., 2005, Chen and Gao, 2006, Kalpana and Selvaraj, 2016). The strong control over the reaction parameters achieves nano-sulfides with high crystallinity, small size and well-defined shape. In general, precursor solutions are dissolved in water (solvothermal also uses organic solvents). The solution is sealed in an autoclave reactor, and heated above the boiling point of the solvent (100-200 °C). Generally, the reaction is completed after 6-24 hours. The diversity of precursors, operational conditions and solvent offer a wide variety of different morphologies (Zhuang et al., 2008, Ni et al., 2007).

#### 2.2.3.3.5. Continuous-flow hydrothermal synthesis of metal sulfides

Recently, continuous-flow hydrothermal synthesis (CFHS) has been used to synthesise a great variety of nano-sulfides with different temperatures and synthesis configurations, resulting in a wide range of nano-sulfides (Dunne et al., 2015b, Dunne et al., 2014). This technique permits the synthesis of nano-sulfides in seconds (< 1 min) with a high quality product. In a similar approach to LFP nanoparticle synthesis, the metal salt solution is driven into the reactor at 250 bar and mixed with superheated water (200-400 °C). Nanoparticles are instantly produced, and varying the temperature, mixing dynamics and precursor chemistry allows different

morphologies to be achieved. Finally the suspension of nanoparticles is cooled down before being dried.

### 2.2.4. Concluding remarks for the production of nanomaterials

Generally solid-state methods are able to produce large amounts of nanoparticles. Also, these processes show potential to be scaled-up for industrial production. The most significant disadvantage of solid-state processes is the use of high temperatures (>500 °C) over long periods of time (1-24 hours per stage), which can lead to a higher cost with the increased energy demand. In addition, the lower quality that solid-state methods offer in terms of size, homogeneity and agglomeration limits their possibilities in the long-term as the leading industrial process. Vapour phase methods use shorter periods, but drawbacks include a high reaction temperature (>700 °C), a higher capex investment and the toxicity of some reactants leading to questions around sustainability. Alternatively, solution methods operate at lower temperatures and shorter periods. They are also able to synthesise high purity, small and homogenous nanoparticles as it has been demostrated in many publications. However, many of them operate in batch and use organic solvents and additives that undermine their potential as industrial processes for financial or enviromental reasons. Unlike many of them, CFHS is a continuous, water-based process that has proven its capacity of production at pilot and industrial scale for many nanoparticles (Johnson et al., 2016, Adschiri et al., 2011, SHYMAN-project, 2015). In addition, CFHS offers a large variety of nanoparticles under similar operational conditions and a flexible production route for nanomaterials.

# 3. Chapter 3 – Experimental

This chapter describes the principles and methods carried out for the synthesis, characterisation and environmental assessment of nanomaterials used in this thesis. Firstly, there is a description of the nozzle reactor used for the synthesis of nanomaterials in Chapters 5, 6 and 7. Secondly, a detailed explanation of the characterisation techniques used to analyse the properties such as size, crystal structure and morphology as well as, a description of the techniques used to evaluate the behaviour of nanoparticles as lubricant additives in Chapters 5, 6 and 7. Finally, the environmental methodology of the life cycle assessment (LCA) is described alongside the LCA software utilized to evaluate the environmental impacts in Chapters 4, 5, 6 and 7.

# Chapter 3

## 3.1. Nozzle reactor

The nanoparticles synthesised in this thesis were produced using the reactor developed at The University of Nottingham (Lester et al., 2006, Lester and Azzopardi, 2004) known as “Nozzle Reactor” or “Counter-current Reactor”. Figure 3.1 shows a schematic flowchart of the most common configuration of the process and reactor flow arrangement. The reactor has two inlet streams. On the top, the hot-stream is usually an inlet of water that has been previously heated up to supercritical conditions (>375 °C and 240 bar). This stream is driven downwards into the reaction zone (bottom reactor) through of a narrow pipe. From the bottom, the cold-stream is a metal salt solution, generally aqueous, at room temperature. The reactor consists of two vertically aligned pipes -“pipe in pipe”-. A detailed description is shown in Figure 3.2. The counter-current generates a flow in the reactor that takes the advantage of the low density of supercritical water to achieve symmetric mixing and a narrow residence time distribution. As a result, almost instantaneous nucleation of the nanoparticles occurs in the mixing or reaction zone. The design of the reactor for the synthesis of nanomaterials permits reproducibility in a continuous process. The nanoparticles then leave the reactor by the top right stream to pass through of a heat exchanger to cool down. The size of the laboratory scale consists in an outer tube of 3/8” diameter (0.065” wall thickness) and an inner tube of 1/8”. The flow of the inlet-streams is supplied by Gilson HPLC pumps. Before the reactor, a heater (coiled tube) heats the hot-stream up to the reaction temperature. The whole system is maintained at 240 bar with a back pressure regulator (BPR). The laboratory reactor and all of the pipes of the rig are made of Swagelok components, generally with 316L stainless steel.

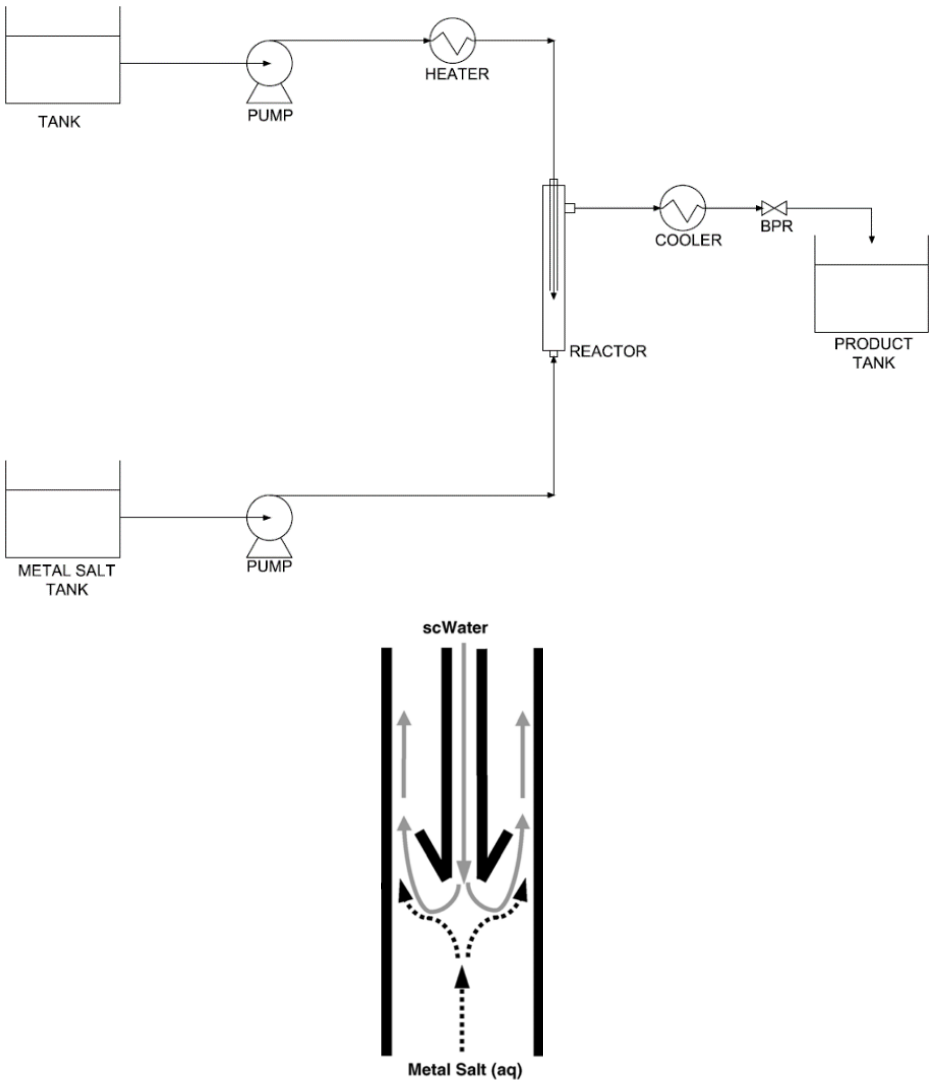



Figure 3.1: Schematic flow diagram of the continuous-flow hydrothermal synthesis (top) and a scheme of the inside Nozzle reactor (down) (Lester et al., 2006).

The configuration described in Figure 3.1 is the most common, but the system can be reconfigured with multiple reactors or cascaded reactors depending on the material synthesis protocol. Using the same reactor, metal oxides, sulfides and phosphates such as $TiO_2$, ZnS and $Ca_5(PO_4)_3OH$ have been synthesised, but also complex nanomaterials like metal organic framework (MOFs) (Dunne et al., 2015a). Some modifications in the configuration have been used to synthesise $TiO_2$ and metal sulfide nanoparticles and these modifications are detailed in Sections 3.1.1, 3.1.2 and 3.1.3.

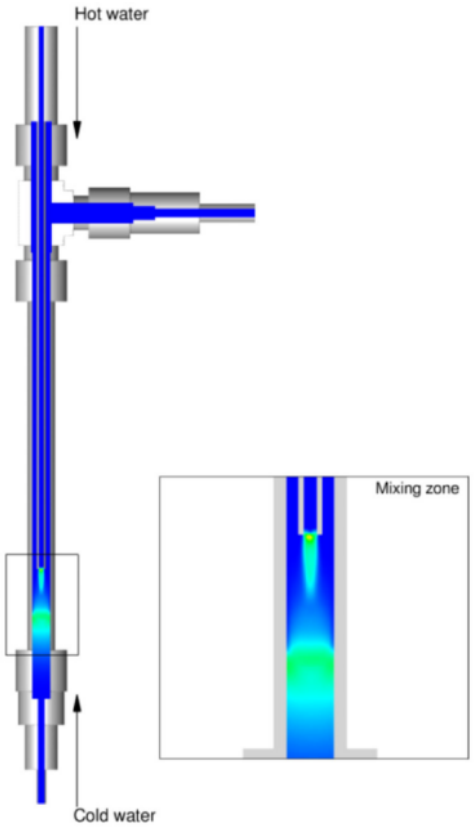



Figure 3.2: Sketch of the reactor section with the inlets of supercritical water (top) and metal salt solution (bottom), as well as the reaction or mixing point (right) (Sierra-Pallares et al., 2016).

### 3.1.1. Synthesis of titanium dioxide nanoparticles

Five different precursors were selected to synthesise nano-$TiO_2$ with the nozzle reactor:

i. TiOS: Titanium (IV) oxysulfate (99.99%) 15 wt% in dilute sulfuric acid

ii. $TiCl_4$: Titanium (IV) chloride (99.9%)

iii. TiPO: Titanium (IV) isopropoxide (97%)

iv. TiBALD: Titanium (IV) bis(ammonium lactate) dihydroxide solution (50 wt% in $H_2O$)

v. PTOOD: Potassium titanium oxide oxalate dehydrate powder (98%)

All precursors were supplied by Sigma Aldrich and used as received. Deionised water and 2-propanol (99.5%), also from Sigma Aldrich, were used as solvents. Some precursors can be unstable in water which means that alternative solvents are needed in the cold-stream. 0.05 M solutions of each precursor were prepared:

A. TiOS + Deionised water
B. $TiCl_4$ + 2-Propanol
C. TiPO + 2-Propanol
D. TiBALD + Deionised water
E. PTOOD + Deionised water

Deionised water was used as the heated hot-stream for the production of nano-$TiO_2$ when solutions A, B and C were pumped as metal salts. For solutions D and E, the hot-stream was a solution of water with a 5% volume solution of hydrogen peroxide ($H_2O_2$, 1.108 g $ml^{-1}$, 100 volumes 30% supplied by Fisher Scientific) to ensure the decomposition of the organic components of the TiBALD and TIPO precursor.

The pressure of the system was established at 240 bar, while the temperature for the reaction was varied from 200 °C to 400 °C at increments of 50 °C, such that product was collected for five different temperatures for each precursor (200, 250, 300, 350, 400 °C). The flows were consistent for each reaction at 20 ml $min^{-1}$ of the supercritical fluid and 10 ml $min^{-1}$ for the precursor stream (see Figure 3.3).

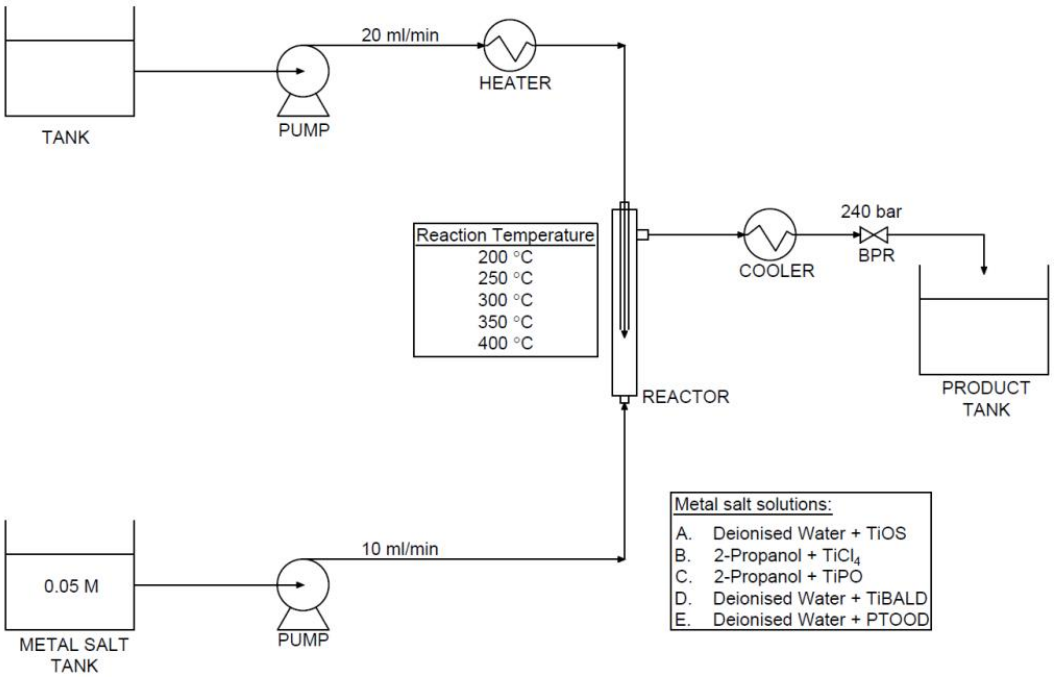



Figure 3.3: Configuration for the synthesis of the $TiO_2$ with different precursors.

### 3.1.2. Synthesis of silver sulfide nanoparticles

Silver sulfide ($Ag_2S$) nanoparticles were similarly synthesised with the counter-current reactor (See Figure 3.4). All the chemicals were purchased from Sigma-Aldrich and used as received without further purification. An aqueous solution of silver nitrate ($AgNO_3$) was prepared with a concentration of 0.025 M (Precursor solution) and pumped at 10 ml $min^{-1}$. In the heated downflow a solution of thiourea 0.0125 M in deionised water was pumped at 20 ml $min^{-1}$. The pressure was kept at 240 bar by a back pressure regulator, while the temperature was set from 250 °C to 400 °C with a step of 50 °C (200, 250, 300, 350, 400 °C). All of the aqueous suspensions were obtained as product for each temperature. The suspensions were centrifuged and washed with deionised water before being dried at 70 °C for 24 h.

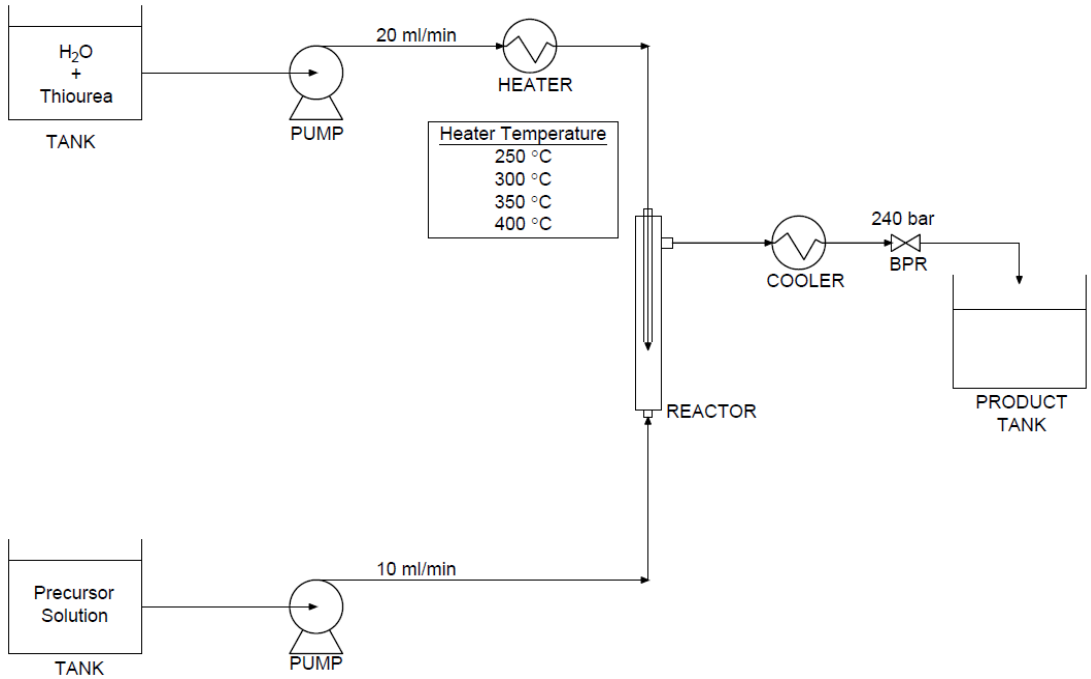



Figure 3.4: Schematic configuration for the synthesis of silver sulfide nanoparticles.

### 3.1.3. Synthesis of metal sulfide nanomaterials

Ten different metal sulfides or nano-sulfides were synthesised using the nozzle reactor (Table 3.1) (Page 47). Two configurations and methods were used to their production according to literature (Dunne et al., 2015b, Dunne et al., 2014). The precursors used to produce the nano-sulfides materials were purchased from Sigma-Aldrich and used as received; $FeSO_4 \cdot 7H_2O$, $Cd(NO_3)_2 \cdot 4H_2O$, $Zn(NO_3)_2 \cdot 6H_2O$, $Pb(NO_3)_2$, $Cu(NO_3)_2 \cdot 3H_2O$, $AgNO_3$, $(NH_4)_6Mo_7O_{24} \cdot 4H_2O$. Thiourea was used in excess as the sulfur source for all of the precursors. Deionised water was used as a solvent and supercritical fluid for the CFHS. The synthesis of molybdenum sulfide ($MoS_2$) required a stream of acetic acid to enhance the reaction. The configurations and methods carried out for the production of nano-sulfides materials are described in next sections. Table 3.1 details all of the concentrations and temperatures used to produce all of the nano-sulfides materials.

### 3.1.3.1. Standard configuration for metal sulphide production

This configuration involved the use of the standard configuration (Lester et al., 2006), shown previously in the Figure 3.1. However from the standard procedure, two different approaches or methods were used to produce the nanoparticles, Method A and Method B.

#### 3.1.3.1.1. Method A

A solution of metal precursor was prepared with deionised water. To this solution, a stoichiometry excess of thiourea was added (2:1 thiourea:metal-salt) to improve the yield of the reaction. The solution was pumped altogether into the reactor with a flow rate of 10 ml $min^{-1}$. The hot-stream consisted only in deionised water at 400 °C and 20 ml $min^{-1}$ of flow rate. The reaction temperature was set at 400 °C approximately (see Figure 3.5).

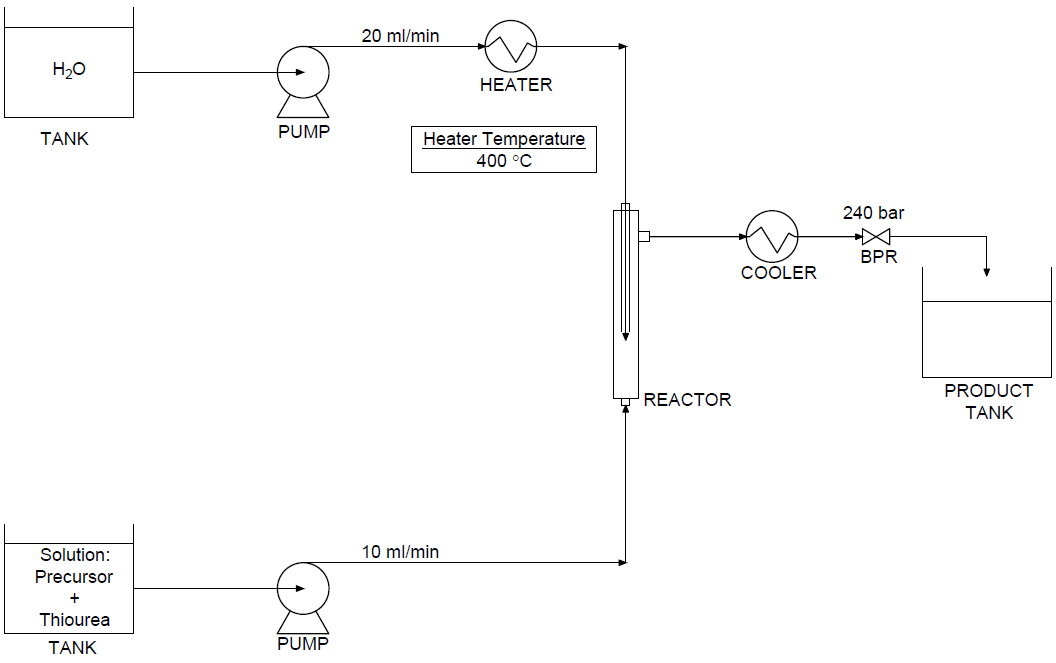



Figure 3.5: Standard configuration method A for the synthesis of the nano-sulfide materials.

### 3.1.3.1.2. Method B

The precursor was dissolved into deionised water and pumped at 10 ml $min^{-1}$. On the other side, a solution of thiourea and deionised water was prepared and pumped downwards into the reactor at 20 ml $min^{-1}$ after the heater. The pre-heating of the thiourea and the long residence time of the heater was used to improve the decomposition of thiourea, producing higher concentration of sulfur in the reactor (see Figure 3.6). The reaction temperature varied between 300 °C to 400 °C, in order to produce different nanoparticles in terms of shape, size and morphology (Dunne et al., 2014).

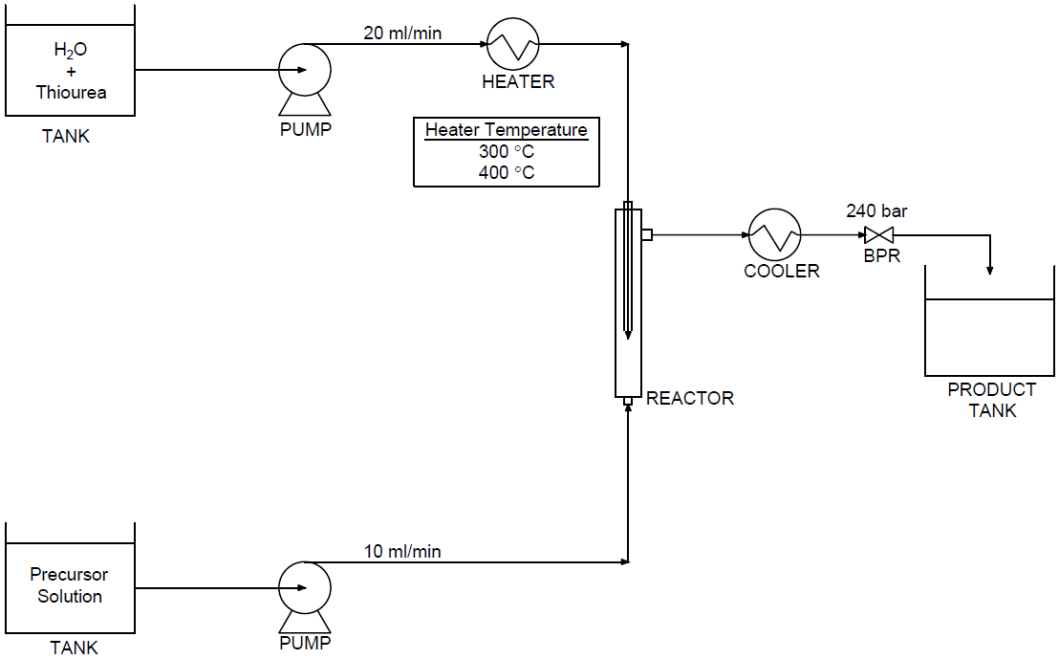



Figure 3.6: Standard configuration method B for the synthesis of the nano-sulfides materials.

### 3.1.3.2. Extended residence time reaction with acid addition

This configuration was only carried out for the synthesis of $MoS_2$ (Dunne et al., 2015b). It requires an extra inlet stream in the reactor, as well as an extra heater to increase the residence time of the reaction. The hot-stream (20 ml $min^{-1}$) consisted in

a solution of 0.1M of thiourea in deionised water, while the cold-stream (10 ml $min^{-1}$) was an aqueous solution of ammonium heptamolybdate at 0.05 M. The new inlet was an acetic acid solution at 20% (v/v) with a flow rate of 10 ml $min^{-1}$. It was driven into the reactor after the reaction zone and before the reactor outlet (see Figure 3.7). The heater temperature was set at 400 °C, while post-heater reaction was kept at 250 °C to maintain high temperature and to improve the formation of nanoparticles.

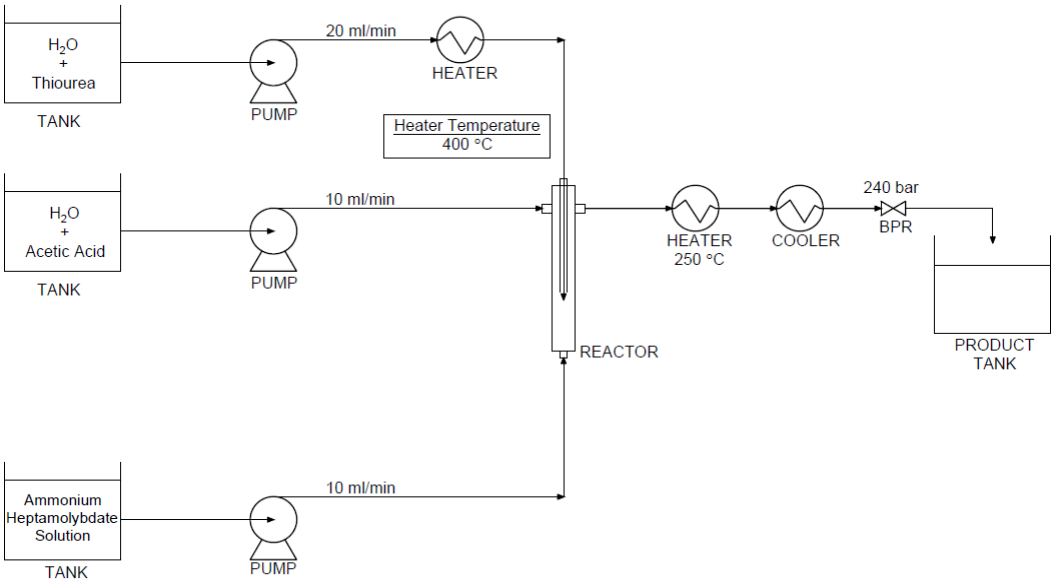



Figure 3.7: Extended residence time with acid addition configuration for the synthesis of the $MoS_2$ nanoparticles.

Table 3.1. Details of the nano-sulfide materials synthesised using different operational conditions and configurations.

| Compound | Formula | Method | Temperature | Precursor Concentration | Thiourea Concentration | Configuration |
|---|---|---|---|---|---|---|
| | | | °C | mol $l^{-1}$ | mol $l^{-1}$ | |
| Iron Sulfide | FeS | A | 400 | 0.025 | 0.05 | Standard |
| | | B | 400 | 0.025 | 0.025 | |
| Cadmium Sulfide | CdS | A | 400 | 0.05 | 0.1 | Standard |
| | | B | 400 | 0.025 | 0.025 | |
| Zinc Sulfide | ZnS | B | 300 | 0.025 | 0.025 | Standard |
| | | | 400 | | | |
| Lead Sulfide | PbS | B | 300 | 0.025 | 0.025 | Standard |
| Copper Sulfide | CuS | B | 300 | 0.025 | 0.025 | Standard |
| Silver Sulfide | $Ag_2S$ | B | 400 | 0.025 | 0.0125 | Standard |
| Molybdenum Disulfide | $MoS_2$ | 20% (v/v) Acetic acid | 400 | 0.05 | 0.1 | Extended residence time & Acid addition |

## 3.2. Characterisation

All of the nanoparticles synthesised by CFHS were separated from the liquid by precipitation and centrifugation, a Hettich-Rotofix 32A was used at 4000 rpm between 5-15 minutes. Also, some samples of $TiO_2$ nanoparticles required hydrochloric acid to settle down (see table 5.6 in Chapter 5). Any solids obtained were dried in an oven for 24 h at 70 °C before characterisation.

### 3.2.1. X-ray diffractometry

X-ray diffractometry was used to measure the crystal structure and phase of nanomaterials. An X-ray beam is emitted to strike the surface crystal (nanoparticles) with a determined angle θ and a known wavelength λ. The first layer of atoms, which form the surface of the crystal, disperses the beam. A portion of the beam is reflected, while another portion penetrates between the atoms and electrons to be scattered later by a second plane. The scattered X-rays are registered by a detector. This operation is repeated several times over the surface of the sample (Figure 3.8) to get a pattern diffraction.

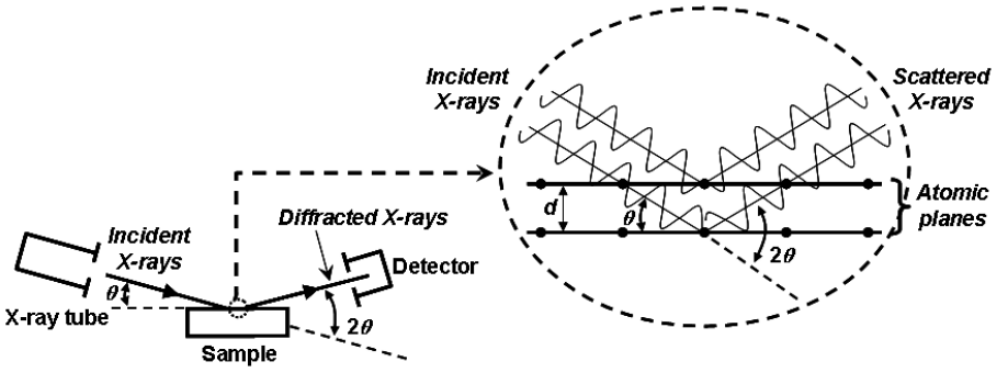



Figure 3.8: Illustration of the diffraction of X-rays by crystal planes (Klugg and Alexander, 1974).

The reflection of the X-rays by the planes of the crystal permits to derive lattice spacings by using the Bragg's law (Ramachandran and Beaudoin, 2000):

$$n\lambda = 2d \sin\theta \qquad (3.1)$$

Where n is an integer, λ wavelength of X-rays, d is the characteristic spacing between the crystal planes and θ is the incident angle. The diffraction of the X-rays beam with different angles and the same wavelength λ, produces a diffraction pattern. This pattern is defined by the d values and the relative intensities of the diffraction lines in order to compare it with a database to determine the characteristics of the crystalline material.

The diffraction pattern consists of a series of intensity peaks at different incident angle θ. An ideal sample shows sharp and very narrow diffraction peaks. When the size of the nanoparticles are smaller of 100 nm (our case), there is not enough planes to produce complete destructive interference and the X-rays are out phase. This lack of destructive interference generates further line broadening of the peaks. As a result, the Scherrer equation relates this breadth of the peak and the size of the nanoparticle (Ramachandran and Beaudoin, 2000):

$$L = \frac{K\lambda}{\beta cos\theta} \qquad (3.2)$$

Where L is a crystalline size (perpendicular to the reflecting plane), K is the crystalline shape constant (0.9-1), λ is the X-rays wavelength, β is the peak width and θ the incident angle. It must be taken into account that due to different size and shape of the nanoparticles, generally the Scherrer equation is used to give an estimation.

Dry nanoparticles were analysed using an X-ray powder diffraction (XRD). XRD patterns were collected on a Bruker AXS D8 Advance X-ray diffractometer with Cu Kα radiation (λ = 0.15418 nm) across a 2θ range of 15-65 ° with step size of 0.04 ° at

collection time of 5 s/step for nano-$TiO_2$. $Ag_2S$ characterisation was carried out between 10-70 ° with a step size of 0.05 ° and a collection time of 4 s/step (Chapter 5 and 6). Crystalline diameters were calculated using the Scherrer equation from the FWHM determined by profile fitting with Xfit software.

### 3.2.2. Transmission electron microscopy

Transmission electron microscopy (TEM) uses an electron beam and magnetic lens to magnify images of specimens at nanoscale (Oku, 2014). The sample is introduced in a vacuum column via a sample holder. The pressure in the column is maintained approximately at $10^{-5}$ Pa. Heated tungsten cathodes generate an electron beam. The beam is irradiated on the sample and transmitted to the other side. Finally the beam passes through a series of lenses and an aperture to eliminate scattered electrons. Clearly, an image can be observed on a fluorescent screen and digitally photographed (Buseck et al., 1989). In general, it is able to image materials at resolutions of low nanometers when operating at magnifications of 500,000 to 1,000,000 times. The morphology can also be determined by this technique. If the nanoparticle is small then the internal structure of the particle may also be observed. Energy dispersive X-ray (EDX) analysis allows the determination of the chemical composition of the sample. The incident electrons that are inelastically scattered with the atoms of the sample lose energy. This loss of energy is analysed to produce EDAX patterns.

Transmission electron microscopy was used to estimate with more accurate the crystalline morphology and size of the nano-$TiO_2$ and silver sulfide nanoparticles in Chapters 5 and 6, mainly due to issues with agglomeration and amorphous content.

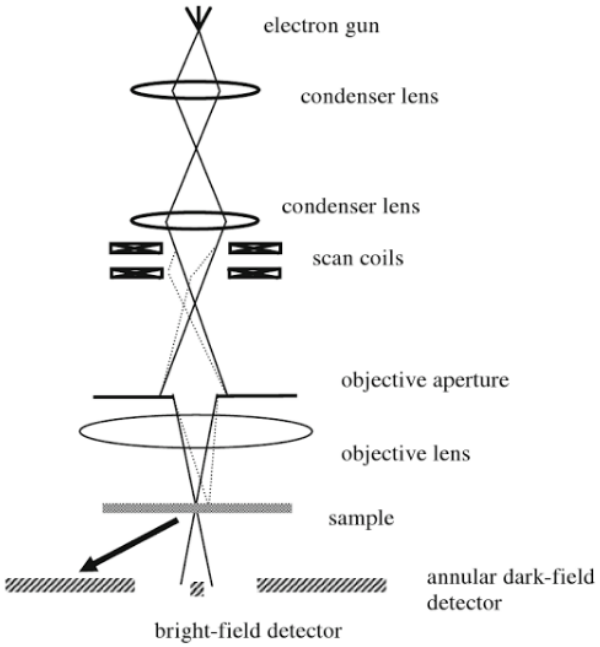



Figure 3.9: Illustration of the Transmission electron microscope (Pennycook and Nellist, 2011).

Samples were prepared for TEM by resuspending a small quantity of dried powder in acetone and depositing it onto lacey carbon coated copper grids (300 mesh). TEM images were obtained using a JEOL 2100 high resolution TEM at an accelerating voltage of 200 kV. Particle size distributions were measured using ImageJ® using a previously described approach (Lester et al., 2012).

### 3.2.3. Thermogravimetric analysis

Thermogravimetric analysis (TGA) measures the mass change in small samples (2-20mg) during heating in a controlled atmosphere (Figure 3.10). The platinum pan supports the sample and is connected to a microbalance that measures 4 decimal places of a milligram. The chamber can use different gases to have an oxidising or inert atmosphere, such as pure oxygen, air or nitrogen. In this work, the sample was heated at constant rate to a maximum temperature for a period before being cooled down. The changes of weight are measured and saved to be plotted later. The graph

describes a TGA curve in which weight (micrograms) or % weight is represented against temperature or time. It is also possible to represent the first derivative of the TGA curve with respect to temperature or time, which is known as differential thermogravimetric curve (DTGA). The loss of mass is due to high temperature which produces evaporation, thermal decomposition, reaction of oxidation or combustion by the interaction with the atmosphere. In general, the first loss of weight is adsorbed water (<150 °C). Over this temperature range there can be different causes for a loss of weight such as $CO_2$ (330 °C) or $SO_2$ (≈550 °C) (Gabbott, 2008, Haines, 2012).

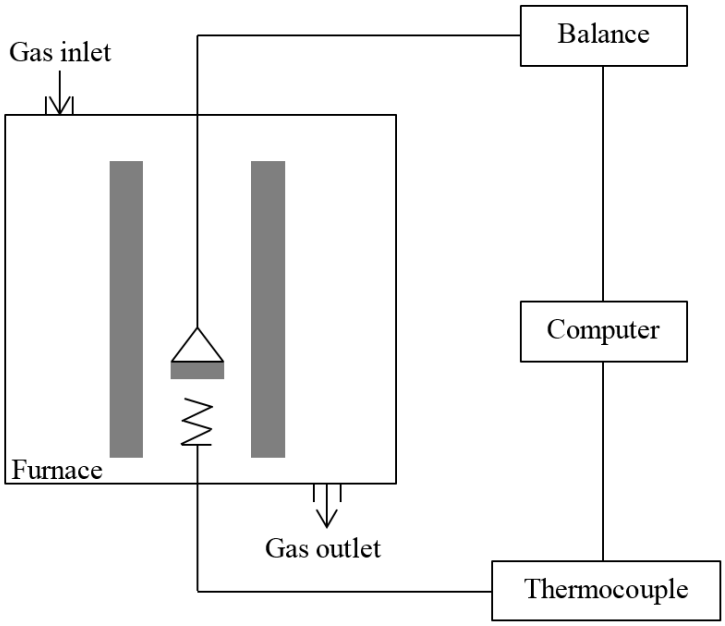



Figure 3.10: Schematic diagram of the Thermogravimetric Analyser.

TGA of the dried powders was carried out in a TA instruments Q500 TGA analyser. Samples of $TiO_2$ nanoparticles (Chapter 5) were heated up to 900 °C for 10 minutes with a rate of 10 °C $min^{-1}$. After this, the samples were cooled down to 100 °C with a rate of 50 °C $min^{-1}$. The data was saved in a computer with a collection step of 0.5 seconds. Air was used as inert gas into the chamber with a flow rate of 100 ml $min^{-1}$. This enabled the actual $TiO_2$ content in the collected solids to be calculated in Chapter 5.

### 3.2.4. Tribological analysis

Tribology measures wear, friction and lubrication between contacting materials (Hirani, 2016). A tribometer is the most common device for measuring friction and wear during tribological analysis. The principal purpose of a tribometer is to determine the friction and wear under controlled and known conditions. There is a vast variety of conditions and factors, like temperature, load, motion or type of lubricant. For this reason, there are many different tribometers with different mechanisms e.g. sliding, rotating, rolling ball-on-slab and pin-on-slab etc. According to the Society of Tribologist and Lubrication Engineers, there are 243 recognized designs of tribometer (Stachowiak and Batchelor, 2004), although the number of tribometers used by scientists is reduced. Generally, a tribometer has a contact area, motion and load equipment, instrumentation to measure friction coefficient and wear rates. In our research ball-on-slab was used as tribometer. The ball-on-slab method consists in fixed ball under an applied load in contact with a sliding slab. The repetitive movement of the slab and the load is linear. The velocity, frequency, distance and load are defined before to start the experiment via software settings (see Figure 3.11). The coefficient of friction (COF) is determined according to the equation (3):

$$F = \mu N \qquad (3.3)$$

Where F is the loading force, μ is the COF and N is the normal force that is known. The continuous movement with a constant load in a period of time determines the COF, which are plotted in a graph. The average result over a period of time is the final value of COF.

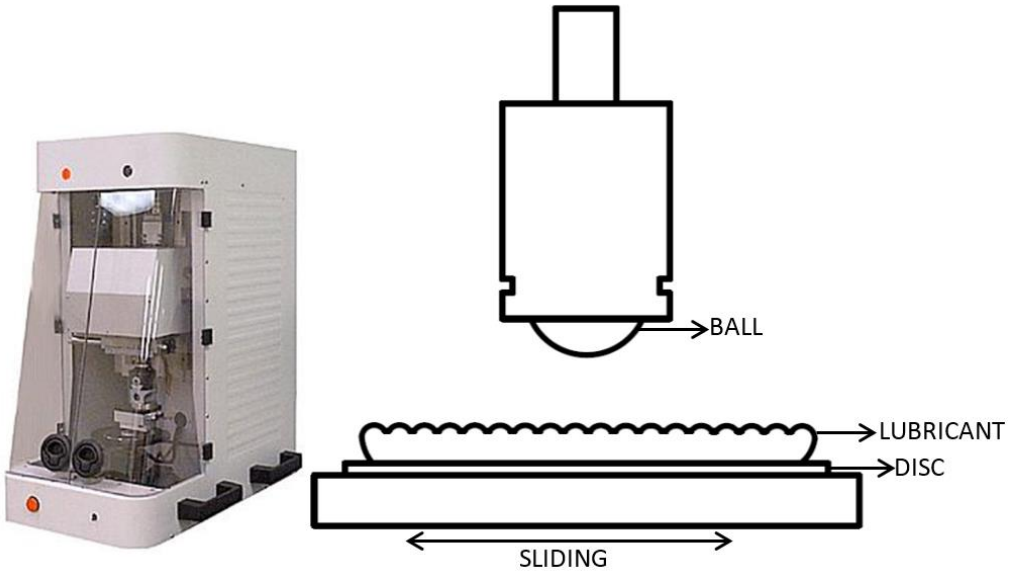



Figure 3.11: Photo and schematic diagram of a Tribometer.

Ten different nano-sulfides materials were selected and dispersed in deionised water and mineral oil pure (Acros Organics) as lubricant additive to estimate their effect (Chapter 6 and 7). The mixture was sonicated using an ultrasonic bath to get a uniform suspension. The percentage of weight (wt%) of nanoparticles was adjusted to 1, 2, 5 or 7% ±0.1%, depending on the tribological test conditions (see Table 3.2 and Table 3.3). The friction experiments were performed on a wear tribometer using a ball-on-slab configuration in linear reciprocating mode. A stainless steel ball of 6.35 mm of diameter (ABCO Ltd.) was used against the pre-polished flat sample surfaces. The tests were carried out at 10 N, at fixed sliding speed of 60 rpm with a reciprocating stroke of 10 mm and duration of 10 minutes. The friction force transferred to a load cell was recorded throughout the tests. A deionised water and mineral oil sample (without nanoparticles) were tested as reference value.

Table 3.2. Details of the nano-sulfide materials used as additives with water as lubricant.

| Compound | Formula | Method | Temperature | Nanoparticle Content |
|---|---|---|---|---|
| | | | °C | wt% |
| Iron Sulfide | FeS | A | 400 | 5 |
| | | B | 400 | 5 |
| Cadmium Sulfide | CdS | A | 400 | 5 |
| | | B | 400 | 5 |
| Zinc Sulfide | ZnS | B | 300 | 5 |
| | | | 400 | 5 |
| Lead Sulfide | PbS | B | 300 | 5 |
| Copper Sulfide | CuS | B | 300 | 5 |
| Silver Sulfide | $Ag_2S$ | B | 400 | 5 |
| Molybdenum Disulfide | $MoS_2$ | - | 400 | 5 |

Table 3.3. Details of the nano-sulfide materials used as additives with mineral oil as lubricant.

| Compound | Formula | Method | Temperature | Nanoparticle Content |
|---|---|---|---|---|
| | | | °C | wt% |
| Iron Sulfide | FeS | A | 400 | 5 |
| | | B | 400 | 5 |
| Cadmium Sulfide | CdS | A | 400 | 5 |
| | | B | 400 | 5 |
| Zinc Sulfide | ZnS | B | 300 | 5 |
| | | | 400 | 5 |
| Lead Sulfide | PbS | B | 300 | 2<br>5<br>7 |
| Copper Sulfide | CuS | B | 300 | 2<br>5<br>7 |
| Silver Sulfide | $Ag_2S$ | B | 400 | 5 |
| Molybdenum Disulfide | $MoS_2$ | 20% (v/v) Acetic acid | 400 | 2<br>5<br>7 |

## 3.3. Environmental methodology

LCA is a method for evaluating the environmental consequences of a product from its origin to the end of its life, “Cradle-to-grave”. Considering all of the steps and aspects of a product life and the necessary sources for extraction of raw materials, product use, recycling and end-of-life. The LCA has a standardised and detailed code defined by the International Organization for Standardisation (ISO), which presented the following LCA standard normative (Baumann and Tillman, 2004).

- ISO 14040 Life Cycle Assessment – Principles and Frameworks
- ISO 14041 Life Cycle Assessment – Goal and scope definition and inventory analysis
- ISO 14042 Life Cycle Assessment – Life cycle impact assessment
- ISO 14043 Life Cycle Assessment – Life cycle interpretation
- ISO 14044 Life Cycle Assessment – Requirements and guidelines
- ISO/TS 14048 Life Cycle Assessment – Data documentation format

According to these standards the order to carry out a LCA is following in order. Firstly, the goal and scope of the study is defined. Secondly, the life cycle inventory (LCI) is developed to collect the necessary information. After this, the life cycle impact assessment (LCIA) represents the results of the environmental impacts. Finally the interpretation of the results to address conclusions and recommendations. These sections are constantly feedback the information to improve the quality of the results (see Figure 3.12).

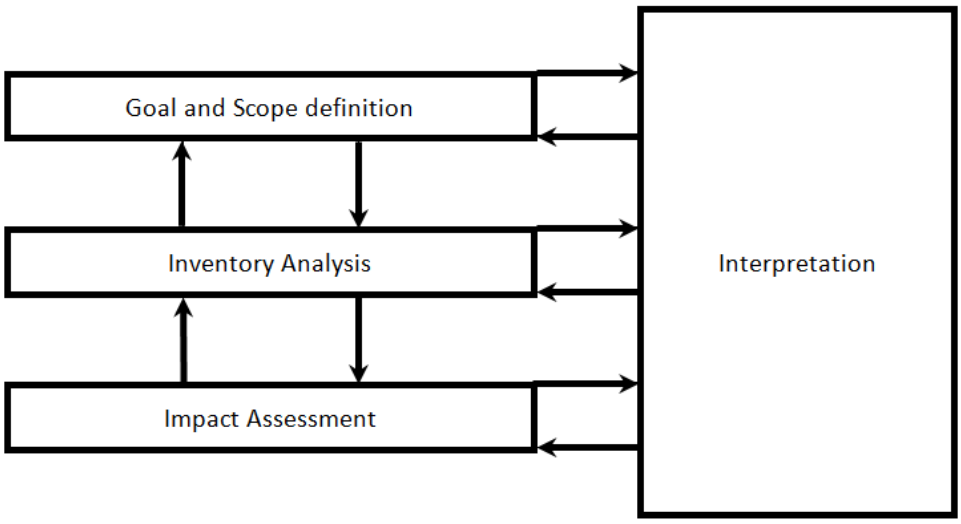



Figure 3.12: Schematic diagram of the Life Cycle Assessment methodology (Baumann and Tillman, 2004).

### 3.3.1. Goal and scope

The first step in a LCA is the definition of the goal, which consists in the declaration unequivocally of intended application, the reason for developing the LCA and the intended audience (Guinée et al., 2001). Scope must also include the information necessary for the product studied such as functions of the system, type of study, functional unit (which is the quantitative term that relates the environmental impacts and the product), system boundaries (cradle-to-gate, cradle-to-grave), allocation procedures, data quality requirements, assumptions and limitations.

### 3.3.2. Life cycle inventory

LCI is a data collection that includes all of the inputs and outputs of the product life studied. Basically, the inputs such as raw materials, energy for manufacturing or use, maintenance requirements etc., while the outputs can be emissions, wastes, by-products, etc. The collected information is classified and processed into different categories.

### 3.3.3. Life cycle impact assessment

In this section, the environmental impacts are evaluated with the collected and categorised information from the LCI using the help of environmental indicators, so that the effects over the environment (ecosystem, health, humans, animals, etc.) are estimated and assessed quantitatively and qualitatively. Also, an evaluation of objectives is carried out to confirm if the goal and the scope have been achieved.

In general, LCIA is carried out with the help of LCA software, such as SimaPro (Pini et al., 2015, Stieberova et al., 2017) or Gabi (Vince et al., 2008, Luz et al., 2010). These tools are based on integrated models to classify the data from the LCI, showing the results in different environmental impacts and relative contribution.

### 3.3.4. Interpretation

The final phase of an LCA is the interpretation of the results obtained in the LCIA. The main objective is to draw broader conclusions from the LCA, to find out 'hot-points' of the product's life and to recommend modifications or improvements to reduce the environmental impacts of the system under study.

The environmental methodology section has been described to provide a general overview of the LCA procedure. More detailed information for each particular case study can be found in Chapters 4, 5, 6 and 7.

### 3.3.5. Environmental software

Two environmental programs (SimaPro and CCaLC) were used to estimate the different impact categories. Chapter 5 on nano-$TiO_2$ production used commercial SimaPro software (Section 3.3.5.1), while Chapters 4, 5 and 6 used the freeware CCaLC (Section 3.3.5.2).

#### 3.3.5.1. SimaPro software

SimaPro is professional software developed by Prè Consultants from Netherlands. It is widely used by scientist and environmental researchers to carry out LCA studies. It uses databases such as Ecoinvent 3 and Ecospold 2 to estimate the environmental impacts. It also uses a combined data collection from a large variety of origins of different process and products. The results can be presented in different ways with different indicators and methods such as ReCiPe and BEES. In this thesis, SimaPro version 8.0.4 was used to estimate the global warming potential (GWP) and cumulative energy demand (CED) as indicators for the production of nano-$TiO_2$ at different operational conditions.

#### 3.3.5.2. CCaLC software

CCaLC is an award winning, freeware developed by the University of Manchester for estimating of carbon footprint of any given product, material or process. CCaLC is an integrated environmental and economic software which follows the normative of ISO 14044 and PAS 2050. In general, it is used to estimate the carbon footprint of a product life, but calculating more environmentally indicators, like acidification, ozone depletion, water footprint, etc. It features two combined databases, Ecoinvent 3 and a general LCA database developed by industry partners and policy makers. CCaLC version 2 was used to estimate the GWP at different scales-up for the production of lithium iron phosphate (LFP) nanoparticles and some of the nano-sulfides production such as $Ag_2S$ or $MoS_2$ in Chapters 4, 6 and 7.

# 4. Chapter 4 – Ex-ante life cycle assessment for the scale-up of a continuous flow hydrothermal synthesis of lithium iron phosphate nanoparticles.

The use of continuous-flow hydrothermal synthesis (CFHS) and the "nozzle" reactor to synthesise nanomaterials have been described in Chapter 2. This technique mainly uses water as the solvent, with lower temperature reaction and shorter reaction time than other techniques like sol-gel synthesis. At the time of starting this PhD, laboratory and pilot scales could already successfully synthesise many nanomaterials; the remaining challenge was the scale-up of the process to industrial scale and uncertainties related to process performance (yield, energy efficiency), material properties, and environmental impact. In addition, the lack of public information of emergent materials and their production routes was also another reason to carry out the environmental assessment of the industrial CFHS. Hence, in this chapter, the use of the industrial plant to produce large scale quantities was assessed using life cycle assessment (LCA). As a promising material, lithium iron phosphate (LFP) cathode was selected by its potential use in new technologies. Laboratory, pilot and industrial scale are all assessed to verify the benefits of the scale-up, the influence of more concentrated solutions and lower yield for industrial scenario. Clearly, the scale-up reduces drastically the greenhouse gas (GHG) emissions, from 869.57 kg $CO_2$-eq/kg product (laboratory) to 18.82 kg $CO_2$-eq/kg product (industry), due mainly to higher production and a well-optimized design of the industrial plant. Higher reactant concentrations and yield both lead to a decrease in $CO_2$ emissions due to a greater production under same operational conditions. The present study provides valuable environmental insights about LFP nanoparticles production for CFHS.

# Chapter 4

## 4.1. Introduction

Lithium-ion compounds are some of the most promising cathode materials, which have been intensively studied for electrical applications such as rechargeable lithium-ion batteries (LIBs) in electric vehicles or energy storage systems (Horiba, 2014, Howell, 2008, Yuan et al., 2011). The high electrical capacity and density, as well as a good cyclability, have increased the commercial interest of these batteries. The most used cathodes of LIBs are layered oxides ($LiCoO_2$ and $LiNiO_2$), spinel oxides ($LiMn_2O_4$) and phospho-olivine ($LiFePO_4$) compounds (Cheruvally, 2008). Some of these materials have important disadvantages, for instance $LiCoO_2$ and $LiNiO_2$ are highly toxic and composed of very expensive materials (Co and Ni, respectively), while $LiMn_2O_4$ is not a stable material at high voltage (Xu et al., 2012). However, Lithium iron phosphate (LFP or $LiFePO_4$) looks an attractive cathode material due to its relatively high capacity (170 mAh $g^{-1}$), low cost and toxicity, thermal stability and good performance at high current loadings (Padhi et al., 1997b, Kang and Ceder, 2009, Padhi et al., 1997a, Cheruvally, 2008). LFP has only two disadvantages: low electronic conductivity ($\approx 10^{-10}$ S $cm^{-1}$) and sluggish $Li^+$ ion diffusivity ($10^{-14}$ – $10^{-17}$ $cm^2$ $S^{-1}$). These barriers, however can be addressed by carbon coating, cation doping and the reduction of particle size during synthesis (Gaberscek et al., 2007, Wang and Sun, 2012, Chung et al., 2002).

Although LFP can be easily found in nature (triphylite), the impurities of the mineral render it unsuitable for use in batteries. A diverse variety of synthesis procedures have been developed and analysed to find a competitive large-scale production of LFP with high quality product such as solid-state (Jugović and Uskoković, 2009, Hong et al., 2012), carbothermal reduction (Barker et al., 2003), batch hydro/solvothermal syntheses (Devaraju and Honma, 2012, Murugan et al., 2008,

Lee and Teja, 2006, Yang et al., 2001), microwave (Murugan et al., 2008, Higuchi et al., 2003) and continuous-flow hydrothermal synthesis (CFHS) (Xu et al., 2008, Johnson et al., 2016, Hong et al., 2013b, Hong et al., 2013a, Hong et al., 2011a, Hong et al., 2012, Hong et al., 2011b). CFHS technique has greatly demonstrated its potential as a scalable process for the industrial production of LFP (Johnson et al., 2016, Hong et al., 2013b, Adschiri et al., 2011), but also with other nanomaterials like metal oxides, metal sulfides and metal organic frameworks (MOFs) (Dunne et al., 2015a, SHYMAN-project, 2015). Also, CFHS uses shorter period of time for the reaction, non-use of organic solvents and lower temperature than other methods (Devaraju and Honma, 2012, Dunne et al., 2015a).

### 4.1.1. Processing parameters for the CFHS of LFP

The most critical parameters for the synthesis of LFP nanoparticles are identified and extensively studied through a literature review in this section (Hong et al., 2011a, Aimable et al., 2009, Hong et al., 2013a, Hong et al., 2013b, Hong et al., 2012, Hong et al., 2011b, Wenli et al., 2009, Xu et al., 2008). All of these parameters affect the purity, cyclability and capacity of the final LFP product and therefore they have to be analysed.

#### 4.1.1.1. Temperature

Production temperature is a determining factor in LFP quality in terms of crystallinity, agglomeration and size-distribution. Several prior studies evaluated subcritical and supercritical conditions, concluding that an increase of temperature reduced the agglomeration and enhanced the crystallinity and uniformity of the product. The only disadvantage was the formation of nanoparticles with larger sizes (Xu et al., 2008, Wenli et al., 2009, Aimable et al., 2009). However, Hong et al.

(2013b) concluded that supercritical conditions lead to smaller nanoparticles of LFP. This fact could be due to difference of residence time between the experimental results reported in these publications, supercritical and subcritical synthesis, since Aimable et al. (2009) operated with the same residence time (6 s) at different temperatures (250 °C and 400 °C), resulting in higher quality product at supercritical temperature, although this also leads larger nanoparticle size.

#### 4.1.1.2. Precursor concentration

The concentration of precursor input to CFHS also impacts product quality. It was found that lower precursor concentration results in larger nanoparticles with fewer impurities of $Fe^{3+}$ ($Fe_2O_3$ and $Fe_3O_4$) (Hong et al., 2013b), due to the higher supersaturation ratio when the concentration increased. These impurities negatively affect the quality of the product, the ions block diffusion of $Li^+$ reducing significantly the capacity (Hong et al., 2011a, Salah et al., 2006). By this reason, extremely high precursor concentrations should be avoided to improve the electrical properties. Carbon coated LFP nanoparticles were synthesised at 0.01:0.01:0.03 ($Fe:PO_4:Li$) M with a capacity of 141 mAh $g^{-1}$ at laboratory scale (Hong et al., 2013b). A pilot plant operated with a higher precursor concentration 0.25:0.375:0.8625 ($Fe:PO_4:Li$) M and the cathode material showed a capacity higher 150 mAh $g^{-1}$ at 0.3 C. This fact demonstrates that the scale-up of the process can be carried out with an increase of precursor concentrations without negative effects in the capacity of the product.

Previous hydrothermal studies recommend to adjust the molar ratio of reactants to 1:1:3 ($FeSO_4:H_3PO_4:LiOH$) to maintain slightly basic or neutral pH. In addition, moderate pH reduces impurities (Lee and Teja, 2006, Wenli et al., 2009), as well as improving precipitation of the LFP nanoparticles (Lee and Teja, 2005).

#### 4.1.1.3. Water and solutions flow rates

Operating at low flow rate product quality improves in terms of crystallinity, absence of impurities and higher content of lithium in the nanoparticles (Aimable et al., 2009, Hong et al., 2011a, Hong et al., 2013b). However, it was also found that an increase in the flow rates produce smaller, more uniform and less agglomerated nanoparticles (Hong et al., 2013a, Hong et al., 2011a, Hong et al., 2013b). In this point, there is a trade-off between high flow rates (smaller, more uniform and less agglomerated) and low flow rates (fewer impurities, higher crystallinity and Li content), which can be balanced by the desired material properties. Hong et al. (2011a) analysed the relation between flow rate and capacity, concluding that lower flow rates result in higher capacity performance, due mainly to the absence of impurities, which affect negatively to the electrical capacity of the cathode.

#### 4.1.1.4. Reactor design

Different reactor designs have been used for CFHS of LFP nanoparticles at laboratory scale. From the simplest "tee reactor" to more developed such as "Swirling-tee rector" (Hong et al., 2013a). A "tee reactor" basically consists in a T-pipe, in which the supercritical water and the precursor solution are mixed. After the reactor a straight-pipe or long coil-pipe can be added to crystallize the nanoparticles and control the residence time (Xu et al., 2008, Wenli et al., 2009, Hong et al., 2011a, Aimable et al., 2009). The synthesis of LFP nanoparticles with three different reactors ("tee reactor", "50° reactor" and "Swirling-tee rector") presented similar nanoparticles (Hong et al., 2013a). Despite this fact, the "Swirling-tee reactor" synthesised smaller and higher crystallinity nanoparticles with fewer impurities and higher capacity performance, possibly due to a better mixing of precursors and

supercritical water. The less favourable mixing regime between the precursor flow solution and the supercritical water flow in the "tee reactor" could be the cause of the lower capacity results.

#### 4.1.1.5. Carbon coating

The carbonization of LFP has demonstrated to enhance the capacity, electronic conductivity and cycle life (Ravet et al., 2001, Julien et al., 2006, Zaghib et al., 2005). Carbon-coated LFP (C-LFP) samples have been synthesised with numerous organic compounds including cellulose, fructose, glucose, sucrose, and others (Devaraju and Honma, 2012). Also, C-LFP has been produced trough of different synthesis techniques such as solid state, hydrothermal reaction or CFHS, all of them using in-situ or post-mixing carbon coating (Wenli et al., 2009, Johnson et al., 2016, Hong et al., 2011a, Hong et al., 2012, Liang et al., 2008).

The carbonization of LFP synthesised by CFHS requires input of additional energy and materials. These inputs are clearly justified by the higher electrical performance that C-LFP samples have demonstrated over simple LFP samples produced by the same technique (up to 40-50% better capacity >140 mAh $g^{-1}$). This increase is mainly due to reduction of impurities and carbon coating, which improves the electron and $Li^+$ transport between the nanoparticles surface (Hong et al., 2011a, Hong et al., 2013a).

The post-mixing carbon coating technique has been widely studied (Hong et al., 2011a, Hong et al., 2012, Hong et al., 2013a). Sucrose was mixed with deionized and distillate water to prepare a set of solutions with concentrations from 4 wt% to 24 wt%. Four grams of LFP were mixed with the previous solution and dried at 80 °C in vacuum oven for 24 h. After that, the powder samples were heated at different

temperatures (500-700 °C) and various periods (3-6 h) under a flow of 5% hydrogen in argon at flow rate of 100 ml $min^{-1}$. The experiments were carried out to determine the optimum carbon coating. The sample of 12 wt% sucrose solution that was treated at 600 °C for 3 h showed the best results of capacity and conductivity, as well as good cycle life after 30 cycles. This sample of C-LPF had a carbon content of 6 wt% approximately after carbonization.

The in-situ mixing carbon coating was carried out at pilot scale using fructose as a carbon source (Johnson et al., 2016). The CFHS of C-LFP used a confined jet mixer (CJM) reactor (Gruar et al., 2013). The molar rate of Fe:$PO_4$:Li was 1:1.5:3.45 and two different concentrations of fructose were used (0.75 and 0.875 M) in the solution precursor, concluding that the sample of higher fructose concentration resulted in better capacity performance at different current rates. The total carbon content of this sample was 12.7 wt%. The dried powder was heated up to 700 °C for 3 h with an unknown argon flow rate.

### 4.1.2. Prior LCA studies of LFP

In recent years, the higher demand for environmentally friendly technologies has caused an increase of the environmental evaluation of new emergent chemical processes and new materials at initial stages of development (Tsang et al., 2016, Pini et al., 2015, Kralisch et al., 2015) to minimise negative environmental impacts. Also, it has been essential to compare between traditional and incipient industries (Middlemas et al., 2013, Pourzahedi and Eckelman, 2015) the benefits and drawbacks of each process and these novel materials. As a new material for leading technologies, LFP has been previously evaluated in LCA studies of LIBs and synthesis comparison (Zackrisson et al., 2010, Majeau-Bettez et al., 2011, Liang et

al., 2017, Yu et al., 2014), Table 4.1 details them briefly. The first one was carried out for plug-in hybrid vehicles (Zackrisson et al., 2010). Results shown that the production of the cathode material represented approximately 10% of the total $CO_2$ emissions during the battery manufacturing, being C-LFP nanoparticles the major contributor of this category. Also, this LCA study mentioned that the synthesis of C-LFP nanoparticles was based on rough assumptions and approximations of a laboratory solid-state synthesis due to lack of cooperation and information of the industry (Zackrisson et al., 2010). A solid-state technique is also used for the production of C-LFP nanoparticles in the LCA study of three different cell batteries manufacturing (Liang et al., 2017) and the technical and environmental assessment of four cathode materials (Yu et al., 2014). Both LCAs defined their life cycle inventories (LCI) by the experimental information collected at laboratory scale. Solid-state techniques are typically batch processes, wherein precursors are subjected to high temperature (400-800 °C) for long periods (10 to 24 hours) (Jugović and Uskoković, 2009). The last LCA study modelled a batch hydrothermal synthesis, estimating production inputs and emissions for a hypothetical industrial scale production based on laboratory conditions and assuming stoichiometric molar ratios and 95% yield (Majeau-Bettez et al., 2011, Chen and Whittingham, 2006). This environmental assessment makes a number of simplifications: heat recovery of 50% is assumed from the batch process; nanoparticle drying is ignored; addition of materials like carbon nanotubes, which are required by the hydrothermal synthesis, are not included within the life cycle inventory analysis. Overall, prior LCA studies share a common limitation in that they are reliant on data from laboratory scale batch production processes and simple energy balance models are utilised to estimate the material and energy requirements of LFP production. Reliance on this data is

necessary due mainly to the lack of publicly available information on industrial and emerging techniques, but introduces significant uncertainty into assessments of environmental impact of LFP production.

These facts hinder the comparison between LFP nanoparticles production methods and their environmental impacts. By this, in this chapter a LCA from "cradle-to-gate" is only carried out for CFHS of C-LFP nanoparticles. The environmental evaluation is also developed at three scales; laboratory, pilot and industrial, providing valuable insights of an innovative process at initial phase of scale-up and design. The realization of this anticipatory LCA contributes to scientific and technical knowledge and how environmental performance may be affected by an industrial production.

Table 4.1. Summary of LCAs studies with LFP cathode material.

| LCA study | Comparison of the study | Functional unit | Technique of synthesis | Data source |
|---|---|---|---|---|
| Zackrisson et al. (2010) | Two different solvents for the cell manufacturing | 10 kWh battery for a hybrid car | Solid-state | Industry, the lacked cooperation with battery manufacturer caused rough assumptions and approximations in LFP production. |
| Majeau-Bettez et al. (2011) | Three batteries of nickel and lithium compounds | 50 MJ | Batch hydrothermal | Industrial modelling from a laboratory scale publication. Estimation of material and energy according to the modelling. |
| Liang et al. (2017) | Lithium, nickel and solar cell batteries | 1000 kWh | Solid-state | Experimental laboratory scale synthesis. |
| Yu et al. (2014) | Four cathode materials | 10000 mAh and 20 cycles | Solid-state | Experimental laboratory scale synthesis. |

## 4.2. Life cycle assessment methods

The aim of this research is to understand the impact of production scale on the environmental impacts of $LiFePO_4$ nanoparticle production. "Cradle to gate" models are developed to assess the life cycle environmental impacts of C-LFP nanoparticles production by CFHS at three different scales: laboratory, pilot and industrial scale. To assess the impacts of key production characteristics, two additional industrial-scale synthesis pathways are considered: high feedstock concentration (0.75M vs 0.5M in base case) and low product yield (80% vs 95% in base case) (Table 4.2).

Table 4.2. Scenarios considered in this study.

| | | Parameters | | | |
|---|---|---|---|---|---|
| Scenario | Based on | Scale | Molar Concentration ($Fe:PO_4:Li$) (mol $l^{-1}$) | Yield (%) | Temperature inlet reactor heater-boiler (°C) |
| 1 | Hong et al. (2013b) | Laboratory | 0.03:0.03:0.09 | 95 | 540 |
| 2 | Johnson et al. (2016) | Pilot | 0.25:0.375:0.8625 | 95 | 450 |
| 3 | Plant | Industrial | 0.5:0.5:1.5 | 95 | 450 |
| 3i | Plant | Industrial, High Feedstock Concentration | 0.75:0.75:2.25 | 95 | 450 |
| 3ii | Plant | Industrial, Low Product Yield | 0.5:0.5:1.5 | 80 | 450 |

*Scenario 3, the most likely scenario for the industrial production.*

Production of C-LFP at laboratory and pilot scale are evaluated based on published data for operating conditions and material requirements (Hong et al., 2013a, Johnson et al., 2016). Energy requirements for these pathways are estimated by process simulation with Aspen HYSYS V8.4 (UNIQUAC property package), assuming all thermal energy is provided by electric heating. For the industrial scale, an exhaustive

literature review is carried out to specify the operational conditions of temperature and precursors concentration for the industrial plant (Section 4.2.3.1. Processing parameters analysis). Once defined the temperature and metal salt concentrations, the materials are established according to the mass balance (widely detailed in section 4.2.3. Industrial scale) and previous nanoparticles production of the plant built under the EU-funded SHYMAN project. Technical information determined the electrical consumption of the equipment (pumps, system control, mixers, etc.) and natural gas used in boiler. Only the evaporation and calcination steps are simulated in Aspen HYSYS to determine the material and energy requirements of these industrial stages.

Life cycle models for the five production scenarios include the direct impacts of C-LFP manufacture as well as the production of all process inputs, including feedstocks, process chemical inputs, and energy requirements, as well as, the treatment of the waste water. Transportation, specific use and end of life of C-LFP nanoparticles are excluded of the environmental evaluation, since the approach of the present study is to assess the scale-up and design of the CFHS as emergent process. The functional unit is defined as 1 kg of dry C-LFP nanoparticles for all production scenarios. Environmental impact is estimated in greenhouse emissions (GHG) that is expressed in kilograms of $CO_2$-equivalent (kg $CO_2$-eq) per kilogram of product. As environmental software, CCaLC2 carbon footprint is used. This software has been developed by University of Manchester (Azapagic, 2015), and previously used in other LCAs studies (Amienyo et al., 2013, Jeswani et al., 2013, Iriarte et al., 2014). CCaLC2 software also includes a set of databases such as Ecoinvent 3 database v.3.

### 4.2.1. Laboratory scale

The synthesis of C-LFP at laboratory scale has widely been detailed in previous studies (Hong et al., 2013a, Hong et al., 2013b). The literature is used to define the material and energy inputs and the generation of process wastes (waste water). In general, two aqueous solutions of precursors are driven into the reactor (Solution A: LiOH and Solution B: $FeSO_4$+$H_3PO_4$) with a flow rate of 1.7 g $min^{-1}$ each one. The mole concentration ratio of LiOH: $FeSO_4$:$H_3PO_4$ is maintained at 0.09:0.03:0.03 M in order to keep slightly basic conditions (pH≈8). The temperature in the reactor is kept at 400 °C with a flow rate of 9 g $min^{-1}$ of deionised water previously heated up to 540 °C approximately. The system keeps a pressure of 250 bar using a back pressure regulator (BPR). After the reaction, the suspension is cooled down and depressurised to be collected. Then the product is washed and decanted before to be dried. To improve the capacity, a calcination process is carried out, 4 g of LFP nanoparticles are mixed into 2 ml of a sucrose solution at 12 wt%. Later the mixture is dried to evaporate the water content and nanoparticles with sucrose are calcined at 600 °C with a flow of 100 ml $min^{-1}$ of argon with 5% hydrogen for 3 hours. A typical yield of 95% is adopted in the present work for supercritical conditions according to literature review (Lee and Teja, 2005).

A complete process model of the laboratory-scale production scenario is developed by modelling and simulation in Aspen HYSYS of pumps, heating, cooling water, product drying and calcination stages. The electrical consumption of the pumps and the heater, as well as the amount of cooling water are defined by the simulation of the laboratory scale water streams (See Appendix). It is assumed that 5% of the total nanoparticles suspension volume is decanted during the first separation stage. Later a washing stage is carried out adding the same volume of deionised water that has

suspension. The electrical energy to evaporate the water content in the evaporation stage is estimated by increase the temperature up to 100 °C in Aspen (water vaporization). The calcination stage is established according to the previously mentioned and literature review (Hong et al., 2013a). 1 kg of LFP is mixed with 500 ml of sucrose solution at 12 wt%, then the mixture is driven into a furnace at 600 °C for 3 h under constant flow rate of 100 ml $min^{-1}$of inert gases (Ar and $H_2$). This stage is also simulated in Aspen HYSYS to get the heating energy and materials inputs. Figure 4.1 shows a flowchart of the laboratory synthesis of C-LFP nanoparticles.

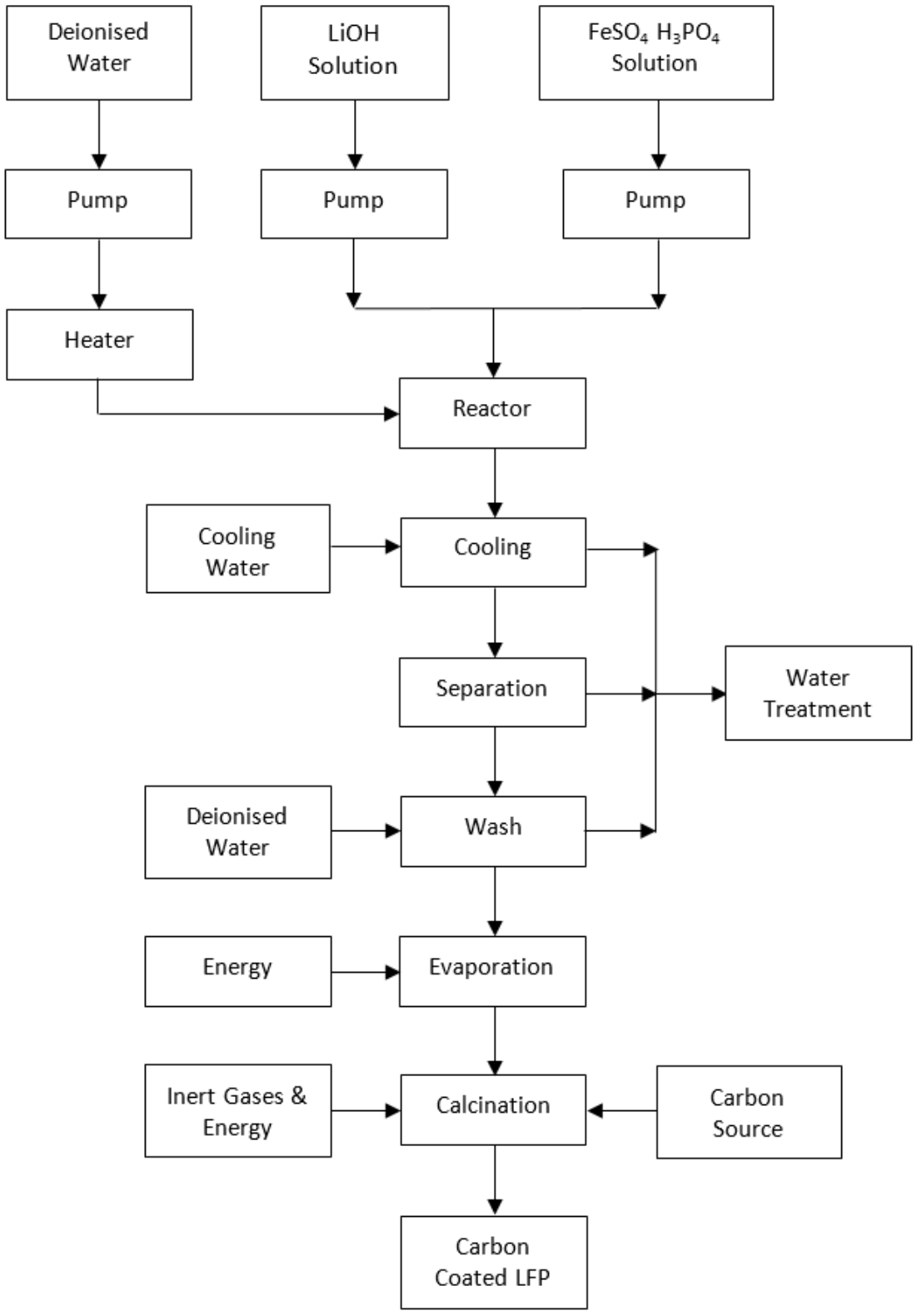



Figure 4.1: Flowchart of the CFHS of LFP nanoparticles at laboratory scale.

### 4.2.2. Pilot scale

Pilot scale synthesis of C-LFP is assessed according to previous synthesis publication (Johnson et al., 2016). In this case, the carbon coating is carried out in-situ, fructose is mixed in an aqueous solution with $FeSO_4$ and $H_3PO_4$, maintaining a molar concentration of 0.875, 0.25 and 0.375 M respectively. A second solution of LiOH with deionised water was also prepared at 0.8625 M. Both solutions are pumped at 200 ml $min^{-1}$ each one. Deionised water is used as a hot fluid and heated up to 450 ºC before to be mixed in the reactor with a flow rate of 400 ml $min^{-1}$. After the reaction, the nanoparticle suspension is cooled down and depressurized. Finally, the nanoparticles are decanted and washed to remove impurities before drying and calcining at 700 ºC for 3 hours under a flow of argon.

Similar to laboratory scale, the pilot scale is modelled to estimate energy and material inputs. Chemicals and solvents are calculated according to literature review (Johnson et al., 2016), while Aspen HYSYS is used to define pumps, heating, cooling water, drying and calcination stages requirements (See Appendix). The decantation is adopted at 5% suspension volume, before to be washed with the same volume of deionised water. Energy requirements to evaporate the water content of the suspension is again calculated by the simulation of vaporization of nanoparticles suspension. In this case, calcination stage is carried out for 1 kg of dried product under constant flow of argon gas at 100 ml $min^{-1}$ for 3 h at 700 °C, simulating this stage in Aspen according to literature review to obtain material and energy inputs (Johnson et al., 2016). Figure 4.2 show a schematic flowchart for the synthesis of C-LFP nanoparticle at pilot scale.

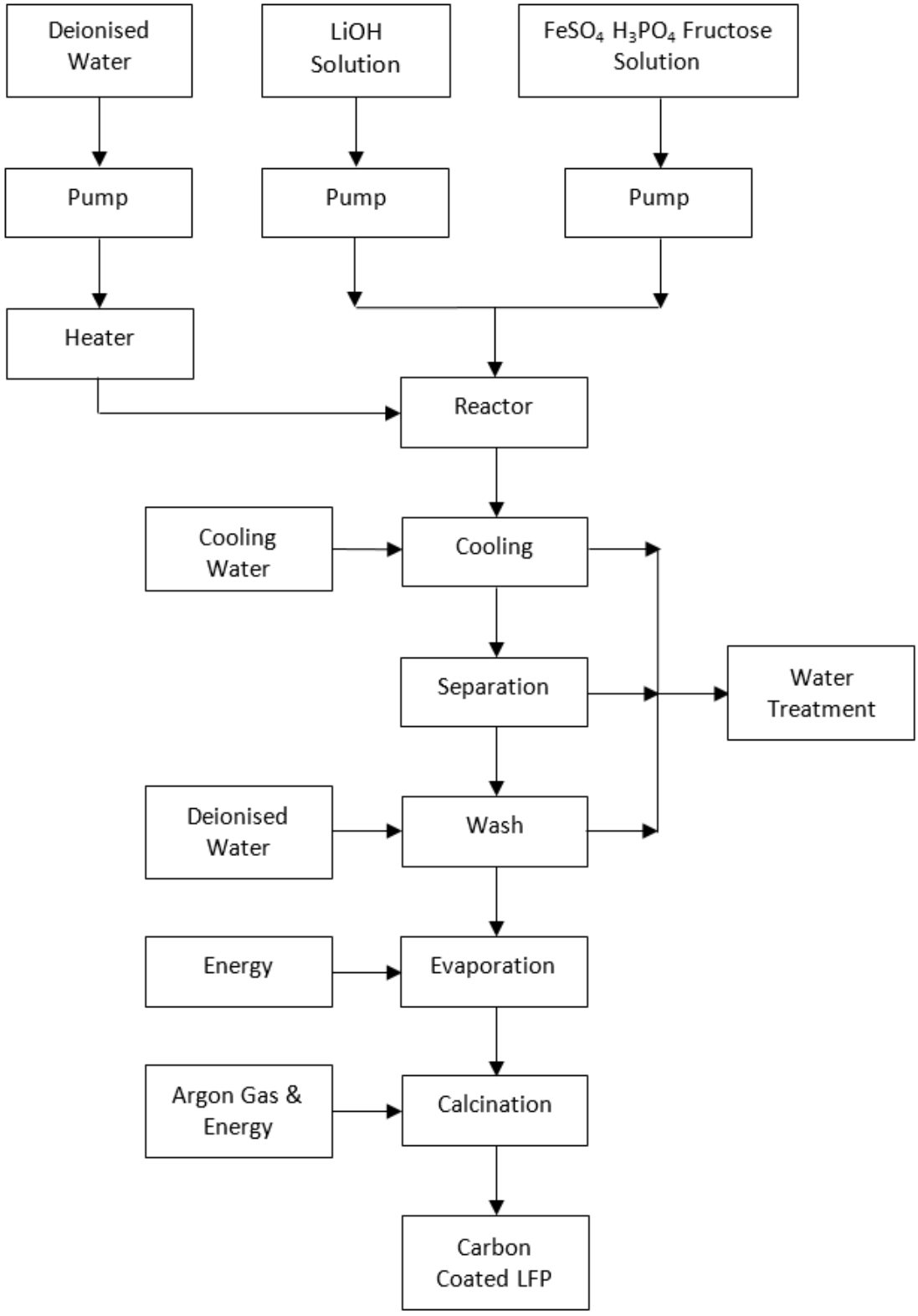



Figure 4.2: Flowchart of the CFHS of LFP nanoparticles at pilot scale.

### 4.2.3. Industrial scale

#### 4.2.3.1. Scale-up for the production of C-LFP nanoparticles

The operational conditions for the industrial production of C-LFP are shown in Table 4.3 (Page 78) and were defined according to the literature review analysed in Section 4.1.1. Similar to the laboratory and pilot scales, the temperature for the production of LFP nanoparticles is kept at supercritical conditions (450 °C and 240 bar). The scale-up from laboratory to pilot plant permitted the increase of precursor concentrations (Johnson et al., 2016). The metal salts concentration was approximately ten times higher in the pilot plant than the laboratory scale. For the industrial scale-up the increase of precursor concentrations is more conservative to guarantee a high quality product with low impurities and high capacity (>140 mAh $g^{-1}$). The base case establishes the first solution of $FeSO_4$ and $H_3PO_4$ at 0.5 M and second solution of LiOH at 1.5 M. Therefore the molar rate (1:1:3 - $Fe:PO_4:Li$) maintains slightly basic pH as literature recommends. The flow rates of the metal solutions are defined at 0.75 $m^3\ h^{-1}$ each one and 3 $m^3\ h^{-1}$ of deionised water as supercritical fluid. These flows correspond with the typical flows of the industrial plant and keep a relationship 2:1 (Deionised water:Metal salt solutions), which is an intermediate value between laboratory (3:1) and pilot (1:1) flow rate ratio. The counter-current reactor is used in plant (Lester et al., 2006, Lester and Azzopardi, 2009), which clearly is a developed reactor as swirling-tee rector or CJM. The post-mixing carbon-coated is adopted for the industrial scenario, this process guarantees a higher control of the final carbon content in the nanoparticles, as well as it has been widely studied in many continuous syntheses publications.

The material inputs are calculated according to the operational conditions with a yield of 95% (Lee and Teja, 2005). The electrical and natural gas consumption required for the production of C-LFP nanoparticles is defined by the specifications of the equipment (pumps, boiler, control system, etc.). The industrial plant was built with a heat exchanger to recover approximately 50% of the heat produced by the boiler. Also, a loop cooling system decreases the temperature, avoiding the use of water and reducing the waste water. After cooling stage, decantation tanks permit to settle down the nanoparticles in a suspension that represent the 5% of the total volume. Before drying the nanoparticles, a wash step is carried out adding the same volume that the suspension volume. Drying and calcination stages are simulated in Aspen HYSYS following similar conditions to the laboratory scale to establish materials and electrical consumption (See Appendix). Figure 4.3 represents a schematic flowchart of the CFHS for the production of C-LFP nanoparticles at industrial scale.

Information provided from industrial facility operators based on other nanoparticle production suggests that the process could operate with higher precursor concentrations. Evidently it means more kg of C-LPF nanoparticles per hour, but it also involves a higher demand of material inputs and possible loss of product quality. An environmental assessment of a scenario with higher molar concentrations clarifies how an increase of precursor concentrations affects the emissions of GHG. However, until further plant experience is gained in the coming 12 months, C-LFP production will not be carried out meaning that the trade-off between production, environmental impact and quality product cannot be verified. As a result, this thesis will consider a scenario with a higher molar concentrations (0.75 M for the $FeSO_4$ & $H_3PO_4$ solution and 2.25 M of LiOH solution), which can be used as information for

scale up design. In addition, a lower yield scenario (80%) was established to determine the consequences of a drop in process efficiency in the larger scale plant. Unlike the other scenarios, a yield of 80% was adopted to assess the environmental impacts. This scenario contributes to develop a wider study, in order to understand the potential environmental consequences of lower production performance. Table 4.4 summarises the production inputs of materials and energy for the production of 1 kg of C-LFP nanoparticles by CFHS in five different scenarios.

Table 4.3. Summary of the processing parameters analysis for the optimum operational conditions at industrial scale production of C-LFP nanoparticles.

| Parameter | Literature conditions | Operational conditions for the industrial plant |
|---|---|---|
| Temperature | Supercritical conditions | Supercritical water at 450 °C |
| Precursor concentration | Low concentration<br>Molar rate 1:1:3 ($Fe:PO_4$:Li) | $FeSO_4$ & $H_3PO_4$ → 0.5 M<br>LiOH → 1.5 M |
| Water & solutions flow rates | Low flow rates | Water → 3 $m^3$ $h^{-1}$<br>Solutions → 0.75 $m^3$ $h^{-1}$ |
| Reactor Design | Developed reactors better than convectional "tee reactor" | Counter-current reactor (Lester et al., 2006) |
| Carbon Coating | Necessary to improve the capacity | Post-mixing, LFP with a solution 12 wt% sucrose and calcination for 3 h at 600 °C under Ar and $H_2$ flow of 100 ml $min^{-1}$ to achieve 140-160 mAh $g^{-1}$ (Hong et al., 2012, Hong et al., 2013a) |

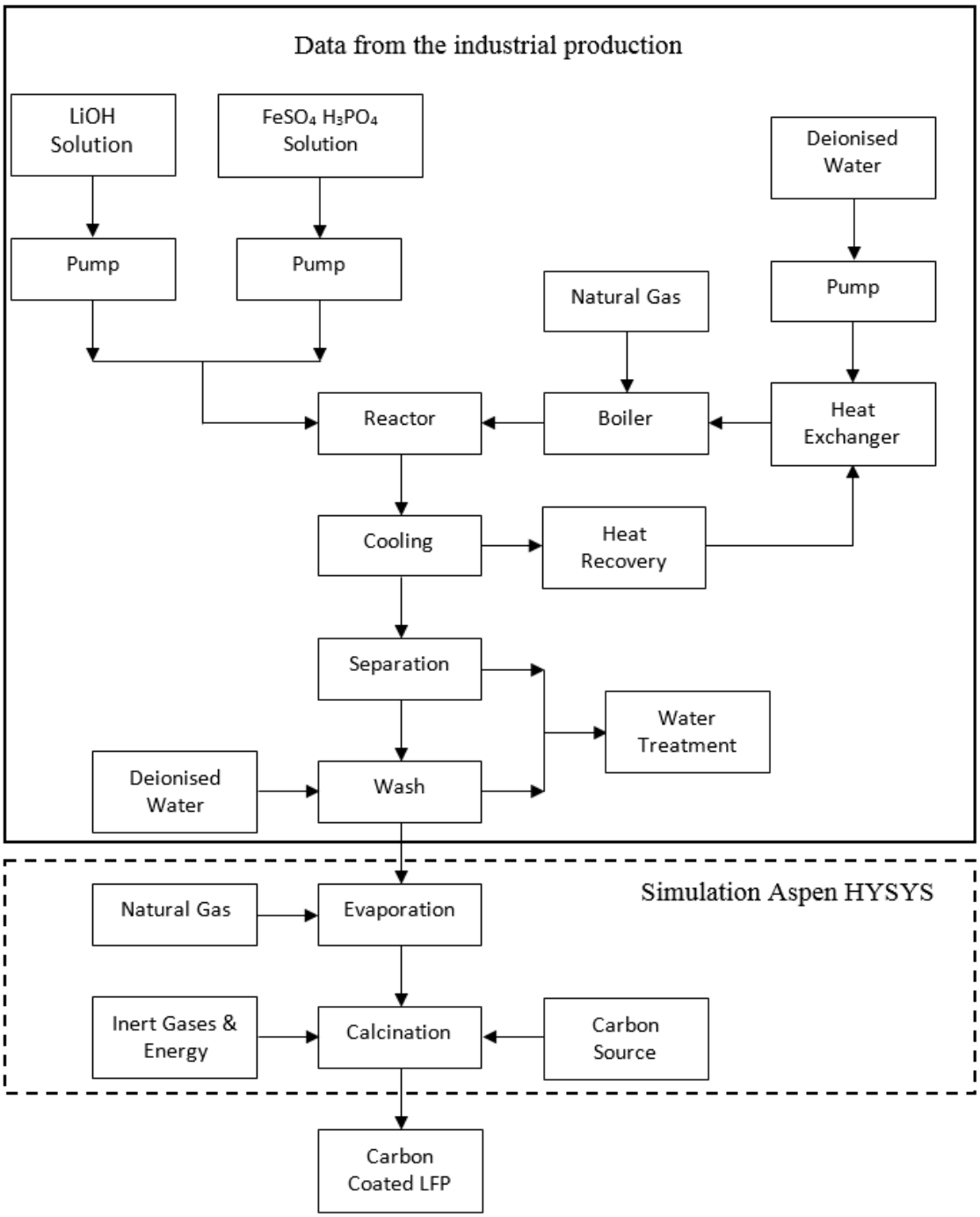



Figure 4.3: Flowchart of the CFHS of LFP nanoparticles at industrial scale.

Table 4.4. Material and energy inputs and outputs to produce 1 kg of C-LFP by a CFHS at different scales and parameters.

| | | Scenario | | | | |
|---|---|---|---|---|---|---|
| Item | Units | Laboratory | Pilot | Industrial | Ind. Higher Concentration | Ind. Yield 80% |
| Iron Sulfate | kg | 1.01 | 1.01 | 1.01 | 1.01 | 1.20 |
| Lithium Hydroxide | kg | 0.48 | 0.55 | 0.48 | 0.48 | 0.57 |
| Phosphoric Acid $_{85\ wt\%}$ | kg | 0.77 | 1.15 | 0.77 | 0.77 | 0.91 |
| Deionised Water | kg | 1703.77 | 112.10 | 84.40 | 56.37 | 100.16 |
| Cooling Water | kg | 37102.33 | 1469.70 | - | - | - |
| Sucrose | kg | 0.07 | 4.20* | 0.07 | 0.07 | 0.07 |
| Argon | kg | 23.44 | 24.66 | 23.44 | 23.44 | 23.44 |
| Hydrogen | kg | 0.06 | - | 0.06 | 0.06 | 0.06 |
| Waste water | kg | 38727.13 | 1579.44 | 82.53 | 55.84 | 98.20 |
| Natural Gas | MJ | - | - | 85.65 | 57.10 | 101.71 |
| Electricity | MJ | 4336.64 | 191.05 | 13.96 | 4.24 | 15.15 |

*Fructose instead of sucrose

## 4.3. Results and discussion

Figure 4.4 shows the total emissions for the five different scenarios studied in the present chapter, being the laboratory scale the most unfavourable of all of them. Table 4.5 (Page 84) also shows the results of GHG emissions for the five scenarios divided in categories. The scale of producing CFHS is a critical parameter: GHG emissions associated with pilot scale production (50.48 kg $CO_2$-eq/kg C-LFP) are approximately 95% less than emissions from laboratory production (869.57 kg $CO_2$-eq/kg C-LFP). Even lower GHG emissions are found for production at industrial scale (18.82 kg $CO_2$-eq/kg C-LFP, approximately 2% that of lab-scale production).

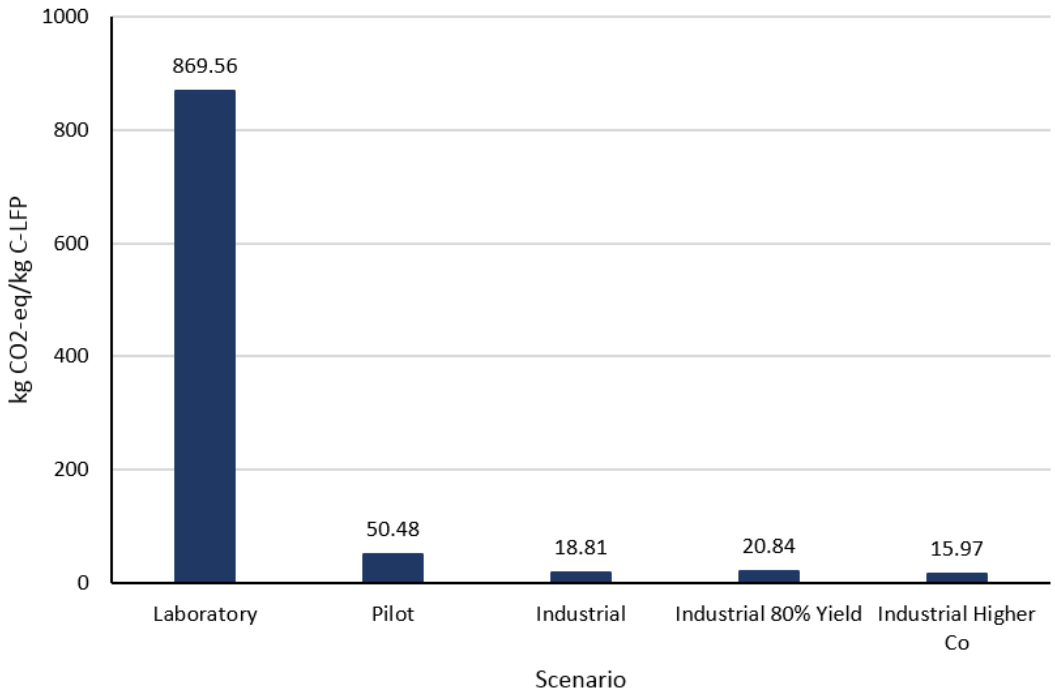



Figure 4.4: Total GHG emissions to produce 1 kg of C-LFP nanoparticles at five different scenarios.

Laboratory synthesis uses low precursor concentration (0.03-0.09 M) and flow rate (1.7-9 g $min^{-1}$), which leads to low productivity (<0.5 g $h^{-1}$ C-LFP). Thus the time necessary to produce 1 kg of LFP nanoparticles reaches approximately 2180 hours,

resulting in a very energy and materials inefficient process. For instance, due to low precursor solutions 1 kg of C-LFP at lab-scale needs a vast amount of deionised water (1703.77 kg) that represents 14.52 kg $CO_2$-eq/kg C-LFP. Production stages emits 833.51 kg $CO_2$-eq/kg C-LFP (>95% of total emissions) at lab-scale, while raw materials contribute 36.06 kg $CO_2$-eq/kg C-LFP (<5% of total emissions). This difference between processing and materials show the inefficiency of laboratory scale systems. Heating and cooling stages are responsible of more than 86% of the total GHG emissions associated with the laboratory scale production scenario (756 kg $CO_2$-eq.), primarily resulting from the lack of energy recovery from the reactor outlet stream. For example, the electrical consumption for heating is 4065 MJ per kg C-LFP (>90% of total electricity) and cooling stage uses 37102.33 kg of water per kg C-LFP, which also contributes to a more intensive water treatment.

The scale-up of CFHS encourages the possibility to operate with higher precursor concentrations and flow rate, which could result in an increase of materials and energy inputs. However, this fact leads a shorter operational time to produce 1 kg of C-LFP (0.45 kg $h^{-1}$ of C-LFP), minimising considerably the total GHG emissions up to 50.48 kg $CO_2$-eq/kg C-LFP (≈95% less than lab-scale). The environmental impact is clearly reduced by a shorter production time. The production stages are responsible of 36.63 kg $CO_2$-eq/kg C-LFP while material inputs emit 13.85 kg $CO_2$-eq/kg C-LFP. Again, the heating and cooling stage is the major contribution with 30.70 kg $CO_2$-eq/kg C-LFP (60.81% of total emissions), confirming it as a hot-spot of the CFHS process. Despite this fact, the GHG emissions of this stage drop 96% by the scale-up of the process. Also, a large reduction in the resources demand is evident for materials like deionised water and cooling water. As a consequence, the GHG emissions produced by material inputs drop more than 60% at pilot scale, up to 13.85

kg $CO_2$-eq/kg C-LFP. For example, both deionised water and cooling water are responsible of 27.13 kg $CO_2$-eq/kg C-LFP in the lab-scale, while that at pilot scale emits 1.46 kg $CO_2$-eq/kg C-LFP. The decrease of materials consumption contributes to a significant reduction in emissions associated with downstream stages such as water treatment, washing and evaporation. In general, the scale-up from laboratory to pilot permits a higher production due to more concentrate solutions and higher flow rates, however there is a large demand of energy in the heating and cooling stage. This is a consequence of a non-optimized process, which does not recover the energy and water used in the heating and cooling stages.

The industrial scale showed the lowest emissions of the three scales, 18.82 kg $CO_2$-eq/kg C-LFP and the highest production rate with 56 kg $h^{-1}$ of LFP. At this scale the production of a kilogram of product is carried out in less than 1 minute. Heating and cooling stages are responsible of the majority of GHG emission for pilot (60.82%) and laboratory (86.94%) scales (Figure 4.5). At industrial scale, a more efficient design exploiting heat recovery and use of a loop cooling system substantially improve the process energy efficiency and reduce GHG emissions for heating and cooling, 99% less than laboratory and 80% less respect to pilot plant. Heat recovery saves approximately 50% of thermal energy consumption and eliminates the need for cooling water (≈1500 kg $h^{-1}$). Knock-on effects, such as reducing the quantity of water requiring treatment, further reduce the impact of industrial scale LFP production. Figure 4.5 shows these differences for the five scenarios in terms of percentages. The well-optimized design of the industrial plant reduces drastically the percentages of the heating and cooling stage, water treatment, washing and evaporation.

Table 4.5. Summary of greenhouse gases emissions to produce 1 kg of C-LFP by a CFHS at five different scenarios.

| | | Scenario | | | | |
|---|---|---|---|---|---|---|
| | | Laboratory | Pilot | Industrial | Ind. Higher Concentration | Ind. Yield 80% |
| Categories | | kg $CO_2$-eq/kg C-LFP | | | | |
| Raw Materials | Lithium Hydroxide | 1.16 | 1.33 | 1.16 | 1.16 | 1.38 |
| | Deionized Water | 14.52 | 0.96 | 0.72 | 0.48 | 0.85 |
| | Cooling Water | 12.61 | 0.50 | - | - | - |
| | Iron Sulfate | 0.17 | 0.17 | 0.17 | 0.17 | 0.20 |
| | Phosphoric Acid $_{85\ wt\%}$ | 1.09 | 1.63 | 1.09 | 1.09 | 1.29 |
| | Argon | 6.40 | 6.75 | 6.40 | 6.40 | 6.40 |
| | Hydrogen | 0.06 | - | 0.06 | 0.06 | 0.06 |
| | Sucrose | 0.04 | 2.52* | 0.04 | 0.04 | 0.04 |
| Production Stages | Pumping | 9.90 | 0.63 | 0.92 | 0.61 | 1.09 |
| | Heating & Cooling | 756.00 | 30.70 | 6.03 | 4.02 | 7.16 |
| | Washing & Evaporation | 39.10 | 2.57 | 0.76 | 0.50 | 0.90 |
| | Calcination | 1.41 | 1.62 | 1.41 | 1.41 | 1.41 |
| | Water Treatment | 27.10 | 1.11 | 0.06 | 0.04 | 0.07 |
| | *Total Raw Materials* | 36.06 | 13.85 | 9.64 | 9.40 | 10.22 |
| | *Total Production Stages* | 833.51 | 36.63 | 9.18 | 6.58 | 10.63 |
| | *Total kg $CO_2$-eq/kg C-LFP* | 869.57 | 50.48 | 18.82 | 15.98 | 20.85 |

*No information of Fructose in database, so sucrose was assumed as raw material.

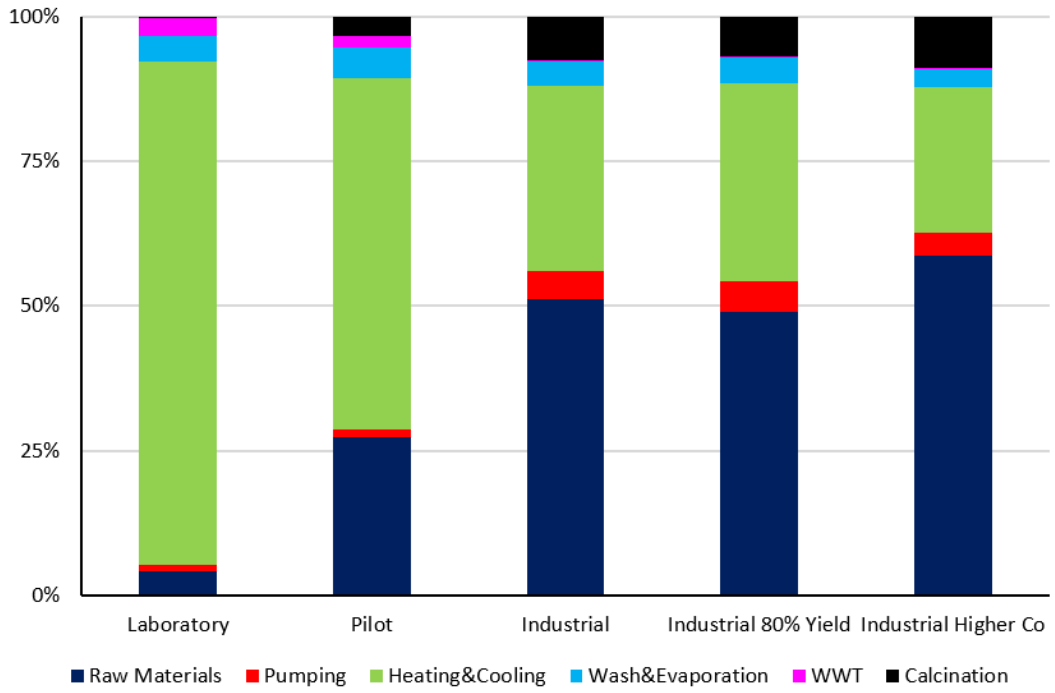



Figure 4.5: Percentages of GHG emission to produce 1 kg of C-LFP nanoparticles at five different scenarios.

The production is definitively benefited by the scale-up of the CFHS due to the higher flow rates and concentration of precursors. Also, the volumetric productivity $\left(\frac{\text{kg of LFP}\cdot\text{h}-1}{\text{Volume Reactor (m}^3)}\right)$ was calculated approximately with the volume of the reactor for each different scenario and the modelling carried out for the batch process (Majeau-Bettez et al., 2011) (Table 4.6). The scale-up again resulted in a higher volumetric production for the same reasons (higher flows and metal salt concentration). The scale-up leads to a higher production for both batch and continuous process. However the volumetric production shows a better value for the CFHS, due to smaller size of the reactor. Batch hydrothermal processes involve large volume reactors and long reaction times to produce similar quantities of product as continuous methods, which would greatly impair the financial viability of batch production methods.

Table 4.6. Production information for each different scenario.

| Scenario | Time to produce 1 kg of LFP | Production (g LFP $h^{-1}$) | Volumetric productivity (kg LFP $h^{-1}$ $m^{-3}$) |
|---|---|---|---|
| 1 | 2180 h | 0.46 | 186 |
| 2 | 2.22 h | 449.61 | 4382 |
| 3 | 1.07 min | 56,200 | 144606 |
| 3i | 0.71 min | 84,301 | 216912 |
| 3ii | 1.27 min | 47,327 | 121775 |
| Majeau-Bettez et al. (2011) Batch Hydrothermal | 2.76 min | 21,705 | 2.17 |

Unlike other production stages, information about calcination step is relatively uncertain, thus a calcination process was roughly and similarly defined for the production of 1 kg of C-LFP nanoparticles in all scenarios (3 h at 600-700 °C under inert gases flow of 100 ml $min^{-1}$). As a result, the total GHG emissions of inert gases and calcination stage are comparable for all of the scenarios. The absence of information in calcination stage encourages future and deeper assessment in order to provide more valuable and realistic information such as the exact quantity of inert gases per kilogram of C-LFP or the possibility to recycle it. If the inert gases could be 100% recycled, which would be optimistic, the total GHG emissions would be reduced 35% by up to 12.42 kg $CO_2$-eq/kg C-LFP.

Laboratory and industrial scale carried out the carbonization of LFP post-mixing, first synthesis of nanoparticles followed by the carbon-coating and calcination steps. The pilot plant according to the literature (Johnson et al., 2016) used fructose in-situ (Fructose was present during the synthesis). The post-mixing method (0.07 kg sucrose/kg C-LFP) demands a quantity of carbon precursor lower than in-situ (4.20 kg fructose/kg C-LFP), thus the GHG emissions are more elevated (2.52 kg $CO_2$-

eq/kg C-LFP). This higher demand of carbon source probably is due to different aspects such as decomposition of fructose under supercritical conditions (Kabyemela et al., 1999) or to achieve a minimum content of carbon in the final product.

A drop in the yield is obviously detrimental to the environment, total emissions rise up 20.85 kg $CO_2$-eq/kg C-LFP. The plant needs more time to produce 1 kg of C-LFP, demanding more energy and resources. Although the production at 95% (56 kg $h^{-1}$) and 80% (47 kg $h^{-1}$) yield do not look extremely different, at industrial scale an immense amount of materials and energy are involved, any change can affect negatively the environment. Resources and production category increased similarly, being this difference clearer in precursors (LiOH, $FeSO_4$ and $H_3PO_4$), heating and cooling stages (Table 4.4).

The impact of a higher concentration of precursors is also studied for the industrial plant. Although larger amount of precursors such as LiOH or $FeSO_4$ are used, a higher throughput is also produced (84.30 kg $h^{-1}$) with the same temperature and flow rates. As a result, the GHG emissions decrease, the time to produce 1 kg of C-LFP is shorter and amount of energy and some materials per kg of product is reduced (natural gas and deionised water) (Table 4.4). The total emissions fall to 15.98 kg $CO_2$-eq/kg C-LFP (≈15% less). The main reduction is showed by the production stages (40%), concreting in the heating and cooling stage. In this step, a large quantity of natural gas is used to heat up the water stream (3 $m^3$ $h^{-1}$) in the boiler, consequently a reduction of time affects favourable to decrease mass input and $CO_2$ emissions.

Lower GHG emissions are showed for scenarios at high yield-rate and the concentrated solutions, although the industrial scenarios vary within a relatively small range between 15.98 and 20.85 kg $CO_2$-eq/kg C-LFP. As previously

mentioned, more concentrated solutions could affect negatively quality of the nanoparticles with appearance of impurities. The present work has been focused on the scale-up of the CFHS and the effects of operational conditions over the GHG emissions at industrial scale. Future work with the industrial plant would help to optimize the trade-off between concentration and quality product. This fact is significant since the industrial plant is able to operate above of 1 M for iron precursor, which means >100 kg $h^{-1}$ of LFP nanoparticles and $CO_2$ emissions lower than 12 kg $CO_2$-eq/kg C-LFP.

### 4.3.1. Prior LCA studies

At first sight, industrial CFHS looks to emit higher GHG emissions than other synthesis routes as it is show in Figure 4.6. However a deeper literature review found that prior LCAs clearly used rough estimations and assumptions, as well as missed key information that results in an underestimate environmental impact.

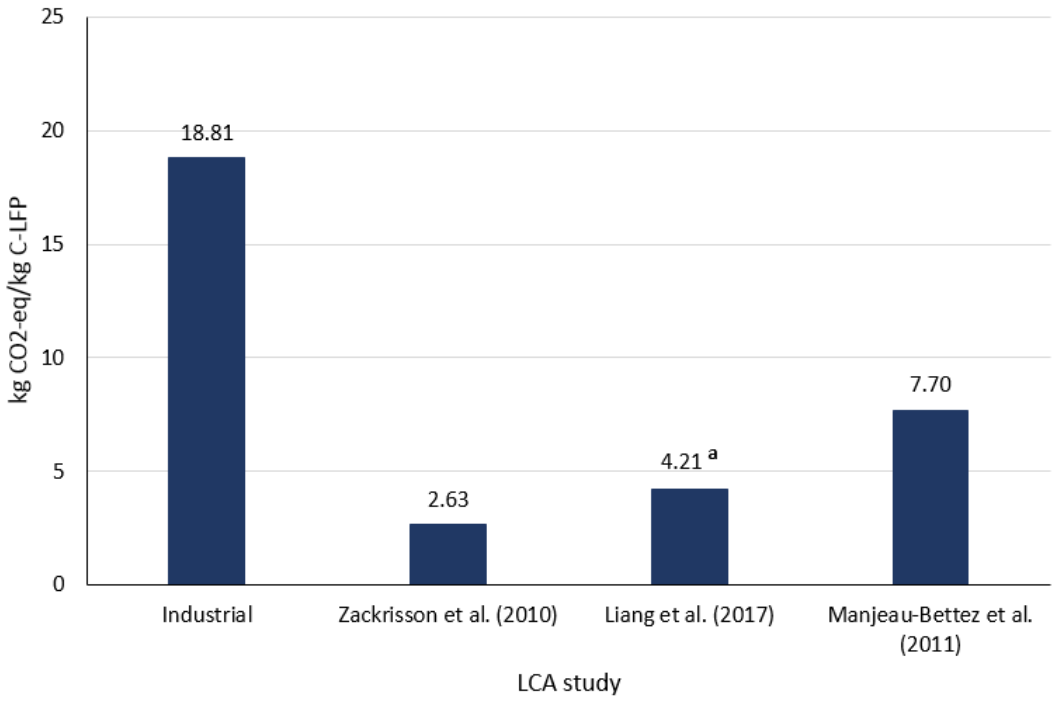


Figure 4.6: Theoretical total GHG emissions to produce 1 kg of C-LFP nanoparticles according to different publications with lack of information. [a] Liang et al. (2017) total GHG emissions for raw materials (excluded processing)

For instance, the lack of information and cooperation by battery manufacturer in the evaluation of LIBs for plug-in hybrid vehicles (Zackrisson et al., 2010). By this, battery manufacturing was defined according to theoretical and laboratory data; precursor inputs were calculated stoichiometrically, material heat capacity of chemicals was assumed (0.9 kJ $kg^{-1}$ $K^{-1}$) and electrical consumption was roughly estimated for production stages (3 kJ $g^{-1}$). The results showed that the global warming impact for 42.2 kg of LFP had a value of 111 kg $CO_2$-eq (2.63 kg $CO_2$-eq/kg C-LFP). Liang et al. (2017) carried out a solid-state synthesis of LFP in the laboratory of Beijing Institute of technology to synthesise C-LFP nanoparticles. The emissions per battery manufacturing were 28.4 kg $CO_2$-eq: 12.7 kg $CO_2$-eq of raw materials and 15.7 kg $CO_2$-eq from production phase. This information is not well-defined and only GHG emission from raw materials (no energy) can be estimated for the synthesis of C-LFP (4.21 kg $CO_2$-eq/kg C-LFP). The precursors and the synthesis of both studies (Zackrisson et al. and Liang et al.) are similar, as well as the GHG emissions. This fact suggests that the total energy assumption of 3kJ $g^{-1}$ LFP that Zackrisson et al. (2010) assumed was insufficient, due probably to the lack of dissemination of information by the battery industries. Also, Yu et al. (2014) synthesised C-LFP at laboratory scale by solid-state method, detailing clearly the amount of precursors and energy used to produce 1 kg of LFP. Material quantities were comparable to the previous publications, but the total electricity involved in the process was of 105 MJ/kg C-LFP. The use of 105 MJ of electricity at UK (low voltage) contributes with 19.5 kg $CO_2$-eq/kg C-LFP (0.19 kg $CO_2$-eq/MJ) (JCR,

2002). Hence, the total GHG emissions of a solid-state techniques (Zackrisson et al., Liang et al. and Yu et al.) could be surpass of 25 kg $CO_2$-eq/kg C-LFP. In addition, in solid-state method is common the use of inert gases like argon or hydrogen to prevent carbon oxidation (Jugović and Uskoković, 2009). Although Yu et al. (2014) mentioned the use of a furnace with argon gas, this does not appear in the life cycle inventory as a material input. In our results, the use of inert gases represents 6.40 kg $CO_2$-eq/kg C-LFP, if this value is considered in solid-state emissions, these could reach the 30 kg $CO_2$-eq/kg C-LFP approximately. Majeau-Bettez et al. (2011) used and modelled a batch laboratory hydrothermal synthesis according to experimental insights (Chen and Whittingham, 2006). The global warming potential (GWP) of the LFP battery production was 22 kg $CO_2$-eq per kg battery, being the production of the cathode responsible for more than 35% (≈7.7 kg $CO_2$-eq/kg LFP). In this case, the use of a furnace and inert gases are not required for the production of LFP nanoparticles, reducing considerably the GHG emissions in this study. However, this LCA study has not included several inputs that can increase drastically the emissions and the demand of energy. The modelling ignored the energy necessary to dry the nanoparticles that in our CFHS represents 10.40 MJ/kg C-LFP. Also, the inventory of the LFP production does not include the use of L-ascorbic acid and carbon nanotubes used during the laboratory synthesis (Chen and Whittingham, 2006). Probably the use of L-ascorbic acid would not increase the GHG emissions, but definitively the synthesis of the carbon nanotubes requires a more intensive and demanding process (nanomaterial synthesis) that results in larger amount of emissions.

With all of these considerations, the CFHS shows its potential as industrial process for the production of C-LFP nanoparticles with a total of GHG emissions ranges

between 15 to 20 kg $CO_2$-eq/kg C-LFP. Further research could reduce the environmental impact with recycling or reducing the amount of inert gases (potential drop of 35% in the total GHG emissions) and increasing the concentration of precursors. Anyway, the current GHG emissions of the present LCA shows lower values than other techniques such as solid-state and batch hydrothermal, which could reach 30 kg $CO_2$-eq/kg C-LFP.

## 4.4. Conclusions

The present chapter has evaluated the environmental impact of five different scenarios to the production of C-LFP nanoparticles by CFHS using LCA methodology and GHG emissions as impact factor. The five scenarios are three scales of production - laboratory, pilot and industrial - and two processing parameters at industrial scale - yield and precursor concentration.

The scale-up of the process leads a significant reduction in emissions, from laboratory to industrial, by up to 98% in the total GHG emissions. Lab-scale is the most unfavourable scenario with 869.57 kg $CO_2$-eq/kg C-LFP, due mainly to an inefficient and basic design. This scale operates with low concentration solutions and flow rates, resulting in an extremely poor productivity. Also, non-optimized stages such as heating & cooling (hot-spot) demand an excessive amount of energy and resources like water cooling, affecting negatively other production stages such as waste treatment.

The scale-up from laboratory to pilot scale permits an increase in the flow rates and precursor concentrations, which is advantageous to the productivity and to reduce up to 50.48 kg $CO_2$-eq/kg C-LFP the GHG emissions (95% less than lab-scale). The

large amount resources and energy saves supported the insight of scale-up. However, this scale is still a non-optimized process, due to the lack of heat recovery.

The industrial scale shows the most respectful values with the environment. The total GHG emissions are 18.82 kg $CO_2$-eq/kg C-LFP, approximately 98% and 62% less than laboratory and pilot scale respectively. These results are due to high production of an industrial plant, a more developed process and design which includes heat recovery and efficient design. For example the most unfavourable stage in laboratory and pilot scale scenarios is heating and cooling stage, after the scale-up and the optimization of the industrial process the GHG emissions drop 99% respect to the laboratory system.

The carbon coating in-situ results in higher GHG emissions than post-mixing, due to the larger demand of carbon source. The calcination stage is defined in this research according to literature review, due to the lack of data and industrial information. All of the scenarios show similar emissions for the use of argon in the furnace (≈6.40 kg $CO_2$-eq/kg C-LFP). Future LCAs and deeper research about calcination process would be considerably valuable to reduce or to recycle the inlet of inert gases, which would lead to lower $CO_2$ emissions.

Although the differences between all of the industrial scenarios are minimum, an increase in the yield and precursor solutions could reduce the GHG emissions between a 10-15%. These parameters increase the production, then the $CO_2$ emissions are lower. Future experience from the CFHS plant from Nottingham should be carried out to study the balance between precursor concentration, quality product and environmental impact in order to provide the best operational conditions of production.

Prior LCAs studies typically show lower GHG emissions than the current analysis. However, this fact is due to ignore or exclude production stages, material and energy inputs. Prior publications mentioned the lack of information and collaboration from the industry, as well as, the rough assumptions considered. Other studies were based on laboratory information and modelling from laboratory to industrial production and it is commonly found the absence of some material and energy requirements. For example, solid-state synthesis frequently requires the use of inert gases like argon in calcination step, but none of the published LCA inventories have considered it. As this fact, there are many examples where carbon nanotubes, inert gases or energy to dry nanoparticles are not included as inputs, resulting clearly in underestimate environmental impact. Despite this fact, our evaluation have considered all necessary data for the CFHS of an industrial production of C-LFP nanoparticles, including all stages, materials and energy requirements, demonstrating to be a potential technique for the industrial production of this new material.

# 5. Chapter 5 - Assessing the life cycle environmental impacts of titania nanoparticle production by continuous flow solvo/hydrothermal syntheses

Continuous-flow hydrothermal and solvothermal syntheses are evaluated from "cradle-to-gate" to assess life cycle assessment (LCA) of an industrial titanium dioxide ($TiO_2$) nanoparticle production. Parameters considered include different operational conditions: precursors, material properties and production capacities. A detailed characterisation of the nano-$TiO_2$ products allows us to link key nanoparticle characteristics to production parameters and environmental impacts, providing useful information. Five precursors are considered, ranging from simple inorganic precursors (titanium oxysulfate, TiOS), to complex organic precursors (titanium bis(ammonium-lactato), TiBALD). Laboratory scale is used to determine the yield, size distribution, crystallinity and phase of the product. The specifications and experience of the plant are used to estimate the mass and energy inputs for the LCA. Overall, higher temperatures result in larger, more crystalline nanoparticles with higher yield. Precursor choice influences nano-$TiO_2$ properties, for example TiOS results in the largest particle sizes, while TiBALD achieves the smallest particles and narrowest size distribution. Precursor choice is also the main factor in determining environmental impacts (>80% in some cases), due to the production impact of complex organic precursors. TiOS shows the lowest global warming potential (<12 kg $CO_2$-eq/kg $TiO_2$) and cumulative energy demand (<149 MJ/kg $TiO_2$) due to the low environmental impact of the precursor, the use of water as a solvent and its high yield even at lower temperatures. Conversely, the TiBALD precursor shows the highest impact (86 kg $CO_2$-eq/kg $TiO_2$ and 1952 MJ/kg $TiO_2$) due to the need for additional post-synthesis steps and the added complexity of precursor manufacturing.

# Chapter 5

## 5.1. Introduction

### 5.1.1. $TiO_2$ production methods

Titanium dioxide or titania ($TiO_2$) is one of the most widely used and studied materials due to its chemical and physical properties, including high thermal and chemical stability (Cargnello et al., 2014), high refractive index, non-toxicity, high hardness, and catalytic and photocatalytic activity (Büchner, 1989, Thompson, 1995). It is used in medical implants (Macwan et al., 2011), water purification (Li et al., 2008), and as pigments in the paper and paints industries (Grubb and Bakshi, 2011), plastics and fibres (Büchner, 1989). Industrial processes have been improved since early last century making $TiO_2$ one of the most commoditised materials in the chemical industry. However alternative routes, capable of producing nano-sized $TiO_2$, have gained interest in recent years e.g. sol–gel (Macwan et al., 2011) spinning disk (Chan et al., 2012) solvothermal and hydrothermal syntheses (Kawasaki et al., 2009, Toft et al., 2009) have been developed to produce nanoparticles of titanium dioxide. With the increase in awareness of environmental concerns, it is ever more important to address the potential environmental impact of industrial processes, both current and emerging.

The sulfate process was the first method to produce titania as a pigment for different paints. In the 1950s, the production increased and the chloride process appeared as an alternative (Reck and Richards, 1999). Unlike these traditional processes, new methods developed in the last few years (sol–gel, solvothermal and hydrothermal) possess better advantages to control the phase, size, shape and composition (Cargnello et al., 2014). Despite these significant benefits, these techniques are typically batch processes with poor scope for scale-up. Continuous-flow

hydrothermal synthesis (CFHS) was developed as a new synthesis approach of metal oxide nanoparticles (Adschiri et al., 1992a, Adschiri et al., 1992b). Continuous-flow solvothermal synthesis (CFSS) has also been shown to produce a larger variety of more complex nanomaterials such as metal–organic frameworks (MOFs) (Toft et al., 2009, Gimeno-Fabra et al., 2012, Bocquet et al., 1999). As continuous methods, CFHS and CFSS are inherently more scalable than conventional batch synthesis. This technique exploits the properties of superheated water – its high dissociation constant and low polarity – to nucleate metal oxide nanocrystals on mixing a stream of a metal salt solution with a superheated water stream. Early work in this field used a simple, off-the-shelf "tee reactor". Later, Lester et al. (2006) designed a new reactor for CFHS and CFSS, known as a "nozzle" or counter-current reactor, taking advantage of the low density of supercritical water to achieve symmetric mixing and a narrow residence time distribution. This reactor has been demonstrated under a wide range of different conditions (temperature, solvents, precursors, etc.), offering an easy and reproducible process, as well as the capacity to produce many materials with distinct shapes and sizes (Gimeno-Fabra et al., 2012, Lester et al., 2006, Aksomaityte et al., 2013, Dunne et al., 2015b, Dunne et al., 2014, Gimeno-Fabra et al., 2013, Hobbs et al., 2009, Lester et al., 2012, Lester et al., 2013, Wang et al., 2013). The nozzle reactor has also achieved the continuous production of nanoparticles from the laboratory scale to the pilot scale to the full scale (Sierra-Pallares et al., 2016). Due to all of these advantages (reproducibility, scalability, flexibility and their potential for an environmentally benign process), CFHS and CFSS stand to play an important role in the large-scale production of nanomaterials.

### 5.1.2. Spectrum of precursors used for $TiO_2$ synthesis

CFHS and CFSS methods have used a wide range of titanium precursors, with both organic and inorganic components, for the production of nanoparticles of $TiO_2$ (Toft et al., 2009, Kawasaki et al., 2009, Malinger et al., 2011, Yasin et al., 2016, Pighini et al., 2007, Makwana et al., 2016, Chen et al., 2012, Baghbanzadeh et al., 2013). Titanium tetrachloride ($TiCl_4$) as a halide salt can be easily hydrolysed (Cargnello et al., 2014) to produce $TiO_2$ with water (Malinger et al., 2011, Yasin et al., 2016). Titanium oxysulfate, or titanyl sulfate (TiOS), which is an intermediate product from the sulfate process (Büchner, 1989), can also be synthesised in a continuous system with an aqueous flow (Makwana et al., 2016). Alkoxides ($Ti(OR)_4$), such as titanium isopropoxide (TiPO or TIPO) are frequently used in non-aqueous sol–gel methods due to their sensitivity to water (Kakihana et al., 2010, Niederberger and Garnweitner, 2006), as well as in CFSS with solvents such as butanol or isopropanol (Toft et al., 2009, Pighini et al., 2007, Baghbanzadeh et al., 2013). Water-soluble titanium complexes (WSTC) are derivatives of $TiCl_4$ or TiPO with an acid such as glycolic, lactic, oxalic, etc., and a base like ammonia ($NH_3$) or potassium hydroxide (KOH) (Ohya et al., 2004, Brisse and Haddad, 1977). Titanium bis(ammonium lactato) dihydroxide (TiBALD), is one of the WSTC precursors that has already been able to produce nano-$TiO_2$ at the pilot-plant scale (kg per day) by CFHS (Chen et al., 2012). Unlike the alkoxides and $TiCl_4$, these complexes are stable in water (Kessler, 2013), permitting their use in aqueous reaction systems. The main difference between precursors is the degree of ease of manufacturing. Inorganic precursors like TiOS and $TiCl_4$ are easily produced by mixing the mineral (raw material) with an acid solution. Alkoxides and WSTC are more complex precursors (and subsequently

more expensive), but with a higher stability due to the interaction of the organic counter ion around the titanium atom.

### 5.1.3. Overview of $TiO_2$ LCA studies

The increased industrial scale use of CFHS and CFSS for production of large quantities of nanoparticles necessitates a thorough assessment of the environmental sustainability of this newly developed process. For this purpose, a standardised method, Life Cycle Assessment (LCA), was used as a tool for quantification of the potential environmental impacts of a product system throughout its life cycle. Prior LCA studies have evaluated $TiO_2$ production from "cradle-to-gate" (excluding the application, product use and end-of-life of nano-$TiO_2$), including traditional and new techniques at different scales and sizes of $TiO_2$ particles. Traditional industries (sulfate and chloride) were evaluated with different feedstocks and waste treatments (Reck and Richards, 1999). This study was based on energy requirements, sulfur oxide emissions, solid waste and metal discharge into water as environmental factors, concluding that the sulfate process (ilmenite) demands less energy but generates more residue and emissions than the chlorine process (slag or rutile). Unlike traditional methods, the Altair Hydrochloride Process (AHP) produces nano-$TiO_2$ using ilmenite and hydrochloric acid (Grubb and Bakshi, 2011). The evaluation of the energy demand for the AHP technique was studied, deducing that energy consumed is similar to that of the sulfate process, despite the fact that the AHP is able to produce nano-$TiO_2$ (Grubb and Bakshi, 2011). The LCA study was also carried out for the process known as Alkaline Roast of Titania Slag (ARTS) (Middlemas et al., 2013, Middlemas et al., 2015). This alternative route uses titanium slag and sodium hydroxide to produce micro-titania particles of 0.2–0.3 μm. The

emissions of $CO_2$ and the cumulative energy demand (CED) were used as impact factors. The results were compared with other LCA studies, concluding that the ARTS process emits less $CO_2$ and demands less energy than the traditional processes and the Altair method (Middlemas et al., 2015). A "cradle-to-gate" LCA was also carried out for the hydrolytic synthesis of $TiO_2$ nanoparticles (Pini et al., 2015). TIPO and water were used in sol–gel synthesis to obtain a suspension of nanoparticles at 6 wt% and 30 nm of size. The LCA results determined that most impacts are produced by the high demand for energy required for operating the process including temperature, as well as the use of an organic precursor with higher environmental impacts as TIPO. The focus of prior studies on single combinations of the titanium precursor and production parameters and the lack of detailed nano-$TiO_2$ characterisation data presented in these studies (i) provide limited insights regarding the effect of the precursor and process parameters on environmental impact; (ii) prevent useful inter-study comparisons and (iii) raise questions on the functional equivalence of the evaluated materials and their suitability for specific end uses.

This chapter evaluates the technical performance and environmental impacts of continuous-flow solvo-hydrothermal synthesis of nano-$TiO_2$. A broad set of titania precursors are considered to characterise the nano-$TiO_2$ in terms of size distribution, crystallinity, phase and yield at the laboratory scale. These experimental data are extrapolated to assess the environmental impacts of commercial scale production based on operational experience, primary data from units, mass and energy balance of a facility (>1000 tons per year) (SHYMAN-project, 2015).

## 5.2. Life cycle assessment methods

The environmental assessment for the synthesis of $TiO_2$ nanoparticles was carried out at a set of temperatures 250–400 °C and precursors. It was modelled using the LCA methods (ISO-14040, 2006, ISO-14044, 2006). Laboratory work for the synthesis of $TiO_2$ nanoparticles, literature review and information from the European Union (EU) funded SHYMAN industrial plant is detailed in this section.

### 5.2.1. Scope and goal

Life cycle assessment models were developed to quantify the environmental impacts associated with industrial-scale nano-$TiO_2$ production using five different precursors at five different temperatures. This means that 25 potential variants of the industrial process were assessed in this study. A “cradle-to-gate” scope of LCA was chosen. The system boundary encompassed all inputs and outputs from raw material excavation for production of precursors, process chemicals and energy including transportation and all processes for nano-$TiO_2$ production. Given the diverse uses of nano-$TiO_2$, the specific use was not considered in the present study. Mass and energy balances of nano-$TiO_2$ production, based on experimental investigations for each precursor and temperature combination at the laboratory scale, and specifications of the industrial facility were used as inputs to the life cycle inventory (LCI). LCA results were calculated with SimaPro 8.0.4, using the necessary databases (e.g. Ecoinvent 3 database v.3). In the cases where the information was unknown, literature sources were used alongside, and chemical simulation engineering software (Aspen Hysys V8.4) was also used. Transportation of all precursors was taken into account, considering an average of 200 km. Packaging of the precursor was defined according to the specifications of the suppliers. Due to the scope of this system from

cradle-to-gate, the final product that leaves the system boundaries is an aqueous suspension with different concentrations of nanoparticles. For this reason, a declared unit (instead of a functional unit) was established and was determined as 1 kg nano-$TiO_2$. Environmental impacts were calculated in two impact categories – cumulative energy demand (CED) and global warming potential (GWP). CED is expressed in megajoules per kilogram of product (MJ $kg^{-1}$). GWP was estimated in kilograms of $CO_2$-equivalent per kilogram of product ($CO_2$-eq. per kg), based on the 100-year global warming potential of greenhouse gas (GHG) emissions.

### 5.2.2. Precursor manufacturing

TiOS and $TiCl_4$ were chosen as they are the most basic inorganic precursor salts. TIPO, TiBALD and potassium titanium oxide oxalate dehydrate (PTOOD) were selected as organic alternatives.

Information about the production of precursors is limited, and, as such, the literature was reviewed to determine the processes of production for the five precursors studied.

TiOS can be obtained from the industrial sulfate process for $TiO_2$ production (Figure 5.1). The process uses ilmenite or slag as raw materials commonly, and these are digested in an exothermic reaction:

$$FeTiO_3 + 2H_2SO_4 \rightarrow TiOSO_4 + FeSO_4 + 2H_2O \quad (5.1)$$

The reaction uses an excess of acid between 1.5–1.7 times the mass requirement (Thompson, 1995) . The yield of titanium is about 95%. When ilmenite is used as the raw material, it is necessary to add scrap iron to reduce any ferric iron to ferrous. After digestion the solution passes different separation methods (filtration and decantation) to remove iron and other impurities (Reck and Richards, 1999). A

literature review detailed the material inputs (Katari et al., 1977, Reck and Richards, 1999). Electricity and natural gas inputs for the production of 1 kg of TiOS were evaluated using Aspen Hysys V8.4 software (UNIQUAC property package) (See Appendix).

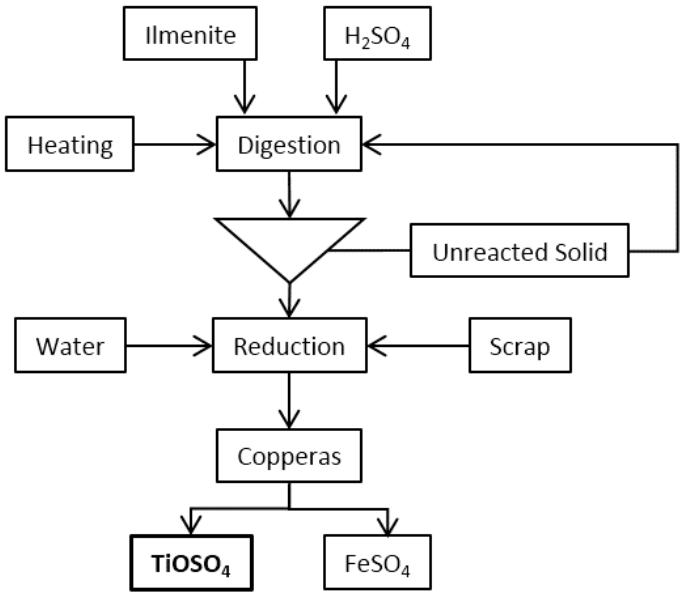



Figure 5.1: Scheme for the production of titanium oxysulfate, which includes the steps of digestion reduction and separation of products.

Table 5.1. Material and energy inputs required for the production of 1 kg of a 15% titanium oxysulfate solution.

| Inputs | |
|---|---|
| Ilmenite (55%$TiO_2$) | 0.14 kg |
| Sulfuric acid (95%) | 0.30 kg |
| Iron | 0.01 kg |
| Water | 0.83 kg |
| Natural Gas | 0.05 MJ |
| Electric Cooling | 0.02 MJ |

$TiCl_4$ is an intermediate product of the chloride process, which generally uses rutile deposits as the raw material. Mineral rutile has a higher percentage of $TiO_2$ content (90–98%) than ilmenite ores (Büchner, 1989), and thus the chloride process produces

less waste than the sulfate method. Firstly, the raw materials (coke, chlorine and rutile) are mixed in a fluidised-bed reactor. The exothermic reaction is maintained at 950 °C. The reaction is:

$$2TiO_2 + 4Cl_2 + 3C \rightarrow 2TiCl_4 + 2CO + CO_2 \quad (5.2)$$

After chlorination, many of the impurities and chlorinated metals are removed as a solid residue. Finally, the gas stream is cooled and the liquid is distilled to form $TiCl_4$ as the final product (Büchner, 1989). Figure 5.2 shows a scheme for $TiCl_4$ manufacturing. Production and purification of $TiCl_4$ were simulated using Aspen Hysys V8.4 (UNIQUAC property package) (See Appendix) according to the literature (Baroch et al., 1955, Francesco et al., 1971) to a defined mass and energy balance, operating at steady state (Table 5.2).

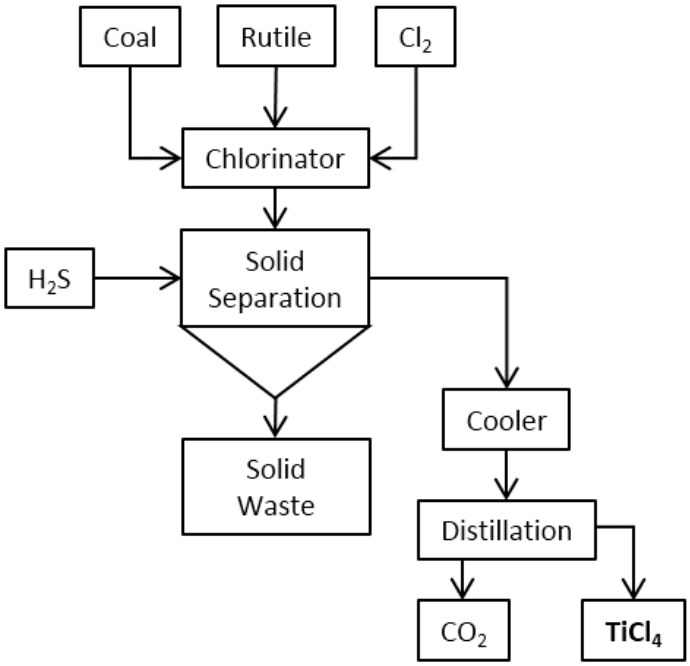



Figure 5.2: Scheme for the production of titanium tetrachloride, including the chlorination process and the stages of separation.

Table 5.2. Material and energy inputs required to produce 1 kg of titanium tetrachloride.

| Inputs | |
|---|---|
| Coal | 0.10 kg |
| Chlorine | 0.75 kg |
| Rutile | 0.43 kg |
| Hydrogen Sulfide | Trace |
| $CO_2$ emission | 0.27 |
| Electric Cooling | 0.03 MJ |

Unfortunately, information about production of TiPO was found to be quite scarce. One of the first methods to produce TiPO was developed by Johannes Nelles in 1940 (Nelles, 1940). Later in 1952, a similar process was described by Bradley and co-workers (Bradley et al., 1952a, Bradley et al., 1952b):

$$TiCl_4 + 4C_3H_8O + 4NH_3 \rightarrow (C_3H_7O_4)Ti + 4NH_4Cl \quad (5.3)$$

According to the literature, the yield is between 72 and 80% (Nelles, 1940, Bradley et al., 1952b). Benzene is used to precipitate the $NH_4Cl$ (Nelles, 1940). The quantity of benzene is not specified, so it was assumed to be a volume equal to the volume of a mixture of 2-propanol (IPA) and $TiCl_4$. The recovery of benzene and IPA was simulated using Aspen Hysys V8.4 (UNIQUAC property package) to quantify the energy used during the separation process (See Appendix). Figure 5.3 and Table 5.3 detailed the process and the energy and material the requirements to produce TiPO.

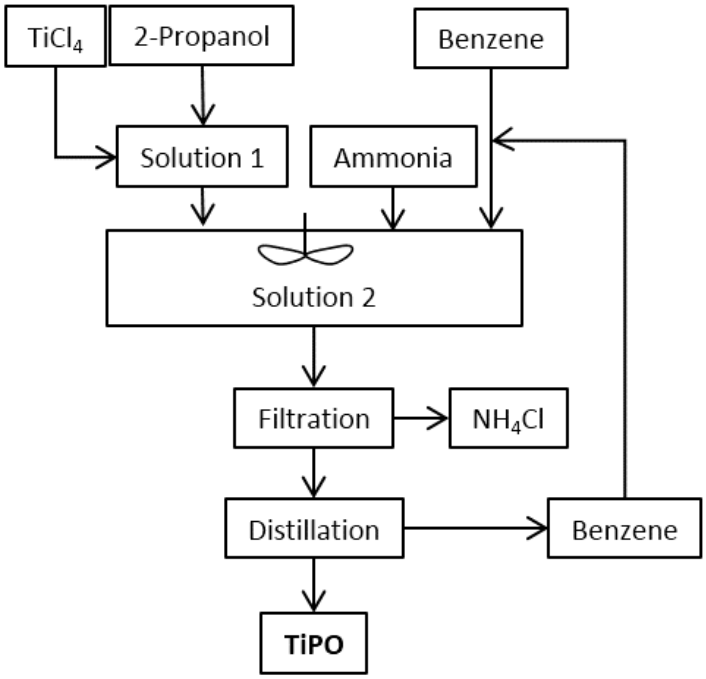



Figure 5.3: Scheme for the production of titanium isopropoxide according to the literature with the stages of mixing and separation.

Table 5.3. Material and energy inputs required to produce 1 kg of titanium isopropoxide.

| Inputs | |
|---|---|
| $TiCl_4$ | 0.83 kg |
| 2-Propanol | 1.05 kg |
| Ammonia | 0.30 kg |
| Benzene | 1.60 kg |
| Natural Gas | 1.19 MJ |
| Electricity | 0.03 MJ |

TiBALD can be synthesized with TiPO, lactic acid and aqueous ammonia solution in water (Ohya et al., 2004). Firstly, both TiPO and lactic acid are mixed at a ratio of 1:2. The addition of water results in a precipitate which re-dissolves under stirring. Finally, ammonia is added, such that the full process can be described in Figure 5.4 - reaction (5.4):

$$2NH_4OH + 2C_3H_6O_3 + (C_3H_7O)_4Ti \rightarrow (C_2H_4(O\text{-})CO_2NH_4)_2Ti(OH)_2 + 4C_3H_8O \quad (5.4)$$

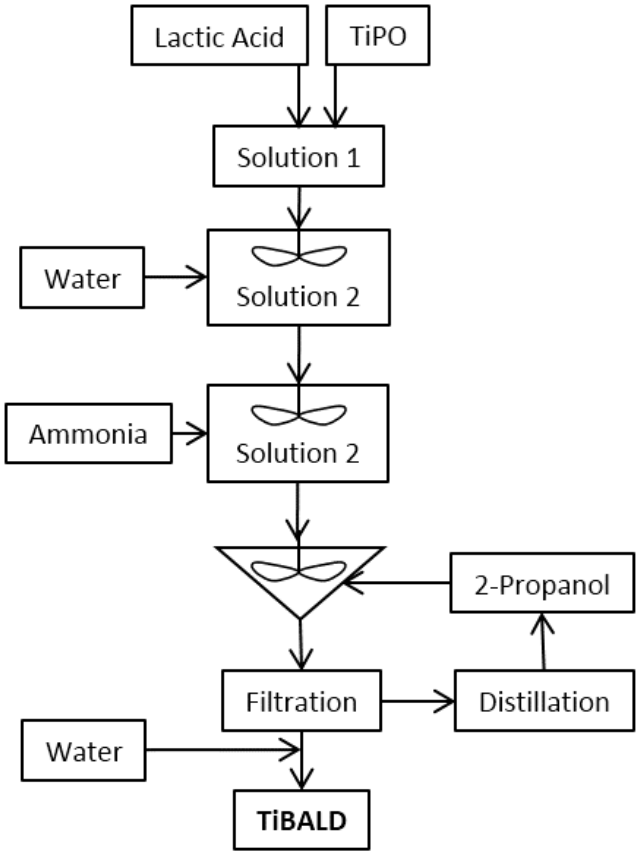



Figure 5.4: Scheme for the production of titanium bis(ammonium lactato) dihydroxide, which includes the inlets of lactic acid and ammonia, the precipitation with 2-propanol and the separation stages.

According to the literature, the yield is 80% (Van de Velde et al., 1974). The stirring energy was estimated by establishing a scaling factor between an industrial stirring system (1 hour stirring 500 litres is 0.25 kW) and the solution volume. The distillation to recover the IPA was simulated by using Aspen Hysys V8.4 (NTRL property package) (See Appendix). Table 5.4 details the inputs to produce 1 kg of TiBALD.

Table 5.4. Material and energy inputs required to produce 1 kg of bis(ammonium lactato) dihydroxide.

| Inputs | |
|---|---|
| TiPO | 0.63 kg |
| Lactic Acid | 0.40 kg |
| Water | 3.78 kg |
| Ammonia (28%) | 0.26 kg |
| 2-Propanol | 0.30 MJ |
| Natural Gas | 9.18 MJ |
| Electric Stirring | 0.15 MJ |

PTOOD can be synthesised in a similar way to TiPO (Figure 5.5). $TiCl_4$, oxalic acid, potassium hydroxide and water are used as reagents (Brisse and Haddad, 1977). Firstly, aqueous solutions of $TiCl_4$ and oxalic acid are mixed, followed by the slow addition of potassium hydroxide. With the formed complex precipitated by the addition of ethanol:

$$TiCl_4 + 2C_2O_2(OH)_2 + 2KOH + H_2O \rightarrow (C_2O_4K)_2TiO{\cdot}2H_2O + 4HCl \quad (5.5)$$

The reactants were adjusted at equimolar values for mass balance. Oxalic acid input production was defined according to literature review (Sullivan et al., 1983). Ethanol distillation was simulated by using Aspen Hysys V8.4 (UNIQUAC property package) (See Appendix), while stirring stages were calculated as mentioned previously. All inputs considered in the production of PTOOD titanium precursor are detailed in Table 5.5.

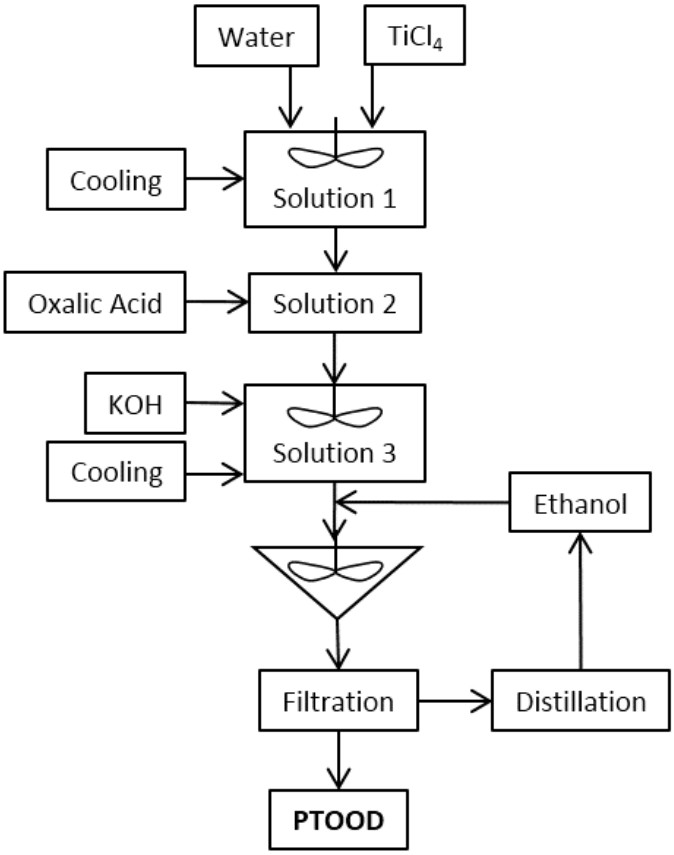



Figure 5.5: Scheme for the production of potassium titanium oxide oxalate dehydrate, which includes all production and separation stages.

Table 5.5. Material and energy inputs required to produce 1 kg of potassium titanium oxide oxalate dehydrate.

| Inputs | |
|---|---|
| $TiCl_4$ | 0.54 kg |
| Water | 8.47 kg |
| Oxalic Acid | 0.51 kg |
| KOH | 0.33 kg |
| Ethanol | 0.01 kg |
| Natural Gas | 21.96 MJ |
| Electric Stirring | 0.04 MJ |
| Electric Cooling | 0.74 MJ |

### 5.2.3. Laboratory synthesis of titania nanoparticles

Laboratory synthesis (Figure 5.6) was widely described in Chapter 3 Experimental. Briefly, five different precursors were selected to synthesise nano-$TiO_2$ nanoparticles with the nozzle reactor; TiOS, $TiCl_4$, TiPO, TiBALD and PTOOD. Deionised water and 2-propanol (IPA or isopropanol) were used as solvents depending on the water sensitivity of the precursor. Deionised water was used as the heated downflow when TiOS, $TiCl_4$ and TiPO were pumped into the system. For TiBALD and PTOOD the hot stream was a solution of water with a 5 volume% solution of hydrogen peroxide ($H_2O_2$) to ensure the decomposition of the organic components of the WSTC precursors. The pressure of the system was established at 240 bar, while the temperature for the reaction was varied from 200 °C to 400 °C at increments of 50 °C (200, 250, 300, 350 and 400 °C). The flows were consistent for each reaction at 20 ml $min^{-1}$ for the downflow and 10 ml $min^{-1}$ for the precursor stream. Samples were treated in order to dry before further characterisation (Chapter 3).

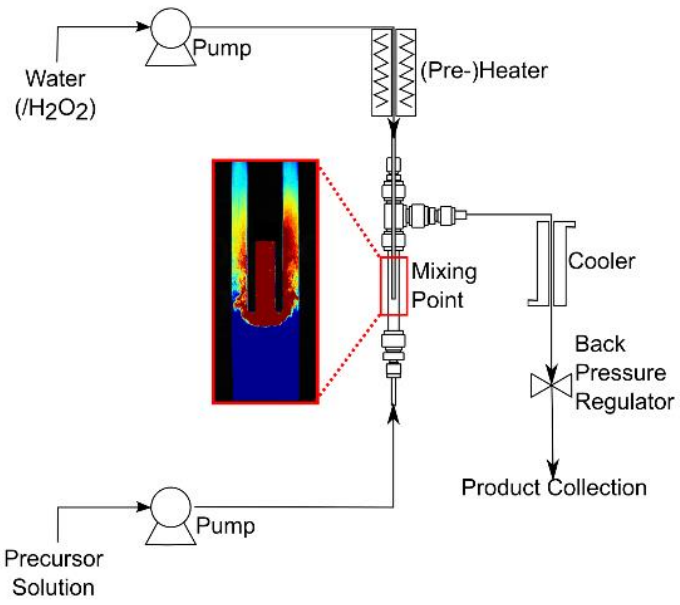



Figure 5.6: Simplified schematic of the counter-current continuous-flow hydrothermal reactor.

### 5.2.4. Scale-up for the production of titania nanoparticles by CFHS

The information necessary for the scale-up of production of nano-$TiO_2$ was analysed and agreed by the chemical engineers of the plant and the chemist experts of the laboratory. The precursor concentration was fixed at 0.05 M at the laboratory scale, as the production of titania with this concentration is known within the group to result in high collection efficiencies with little chance of blockages. The industrial plant, with larger diameter tubing and higher flow rates, is capable of operating at higher concentrations of the precursor. According to industrial design specifications, the plant is able to operate with a precursor concentration higher than 0.5 M. However, for this study the precursor concentration used in the calculations was established as 0.5 M. The increase of the precursor concentration could be carried out in future, according to the work experience, which would provide further reductions in the environmental impact of CFHS and CFSS.

The scale-up has an inherent benefit over the laboratory and pilot scale, due to the energy recovery. In the industrial plant, a high-pressure heat exchanger recovers around 50% of energy. The outlet and inlet streams of the reactor are crossed in the heat exchanger, reducing the requirements of natural gas and associated (GHG) emissions.

For the industrial scenario, separation is carried out by sedimentation. Depending on the precursor and temperature, nitric acid was needed to precipitate the nanoparticles (see Table 5.6). In the scale-up, sulfuric acid ($H_2SO_4$) was selected for the same cases that needed an acid solution. It has been proven in the laboratory that sulfuric acid is able to precipitate nanoparticles as well and, due to its low cost, is most likely to be used in an industrial setting.

After sedimentation, the product is washed with deionised water to remove organic and unreacted compounds, impurities, etc. A second sedimentation is carried out to remove wastewater from the washed nanoparticles. Depending on the precursor and the pH of the wastewater from the process, sodium hydroxide (NaOH) may be needed to neutralize it prior to release. The pH and quantity of NaOH necessary for neutralisation were determined by the chemical acid–base equilibrium laws. The wastewater is neutralized to a pH over 5 before purification in a water treatment plant.

In this study, the boundaries establish a highly concentrated suspension of nano-$TiO_2$ in water as a final product. The wide range of possible applications could require a suspension of nanoparticles or dried nano-$TiO_2$. The last case would involve another stage such as vacuum evaporation, filtration, etc., which could be evaluated and added to our environmental assessment.

The whole process is a closed system; the precursors are dissolved in water and the reaction occurs in a closed reactor. Sedimentation uses a closed tank and results in no emissions into the air. The only emission considered is the release of nanoparticles (1%) into the wastewater before treatment in the water treatment plant (<120 mg $l^{-1}$). According to literature review, a primary water treatment could reduce more than 90% of the concentration of nanoparticles of $TiO_2$ (Honda et al., 2014), so that after the water treatment, the concentration would be lower than 12 mg $l^{-1}$. A recent cytotoxicity assessment was carried out as a collaboration between the SHYMAN and NANOMILE projects which showed that similar concentrations of $TiO_2$ nanoparticles have no toxic effect on HepaRG cells (Nanomile, 2016). In addition, human studies conducted so far do not suggest an association between occupational

exposure to titanium dioxide and an increased risk of cancer (J. Prochazka, personal communication). Figure 5.7 shows the process flow for the industrial scale continuous flow system.

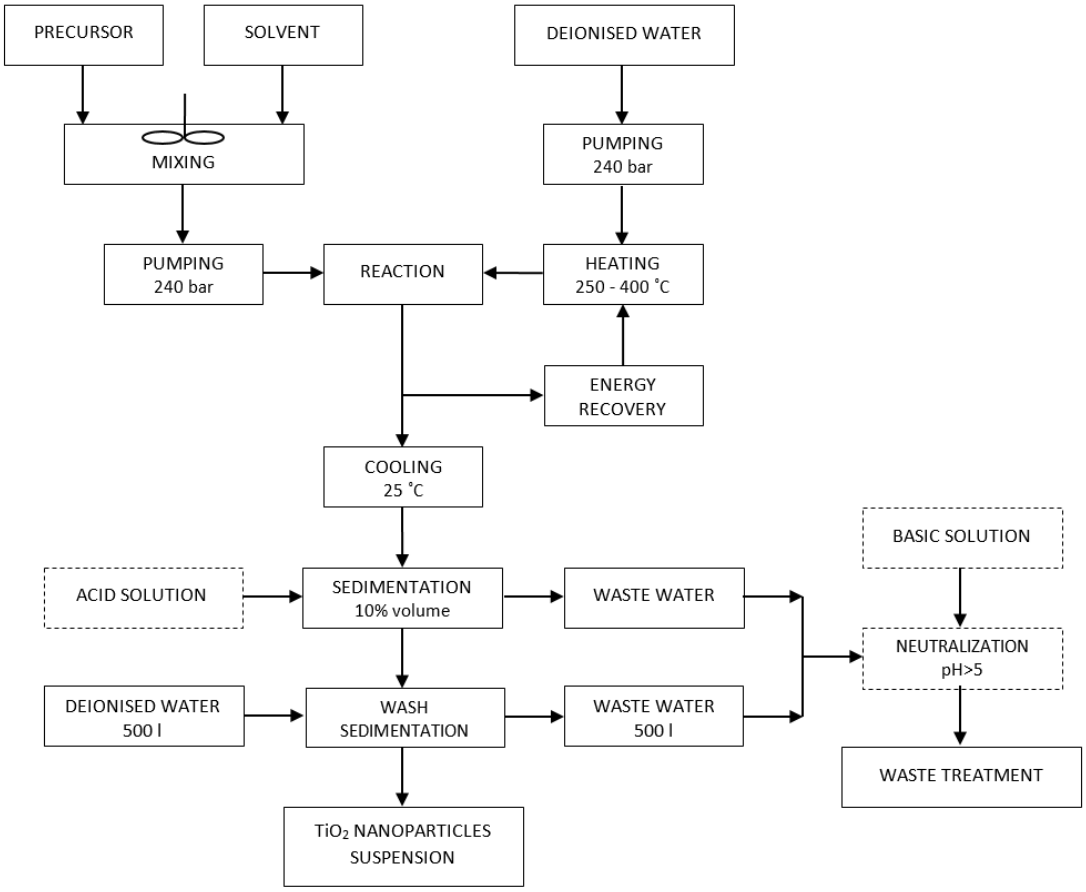



Figure 5.7: Scheme for the large-scale continuous-flow production of titania nanoparticles.

## 5.3. Results and discussion

### 5.3.1. Phase and crystallinity

The powder X-ray diffraction patterns of the obtained materials from all syntheses are shown in Figure 5.8. Samples prepared from $TiCl_4$ show a small peak at a Bragg angle of 31° which can be attributed to brookite (ICDD 01-076-1934). A small

percentage of brookite was also found when the pH was lower than 1 and titanium tetrachloride was used as a precursor (Malinger et al., 2011), consistent with our own observations here. All other diffraction patterns correspond to the anatase phase of titania (ICDD 01-078-2486). A number of samples, notably those prepared from TiPO at 200 and 250 °C and TiBALD at 350 °C, also present extremely broad features centred around 30° 2v, which may be assigned to amorphous titania.

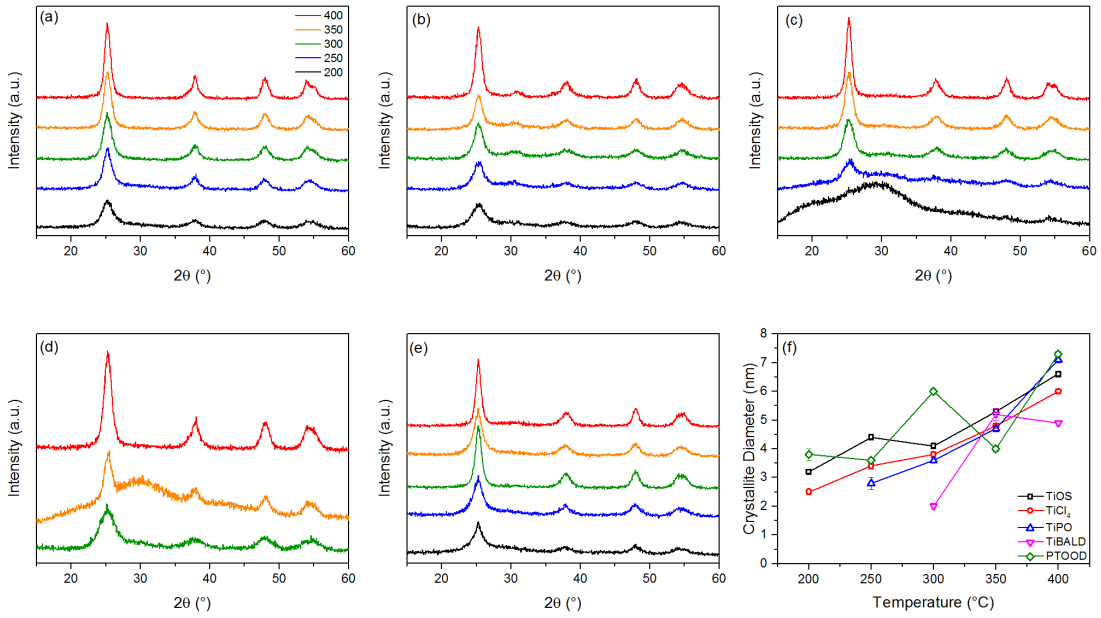



Figure 5.8: Powder X-ray diffraction patterns of products obtained at varying reaction temperatures from five different precursors: (a) titanium oxysulfate, (b) titanium tetrachloride, (c) titanium isopropoxide, (d) titanium bis(ammonium lactato) dihydroxide and (e) potassium titanium oxide oxalate; and (f) the corresponding calculated crystallite diameters.

TEM images show that an increase in synthesis temperature results in an increase in crystallinity of the obtained nanoparticles (see Figure 5.9). The products from all precursors at lower temperatures typically form highly agglomerated clusters, which prohibits accurate size determination using image analysis. Products from higher synthesis temperatures are more crystalline and typically less agglomerated.

Generally, anatase, as the kinetically favoured phase, is the expected product of rapid CFHS and CFSS conditions. The use of $TiCl_4$ as a precursor negatively affects the purity of the final product due to the generation of the brookite phase. Amorphous nanoparticles are produced if the reaction temperature is too low for the precursor type.

Table 5.6. Summary of the properties of products obtained from the lab-scale continuous flow synthesis of titania nanoparticles. An. = anatase, B. = brookite, Am. = amorphous.

| Precursor | Type of Synthesis | Temperature (°C) | Precipitant | Phase | Weight Loss (%) | Yield (%) | XRD Size (nm) | TEM Size (nm) |
|---|---|---|---|---|---|---|---|---|
| TiOS | Hydrothermal | 200 | | An. | 37 | 69 | 3.2 | - |
| | | 250 | | An. | 24.5 | 100 | 4.4 | - |
| | | 300 | | An. | 19.3 | 100 | 4.1 | 5.1 ± 1.4 |
| | | 350 | | An. | 14.5 | 98 | 5.3 | 6.1 ± 1.7 |
| | | 400 | | An. | 15.0 | 100 | 6.6 | 9.4 ± 3.1 |
| $TiCl_4$ | Solvothermal | 200 | ✓ | An. | 30.6 | 45 | 2.5 | - |
| | | 250 | ✓ | An. | 16.9 | 55 | 3.4 | - |
| | | 300 | ✓ | An./ B. | 16.3 | 56 | 3.8 | 6.2 ± 1.3 |
| | | 350 | ✓ | An./ B. | 16.9 | 67 | 4.8 | 6.6 ± 2.2 |
| | | 400 | ✓ | An./ B. | 17 | 77 | 6.0 | 7.7 ± 1.6 |
| TiPO | Solvothermal | 200 | | Am. | 10.6 | 87 | - | - |
| | | 250 | | An./ Am. | 11.5 | 98 | 2.8 | |
| | | 300 | | An. | 11.9 | 97 | 3.6 | 4.7 ± 1.3 |
| | | 350 | ✓ | An. | 10.5 | 93 | 4.7 | 6.5 ± 1.8 |
| | | 400 | ✓ | An. | 8.8 | 67 | 7.1 | 7.5 ± 2.4 |
| TiBALD | Hydrothermal | 200 | ✓ | An./ Am. | 34 | 30 | - | |
| | | 250 | ✓ | An./ Am. | 30.6 | 56 | - | |
| | | 300 | ✓ | An. | 29 | 72 | 2.0 | 6.2 ± 1.8 |
| | | 350 | | An. | 12.8 | 75 | 5.2 | - |
| | | 400 | | An. | 8.3 | 93 | 4.9 | 6.2 ± 1.6 |
| PTOOD | Hydrothermal | 200 | ✓ | An./ Am. | 45.5 | 55 | 3.8 | - |
| | | 250 | ✓ | An. | 28.5 | 64 | 3.6 | - |
| | | 300 | ✓ | An. | 23 | 78 | 6.0 | 7.5 ± 2.1 |
| | | 350 | | An. | 11.5 | 83 | 4.0 | 5.8 ± 1.5 |
| | | 400 | | An. | 6.5 | 88 | 7.3 | 7.9 ± 2.0 |

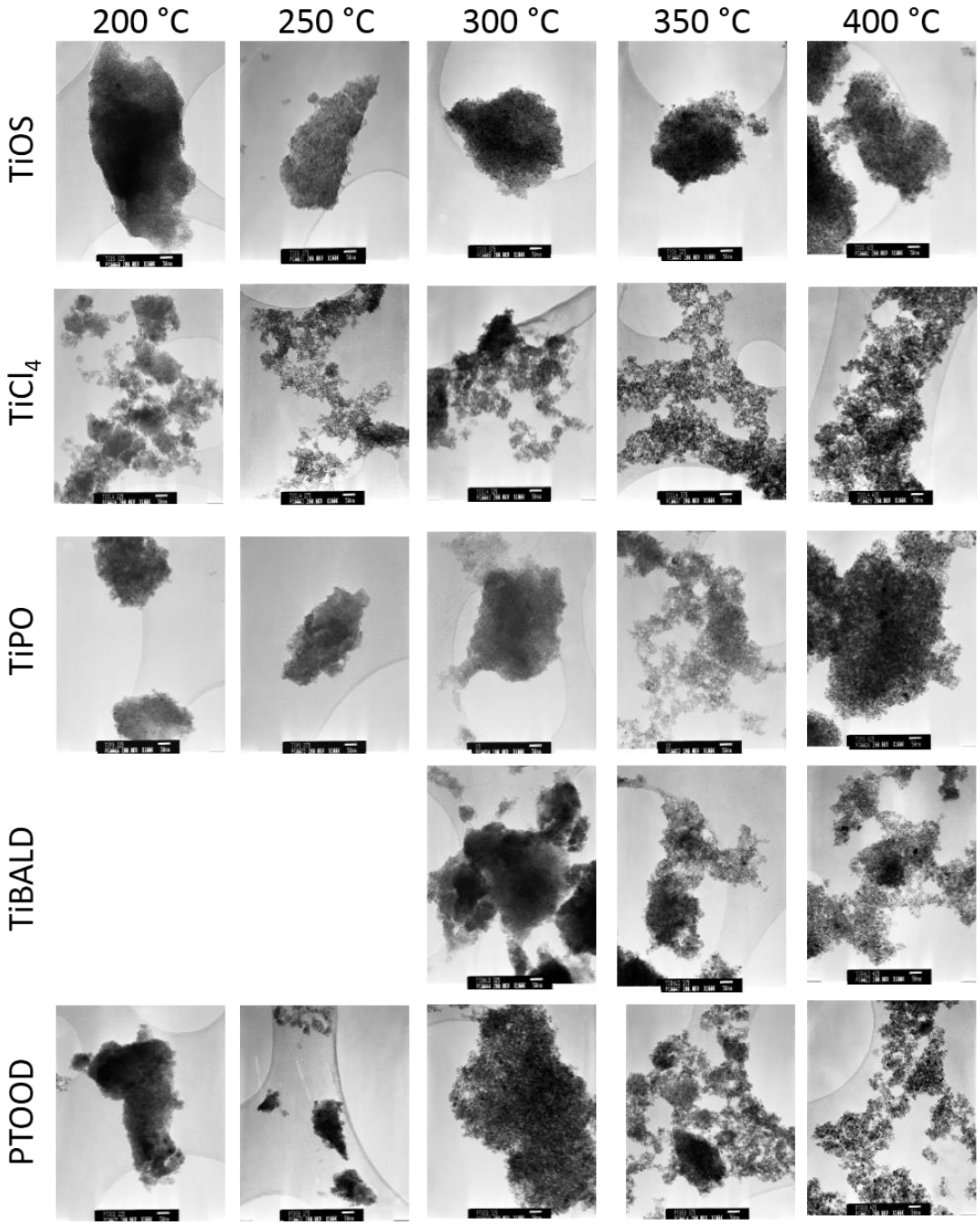



Figure 5.9: Representative TEM images of all samples acquired.

### 5.3.2. Size

The calculated crystallite diameters from the XRD analysis are shown in Figure 5.8 (f). In all cases the crystallite sizes are calculated to be between 2.5 and 8 nm. There is a general trend towards increasing crystallite diameter with increasing temperature.

TEM images confirm similar results to the XRD; an increase in reaction temperature leads to an increase in the size of the nanoparticles (see Figure 5.9). TEM images and the corresponding size distributions are shown in Figure 5.10 for samples prepared at 400 °C from all precursors. In all cases the measured particle sizes were between 3 and 20 nm. The sample prepared from TiOS at 400 °C showed the largest mean particle size at 9.4 nm, as well as the broadest distribution. All other samples prepared at 400 °C, with the exception of those obtained from the reaction of TiBALD, exhibited mean particle sizes between 7.5 and 8 nm. The product from TiBALD at 400 °C shows both the smallest particles and the tightest size distribution, with sizes of 6.2 ± 1.6 nm. TEM size distributions, where possible, of all samples are provided in the Figure 5.11.

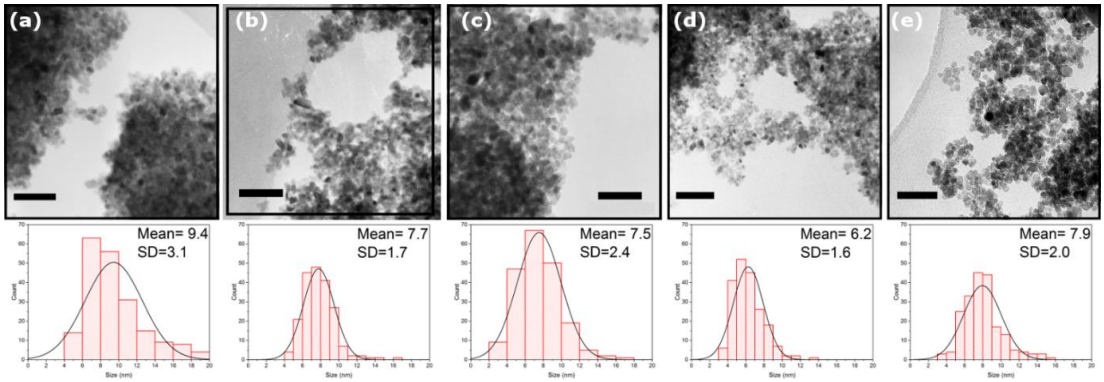



Figure 5.10: TEM images and corresponding size distributions (n = 200) of samples prepared at 400 °C from (a) titanium oxysulfate, (b) titanium tetrachloride, (c) titanium isopropoxide, (d) titanium bis(ammonium lactato) dihydroxide and (e) potassium titanium oxide oxalate. Scale bars represent 50 nm.

## Chapter 5

Nanoparticles of $TiO_2$ were synthesised in a range of temperatures of 120–220 °C by a continuous hydrothermal process, concluding that an increase of temperature leads to an increase of size and crystallinity (Malinger et al., 2011), but at the expense of an increase in energy consumption. Our XRD and TEM results suggest similar conclusions i.e. higher temperatures lead to bigger and more crystalline nanoparticles. Obviously the demand of energy is higher when the temperature increases, but this affirmation should be estimated by kilograms of nano-$TiO_2$, because an increase of temperature could also increase the yield of the precursors (Hobbs et al., 2009). The use of different precursors leads to differences in the nano-$TiO_2$ product. A complex organic precursor like TiBALD generates small, non-agglomerated and highly crystalline nanoparticles, whilst the use of simple inorganic precursors like TiOS produces the biggest nanoparticle size and the broadest size distributions.

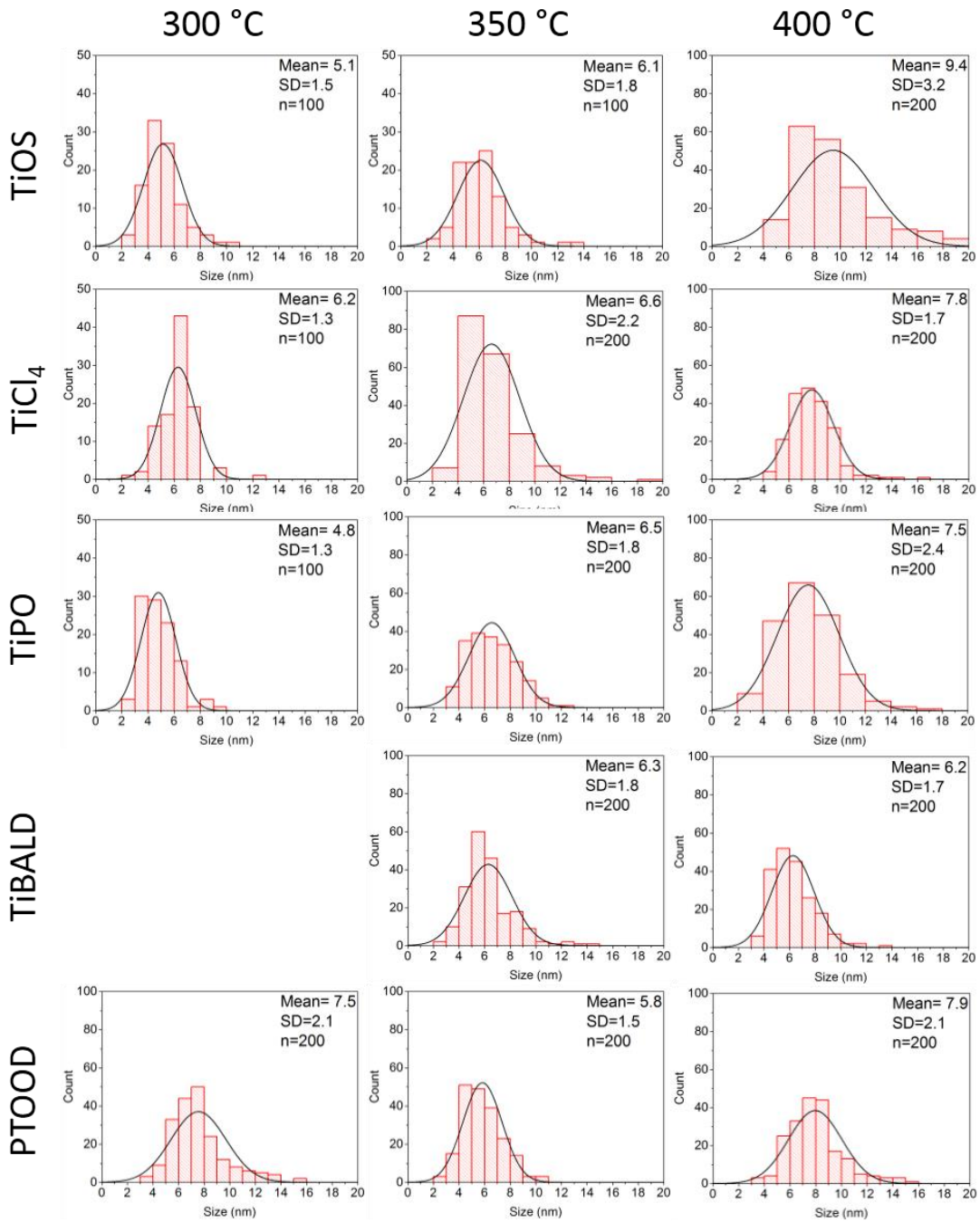



Figure 5.11: Size distribution histograms of all samples where possible.

### 5.3.3. Yield

The solids obtained were subjected to thermogravimetric analysis, as shown in Figure 5.12 (a–e). All samples show some degree of mass loss, as would be expected, but the nature of the weight loss can be used as an indicator of downstream separation/wastewater processing issues. Samples prepared from TiOS at temperatures of 200 and 250 °C show a gradual weight loss up to ~130 °C due to the loss of surface bound water and hydroxides, followed by a small sharp weight loss at 330 °C which may be due to adsorbed $CO_2$. An additional weight loss step between 520 and 640 °C is attributed to the loss of $SO_2$ from the residual sulfate species. Samples prepared at higher temperatures of 300, 350 and 400 °C show a faster weight loss at low temperatures due to the removal of physisorbed water, while the $SO_2$ weight loss is significantly lessened. Samples prepared from $TiCl_4$ all show a sharp weight loss up to 100 °C with a further extended weight loss up to 300 °C ascribed to the loss of physisorbed and chemisorbed water and hydroxide groups, respectively. The total weight losses are typically 15–17%, with the exception of the sample prepared at 200 °C which loses 30% of its initial mass on heating to 900 °C in a TGA. Samples prepared from TiPO all show similar thermal behaviour, with only slight weight losses of ~10% up to temperatures of 350 °C. It is worth noting that samples prepared at reaction temperatures less than 350 °C all show a weight loss, suggesting only adsorbed water (<300 °C) while those prepared at 350 and 400 °C show an additional step which is likely due to dehydroxylation. Samples prepared from both WSTCs, TiBALD and PTOOD, at temperatures of 200–300 °C show significant weight losses between 28 and 47%, largely resulting from the high water content and incomplete breakdown of the organic counter ion. At higher synthesis temperatures, weight losses are between just 5 and 10% and can be attributed solely

to the dehydration and dehydroxylation of the nanopowders. These results indicate that the increase of temperature reduces the amount of impurities in the post-reaction product, which are washed away in the later stages of the process.

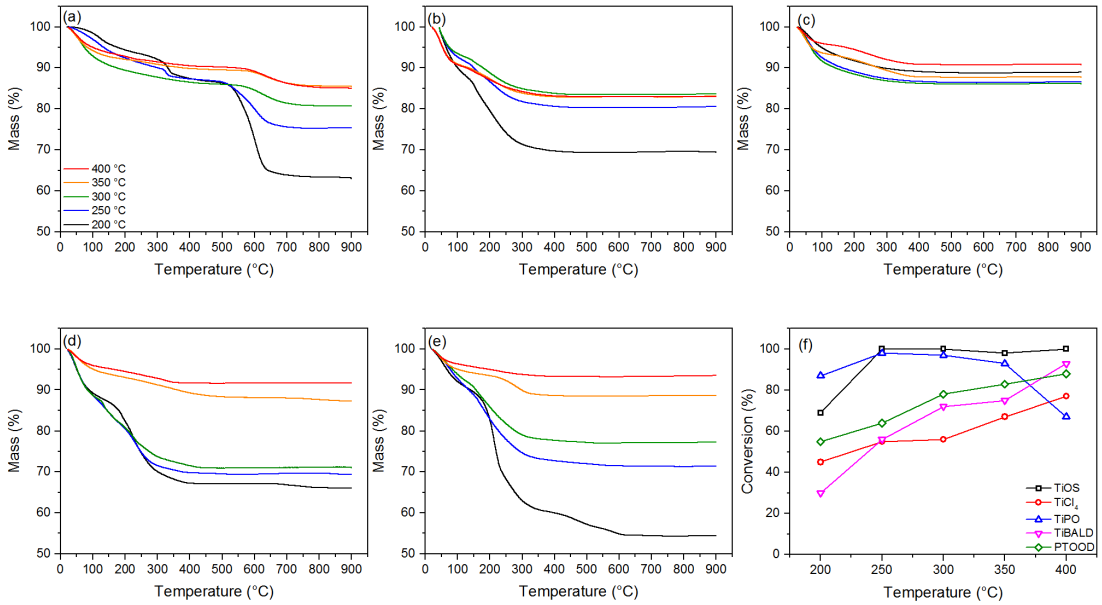



Figure 5.12: Thermogravimetric traces of products obtained at varying reaction temperatures from five different precursors: (a) titanium oxysulfate, (b) titanium tetrachloride, (c) titanium isopropoxide, (d) titanium bis(ammonium lactato) dihydroxide and (e) potassium titanium oxide oxalate; and (f) the % conversion for each synthesis.

It is reasonably assumed that the final mass after TGA analysis is pure $TiO_2$. The temperature reached 900 °C, removing all organic impurities and water content. The initial mass of the solid obtained after drying is adjusted according to these TGA results to ascertain an accurate conversion. The % yield as a function of temperature is shown in Figure 5.12 (f) for all precursors. It is generally observed that increasing the temperature of the reaction, regardless of the precursor, results in fewer impurities and a higher conversion. The sole exception to this is TiPO, which shows a significantly decreased ongoing yield from 350 °C (93%) to 400 °C (67%). The

reactions involving TiPO were carried out in IPA, the critical point of which is 235 °C and 53 bar. When the temperature of mixing in the reactor is around this point the particle size can drop (Toft et al., 2009), while in our case it has been demonstrated that the yield decreased. $TiCl_4$, which also uses IPA as a solvent, exhibits low yield for all temperatures. This suggests that the use of IPA leads to lower conversion, relative to water. Also, the use of water is associated with a lower environmental impact than the organic solvent. The WSTC precursors (PTOOD and TiBALD) have high yield (>70%) when the system operates above 300 °C. Of the five precursors studied, only TiOS shows good conversions across all synthesis temperatures, with 100% yield achieved above 200 °C.

The general properties and characteristics of all products are summarised in Table 5.6.

### 5.3.4. Cumulative energy demand and global warming potential

Cumulative energy demand (CED) and global warming potential (GWP), quantified on a cradle-to-gate basis, vary substantially between the nano-$TiO_2$ production routes (Figure 5.13 and 5.14, respectively) (Tables 5.7 and 5.8). Generally, the precursor is found to be the main contributing factor to CED for the organic precursors, as shown in Figure 5.13. Also, precursors which result in low yield and which contain organic components or solvent significantly increase the CED values. TiBALD, which is a third generation precursor (prepared from TiPO, which is itself prepared from $TiCl_4$), has the highest CED values, from 1952 to 6157 MJ $kg^{-1}$ $TiO_2$ depending on the synthesis temperature/conversion. On the other hand, TiOS has CED values between 102 and 149 MJ $kg^{-1}$ $TiO_2$. This is predominantly due to the fact that TiOS manufacturing requires fewer production steps and thus less energy.

Low yield extends production time, increasing the quantity of precursors, energy, solvents, etc. which are crucial during production. For example, using TiPO at 400 °C, with a yield to $TiO_2$ of just 67%, results in a higher CED than the same precursor at other temperatures where the yield is up to 90% (Figure 5.13 (c)).

According to the yield conclusions, it could be similarly suggested that working at higher concentrations, the energy and solvent requirements would be reduced significantly by the production of a higher quantity of product. The increase of the concentration has a clear and important limitation, i.e. potential blockages in the industrial plant. A blockage would produce a huge loss of solvents, materials, energy etc., as well as large generation of waste.

Process chemicals also represent significant life cycle energy requirements for some nano-$TiO_2$ pathways. The use of the IPA as a solvent, i.e. when using TiPO and $TiCl_4$ precursors, contributes between 100 and 172 MJ $kg^{-1}$ $TiO_2$. The bulk of this energy consumption is related to the distillation process used to recover the isopropanol, post-production. Precursors compatible with water as the solvent avoid this significant energy demand (TiOS; TiBALD; PTOOD). The use of acid to precipitate nanoparticles, as is required for all $TiCl_4$ preparations and several others (see Table 5.6) requires additional input of sulfuric acid as well as a subsequent neutralization stage and higher energy demands for wastewater treatment. For this reason the post-processing and wastewater treatment stages can make a significant contribution to CED for some nano-$TiO_2$ production routes. For PTOOD, acid addition is necessary for precipitation at reaction temperatures below 350 °C, contributing an additional ~80 MJ $kg^{-1}$ $TiO_2$ to CED compared to production at higher temperatures that do not require acid addition.

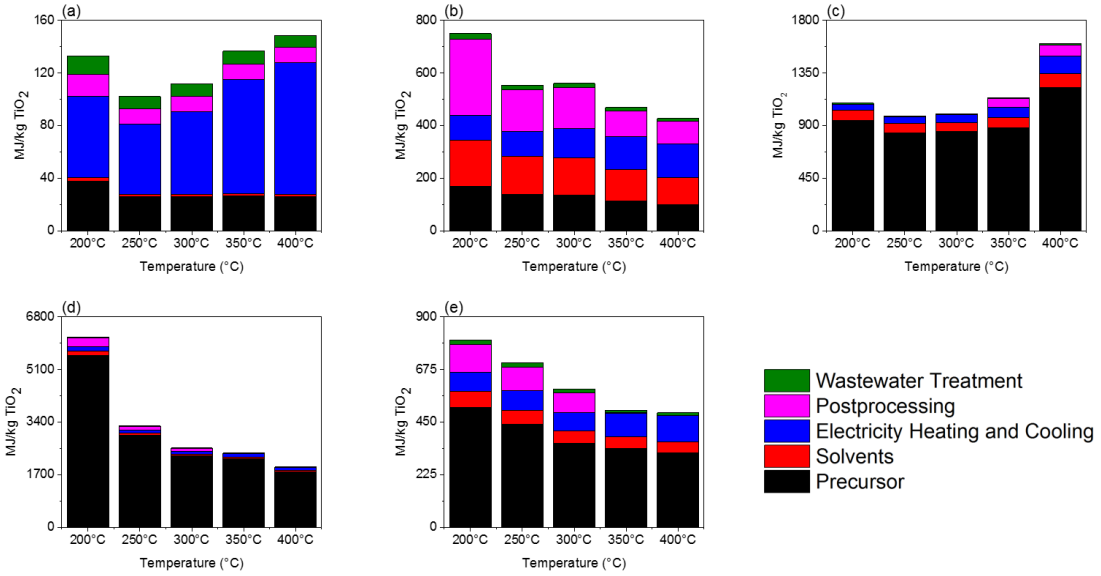



Figure 5.13: The cumulative energy demand (CED) to produce 1 kg of titania nanoparticles at each synthesis temperature from: (a) titanium oxysulfate (b) titanium tetrachloride, (c) titanium isopropoxide, (d) titanium bis(ammonium lactato) dihydroxide and (e) potassium titanium oxide oxalate.

Nano-$TiO_2$ production from the TiOS precursor was found to have the lowest CED, ranging from 102 to 149 MJ $kg^{-1}$ for the reaction temperatures considered in this study. This arises from a combination of a number of favourable parameters: TiOS is a "first generation" precursor with low energy requirements; it is compatible with water as a solvent; it has a yield of ~100% when reacted at 250 °C; and does not require acid inputs for precipitation. Here the electricity, heating and cooling section is the most demanding in terms of energy. The CED increases from 53 to 100 MJ $kg^{-1}$ $TiO_2$, when the temperature increases from 250 to 400 °C. In contrast, the CED for TiPO and TiBALD is an order of magnitude larger, due primarily to the energy-intensity of precursor materials and, to a lesser extent, the use of IPA as a solvent (TiPO) and acid-assisted precipitation.

Our results indicate that nano-$TiO_2$ production can be achieved with similar life cycle energy expenditure as reported for micron-size $TiO_2$, which ranges from 75 to 110 MJ $kg^{-1}$ (Reck and Richards, 1999, Middlemas et al., 2015). Given that the production of micro-size particles is comparatively less demanding, these results indicate that CFHS can be an energy-efficient means of producing nano-$TiO_2$. Only the Altair process (studied by Grubb and Bakshi) was able to produce nano-$TiO_2$ of 40 nm, with a CED value of approximately 105 MJ $kg^{-1}$ $TiO_2$. However, the authors highlight certain omissions and incomplete data inputs (Grubb and Bakshi, 2011) and so their results may underestimate the impact of the Altair process.

The GWP of each system, as shown in Figure 5.14, shows similar trends as the CED analysis. Key factors affecting GHG emissions include the choice of precursor (TiPO, TiBALD, and PTOOD are associated with relatively high GWP), the use of isopropanol as a solvent, and additional process steps associated with acid-assisted precipitation. As a consequence, the TiBALD production route results in the highest GHG emissions, from 85.5 to 276.8 kg $CO_2$-eq. per kg $TiO_2$ depending on the reaction temperature. On the other hand, TiOS gives the lowest emissions, of only 8.8 to 11.9 kg $CO_2$-eq. per kg $TiO_2$. The GWP values for TiPO, PTOOD and $TiCl_4$ range between 29 and 75 kg $CO_2$-eq. per kg $TiO_2$ depending on conversion, the use of NaOH to neutralize the effluent or the use of IPA.

Previous synthesis by the sol–gel method used TiPO as precursor for the production of 30 nm anatase nanoparticles (Pini et al., 2015). The GWP impact of this process for 1 kg of $TiO_2$ nanoparticles is approximately 48 kg of $CO_2$-eq. With CFSS, the TiPO precursor has emissions between 40.3 and 73.7 kg $CO_2$-eq. per kg of $TiO_2$. This indicates that the use of both an organic precursor and a solvent is not as beneficial, independent of the process used.

The only reported GWP emissions similar to our results for TiOS are from the ARTS process (7.47 kg $CO_2$-eq. per kg $TiO_2$) (Middlemas et al., 2015) and traditional sulfate and chloride processes (5.31 and 6.85 kg $CO_2$-eq. per kg $TiO_2$) (Weidema et al., 2013), but they produced $TiO_2$ of micron-size instead of nano-size.

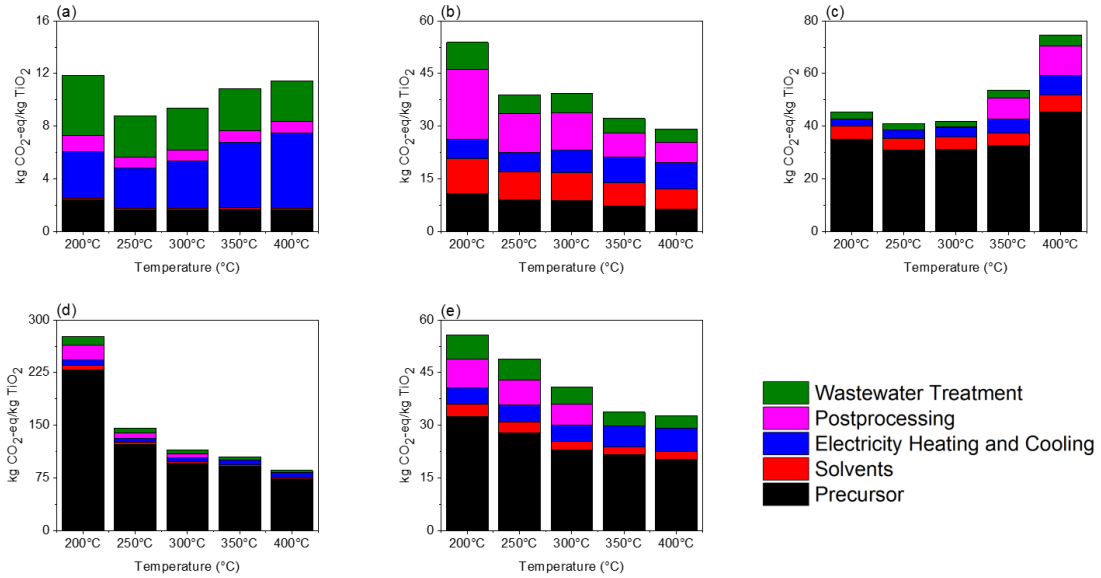



Figure 5.14: The global warming potential (GWP) to produce 1 kg of titania nanoparticles at each synthesis temperature from: (a) titanium oxysulfate (b) titanium tetrachloride, (c) titanium isopropoxide, (d) titanium bis(ammonium lactato) dihydroxide and (e) potassium titanium oxide oxalate.

Table 5.7. Cumulative energy demand values in MJ $kg^{-1}$ $TiO_2$ for all of the precursors and temperatures at industrial-scale production. Temp. = Temperature, Pre. = Precursor, IPA = Isopropanol, IPA dis. = Isopropanol distillation, $H_2O_2$ = Hydrogen Peroxide, Pack. = Packaging, Trans. = Transport, DIW = Deionised Water, Elec. = Electricity, H&C = Heating and Cooling, CP = Cleaning process, PP = Postprocessing, Wash = Washing, Neu. = Neutralization and WWT = Water waste treatment.

| Precursor | Temp. (°C) | Pre. | IPA | IPA dis. | $H_2O_2$ | Pack. | Trans. | DIW | Elec. | H&C | CP | PP | Wash | Neu. | WWT |
|---|---|---|---|---|---|---|---|---|---|---|---|---|---|---|---|
| TiOS | 200 | 26.7 | - | - | - | 4.7E-02 | 10.8 | 2.7 | 15.4 | 46.5 | 2.2E-02 | 0.2 | 0.7 | 16.2 | 13.7 |
| | 250 | 18.4 | - | - | - | 3.2E-02 | 7.5 | 1.9 | 10.6 | 42.6 | 1.1E-02 | 0.1 | 0.5 | 11.2 | 9.5 |
| | 300 | 18.4 | - | - | - | 3.2E-02 | 7.5 | 1.9 | 10.6 | 52.3 | 1.1E-02 | 0.1 | 0.5 | 11.2 | 9.5 |
| | 350 | 18.8 | - | - | - | 3.3E-02 | 7.6 | 1.9 | 10.8 | 75.8 | 1.1E-02 | 0.1 | 0.5 | 11.4 | 9.7 |
| | 400 | 18.4 | - | - | - | 3.2E-02 | 7.5 | 1.9 | 10.6 | 89.3 | 1.1E-02 | 0.1 | 0.5 | 11.2 | 9.3 |
| $TiCl_4$ | 200 | 171.3 | 7.5 | 164.1 | - | 3.0E-02 | 3.0 | 3.2 | 23.6 | 71.3 | 3.3E-02 | 61.7 | 1.1 | 225.2 | 22.7 |
| | 250 | 140.2 | 6.1 | 134.3 | - | 2.5E-02 | 2.5 | 2.6 | 19.3 | 77.4 | 2.2E-02 | 33.7 | 0.9 | 122.8 | 16.5 |
| | 300 | 137.6 | 6.0 | 131.9 | - | 2.4E-02 | 2.4 | 2.6 | 19.0 | 93.3 | 2.2E-02 | 33.1 | 0.9 | 120.6 | 16.2 |
| | 350 | 115.1 | 5.0 | 110.3 | - | 2.0E-02 | 2.0 | 2.1 | 15.9 | 110.9 | 2.2E-02 | 20.8 | 0.7 | 75.6 | 12.6 |
| | 400 | 100.1 | 4.4 | 95.9 | - | 1.8E-02 | 1.8 | 1.9 | 13.8 | 115.9 | 2.2E-02 | 18.1 | 0.6 | 65.8 | 11.0 |
| TiPO | 200 | 945.0 | 3.9 | 83.1 | - | 1.6E-02 | 2.3 | 1.6 | 14.0 | 36.9 | 1.1E-02 | 0.1 | 0.5 | - | 7.8 |
| | 250 | 839.1 | 3.4 | 73.8 | - | 1.4E-02 | 2.3 | 1.5 | 12.4 | 43.4 | 1.1E-02 | 0.1 | 0.5 | - | 7.0 |
| | 300 | 847.6 | 3.5 | 74.6 | - | 1.4E-02 | 2.1 | 1.5 | 12.5 | 53.9 | 1.1E-02 | 0.1 | 0.5 | - | 7.0 |
| | 350 | 884.1 | 3.6 | 77.8 | - | 1.5E-02 | 2.2 | 1.5 | 13.1 | 79.9 | 1.1E-02 | 15.0 | 0.5 | 54.3 | 9.2 |
| | 400 | 1227.3 | 5.0 | 108.0 | - | 2.0E-02 | 3.0 | 2.1 | 18.2 | 133.2 | 2.2E-02 | 20.8 | 0.7 | 76.7 | 12.8 |
| TiBALD | 200 | 5547.1 | - | - | 124.5 | 0.8E-02 | 18.3 | 6.3 | 35.7 | 107.0 | 4.4E-02 | 61.8 | 1.6 | 225.2 | 39.0 |
| | 250 | 2971.1 | - | - | 66.7 | 4.3E-02 | 9.8 | 3.4 | 19.1 | 76.0 | 2.2E-02 | 24.9 | 0.9 | 90.5 | 19.9 |
| | 300 | 2311.2 | - | - | 51.9 | 3.3E-02 | 7.6 | 2.6 | 14.9 | 72.6 | 2.2E-02 | 19.3 | 0.7 | 70.4 | 15.7 |
| | 350 | 2218.6 | - | - | 49.8 | 3.2E-02 | 7.3 | 2.5 | 14.3 | 99.1 | 2.2E-02 | 0.1 | 0.6 | - | 12.5 |
| | 400 | 1789.3 | - | - | 40.1 | 2.6E-02 | 5.9 | 2.0 | 11.5 | 96.0 | 1.1E-02 | 0.1 | 0.5 | - | 10.0 |
| PTOOD | 200 | 507.1 | - | - | 67.9 | 7.2E-03 | 6.7 | 3.8 | 20.9 | 58.3 | 2.2E-02 | 25.3 | 0.9 | 92.1 | 20.8 |
| | 250 | 435.8 | - | - | 59.3 | 3.1E-02 | 5.8 | 3.2 | 16.7 | 66.5 | 2.2E-02 | 21.8 | 0.7 | 79.2 | 17.9 |
| | 300 | 357.7 | - | - | 47.9 | 2.5E-02 | 4.7 | 2.7 | 13.7 | 67.0 | 2.2E-02 | 17.9 | 0.6 | 65.0 | 14.7 |
| | 350 | 336.1 | - | - | 45.0 | 2.4E-02 | 4.5 | 2.5 | 12.9 | 89.5 | 2.2E-02 | 0.1 | 0.6 | - | 11.7 |
| | 400 | 317.0 | - | - | 42.4 | 1.6E-02 | 4.2 | 2.4 | 12.2 | 101.4 | 1.1E-02 | 0.1 | 0.5 | - | 11.0 |

Table 5.8. Global warming potential values in kg $CO_2$-eq per kg $TiO_2$ for all of the precursors and temperatures at industrial-scale production. Temp. = Temperature, Pre. = Precursor, IPA = Isopropanol, IPA dis. = Isopropanol distillation, $H_2O_2$ = Hydrogen Peroxide, Pack. = Packaging, Trans. = Transport, DIW = Deionised Water, Elec. = Electricity, H&C = Heating and Cooling, CP = Cleaning process, PP = Postprocessing, Wash = Washing, Neu. = Neutralization and WWT = Water waste treatment.

| Precursor | Temp. (°C) | Pre. | IPA | IPA dis. | $H_2O_2$ | Pack. | Trans. | DIW | Elec. | H&C | CP | PP | Wash | Neu. | WWT |
|---|---|---|---|---|---|---|---|---|---|---|---|---|---|---|---|
| | 200 | 1.7 | - | - | - | 1.4E-02 | 0.7 | 0.1 | 0.9 | 2.7 | 1.2E-03 | 8.9E-03 | 3.5E-02 | 1.2 | 4.6 |
| | 250 | 1.2 | - | - | - | 9.9E-03 | 0.4 | 0.1 | 0.6 | 2.5 | 6.1E-04 | 6.1E-03 | 2.4E-02 | 0.8 | 3.2 |
| TiOS | 300 | 1.2 | - | - | - | 9.9E-03 | 0.4 | 0.1 | 0.6 | 3.0 | 6.1E-04 | 6.1E-03 | 2.4E-02 | 0.8 | 3.2 |
| | 350 | 1.2 | - | - | - | 1.0E-02 | 0.5 | 0.1 | 0.6 | 4.4 | 6.1E-04 | 6.2E-03 | 2.5E-02 | 0.8 | 3.2 |
| | 400 | 1.2 | - | - | - | 9.9E-03 | 0.4 | 0.1 | 0.6 | 5.2 | 6.1E-04 | 6.1E-03 | 2.4E-02 | 0.8 | 3.1 |
| | 200 | 9.5 | 0.2 | 9.5 | - | 4.5E-03 | 0.2 | 0.2 | 1.3 | 4.1 | 1.8E-03 | 3.7 | 5.4E-02 | 16.4 | 7.6 |
| | 250 | 7.8 | 0.2 | 7.8 | - | 3.7E-03 | 0.1 | 0.1 | 1.1 | 4.5 | 1.2E-03 | 2.0 | 4.4E-02 | 8.9 | 5.5 |
| $TiCl_4$ | 300 | 7.6 | 0.2 | 7.6 | - | 3.6E-03 | 0.1 | 0.1 | 1.1 | 5.4 | 1.2E-03 | 2.0 | 4.3E-02 | 8.8 | 5.4 |
| | 350 | 6.4 | 0.2 | 6.4 | - | 3.0E-03 | 0.1 | 0.1 | 0.9 | 6.4 | 1.2E-03 | 1.2 | 3.6E-02 | 5.5 | 4.2 |
| | 400 | 5.5 | 0.1 | 5.5 | - | 2.6E-03 | 0.1 | 0.1 | 0.8 | 6.7 | 1.2E-03 | 1.1 | 3.1E-02 | 4.8 | 3.7 |
| | 200 | 34.0 | 0.1 | 4.8 | - | 3.2E-03 | 0.1 | 0.1 | 0.8 | 2.1 | 6.1E-04 | 7.0E-03 | 2.8E-02 | - | 2.6 |
| | 250 | 30.2 | 0.1 | 4.3 | - | 2.9E-03 | 0.1 | 0.1 | 0.7 | 2.5 | 6.1E-04 | 6.2E-03 | 2.5E-02 | - | 2.3 |
| TiPO | 300 | 30.5 | 0.1 | 4.3 | - | 2.9E-03 | 0.1 | 0.1 | 0.7 | 3.1 | 6.1E-04 | 6.3E-03 | 2.5E-02 | - | 2.3 |
| | 350 | 31.8 | 0.1 | 4.5 | - | 3.0E-03 | 0.1 | 0.1 | 0.7 | 4.6 | 6.1E-04 | 3.9 | 2.6E-02 | 3.9 | 3.1 |
| | 400 | 44.1 | 0.2 | 6.2 | - | 4.2E-03 | 0.2 | 0.1 | 1.0 | 6.4 | 1.2E-03 | 5.6 | 3.6E-02 | 5.6 | 4.3 |
| | 200 | 224.8 | - | - | 6.2 | 2.2E-02 | 1.2 | 0.3 | 2.0 | 6.2 | 2.4E-03 | 3.7 | 8.1E-02 | 16.4 | 13.0 |
| | 250 | 120.4 | - | - | 3.3 | 1.2E-02 | 0.6 | 0.2 | 1.1 | 4.4 | 1.2E-03 | 1.5 | 4.3E-02 | 6.6 | 6.6 |
| TiBALD | 300 | 93.7 | - | - | 2.6 | 9.4E-03 | 0.5 | 0.1 | 0.8 | 4.2 | 1.2E-03 | 1.2 | 3.4E-02 | 5.1 | 5.2 |
| | 350 | 89.9 | - | - | 2.5 | 9.0E-03 | 0.5 | 0.1 | 0.8 | 5.7 | 1.2E-03 | 8.1E-03 | 3.2E-02 | - | 4.1 |
| | 400 | 72.5 | - | - | 2.0 | 7.2E-03 | 0.4 | 0.1 | 0.6 | 5.5 | 6.1E-04 | 6.6E-03 | 2.6E-02 | - | 3.3 |
| | 200 | 31.1 | - | - | 3.4 | 8.5E-03 | 0.4 | 0.2 | 1.2 | 3.4 | 1.2E-03 | 1.5 | 4.4E-02 | 6.7 | 6.9 |
| | 250 | 26.7 | - | - | 2.9 | 7.3E-03 | 0.4 | 0.2 | 0.9 | 3.8 | 1.2E-03 | 1.3 | 3.8E-02 | 5.8 | 6.0 |
| PTOOD | 300 | 21.9 | - | - | 2.4 | 6.0E-03 | 0.3 | 0.1 | 0.8 | 3.8 | 1.3E-03 | 1.1 | 3.4E-02 | 4.8 | 4.9 |
| | 350 | 20.6 | - | - | 2.3 | 5.6E-03 | 0.3 | 0.1 | 0.7 | 5.2 | 1.2E-03 | 7.4E-03 | 3.1E-02 | - | 3.9 |
| | 400 | 19.4 | - | - | 2.1 | 3.8E-03 | 0.3 | 0.1 | 0.7 | 5.9 | 6.1E-04 | 6.9E-03 | 2.7E-02 | - | 3.7 |

## 5.4. Conclusions

The production of titanium dioxide nanoparticles from five different precursors at a range of temperatures using a counter-current continuous-flow hydrothermal reactor results in anatase nanoparticles with a mean particle diameter of less than 20 nm. The precursors selected ranged from “first generation” titanium sources derived from the mining and refining of titanium ores (TiOS and $TiCl_4$) to more complex second (alkoxides and PTOOD) and third generation water soluble titanium complexes (TiBALD).

In general, increasing the reaction temperature was found to give larger, more crystalline, nanoparticles as shown by XRD and TEM analysis. Higher synthesis temperatures also increased the purity and yield. While TiOS showed the highest particle sizes and broadest size distributions, the third generation precursor, TiBALD, shows the smallest particle size and narrowest size distribution of samples prepared at the highest synthesis temperature. Also, the TGA results indicate that the increase in reaction temperature reduced the impurities in the post-reaction products. Samples from TiOS contained residual sulfate species, while those obtained from the WSTCs at low temperatures showed residual organics.

The life cycle assessment demonstrated that the most important factor in determining the environmental impact of the process for the production of anatase nanoparticles is the choice of precursor. Additionally, other factors that contributed to increase the environmental impact were the use of organic precursors and solvents, acid solution, and the low yield of some analysed routes.

Titanium oxysulfate shows the lowest environmental impact for the production of nano-$TiO_2$. It is a low-cost, first generation precursor, with a few steps in its

production. Its use as a precursor in the CFHS process does not necessitate the use of organic solvents, and it shows high yield across a wide range of temperatures. As a result of these factors, the GWP of TiOS is between 8 and 12 kg $CO_2$-eq. per kg $TiO_2$ for all of the temperatures. CED values range between 100 and 150 MJ $kg^{-1}$ $TiO_2$ approximately and are similarly the lowest among the precursors considered in this study. The highest impact production route is from TiBALD, due to its low yield at low reaction temperatures, the need for additional post-synthesis steps and complexity of manufacturing the precursor complex in the first place.

Results demonstrate the potential for CFHS to achieve low environmental impacts for nanoparticle synthesis when compared with competing technologies and CFSS. Prior studies have demonstrated technical advantages of this approach, including scalability, short reaction time, high crystallinity and nano-sized production with narrow size distribution. CFHS production of nano-$TiO_2$ is shown to achieve similar CED and GWP compared to micro-sized particles manufactured by processes involving high temperatures and long reaction times.

In common with prior cradle-to-gate analyses of nano-$TiO_2$ production, care must be taken while interpreting results. The full product life cycle should be considered for the evaluation of the use of nano-$TiO_2$ in specific applications. Such an analysis must be performed by an understanding of the implications of nano-$TiO_2$ properties on environmental impacts during the use and end-of-life phases. To our knowledge, this is first time that the environmental impacts of $TiO_2$ production have been linked to precursor selection, process parameters, and key $TiO_2$ characteristics (size distribution, crystallinity). This chapter therefore provides a useful foundation to future work evaluating potential applications of nano-$TiO_2$ and their life cycle environmental impacts.

# 6. Chapter 6 – Synthesis, friction performance and environmental assessment of silver sulfide nanoparticles as lubricant additive by continuous flow hydrothermal synthesis

In this chapter silver sulfide ($Ag_2S$) nanoparticles were prepared by continuous-flow hydrothermal synthesis (CFHS) for first time at laboratory scale. The synthesis was carried out with water, silver nitrate and thiourea with a range of temperatures from 250 °C to 400 °C. The characterization of the nanoparticles shows α-$Ag_2S$ phase nanoparticles above 300 °C to 400 °C. However, subcritical conditions resulted in poor uniformity and dispersion product. Supercritical conditions showed $Ag_2S$ nanoparticles with smaller size, more uniformity and less agglomeration. Tribological tests were performed to determine the effect of these $Ag_2S$ nanoparticles as additives in water and mineral oil lubricants. Although the friction was reduced in all of the samples with nanoparticles content, water-based nanoparticles samples showed higher coefficient of friction than mineral oil lubricant. The results showed that incorporating 5 wt% $Ag_2S$ nanoparticles into mineral oil reduced the coefficient of friction (COF) by approximately 60% relative to pure mineral oil lubricants. The greenhouse gas emissions (GHG) for the industrial production of 1 kg of lubricant with 5 wt% of $Ag_2S$ nanoparticles were evaluated by an environmental assessment. Total GHG emissions were 4.06 kg $CO_2$-eq per kg lubricant, with the silver nitrate precursor being the main contributor with a 68.35% of total $CO_2$ emissions. The present study presents valuable information about potential industrial and continuous production of $Ag_2S$ nanoparticles with a lubricating application as well as an environmental assessment for their production.

# Chapter 6

## 6.1. Introduction

Interest in silver sulfide ($Ag_2S$) nanoparticles has recently increased due to their extensive use in emergent applications such as electrical (Tian et al., 2014, Yang et al., 2013, Mo et al., 2012, Wang et al., 1998), photocatalytic (Kalpana and Selvaraj, 2016, Kumari et al., 2014), antimicrobial (Kumari et al., 2014) and tribological (Ding et al., 2005, Zhao and Bahadur, 1998). Owing to this variety of applications, various synthesis methods for the generation of $Ag_2S$ nanoparticles have been widely studied in recent years. Many studies focused on new synthesis routes, such as precipitation (Wang et al., 1998, Lu et al., 2002), hydrothermal (Qian et al., 2001, Yu et al., 2012), solvothermal (Ma et al., 2007, Chen and Gao, 2006, Yan et al., 2009), electrodeposition (Peng et al., 2002), microwave (Gao et al., 2005, Yan et al., 2008), gas-solid (Wen et al., 2005) and template (Niu et al., 2007). Also, other reports were concentrated on the control of the morphology through variation of temperature (Li et al., 2011), reaction time (Xing et al., 2011), concentration (Sadovnikov et al., 2015) or addition of surfactants like polyvinylpyrrolidone (PVP) (Xu et al., 2004), amines (Lim et al., 2004) and cetyl trimethyl ammonium bromide (CTAB) (Dong et al., 2008). Although many of them have demonstrated an impressive control of shape and size of the nanoparticles, the use of complex-techniques, organic compounds or long periods of time hinder an economic and environmentally friendly industrial process. Unlike these batch techniques, continuous-flow hydrothermal synthesis (CFHS) has been shown to be a fast, scalable, and green water-based process for the production of metal oxide (Dunne et al., 2015a) and metal sulfide (Dunne et al., 2014, Dunne et al., 2015b) nanomaterials. This continuous method synthesises highly crystalline nanoparticles in seconds (<5 s) with facile size and shape control,

avoiding high temperature, long reaction times and the use of organic compounds and solvents.

Previous studies showed the promising potential of $Ag_2S$ nanoparticles as additives for lubricants. Spherical $Ag_2S$ nanoparticles of 2-3 nm were previously synthesised by a template technique with the use of Triton X-100 and decanol (Ding et al., 2005). A high-speed ring-block was used to study their tribological behaviour, concluding that the presence the $Ag_2S$ nanoparticles and Triton X-100 improved the anti-wear properties. Also, tribological properties of polyphenylene sulfide (PPS) reinforced with $Ag_2S$ and PbTe nanoparticles were studied at different contents (10-30 vol.%) (Zhao and Bahadur, 1998). In this case, a pin-on-disk was used to determine the wear and coefficient of friction. The results showed that the $Ag_2S$ nanoparticles reduced the wear and COF, with 20-30 vol% identified as the optimum content of inorganic nanoparticles to improve the tribological properties of the lubricant.

As nanotechnology becomes more ubiquitous, it is increasingly important that environmental assessments are carried out in order to confirm the advantages of nanomaterials in energy efficiency, material reduction, longer period of life and superior performance in their applications and manufacturing process. For example, the use of ZnO nanoparticles in metal panels as self-cleaning coating has been compared with protective coating without nanoparticles (Stieberova et al., 2017). The assessment showed lower environmental impacts when ZnO nanoparticles were used as coating, due to elimination of environmental impacts during the use stage where no maintenance is needed in the case of the coating with nanoparticles. To this end the environmental impact of the production of a lubricant containing silver sulfide nanoparticles as an additive has also been assessed in this work.

To the best of our knowledge, both the continuous synthesis of $Ag_2S$ nanoparticles and its environmental impact as potential lubricant additive have never been reported. Herein, we introduced a facile, scalable and continuous technique to their production by the only use of water, thiourea and silver nitrate. Also, we studied the tribological performance of $Ag_2S$ nanoparticles as additive in water and mineral oil to reduce the COF as well as we evaluated the environmental impact of this nanomaterial as lubricant additive in an industrial production.

## 6.2. Methodology

The aims of the present Chapter are; the synthesis of $Ag_2S$ nanoparticles by CFHS at laboratory scale, their performance as nano-lubricant in water and mineral oil and their environmental assessment for a potential industrial production in the plant built in Nottingham under the funded European SHYMAN project.

### 6.2.1. Laboratory synthesis of $Ag_2S$ nanoparticles and tribological tests

Experimental procedures are detailed in Chapter 3 (Sections 3.1.2. and 3.2.4.) but, in brief, the synthesis of $Ag_2S$ nanoparticles was carried out at laboratory scale by CFHS, using thiourea and silver nitrate ($AgNO_3$) as precursors (Figure 3.4, Chapter 3). An aqueous solution of $AgNO_3$ was prepared at 0.025 M and pumped at 10 ml $min^{-1}$, while a solution of thiourea at 0.0125 M in deionised water was driven into the system at 20 ml $min^{-1}$ after being heated in the electrical heater, varying the temperature from 250 to 400 °C (50 °C step) to produce nanoparticles under different operational conditions. A set of aqueous suspensions were obtained as product for each temperature. The suspensions of nanoparticles were centrifuged and washed

before drying in the oven to remove the water content at 70 °C for 24 h. Finally, all of the nanomaterials were carried out to be characterised (XRD, TEM and EDX).

$Ag_2S$ nanoparticles synthesised under supercritical (400 °C) conditions were used for the tribological performance as lubricant additive in water and pure mineral oil due to smaller size and higher crystallinity. The percentage of weight (wt%) of nanoparticles was adjusted to 5 wt% ± 0.1% in water and mineral oil. Ultrasonic sonicated the mix to get a uniform suspension (5-15 min). The friction experiments were performed on a tribometer device using ball-on-slab configuration.

### 6.2.2. Life cycle assessment methods

The main aim of the present research is to provide environmental foundation for the potential application of $Ag_2S$ nanoparticles as a lubricant additive and the industrial production by CFHS. International life cycle methodology (ISO-14040, 2006, ISO-14044, 2006) is used to conduct an environmental assessment of 1 kg of lubricant with 5 wt% of $Ag_2S$ nanoparticles (50 g of nanoparticles and 950 g of mineral oil). Figure 6.1 shows the boundaries of the present study, which include extraction of raw materials, chemicals and energy requirements for the industrial production of the lubricant suspension with nanoparticles ("Cradle-to-gate"). The use and end-of-life are excluded the present assessment. Future work considering specific applications of lubricants could expand on the present work. Transportation of raw materials is considered with 200 km as average for the chemicals used in the synthesis and preparation of the nano-lubricant. Information based on the current plant built in Nottingham is used to determine electrical consumption, natural gas requirements, typical flow rates and volume used during the manufacturing of nanoparticles. Evaporation stages were simulated in Aspen HYSYS (UNIQUAC property package)

to define the natural gas required for the evaporation of water (See Appendix). CCaLC2 is an integrated environmental software which follows the normative of ISO 14044 and PAS 2050. In the present study CCaLC2 is used to determine the impact of the industrial production in greenhouse emissions (GHG); kg of $CO_2$ equivalent per functional unit (kg $CO_2$-eq per kg of lubricant). A set of databases like Ecoinvent 3 database v.3 are included in CCaLC2, which are used to define the impact of the raw material and energy inputs for the industrial production of 1 kg of lubricant.

#### 6.2.2.1. Precursor manufacturing

Two precursors, $AgNO_3$ and thiourea, are not included in the CCalC2 databases, and therefore a literature review was carried out to determine the production requirements of these materials.

$AgNO_3$ was determined by literature review of previous LCA studies of silver nanoparticle synthesis routes (Pourzahedi and Eckelman, 2015, Slotte et al., 2015). These publications considered the "cold process" to produce $AgNO_3$, which consists in the mixing of silver metal with nitric acid. The material requirements for the production of 1 kg of $AgNO_3$ were easily calculated according to the stoichiometry of the reaction (6.1), 0.99 kg of $HNO_3$ 50 wt% in $H_2O$ and 0.64 kg of high purity silver metal.

$$3Ag + 4HNO_3 \rightarrow 3AgNO_3 + NO + 2H_2O \quad (6.1)$$

Thiourea can be synthesised by the isomerization of ammonium thiocyanate, heating it up to 150 °C (Mertschenk et al., 1995) (Reaction (6.2)). The heat capacity of ammonium thiocyanate is 30 cal $mol^{-1}$ $k^{-1}$ approximately (Vanderzee and Westrum,

1970). This data is used to determine that 1 kg of thiourea requires at least 1 kg of ammonium thiocyanate and 214.36 kJ of heating energy.

$$NH_4\text{-}SCN \xrightarrow{\Delta T\ 150\ ^\circ C} NH_2\text{-}CS\text{-}\ NH_2 \quad (6.2)$$

#### 6.2.2.2. Scale-up for the production of lubricant with $Ag_2S$ nanoparticles

Laboratory experience is used to specify the operational conditions for the industrial production; temperature, precursor concentrations and flow rates, which are briefly described in Table 6.1. $Ag_2S$ nanoparticles were synthesised with low concentration solutions due mainly to the likelihood of blockage during the synthesis in the laboratory scale. For the industrial scale scenario this fact is also considered. The precursor solution of $AgNO_3$ (cold stream) is established at 0.25 M while that the thiourea solution concentration is 0.125 M (hot stream). Typical metal salt concentrations for industrial production are higher, 0.5 M. However for $Ag_2S$ nanoparticles production, this prevention is carried out to avoid blockages and production stoppages. The flow rate ratio between both solutions is generally 2:1 (hot stream:cold stream), being 3 $m^3\ h^{-1}$ for the hot stream and 1.5 $m^3\ h^{-1}$ the cold stream. With these parameters and a yield of 95% for the industrial production all of the material inputs -deionised water and chemicals- and outputs –product and wastewater- are defined to produce 1 kg of lubricant with 5 wt% of $Ag_2S$ nanoparticles. Energy requirements –electrical and natural gas cosumption- are easily determined by the information from the Nottingham plant for all of the production stages, except for evaporation of water in the drying stage (Aspen HYSYS simulation). The separation stage is assumed with a decantation of 10 vol% and later washed with 450 L of deionised water in the washing stage.

Table 6.1. Summary of the operational conditions for the laboratory and industrial production.

| Parameter | Laboratory synthesis | Industrial plant production |
|---|---|---|
| Temperature | 400 °C | 400 °C |
| $AgNO_3$ concentration | 0.025 M | 0.25 M |
| Thiourea concentration | 0.0125 M | 0.0125 M |
| Flow rate | Hot stream → 20 ml $min^{-1}$<br>Cold stream → 10 ml $min^{-1}$ | Hot stream → 3 $m^3$ $h^{-1}$<br>Cold stream → 1. 5 $m^3$ $h^{-1}$ |

CFHS is based on water solutions reacting in a closed system, the nanoparticles are synthesised inside of the reactor to produce an aqueous suspension. As a result there are no emissions of nanomaterials into the air. However it is possible that a tiny quantity of nanoparticles (< 1% total mass) could be accumulated in the waste water before to be treated in the water treatment plant. Publications about the effects of $Ag_2S$ nanoparticles in water are practically non-existent. However, some publications have recently been focused on the potential risk effects of silver release from silver components and nanoparticles (Ratte, 1999, Navarro et al., 2008). Jacobson et al. (2005) studied the reduction of silver solubility by humic acid and thiol ligands during $Ag_2S$ dissolution, since sulfidation of silver results in a considerable reduction of the toxicy (Levard et al., 2012), due to the absence of silver ions and nanoparticles. This study concluded that humic acids are able to decrease the solubility of silver by about 75% while other components like cysteine and thiosulfate almost completely reduced the release of silver. To the best of our knowledge investigations about possible toxic effects of $Ag_2S$ nanoparticles themselves have not been reported and toxic effects should carry out to determine and characterize its impact in water.

Table 6.2 describes all inputs and outputs of raw materials, chemicals and energy processing of the nano-lubricant production involved in this assessment per functional unit and Figure 6.1 represents a schematic flowchart of the nano-lubricant production.

Table 6.2. Material and energy inputs and outputs to produce 1 kg of lubricant with 5 wt% of $Ag_2S$ nanoparticles.

| Item | Units | Amount per Functional Unit |
|---|---|---|
| Deionised Water | g | 5607.24 |
| Mineral Oil | g | 950 |
| Thiourea | g | 32.34 |
| Silver nitrate | g | 72.16 |
| Wastewater | g | 5151.98 |
| Natural Gas | MJ | 5.84 |
| Electricity | MJ | 0.40 |

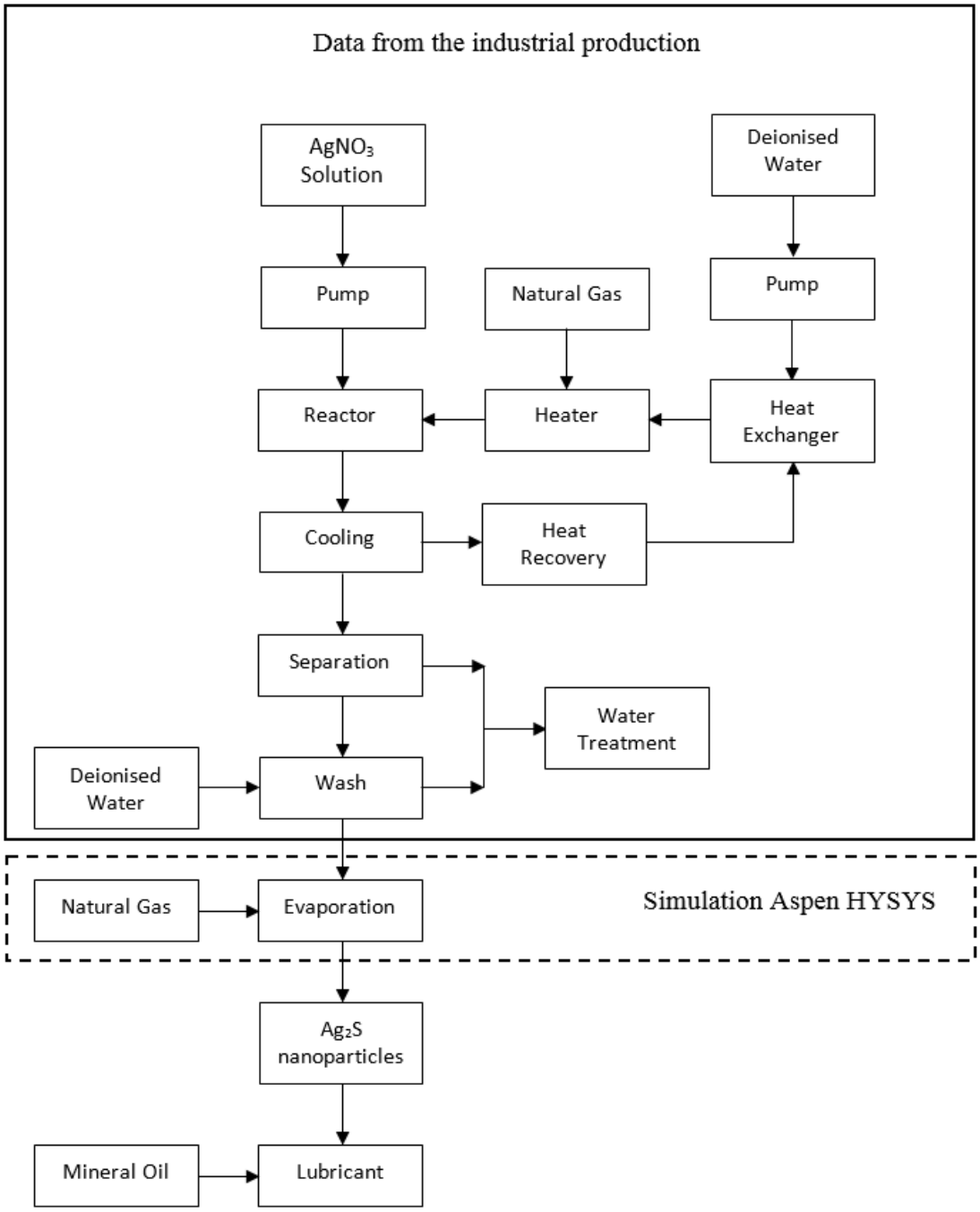



Figure 6.1: Flowchart of the lubricant production with $Ag_2S$ nanoparticles synthesised by continuous-flow hydrothermal synthesis.

# Chapter 6

## 6.3. Results and discussion

### 6.3.1. Characterization

Figure 6.2 shows the XRD patterns obtained for the four samples synthesised between 250 ˚C and 400 ˚C. The diffraction peaks of the product synthesised at 250 ˚C correspond with silver thiocyanate (AgSCN). Other hydrothermal synthesis studies found AgSCN as a final product when the temperature was below 180 °C. This fact is due to the stability and low solubility of AgSCN (Chen and Gao, 2006, Ma et al., 2007). Although the temperature after the heater was 250 ˚C, the post-mixing point temperature was 155 ˚C approximately, hindering the yield into $Ag_2S$ nanoparticles. Similarly, the synthesis of copper sulfide (CuS) resulted in copper thiocyante (CuSCN) at the same temperature, concluding that the low temperature likely results in incomplete breakdown of thiourea and low yield (Dunne et al., 2014). Hence, low temperature and short residence times negatively affect the reaction, resulting in an incomplete decomposition of thiourea and the formation of AgSCN. The samples produced at higher temperatures (≥300 ˚C) showed XRD patterns consistent with α-phase $Ag_2S$ nanoparticles (JCPDS 00-014-0072) (Blanton et al., 2011). Under subcritical conditions (300 and 350 °C) pure monoclinic α-$Ag_2S$ nanoparticles were formed. The monoclinic α-phase is stable until 180 °C, above this temperature the phase changes to body-centered cubic β-phase. In general, hydrothermal and solvothermal syntheses previously reported formed α-phase $Ag_2S$ (Xu et al., 2004, Chen and Gao, 2006, Dong et al., 2008, Xiang et al., 2008, Yu et al., 2012, Tian et al., 2014, Ma et al., 2007).

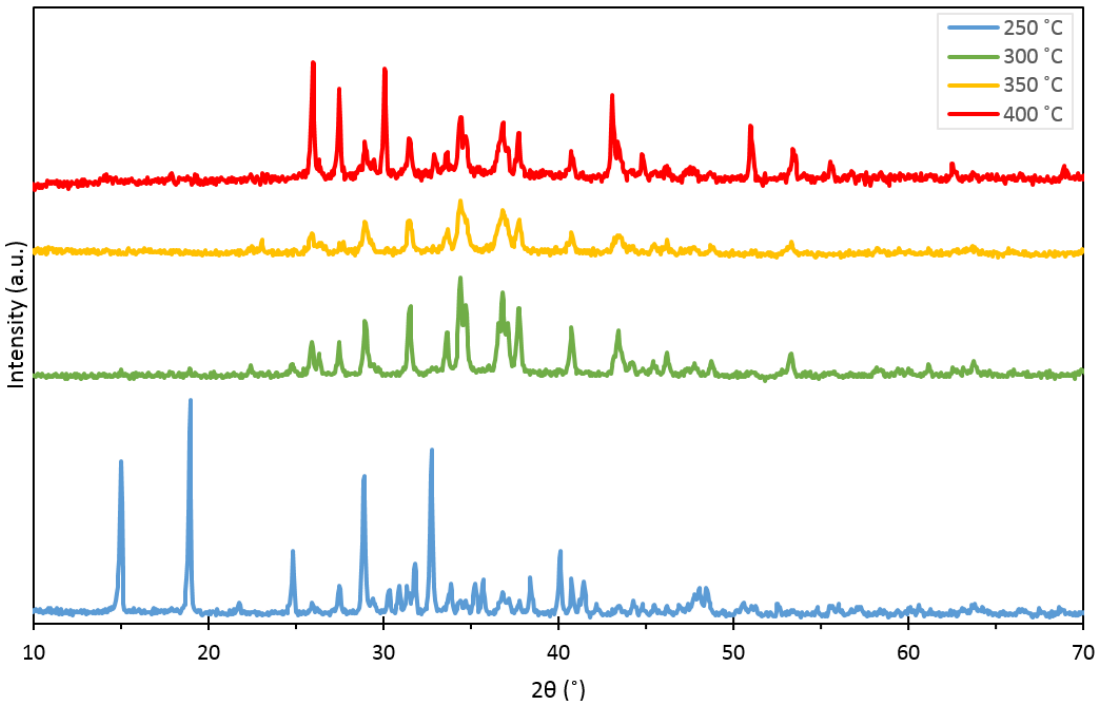



Figure 6.2: Powder X-ray diffraction patterns of products obtained at varying reaction temperatures for the synthesis of $Ag_2S$ nanoparticles.

TEM images of $Ag_2S$ nanoparticles synthesised at temperatures between 300 °C and 400 °C are shown in Figure 6.3. $Ag_2S$ prepared at 300 °C is comprised of agglomerated nanoparticles with poor uniformity with sizes ranging from 50 nm to 120 nm (Figure 6.3 (a & b)). Figure 6.3 (c) and (d) correspond with $Ag_2S$ nanoparticles synthesised at 350 °C, which shows better uniformity and less agglomeration. The increase of the temperature improved the dispersion and uniformity as well as reduced the diameter of the nanoparticles (50 nm to 100 nm), with the majority being 50 nm lozenge shaped particles. The product synthesised at 400 °C correspond with (e), (f) and (g) images in Figure 6.3. The nanomaterials prepared under supercritical conditions are considerably smaller, at 25 nm approximately. The supercritical water has a lower density and dielectric constant causing a higher degree of supersaturation (more nuclei), as well as, a shorter residence time. Also, an increase of temperature leads a higher decomposition of

thiourea into $HS^-$, maximizing concentration and forcing a rapid nucleation of tiny nanocrystals. As a consequence of these facts, nanoparticles with smaller size are generated (Cabanas et al., 2007, Dunne et al., 2014). Figure 6.3 (f) and (g) show these smaller nanoparticles produced at the higher temperature. In general, the shape of $Ag_2S$ nanoparticles corresponded with a lozenge shape.

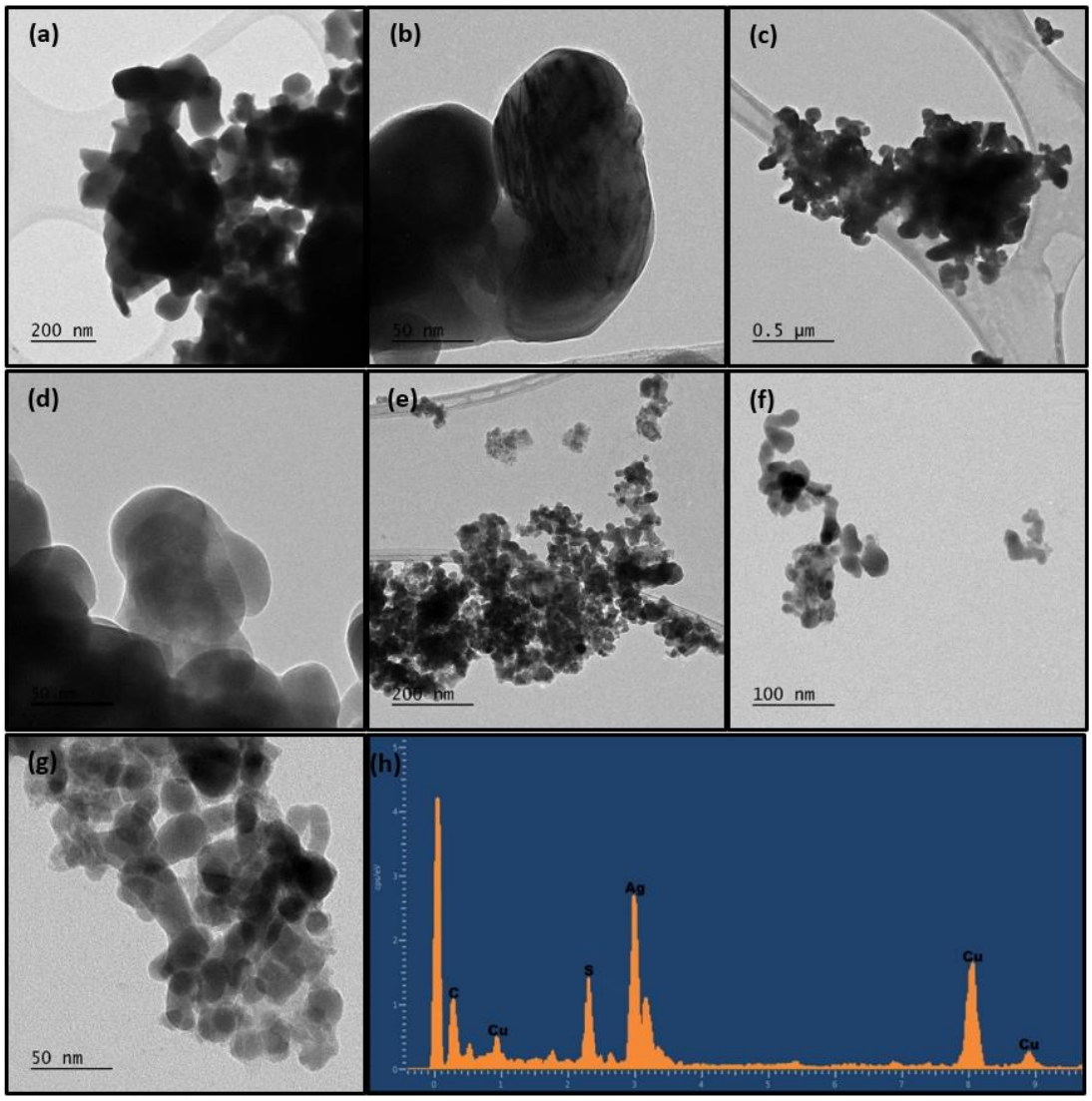



Figure 6.3: TEM images of $Ag_2S$ nanoparticles samples prepared at different temperatures; 300 °C (a-b); 350 °C (c-d) and 400 °C (e-g) and EDX spectrum (h) of $Ag_2S$ nanoparticles at 400 °C.

Figure 6.3 (h) represents the EDX spectrum of the product made at 400 °C. Four elements were found in the EDX analysis: carbon, copper, silver and sulfur. While carbon and copper are due to use of lacey carbon coated copper grid, the silver and sulfur correspond to the atomic ratio of $Ag_2S$ nanoparticles with the expected Ag:S ratio of 2:1 approximately.

### 6.3.2. Tribological tests of lubricants formed with $Ag_2S$ nanoparticles

Tribological tests are represented in Figure 6.4, which corresponds with (a) water, (b) water-based suspension 5 wt% $Ag_2S$ nanoparticles, (c) mineral oil lubricant and (d) mineral oil-based suspension 5 wt% $Ag_2S$ nanoparticles tests. As the effect to reduce the COF can depend on chemical composition, size and morphology of nanoparticles, $Ag_2S$ nanoparticles synthesised at 400 °C were used for the tests. These operational conditions synthesised nanoparticles with smaller size, less agglomeration, higher uniformity, which is expected to enhance the lubricating effect (Dai et al., 2016), as the small size of nanomaterials permit them to easily form a layer between the two surfaces in contact.

The use of pure water (without nanoparticles) as lubricant fluid resulted in the most unfavourable scenario to minimise the friction between the ball and the disc with a COF value of 0.425 ± 0.089. $Ag_2S$ nanoparticles were added to water in order to reduce the friction in the tribometer. This fact resulted in lower COF (9% less), the average of the coefficient of friction was of 0.387 ± 0.036 and thus the $Ag_2S$ nanoparticles demonstrated the lubricating effect. The drawback of using water and nanoparticles was the lack of dispersion and uniformity: precipitation of nanoparticles occurred during the test and the deviation in the values COF was higher in the latter part of the experiment (See Figure 6.4 (b)).

The results of mineral oil samples were more favourable than water samples, due to its lubricating nature and the homogeneity of the suspension shown during the tests. The COF for mineral oil was of 0.287 ± 0.058, while that the addition of $Ag_2S$ nanoparticles in mineral oil resulted in the lowest friction value 0.115 ± 0.019 (Figure 6.4 (d)). This COF was approximately 60% lower than the use of mineral oil without nanoparticles. Also, this represented the maximum reduction of friction (MRF), due probably to the absence of precipitation of $Ag_2S$ nanoparticles in the mineral oil suspension and the use of a lubricant base like mineral oil.

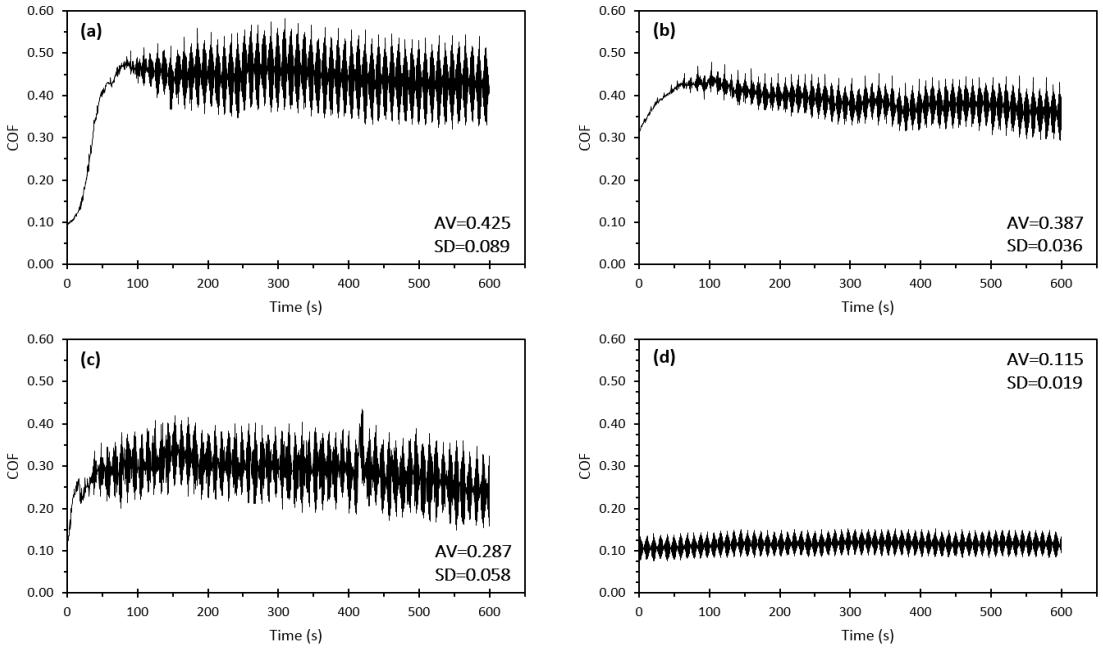



Figure 6.4: Coefficient friction tests of (a) water, (b) water-based suspension 5 wt% $Ag_2S$ nanoparticles, (c) mineral oil and (d) mineral oil-based suspension 5 wt% $Ag_2S$ nanoparticles.

Figure 6.5 shows all COF average values with the standard deviation of the lubricant used in this study. The diminution of COF and the standard deviation between the samples with and without nanoparticles clearly demonstrate the lubricating effect and enhanced performance due to the addition of $Ag_2S$ nanoparticles.

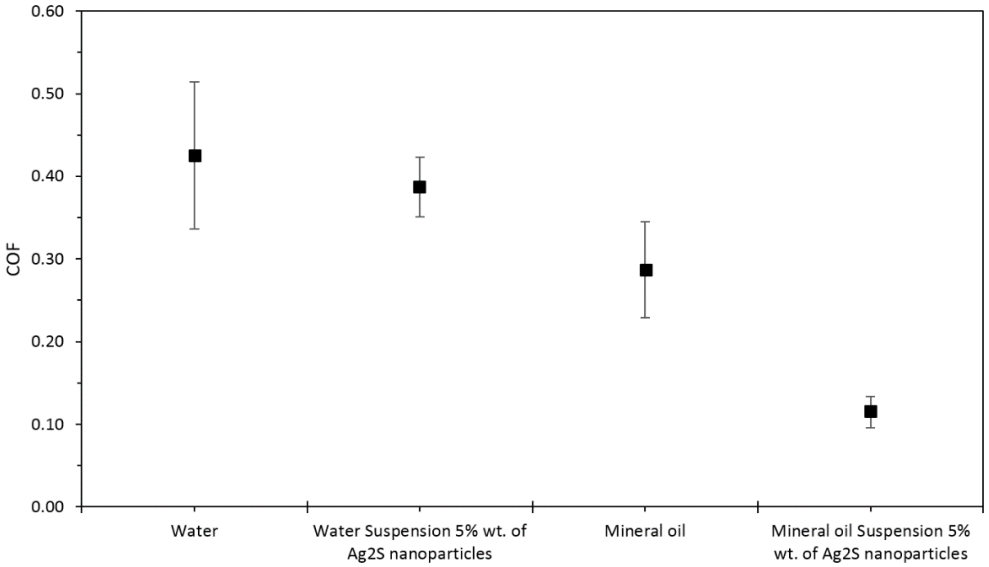



Figure 6.5: Average and standard deviation of coefficient friction for all of the samples studied.

### 6.3.3. Greenhouse emissions

Table 6.3 shows the results of GHG emissions for the production of 1 kg of lubricant with 5 wt% of $Ag_2S$ nanoparticles. Also, Figure 6.6 details the percentages of the GHG emissions in different categories such as precursors and production stages. The total emissions for the lubricant suspension were 4.06 kg $CO_2$-eq per kg lubricant. Silver nitrate showed the highest emission with 2.78 kg $CO_2$-eq per kg lubricant (> 68% of total emissions). Similarly, Pourzahedi and Eckelman (2015) concluded that the main contributor for all of the synthesis routes to silver nanoparticles was the silver source, due largely to the industrial production and transport (usually by air) of silver metal. The production of silver metal is generally carried out by Parkes process (Britain, 1979), which has a high energy demand in the melting and vaporization stages. These production steps are needed to separate silver from other metals such as lead and zinc. Nanoparticles based on other metals (lead, zinc or iron sulfide) could therefore achieve lower environmental impacts, but also the tribological performance has to be studied for lubricant applications (Chapter 7). The emissions

associated with nitric acid are significantly lower than silver metal, even so the main contributor in GHG emissions corresponds with the use of $AgNO_3$ (silver metal and nitric acid) as precursor in the production of $Ag_2S$ nanoparticles.

Table 6.3. Summary of greenhouse gases emissions to produce 1 kg of lubricant with 5 wt% of $Ag_2S$ nanoparticles.

| | Categories | kg $CO_2$-eq per kg lubricant with 5 wt% nanoparticles |
|---|---|---|
| Raw Materials | Deionized Water | 0.05 |
| | Mineral Oil | 0.51 |
| | Thiourea | 0.07 |
| | Silver nitrate | 2.78 |
| Production Stages | Pumping | 0.06 |
| | Heating & Cooling | 0.36 |
| | Post-reaction stages | 0.10 |
| | Transport | 0.14 |
| | *Total Raw Materials* | 3.40 |
| | *Total Production Stages* | 0.66 |
| | *Total emissions* | 4.06 |

As mentioned in the introduction, many studies have used organic solvents and compounds (Ma et al., 2007, Chen and Gao, 2006, Xu et al., 2004, Wu et al., 2004, Lim et al., 2004, Dong et al., 2008) for the synthesis of $Ag_2S$ nanoparticles in order to enhance the control of morphology. In general these hazardous substances lead more energy intensive processes and higher emissions (Tsang et al., 2016, Caramazana-Gonzalez et al., 2017, Şengül et al., 2008). In our CFHS, the use of water as solvent resulted in low emissions in the raw materials and post-processing stages of 0.05 and 0.10 kg $CO_2$-eq per kg lubricant respectively. This absence of organic compounds and solvents requires facile and less demanding processes than organic separation steps such as distillation which would otherwise be needed.

Although the 95% of the total mass in the lubricant suspension is mineral oil, the emissions associated with it represents the 12.63% of the total (0.51 kg $CO_2$-eq per kg lubricant). According with literature review the production of 1 kg of lubricant oil emits 0.54 kg $CO_2$-eq (Nielsen et al., 2003), this value is significantly lower than the GHG emissions of our lubricant with 5 wt% nanoparticles. The addition of nanoparticles based on silver element increases the $CO_2$ emissions considerably. However, it is important to highlight that the use of $Ag_2S$ nanoparticles as lubricant additive leads to a drastic reduction of the COF, up to 60% approximately with respect to mineral oil. This fact could also lead a longer product lifetime and greater energy efficiency due to lower friction and wear between surfaces in machines and motors. Future research work can involve a full life cycle assessment of the nano-lubricant applications to deliver the total environmental impacts and the net benefit.

All of the production stages contributed 0.66 kg $CO_2$-eq per kg lubricant (≈ 16% of the total GHG emissions), with the heating and cooling stages being the most unfavourable of the nanoparticles manufacturing with 0.36 kg $CO_2$-eq per kg lubricant (8.92%).

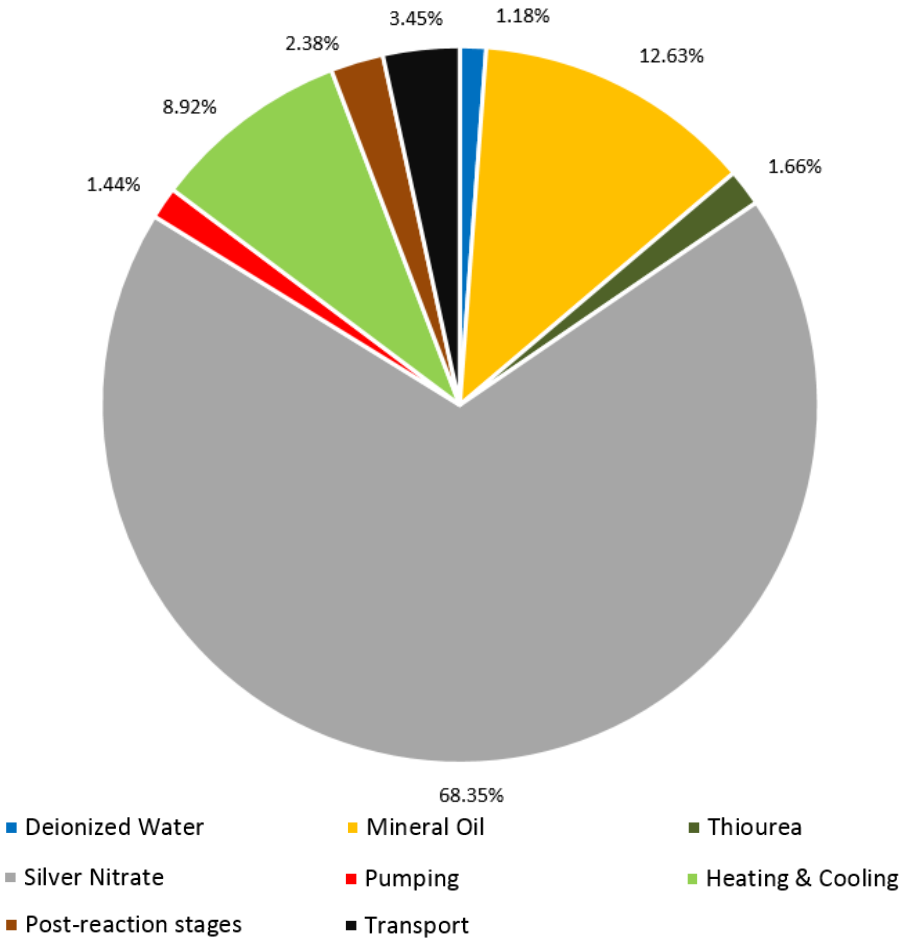



Figure 6.6: Percentage of greenhouse emissions for production of 1 kg of lubricant with 5 wt% $Ag_2S$.

Total emissions for the production of 1 kg of $Ag_2S$ nanoparticles was 68.60 kg $CO_2$-eq per kg $Ag_2S$ nanoparticles. To date an assessment of $Ag_2S$ nanoparticles production has never published; however, similar nanomaterials have previously been studied (Pourzahedi and Eckelman, 2015). A comparative LCA of silver nanoparticle synthesis routes was carried out to determine the environmental impacts of seven different methods. The EPA's tool for the reduction and assessment of chemical and other environmental impacts (TRACI) was used to calculate the impact in ten categories like ozone depletion, acidification or global warming potential (GWP). The GWP results ranged from 128 to 543 kg $CO_2$-eq per kg Ag nanoparticles for reactive magnetron sputtering and flame spray pyrolysis techniques

respectively. These values are clearly higher than the emissions showed by our industrial production of $Ag_2S$ nanoparticles. This is most likely due to the use of water, high yield, simple and optimized (heat recovery in heating stage) process in the CHFS. Table 6.4 details the GHG emissions for the production of 1 kg of $Ag_2S$ nanoparticles, showing similar trends to the production of lubricant with nanoparticles.

Table 6.4. Summary of greenhouse gases emissions to produce 1 kg of $Ag_2S$ nanoparticles.

| | Categories | kg $CO_2$-eq per 1 kg of $Ag_2S$ nanoparticles |
|---|---|---|
| Raw Materials | Deionized Water | 0.96 |
| | Thiourea | 1.35 |
| | Silver Nitrate | 55.44 |
| Production Stages | Pumping | 1.17 |
| | Heating & Cooling | 7.25 |
| | Post-reaction stages | 1.94 |
| | Transport | 0.50 |
| | *Total Raw Materials* | 57.74 |
| | *Total Production Stages* | 10.86 |
| | *Total emissions* | 68.60 |

## 6.4. Conclusions

$Ag_2S$ nanoparticles were synthesised by a continuous-flow hydrothermal synthesis route between 300 °C and 400 °C using a counter-current reactor. Lower synthesis temperatures (250 °C) resulted in AgSCN formation due to incomplete breakdown of thiourea and AgSCN precipitation. Higher temperature (300-400 °C) led the synthesis monoclinic α-phase $Ag_2S$ nanoparticles. The increase of reaction temperature improved the quality product with more uniform, crystalline and less

agglomerated nanoparticles as shown by XRD and TEM characterization. Also, higher synthesis temperature reduced the size of nanoparticles. Samples of $Ag_2S$ nanoparticles produced under supercritical temperature resulted in well dispersed and uniform nanoparticles of approximately 25 nm.

Tribological tests were carried out by the dispersion of $Ag_2S$ nanoparticles at 5 wt% in water and mineral oil. Nanoparticles used as lubricant additive were synthesised under supercritical conditions, due to their smaller size and higher quality. Results showed that the maximum reduction of friction corresponded to the lubricant formed with mineral oil and $Ag_2S$ nanoparticles. The COF was reduced from 0.287 to 0.115 (60% lower) by only the addition of nanoparticles. In water-based samples the COF was higher than mineral oil-based samples, due mainly to absence of lubricant liquid and the lack of uniformity in the aqueous suspension of nanoparticles during the test (precipitation). Therefore the use of $Ag_2S$ nanoparticles as lubricant additive in mineral oil was the best option to reduce the friction.

The environmental assessment determined that the total GHG emissions to produce 1 kg of mineral oil with 5 wt% of $Ag_2S$ nanoparticles were 4.06 kg $CO_2$-eq. The highest impact was associated with the use of $AgNO_3$ as a precursor, which resulted in 2.78 kg $CO_2$-eq per kg lubricant (≈ 68% of total emissions). This is mainly due to the intensive processes required in the production of silver metal as a precursor to the silver salt.

Results showed the potential of the CFHS method with respect to other production techniques. The total emissions of 1 kg of $Ag_2S$ nanoparticles were at least 50% lower than other methods to produce silver nanoparticles, due to the efficiency and optimization of this industrial process and the use of water and inorganic salts in the production of nanoparticles.

# 7. Chapter 7 – The sustainability and tribological performance of various nano-sulfides produced using continuous-flow hydrothermal synthesis

Metal sulfides nanoparticles (nano-sulfides) offer a considerable reduction of friction and anti-wear effect as lubricant additives. In this chapter, ten different nano-sulfides synthesised by continuous-flow hydrothermal synthesis (CFHS) at laboratory scale were used to determine their beneficial use as lubricant additive in water and mineral oil. The broad set of nano-sulfides with diverse morphologies are easily synthesised with the "nozzle" reactor by changing operational conditions such as reaction temperature, synthesis configuration and precursors. The water-based lubricant with nanoparticles results in lower coefficient of friction (COF) in almost all cases, only with ZnS nanomaterials increasing the friction in water, due probably to particle agglomeration. The lubricant formed by mineral oil and nano-sulfides drastically reduced friction (by 56-65%) to create a narrow range of COF values (0.101-0.125). PbS, CuS and $MoS_2$ nano-sulfides are the most favourable in reducing the friction in water and mineral oil, due to their small size, high crystallinity and lack of agglomeration of their nanoparticles. Also, a life cycle assessment (LCA) from "cradle-to-gate" evaluated the industrial production of 1 kg of nano-lubricant (5 wt% nanoparticles) for five nano-sulfides. The main factor to reduce the greenhouse gas (GHG) emissions is the precursor selection, FeS nano-lubricant shows the lowest environmental impact (1.66 kg $CO_2$-eq/kg lubricant) by the use of a simple and low burden processing metal salt. In contrast, CuS, $MoS_2$ and $Ag_2S$ uses nitrate salts, which require more intensive and complex production. As a consequence, $Ag_2S$ represents the most unfavourable nano-lubricant with 4.06 kg $CO_2$-eq/kg lubricant.

# Chapter 7

## 7.1. Introduction

Machines and engines require the use of lubricants to reduce the friction and wear between their components. Lubricants form a film of protection which prevents the increase of temperature, the generation of heat and the deformation by friction. Although there is a large variety of lubricants depending on the working conditions, the most common are hydrocarbon-based with additives (Dai et al., 2016). In recent years, the use of nanoparticles as lubricant additives has increased the interest by their excellent mechanical and tribological properties (Bakunin et al., 2004, Tang and Li, 2014, Gulzar et al., 2016). The small size of nanomaterials enhances the properties of the traditional oil lubricants (Yazdani et al., 2015), due to their effects like rolling, sliding and the creation of a protective film. Also, nanoparticles are able to work under extreme conditions such as high temperature or pressure (Dangsheng, 2001) and their use as lubricant modifier contributes to higher energy efficiency due to reduction of friction between moving parts such as engines (Bakunin et al., 2004).

The wide range of nanoparticles that can be used as lubricant modifier can be categorised by size, morphology or chemical composition. Depending on their composition the most popular correspond with metal, metal oxide and metal sulfide nanoparticles (Dai et al., 2016). The last group has gained interest, of late, in lubricant applications (De Barros et al., 2003), due to low values of friction and high wear effect shown in literature (Dai et al., 2016, De Barros et al., 2003), especially molybdenum disulfide ($MoS_2$) (Rapoport et al., 1997, Deorsola et al., 2012, Chhowalla and Amaratunga, 2000, Zhang et al., 2015, Wang et al., 2016, Kalin et al., 2012, Zhao et al., 2016). $MoS_2$ presents a fullerene-like morphology which is capable of rolling, sliding and exfoliation effects (Tevet et al., 2011), but also other sulfide nanoparticles (nano-sulfides) such as silver, zinc, copper and lead sulfide

have previously demonstrated their potential as a lubricant additive (Ding et al., 2005, Zhao and Bahadur, 1998, Kang et al., 2008, Chen and Liu, 2006, Zhang et al., 2013, Chen and Liu, 2001).

Nano-sulfide syntheses have been carried out by different techniques such as mechanochemical (Tsuzuki and McCormick, 1999, Baláž et al., 2003), precipitation (Lewis, 2010), gas phase reaction (Feldman et al., 1996), chemical vapour deposition (Li et al., 2004) and batch solvo/hydrothermal syntheses (Sun et al., 2014, Hu et al., 2014, Zhuang et al., 2008, Gao et al., 2008, Ni et al., 2007, Wang et al., 2006, Xia et al., 2008, Deorsola et al., 2012, Du et al., 2012). Some of these methods have demonstrated their potential to be scaled-up, but they still present drawbacks like long periods of production, batch stages and no-versatility in the production and products (i.e. only one morphology or particle size). Unlike them, continuous-flow hydrothermal synthesis (CFHS) (Lester and Azzopardi, 2004, Lester et al., 2006) has been able to continuously synthesise a great variety of nano-sulfides with different temperatures and synthesis configurations (Dunne et al., 2015b, Dunne et al., 2014). In addition, the scalability of the CFHS has been previously demonstrated (SHYMAN-project, 2015, Munn et al., 2015), alongside the inherent flexibility to synthesise different nanomaterials like metal oxides (Lester et al., 2012, Caramazana-Gonzalez et al., 2017), metal organic framework (MOFs) (Gimeno-Fabra et al., 2012) and others (Dunne et al., 2015a). The differences between the nano-sulfides are easily visible in their morphology: different phases, sizes and shapes such as rods, tetrapodals, plates, etc. (Dunne et al., 2014), which could result in different tribological behaviour as lubricant additive (Duan and Lei, 2001, Rapoport et al., 1997).

# Chapter 7

In this chapter, a set of nano-sulfides synthesised by CFHS are chosen to determine the coefficient of friction (COF) and the reduction of friction as lubricant additives in water and mineral oil. In addition, due to the emergent demand of environmental assessment for new production techniques and nanomaterials (Akram et al., 2014, Stieberova et al., 2017, Tichá et al., 2016), an anticipatory life cycle assessment (LCA) is carried out for the production of 1 kilogram of each lubricant with 5 wt% nanoparticle addivate (as the 'nano-lubricant'). The chosen nano-sulfides are copper, iron and silver sulfide, as well as, molybdenum disulfide, which were synthesised at different operational conditions (temperature, production configuration and precursors) and therefore their evaluation provides a broad technical and environmental assessment.

## 7.2. Methodology

The present research has two aims. The first is the tribological study of ten nano-sulfides as lubricant additives for water and mineral oil (Table 7.1). The nanoparticles were synthesised at laboratory scale by CFHS, mixed with the lubricant base and tested in a tribometer. The second is the assessment of the environmental impact of the production of 1 kg of nano enhanced lubricant, using FeS, CuS, $Ag_2S$ and $MoS_2$ nanoparticles and information of the industrial plant built in Nottingham.

### 7.2.1. Laboratory synthesis and tribological tests

The list of nano-sulfides synthesised in the laboratory for the tribological tests is shown in Table 7.1. The synthesis of all them is described in the Chapter 3 and literature review (Dunne et al., 2014, Dunne et al., 2015b). Briefly, nine nano-

sulfides were prepared with a standard configuration, using method A or B. Method A consisted of an aqueous solution of metal precursor and thiourea in excess. This solution is pumped into the reactor with a flow rate of 10 ml $min^{-1}$, while a supercritical water stream is also driven into the reactor at 400 °C and 20 ml $min^{-1}$ (Figure 3.5, Chapter 3). Unlike method A, method B dissolves the thiourea with the deionized water of the hot-stream, as well as, this method varies temperature between 300 and 400 °C to synthesise a greater variety of nano-sulfides (Figure 3.6, Chapter 3). $MoS_2$ requires a lower pH and longer time for the sulfidation and precipitation of the nanoparticles (Dunne et al., 2015b), thus the production configuration uses an extra inlet of acetic acid and a second heater (coil-pipe) after the reactor to enhance the synthesis of $MoS_2$ nanoparticles (Figure 3.7, Chapter 3).

The collected suspensions were centrifuged and washed before drying in an oven for 24 h at 70 °C. Finally, dried nanoparticles were mixed with mineral oil and water at different content of nanoparticles (1, 2, 5 and 7 wt%) for the tribological tests.

Table 7.1. Details of the nano-sulfides synthesis at laboratory scale conditions.

| Compound | Formula | Method | Temperature | Configuration |
|---|---|---|---|---|
| | | | °C | |
| Iron Sulfide [a] | FeS | A | 400 | Standard |
| | | B | 400 | |
| Cadmium Sulfide | CdS | A | 400 | Standard |
| | | B | 400 | |
| Zinc Sulfide | ZnS | B | 300 | Standard |
| | | | 400 | |
| Lead Sulfide | PbS | B | 300 | Standard |
| Copper Sulfide [a] | CuS | B | 300 | Standard |
| Silver Sulfide [a] | $Ag_2S$ | B | 400 | Standard |
| Molybdenum Disulfide [a] | $MoS_2$ | - | 400 | Extended residence time & Acid addition |

[a] Nanoparticles evaluated in the LCA

### 7.2.2. Life cycle assessment methods

The present assessment evaluates environmentally the industrial production of 1 kg of nano-lubricant (mineral oil with 5 wt% of nanoparticles) using five nano-sulfide (FeS, CuS, $Ag_2S$ and $MoS_2$) and LCA methodology (ISO-14040, 2006, ISO-14044, 2006). The production of each nano-sulfides involves different operational conditions: three production configurations, two reaction temperatures and various metal salt precursors, which represents 5 scenarios of production. The boundaries includes from extraction of raw materials to nano-lubricant production ("Cradle to gate"); considering 200 km of transport as an average for all chemicals, inputs and outputs of the production, energy requirements and wastewater treatment. Packing and end-of-life are excluded due to lack of information of nano-sulfides as additives. Information from operators and chemical engineers in agreement with the Nottingham Plant (Figure 7.1) is used; electrical consumptions of equipment, natural gas of the boiler, typical volumes treated in separation and washing stages. Only Aspen HYSYS (UNIQUAC property package) software models the evaporation step to estimate the energy requirements of the water content evaporation (See Appendix). CCaLC2 is also used as environmental software to calculate the greenhouse emissions (GHG) in kilograms of $CO_2$-equivalent (kg $CO_2$-eq) per kilogram of nano-lubricant. This environmental tool contains an extensive list of items for raw materials, energy, wastewater treatment, etc. sourced from CCaLC and Ecoinvent databases.

#### 7.2.2.1. Precursor manufacturing

Thiourea ($CH_4N_2S$), silver nitrate ($AgNO_3$), copper nitrate ($Cu(NO_3)_2$) and ammonium heptamolybdate ($(NH_4)_6Mo_7O_{24}$) are not presented in the databases,

therefore literature review was carried out to determine their synthesis procedures and assumptions.

Silver nitrate is adopted in similar way that previous LCA studies (Pourzahedi and Eckelman, 2015, Slotte et al., 2015), which selected the "cold method" to produce $AgNO_3$ by the mixing of silver metal and nitric acid. The material inputs to synthesise 1 kg of $AgNO_3$ are defined by the stoichiometry of the reaction (7.1), being necessary 0.99 kg of $HNO_3$ 50 wt% in $H_2O$ and 0.64 kg of high purity silver metal.

$$3Ag + 4HNO_3 \rightarrow 3AgNO_3 + NO + 2H_2O \quad (7.1)$$

Thiourea can be synthesised by the isomerization of ammonium thiocyanate. This flow requires a heating process up to 150 °C (Mertschenk et al., 1995) as in reaction (7.2). The heat capacity of ammonium thiocyanate is 30 Cal $mol^{-1}$ $k^{-1}$ approximately (Vanderzee and Westrum, 1970). Therefore the isomerization of ammonium thiocyanate requires 1 kg of ammonium thiocyanate and 214.36 kJ of heating energy.

$$NH_4\text{-}SCN \xrightarrow{\Delta T\ 150\ ^\circ C} NH_2\text{-}CS\text{-}NH_2 \quad (7.2)$$

Copper nitrate ($Cu(NO_3)_2$) production is carried out by mixing copper metal in nitric acid solution (Zhang and Richardson, 2000) (Reaction (7.3)). Mass balance according to stoichiometry determines 1.79 kg of $HNO_3$ 50 wt% in $H_2O$ and 0.34 kg of copper metal.

$$3Cu + 8HNO_3 \rightarrow 3Cu(NO_3)_2 + 2NO + 4H_2O \quad (7.3)$$

The synthesis of ammonium heptamolybdate is made by the solution of molybdenum trioxide ($MoO_3$) in aqueous ammonia solution (Sebenik et al., 2000). $MoO_3$ is not presented in databases either, indeed molybdenum concentrate and metallic

molybdenum are only included in databases. Previous LCA study of $MoS_2$ nanoparticles assumed molybdenum metal as input of the precursor synthesis (Deorsola et al., 2012). In addition, the production of metallic molybdenum involved more stages and requirements than heptamolybdate (Sebenik et al., 2000). Therefore in the present assessment 1 kg of ammonium heptamolybdate is also substituted by 1 kg of metallic molybdenum as previous publication.

#### 7.2.2.2. Scale-up for the production of lubricants with nano-sulfide additives

The synthesis of nano-sulfides have been carried out at laboratory scale, thus concentration of precursors are extrapolated according to prior nanoparticles production and experience with the plant (Table 7.2). Current flow rates of industrial scale are 3 $m^3$ $h^{-1}$ for preheated stream and 1.5 $m^3$ $h^{-1}$ for metal salt solution and acetic acid inlet. This information and a yield of 95% were used to define material inputs of deionised water, precursors and other chemicals, as well as, outputs of the process; product and wastewater. Electrical and natural gas consumption were defined by the equipment specifications in the plant, such as pumps, boiler and mixers. Separation stage concentrates the nanoparticles in 10% of volume by precipitation. The same volume of fresh deionised water was used in the washing stage as concentrated suspension. The use of acetic acid reduced the pH in the $MoS_2$ production, thus sodium hydroxide (NaOH) solution is required to neutralize the wastewater before to be treated in the water treatment. Aspen HYSYS was used to determine the energy necessary to dry nanoparticles by evaporation of water. Figure 7.1 describes the nano-lubricant production by the CFHS of nano-sulfides and Table 7.3 shows all material and energy inputs per kilogram of nano-lubricant.

Table 7.2. Scenarios for the industrial production of nano-sulfides considered in this Thesis.

| | | Concentration (mol $l^{-1}$) | | |
|---|---|---|---|---|
| Nano-sulfide | Scale | Metal salt ($M^{X+}$) | Thiourea | Acetic Acid |
| CuS 300B | Laboratory | 0.025 | 0.025 | - |
| | Industrial | 0.25 | 0.25 | - |
| FeS 400A | Laboratory | 0.025 | 0.05 | - |
| | Industrial | 0.25 | 0.5 | - |
| FeS 400B | Laboratory | 0.025 | 0.025 | - |
| | Industrial | 0.25 | 0.25 | - |
| $Ag_2S$ 400B | Laboratory | 0.025 | 0.0125 | - |
| | Industrial | 0.25 | 0.125 | - |
| $MoS_2$ | Laboratory | 0.05 | 0.1 | 20% (v/v) |
| | Industrial | 0.25 | 0.5 | 20% (v/v) |

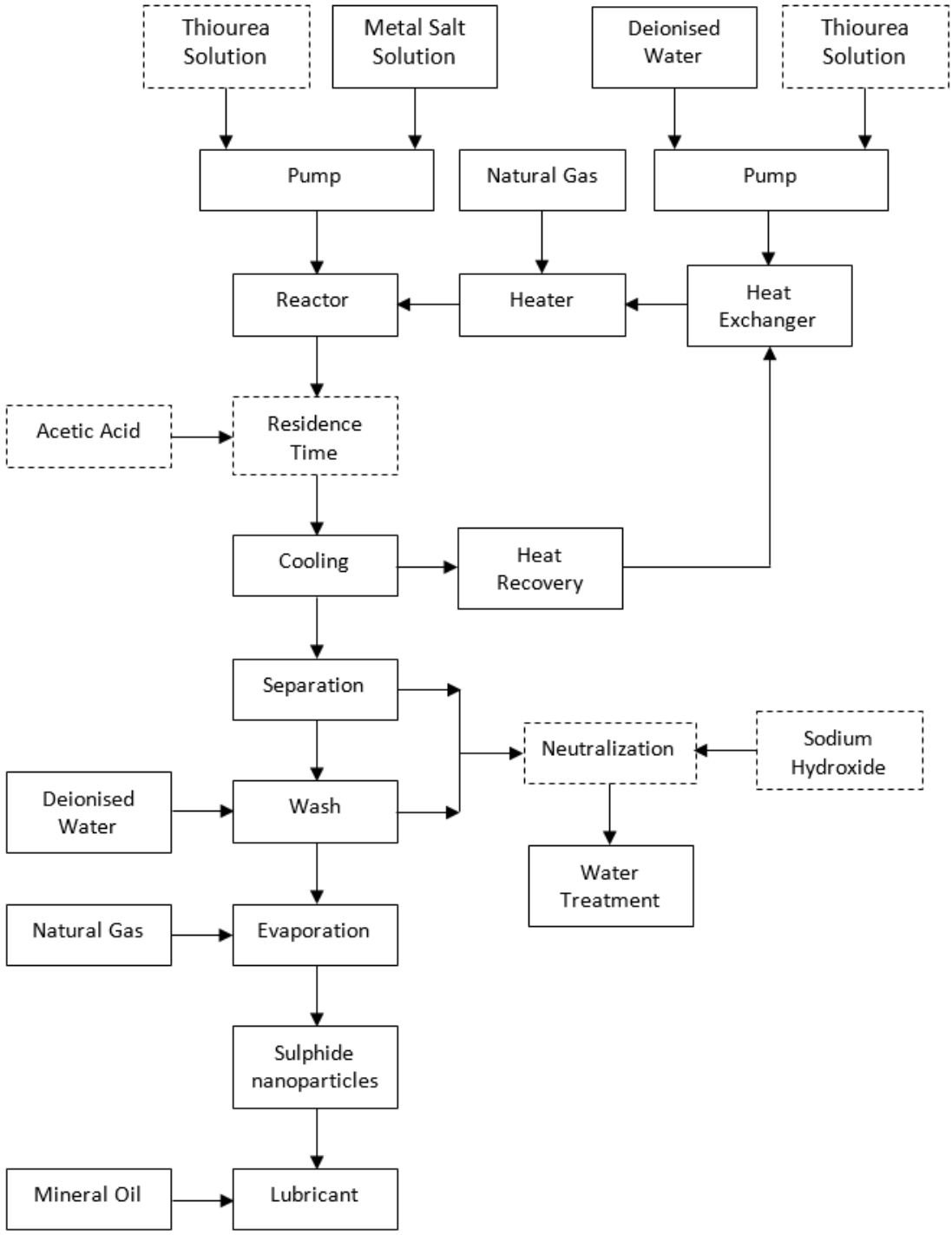



Figure 7.1: Flowchart of the lubricant production with sulfides nanoparticles synthesised by continuous-flow hydrothermal synthesis.

Table 7.3. Material and energy inputs and outputs to produce 1 kg of lubricant with 5 wt% of nanoparticles.

| Item | Units | CuS 300B | FeS 400A & 400B | $Ag_2S$ 400B | $MoS_2$ |
|---|---|---|---|---|---|
| Deionised Water | g | 7266.29 | 7902.82 | 5607.24 | 5523.90 |
| Mineral Oil | g | 950.00 | 950.00 | 950.00 | 950.00 |
| Thiourea | g | 83.80 | 91.15 | 32.34 | 100.11 |
| Copper Nitrate | g | 103.25 | - | - | - |
| Iron Sulfate | g | - | 90.95 | - | - |
| Silver Nitrate | g | - | - | 72.16 | - |
| Ammonium Heptamolybdate | g | - | - | - | 54.67 |
| Acetic Acid | g | - | - | - | 276.19 |
| Sodium Hydroxide Solution | g | - | - | - | 574.54 |
| Wastewater | g | 6742.76 | 7316.48 | 5151.98 | 5979.98 |
| Natural Gas | MJ | 4.82 | 8.23 | 5.84 | 4.83 |
| Electricity | MJ | 0.53 | 0.57 | 0.40 | 0.37 |

## 7.3. Results and discussion

### 7.3.1. Tribological tests of nano-sulfides as lubricant additives

Tribological tests were carried out to determine the COF, samples were tested in a ball-on-slab tribometer at 10 N, sliding speed of 60 rpm with a reciprocating stroke of 10 mm and duration of 10 minutes. While the ball is fixed, the slab slides and the friction produced between the two surfaces is recorded and plotted by the computer. The average of the data is calculated to estimate the COF. Firstly, pure water and mineral oil tests are carried out to determine the COF average (Figure 7.2). These values are used to calculate the total reduction of friction by the addition of nano-sulfides in water and mineral oil. Water test results in a COF of 0.425 while mineral oil, as inherent lubricant, shows a lower COF value of 0.287.

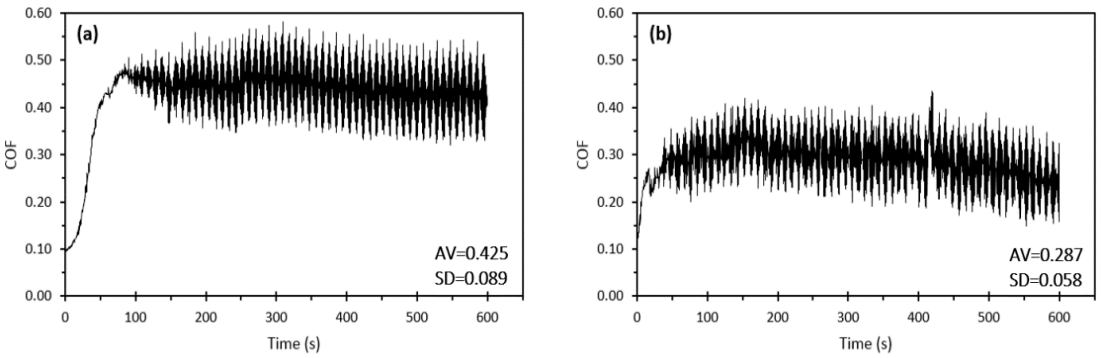



Figure 7.2: Coefficient of friction tests of (a) pure water and (b) pure mineral oil lubricant.

#### 7.3.1.1. Water-based tests

The use of nano-sulfides in water as lubricant is intentionally studied in the present chapter to determine the COF of these suspensions (Figure 7.3). The final product of CFHS is a concentrated water-suspension (5-10 wt%), thus their potential use as

water-based lubricant could also lead a lower environmental impact, due to fewer number of production stages (drying) and materials (mineral oil).

The small size of nanoparticles allows a contact interface to be created, improving the lubrication (Dai et al., 2016). As such, almost all of the nano-sulfides suspensions in water appear to reduce friction between the ball and the slab. Although, ZnS nanoparticles show the smallest size, their tests lead the highest COF results in water. Both ZnS nanomaterials (at 300 and 400 °C, method B) increase the friction with respect to the water test, exceeding the COF value of 0.5. This could be a consequence of the agglomeration showed during their synthesis (Dunne et al., 2014), suggesting that high crystallinity and a non-agglomerated product can offer a better tribological performance in water - like PbS and CuS. The rest of the nanoparticles suspensions show lower COF than pure water, ranging from 0.265 of PbS to 0.387 of $Ag_2S$ nanoparticles (see Table 7.4). PbS and CuS (300B), as well as $MoS_2$ present the most favourable values (0.265-0.297), being even lower or similar to mineral oil (0.287). This significant friction reduction exceeds 30-35% in comparison with the water test. The use of nanoparticles in water clearly decreases the friction. However during the test precipitation of nanoparticles was observed. Figure 7.3 shows that after 300 seconds, the oscillation of friction increases in some of the nano-sulfide suspensions, especially in ZnS, CdS and $Ag_2S$. Future research should study the use of dispersants and surfactants to improve the homogeneity of the water-base lubricant, like recent studies have carried out with glycerol (He et al., 2017, Wu et al., 2017). Phase transfer from the original slurry fluid to the final suspension (whether water or oil) would reduce aggregation and lower the final aggregate size towards primary particles.

A lower content of nanoparticles in water suspensions (1 wt%) was also studied for PbS and $MoS_2$, due to low friction show at 5 wt% (Figure 7.4). For the low concentrate nano-lubricant the COF resulted in higher COF values than suspensions at 5 wt% as well as the loss of stability after a period (precipitation). For example, PbS at 1 wt% in water shows a COF of 0.391, which was similar to the water; and $MoS_2$ suspension rose drastically the COF average after of 200 seconds, negating any lubricant effect.

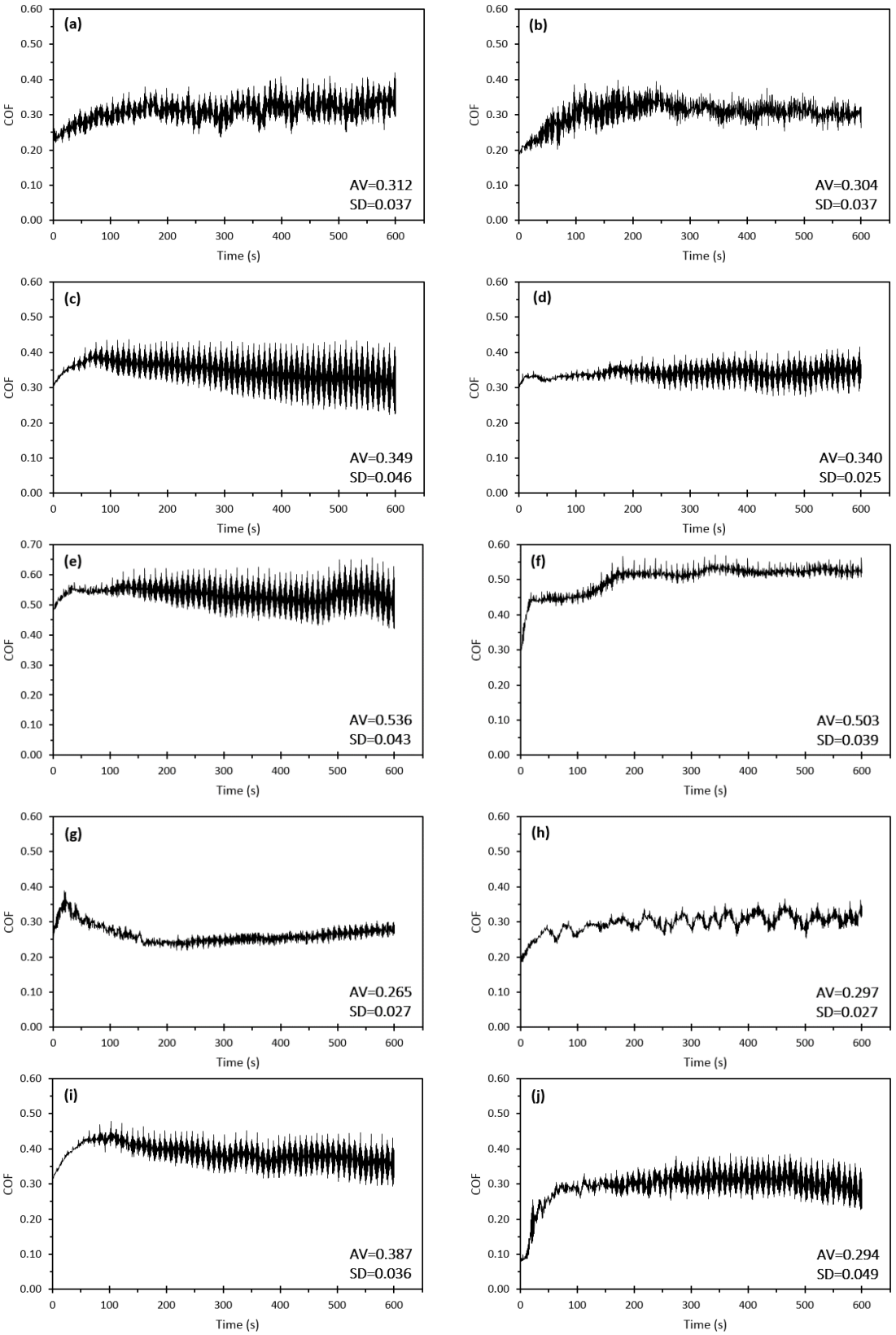



Figure 7.3: Coefficient of friction tests of water suspensions with nano-sulfides at 5 wt% as additive. (a) FeS 400A, (b) FeS 400B, (c) CdS400A, (d) CdS 400B, (e) ZnS 300B, (f) ZnS 400B, (g) PbS 300B, (h) CuS 300B, (i) $Ag_2S$ 400B and (j) $MoS_2$.

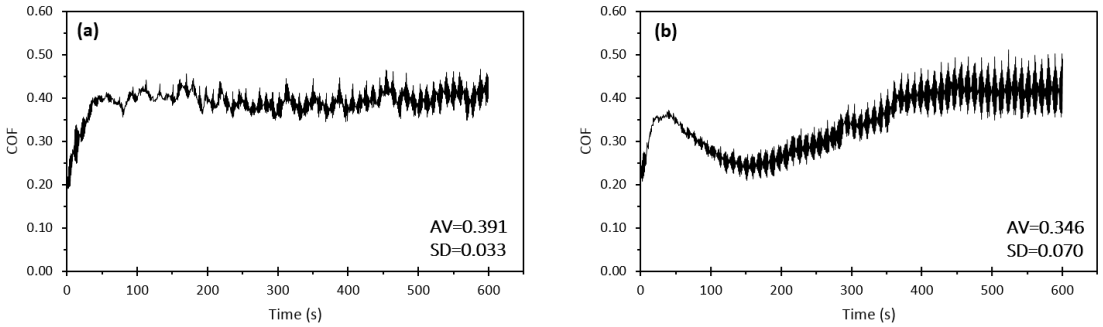



Figure 7.4: Coefficient of friction tests of water suspensions with nano-sulfides at 1 wt% as additive. (a) PbS 300B and (b) $MoS_2$.

Table 7.4. Details of the Nano-sulfides materials used as additives with water as lubricant.

| Compound | Method | Temperature | Nanoparticle content | Average COF |
|---|---|---|---|---|
| | | °C | wt% | |
| FeS | A | 400 | 5 | 0.312 ± 0.037 |
| | B | 400 | 5 | 0.304 ± 0.037 |
| CdS | A | 400 | 5 | 0.349 ± 0.046 |
| | B | 400 | 5 | 0.340 ± 0.025 |
| ZnS | B | 300 | 5 | 0.536 ± 0.043 |
| | | 400 | 5 | 0.503 ± 0.039 |
| PbS | B | 300 | 1 | 0.391 ± 0.033 |
| | | | 5 | 0.265 ± 0.027 |
| CuS | B | 300 | 5 | 0.297 ± 0.027 |
| $Ag_2S$ | B | 400 | 5 | 0.387 ± 0.036 |
| $MoS_2$ | Extended residence time & Acid addition | 400 | 1 | 0.346 ± 0.070 |
| | | | 5 | 0.294 ± 0.049 |
| Water | - | - | - | 0.425 ± 0.089 |

#### 7.3.1.2. Mineral oil-based tests

Figures 7.5 and 7.6 show the tribological tests of mineral oil with nanoparticles at different contents (2, 5 and 7 wt%). Unlike water-base lubricants, nano-lubricants with mineral oil result significantly in lower COF values than water suspensions, all ranging between 0.101 and 0.125. The friction is therefore reduced between 56-65% with respect to the only use of pure mineral oil. Also, the suspensions of mineral oil with nanoparticles showed a better homogeneity and lack of precipitation that can be explained by Stoke's law:

$$v = \frac{2(\rho_{NP} - \rho_F) g r^2}{9\mu} \quad (7.4)$$

Where v is the settling velocity, ρ is the density of the nanoparticle (NP) or the fluid (F), g is gravity, r is the radius of the nanoparticle and μ is the viscosity of fluid. Only two parameters are different, namely fluid density and viscosity. The density of the mineral oil is slightly lower than water, thus the key parameter is in the viscosity value, being typically between 15-30 cP for mineral oil and 1 cP for water. Therefore the settling velocity in mineral oil is considerably slower than in water.

Again the lowest COF is shown by the suspension of PbS nanoparticles (0.104), secondly of CuS (0.112). Both, PbS and CuS show a large reduction with water and mineral oil, at approximately 30% and 60% respectively. Their morphology presents highly non-agglomerated crystalline nanoparticles, with a bilayer of disulfide, which present weak linkages that permit a 'sliding' effect (Du et al., 2012, Evans and Konnert, 1976). In addition, the small size of the cuboidal PbS (27 nm) and hexagonal platelets of CuS (40 x 24.4 nm) could also involve a rolling effect. CdS 400A is the third lowest COF in mineral oil, its morphology of rods and multipodal

unagglomerated nanoparticles results in a COF of 0.112. However, the synthesis of the same nanomaterial by method B at 400 °C formed some fused nanoparticles (similarly $Ag_2S$) that lead to slightly higher COF values. ZnS nanomaterials (300B & 400B) also decrease the friction when they are mixed with mineral oil. Although ZnS COF values are still relatively high, the total friction reduction is still 56% lower than the pure mineral oil.

Three nano-sulfides were also mixed at 2 and 7 wt% with mineral oil (PbS, CuS and $MoS_2$), due to good results in water and mineral oil. Tribological tests are shown in Figure 7.6. In general a higher addition of nanoparticles can lightly reduce the COF. For example PbS and CuS show a COF of 0.101 and 0.106, respectively, at 7 wt% addition (0.104 and 0.112 at 5 wt%). However, the difference is minimal and 5 wt% should be enough to get a 'competitive' COF and a homogeneous product. Therefore a study of net environmental impact of each nano-sulfide vs net "drop" in COF value is not necessary, due to similarity of COF values for different nanoparticle contents. The assessment should be focused on the environmental consequences of production configuration, precursor choice and temperature of each nano-sulfide require to its production, since these factors affect directly to the GHG emissions.

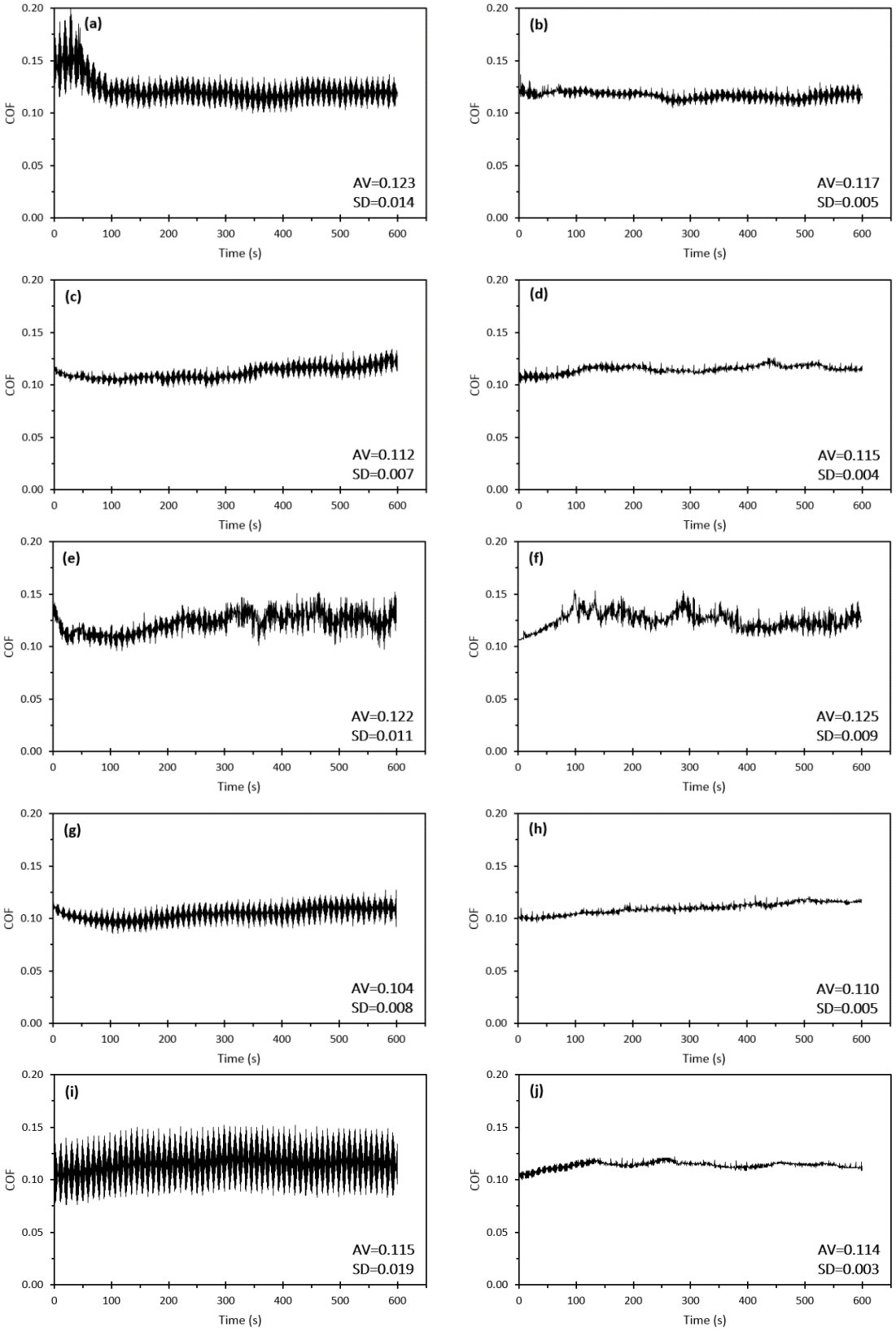



Figure 7.5: Coefficient of friction tests of mineral oil lubricant with nano-sulfides at 5 wt% as additive. (a) FeS 400A, (b) FeS 400B, (c) CdS 400A, (d) CdS 400B, (e) ZnS 300B, (f) ZnS 400B, (g) PbS 300B, (h) CuS 300B, (i) $Ag_2S$ 400B and (j) $MoS_2$.

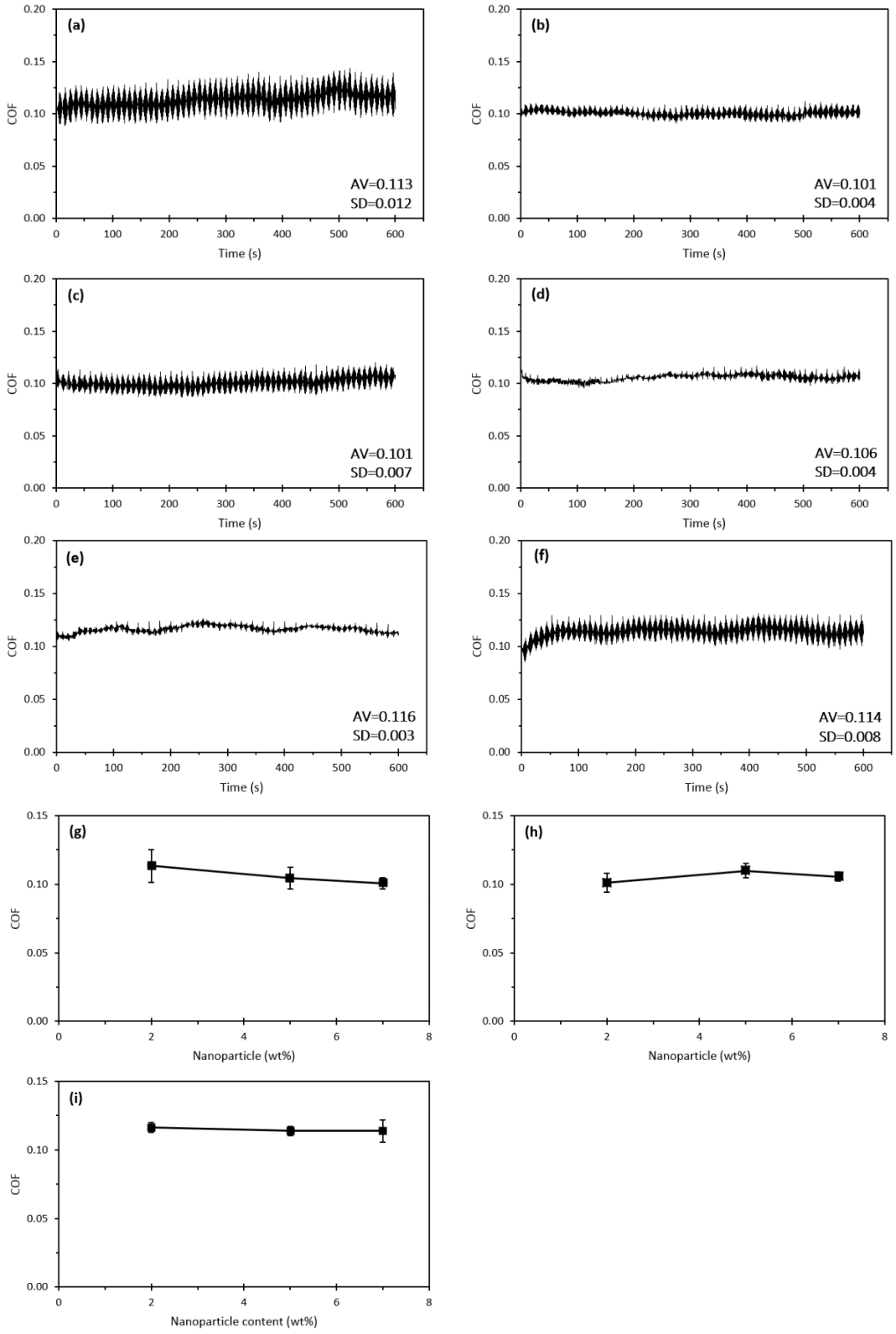



Figure 7.6: Coefficient of friction tests and average of mineral oil lubricant with different content of nano-sulfides as additive. (a) PbS 300B - 2 wt%, (b) PbS 300B - 7 wt%, (c) CuS 300B - 2 wt%, (d) CuS 300B - 2 wt%, (e) $MoS_2$ - 2 wt%, (f) $MoS_2$ - 7 wt%, (g) PbS 300B, (h) CuS 300B and (i) $MoS_2$.

In general, nano-sulfides show a significant reduction in COF in water (Table 7.4) and even more so in mineral oil (56-65%) (Table 7.5). Comparison with previous publications is not straightforward because of the large variety of nanoparticles tested, particle size, particle morphologies, lubricant bases and differences in the tribological tests such as load, time and type of device. Dai et al. (2016) evaluated several publication of nanoparticles in oil lubrication to estimate the average of COF and maximum friction reduction on the nano-additives depending on the composition, size and morphology. According to their conclusions, nano-sulfide additives show an average of minimum COF of 0.05 and maximum friction reduction of 50%. In our case, the nano-sulfides have ranged between 0.101 and 0.125 of COF, which is higher than some values presented in literature review (Dai et al., 2016). However, further research with other tribological conditions, surfactants and lubricant oils could result in lower COF. Regarding to the maximum friction reduction, nano-sulfides synthesised by CFHS and mixed with mineral oil have decreased up to 56-65% the COF, thus this represents a significant reduction and suggests that nano-sulfides have a potential use as lubricant additives.

Table 7.5. Details of the Nano-sulfides materials used as additives with mineral oil as lubricant.

| Compound | Method | Temperature | Nanoparticle content | Average COF |
|---|---|---|---|---|
| | | °C | wt% | |
| FeS | A | 400 | 5 | 0.123 ± 0.014 |
| | B | 400 | 5 | 0.117 ± 0.005 |
| CdS | A | 400 | 5 | 0.112 ± 0.007 |
| | B | 400 | 5 | 0.115 ± 0.004 |
| ZnS | B | 300 | 5 | 0.122 ± 0.011 |
| | | 400 | 5 | 0.125 ± 0.009 |
| PbS | B | 300 | 2 | 0.113 ± 0.012 |
| | | | 5 | 0.104 ± 0.008 |
| | | | 7 | 0.101 ± 0.004 |
| CuS | B | 300 | 2 | 0.101 ± 0.007 |
| | | | 5 | 0.110 ± 0.005 |
| | | | 7 | 0.106 ± 0.004 |
| $Ag_2S$ | B | 400 | 5 | 0.115 ± 0.019 |
| $MoS_2$ | Extended residence time & Acid addition | 400 | 2 | 0.116 ± 0.003 |
| | | | 5 | 0.114 ± 0.003 |
| | | | 7 | 0.114 ± 0.008 |
| Mineral Oil | - | - | - | 0.287 ± 0.058 |

### 7.3.2. Greenhouse emissions

Specific nano-sulfides were selected assess their production as potential lubricant additives. These were as follows:

- $MoS_2$ *by its excellent reduction of COF*;
- CuS 300B *by low COF and reaction temperature*;
- FeS 400A and 400B *due to two synthesis methods (A&B) and the different precursor background (sulfate instead of nitrate salt).*
- $Ag_2S$ as material from Chapter 6.

These five nano-sulfides correspond with three production configurations, two reaction temperatures and different precursors. Other nano-sulfides like lead and cadmium sulfide showed a significant reduction in friction. However, their high toxicity would pose a considerable risk for the industrial production and use, thus they are excluded from the present study.

Table 7.6 shows the results of GHG emissions to produce 1 kg of nano-lubricant with different nano-sulfides. The information is detailed in different categories such as raw materials and production stages. Figure 7.7 represents the percentages of GHG emissions per kg of lubricant, identifying the most unfavourable items and production stages.

Table 7.6. Summary of greenhouse gases emissions to produce 1 kg of lubricant with 5 wt% sulfides nanoparticles.

| | | CuS 300B | FeS 400A & 400B | $Ag_2S$ 400B | $MoS_2$ |
|---|---|---|---|---|---|
| | Categories | kg $CO_2$-eq per kg lubricant with 5 wt% nanoparticles | | | |
| Raw Materials | Deionized Water | 0.06 | 0.07 | 0.05 | 0.05 |
| | Mineral Oil | 0.51 | 0.51 | 0.51 | 0.51 |
| | Thiourea | 0.17 | 0.19 | 0.07 | 0.21 |
| | Copper nitrate | 0.66 | - | - | - |
| | Iron sulfate | - | 0.02 | - | - |
| | Silver nitrate | - | - | 2.77 | - |
| | Ammonium Heptamolybdate | - | - | - | 0.42 |
| | Acetic Acid | - | - | - | 0.33 |
| | Sodium Hydroxide Solution | - | - | - | 0.26 |
| Production Stages | Pumping | 0.08 | 0.08 | 0.06 | 0.06 |
| | Heating & Cooling | 0.26 | 0.51 | 0.36 | 0.28 |
| | Post-reaction stages | 0.13 | 0.14 | 0.10 | 0.09 |
| | Transport | 0.15 | 0.14 | 0.14 | 0.20 |
| | *Total Raw Materials* | 1.40 | 0.87 | 3.40 | 1.78 |
| | *Total Production Stages* | 0.62 | 0.78 | 0.66 | 0.63 |
| | *Total emissions* | 2.02 | 1.66 | 4.06 | 2.41 |

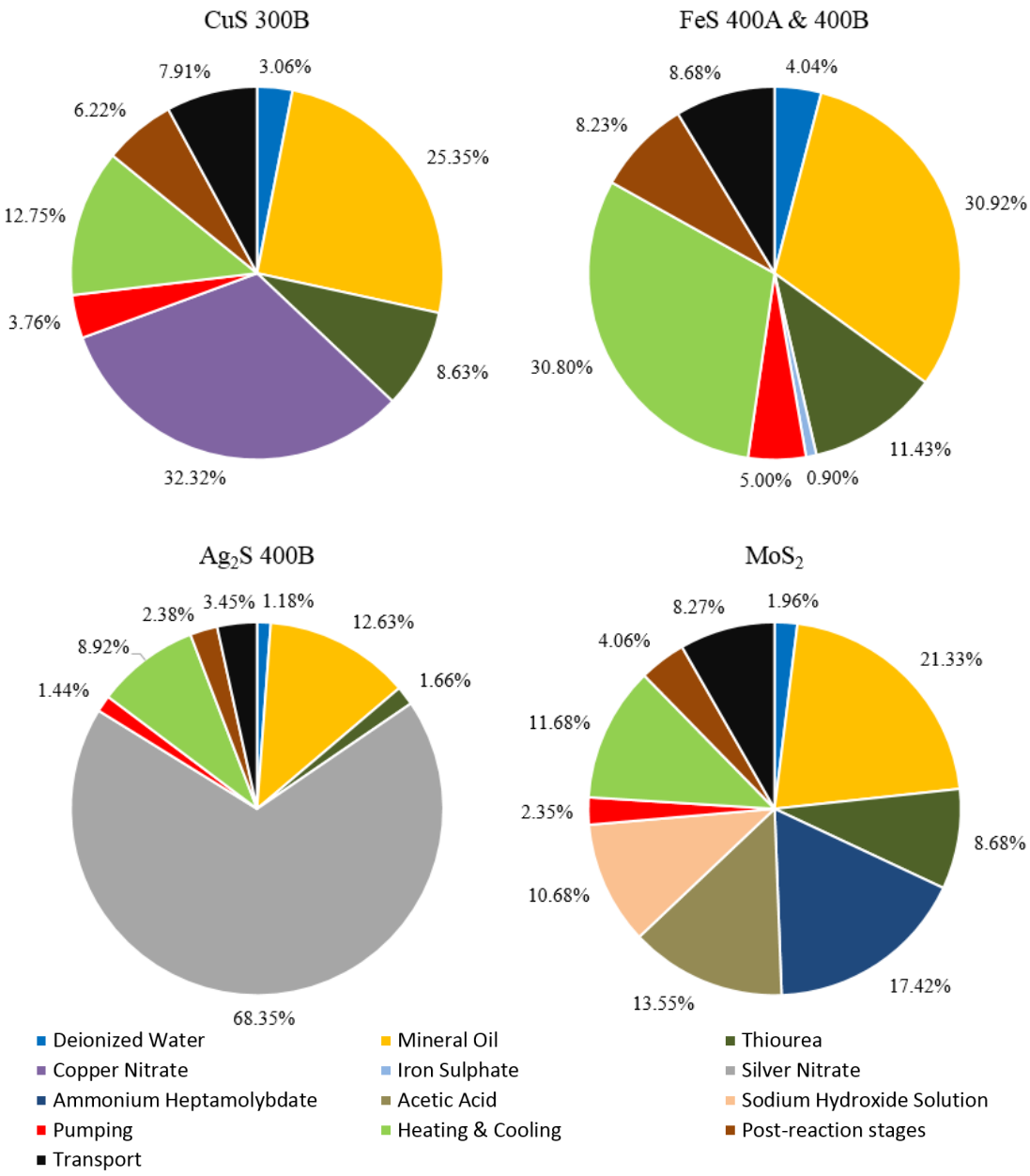



Figure 7.7: Percentage of greenhouse emissions to produce 1 kg of lubricant with 5 wt% sulfides nanoparticles.

The lowest GHG emissions correspond with the nano-lubricant of FeS nanomaterials (FeS 400 A&B), 1.66 kg $CO_2$-eq per kg lubricant. Although FeS nanoparticles are synthesised by different methods, both A and B methods contribute with equal emissions, due to the same reaction temperature, precursors and molar ratio (concentration). FeS nano-sulfides are synthesised with iron sulfate ($FeSO_4$), a by-

product easily produced during the titanium dioxide production (via sulfate process) (Reck and Richards, 1999, Büchner, 1989). The simple manufacturing of $FeSO_4$ does not involve intensive demand of energy and materials, resulting in lower GHG emissions than nitrate salts or more complex molybdenum compounds. For instance $FeSO_4$ constitutes 0.90% of total emissions (0.02 kg $CO_2$-eq per kg lubricant), while that $AgNO_3$ involves the 68.35% of GHG emissions (2.77 kg $CO_2$-eq per kg lubricant) of the nano-lubricant (See Figure 7.7). $AgNO_3$ includes the manufacturing nitric acid and metallic silver, which involve more demanding and complex production stages. For example, silver metal production carries out melting and vaporization stages (Britain, 1979). As consequence, the most unfavourable nano-sulfides is $Ag_2S$ with 4.06 kg $CO_2$-eq per kg lubricant.

CuS nano-lubricant shows 2.02 kg $CO_2$-eq per kg lubricant of total GHG emissions, lower temperature results in half emissions than FeS in the heating and cooling stage (0.26 vs 0.51 kg $CO_2$-eq per kg lubricant). However the use of a nitrate salt leads to an increase in $CO_2$ emissions which equates to a more significant environmental impact. The precursor selection affect clearly more GHG emissions than the reaction temperature for the industrial production of nano-sulfides.

Total GHG emissions for $MoS_2$ is 2.41 kg $CO_2$-eq per kg lubricant, slightly higher than CuS. The production of $MoS_2$ requires the inlet of acetic acid (0.33 kg $CO_2$-eq per kg lubricant), which carries out a neutralization stage with sodium hydroxide (0.26 kg $CO_2$-eq per kg lubricant). These chemicals are approximately 24% of the total GHG emissions per kg of nano-lubricant. Also, the need for transport of more precursor materials contributes to the higher GHG emissions (0.20 kg $CO_2$-eq per kg lubricant). The increase in residence time during production is also a requirement in the $MoS_2$ production, however a longer time only consists of a longer pipe after the

reactor rather than proportional increases in energy demand from heaters. During the laboratory synthesis of $MoS_2$ an electrical heater is used to keep high temperature, however the industrial production would only need an isolated pipe to maintain high temperature and avoid any energy input, thus the outlet of the reactor is over 350 °C.

GHG emissions of the industrial production for these nano-sulfides by the CFHS is also detailed in Table 7.7 and Figure 7.8. Prior LCAs that describe the production of metal sulfides are really limited. $MoS_2$ nanoparticles were evaluated for the hydrothermal synthesis in a batch reactor at laboratory scale (Deorsola et al., 2012). The total global warming potential resulted in 42 kg $CO_2$-eq per kg of $MoS_2$ nanoparticles. However, the synthesis of $MoS_2$ required a heat treatment at 900 °C for 1 hour under argon flow, which was excluded from the analysis by considering only the hydrothermal synthesis. Tungsten disulfide ($WS_2$) nanoparticles, commonly used as lubricant additive (Rapoport et al., 1997), were also assessed for their production by reaction phase, resulting in 39.18 kg $CO_2$-eq per kg $WS_2$ (Bobba et al., 2016). In general, primary information from the pilot plant was used, but also literature review had to be carried out to define the production of precursors ($WO_3$) and some data gaps. Various synthesis methods for the production of silver nanoparticles (discussed in Chapter 6) were evaluated, determining that their production results in 128 - 543 kg $CO_2$-eq per kg of Ag nanoparticles, depending on the production route (Pourzahedi and Eckelman, 2015). The CFHS industrial production shows similar or lower GHG emissions for $MoS_2$ and $Ag_2S$ compared to previous publications, however the production of FeS and CuS result considerably in lower GHG emissions. Therefore the industrial production by CFHS clearly offers a wide operational versatility for various nano-sulfides as lubricant additives, as well as similar and lower GHG emissions compared with other techniques.

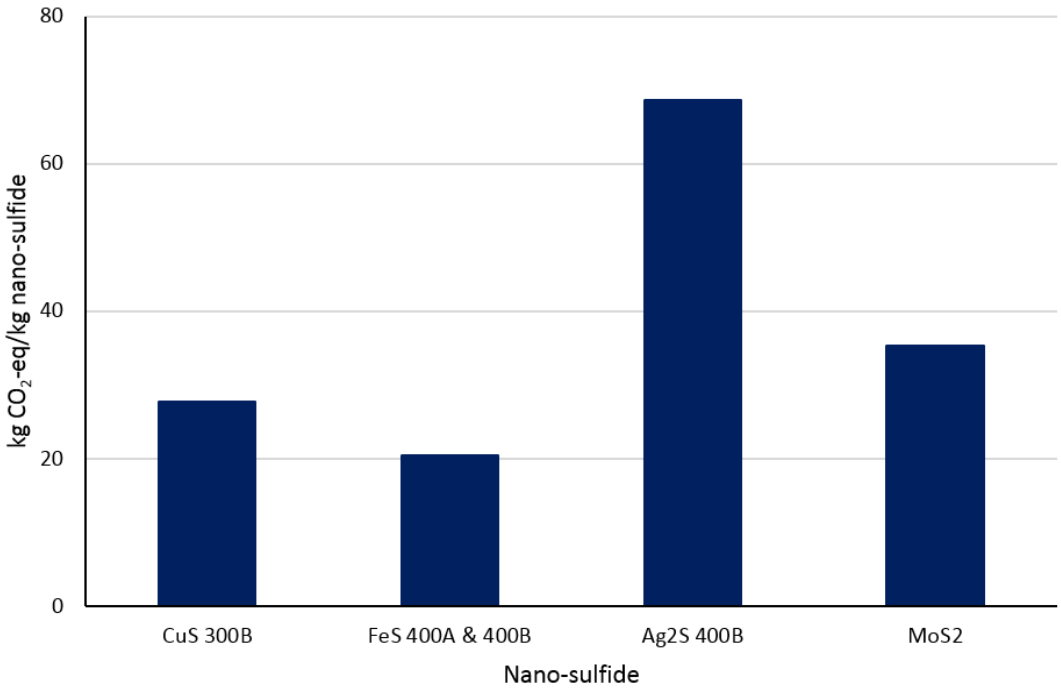



Figure 7.8: Total GHG emissions to produce 1 kg of different nano-sulfides.

Table 7.7. Summary of greenhouse gases emissions to produce 1 kg of sulfide nanoparticles.

| | | CuS 300B | FeS 400A & 400B | $Ag_2S$ 400B | $MoS_2$ |
|---|---|---|---|---|---|
| | Categories | kg $CO_2$-eq per 1 kg of nanoparticles | | | |
| Raw Materials | Deionized Water | 1.24 | 1.35 | 0.96 | 0.94 |
| | Thiourea | 3.50 | 3.80 | 1.35 | 4.18 |
| | Copper Nitrate | 13.04 | - | - | - |
| | Iron Sulfate | - | 0.31 | - | - |
| | Silver Nitrate | - | - | 55.44 | - |
| | Ammonium Heptamolybdate | - | - | - | 8.36 |
| | Acetic Acid | - | - | - | 6.51 |
| | Sodium Hydroxide Solution | - | - | - | 5.13 |
| Production Stages | Pumping | 1.52 | 1.66 | 1.17 | 1.13 |
| | Heating & Cooling | 5.16 | 10.20 | 7.25 | 5.61 |
| | Post-reaction stages | 2.51 | 2.73 | 1.94 | 1.95 |
| | Transport | 0.77 | 0.46 | 0.50 | 1.57 |
| | *Total Raw Materials* | 17.78 | 5.46 | 57.75 | 25.12 |
| | *Total Production Stages* | 9.96 | 15.05 | 10.86 | 10.26 |
| | *Total emissions* | 27.74 | 20.51 | 68.61 | 35.38 |

## 7.4. Conclusions

Ten nano-sulfides were dispersed in water and mineral oil at different weight loadings to form nano enhanced lubricants and to study their tribological performance in a tribometer. All of them were previously synthesised by CFHS and different operational conditions (temperature, process configuration and precursors). Water-lubricants with nano-sulfides show a reduction of COF with respect to water in all of the cases with the exception of ZnS nanoparticles. This material increases friction, probably due to agglomeration and poor crystallinity of the product. Unlike ZnS, PbS, CuS and $MoS_2$ are able to decrease the COF up to 30-35% in water, being similar or lower than commercial pure mineral oil. Water-lubricants also show precipitation of the nanoparticles during the tribological tests, so that future research should study the addition of surfactants to stabilise the suspension and improve performance.

The addition of nanoparticles into mineral oil results in a considerable reduction in the COF, amounting to 56-65% in respect of pure mineral oil. The COF values ranged between 0.101-0.125, showing the potential use of nano-sulfides as lubricant oil additives although there are lower values reported elsewhere. The lower density and higher viscosity of the mineral oil resulted in a more homogeneous nano-lubricant (absence of precipitation during the test). The lowest COF values corresponded to PbS, CuS, CdS and $MoS_2$ nano-sulfides.

GHG emissions of five nano-sulfides are assessed for the industrial production of 1 kg of nano-lubricant (5 wt% nanoparticles in mineral oil). Information from the CFHS plant built in Nottingham is used to estimate the environmental impact in GHG emissions. Results showed that FeS nanoparticles corresponded to the lowest

emissions 1.66 kg $CO_2$-eq per kg lubricant, due mainly to the use of a simple and low environmental burden precursor ($FeSO_4$). In second place, CuS nano-lubricant produced 2.02 kg $CO_2$-eq per kg lubricant. The benefits of lower synthesis temperature is negated by the use of nitrate precursors with a higher 'emissions' value. $Ag_2S$ represented the most unfavourable nano-lubricant, total GHG emissions 4.06 kg $CO_2$-eq per kg lubricant. The use of silver metal and nitric acid to produce $AgNO_3$ precursor requires a greater demand of energy during their manufacture, leading to a 68% increase in total emissions of the lubricant production. $MoS_2$ nanoparticles with mineral oil lubricant resulted in 2.41 kg $CO_2$-eq per kg lubricant, the synthesis of this nanomaterial required more chemicals than other nano-sulfides (Acetic acid and sodium hydroxide) and complex reagents (Molybdenum), which increased GHG emissions.

Results showed the versatility of the CFHS to produce a wide range of nano-sulfides for the same application, by simply changing operational parameters. The large variety of products and operational conditions resulted in GHG emissions that were generally lower or similar to other techniques.

# Chapter 8

# 8. Chapter 8 - Conclusions and future work

## 8.1. General conclusions

Continuous-flow hydrothermal synthesis (CFHS) has previously been described throughout this thesis as an emergent technology for the production of nanomaterials. This fact has been demonstrated by the synthesis of various metal sulfides and titanium dioxide. Their synthesis required a wide range of operational conditions, precursors and configurations, showing the versatility of the "Nozzle reactor" and CFHS. Also, the industrial production of various nanomaterials from different chemical groups; metal sulfides, oxides and phosphates have been assessed to determine their environmental impact and the benefits of the scale-up.

Firstly, the scale-up of the process from laboratory to industrial plant is evaluated for synthesis of lithium iron phosphate (LFP) nanoparticles. Clearly, the optimised design of the industrial plant built in Nottingham as well as higher concentration of precursors and flow rates favour drastically the reduction of greenhouse emissions (GHG) (> 98%). The most unfavourable stages at laboratory and pilot scales, heating and cooling stages minimise considerably the environmental impact in the industrial production due to energy recovery design (>50%). Two operational parameters have also been studied -yield and concentration- in order to estimate future potential industrial scenarios. Reasonably, the increase of yield and concentration lead a decrease of environmental impact, however the GHG emissions results similar and therefore it can be concluded that main factor to reduce the environmental impact is the scale-up of the process. Previous life cycle assessment studies for LFP production typically show similar or lightly lower GHG emissions than CHFS, nevertheless it has to be mentioned that in general these assessments ignore and exclude production

stages, material and energy inputs, which results in a higher environmental impact than CHFS technique.

A broad set of temperatures and precursors were used in the laboratory to synthesise high crystalline and small $TiO_2$ nanoparticles (titania) under hydrothermal and solvothermal conditions. Laboratory synthesises provide valuable information about phase, crystallinity, size, yield and purity of the titania production under a wide range of operational conditions. In general higher reaction temperature favours the yield, crystallinity, larger size and higher purity of the nanoparticles. The information generated is used to evaluate the environmental impact of the industrial production for all of the cases (25). Environmental results conclude that the precursor choice is the most decisive parameter in order to reduce the impact, secondly of solvent, yield and extra requirements such as acid addition to precipitate the nanoparticles. Titanium oxysulphate (TiOS) precursor shows the lowest global warming potential (GWP) and cumulative energy demand (CED) due to water-solubility, simple and easy-manufacturing, high yield and absence of extra requirements. TiOS shows lower emissions and energy demand than the other precursors and nanoparticle synthesis techniques. Only processes that produce micron sized particles show slightly lower or similar impact than the CFHS of nano-$TiO_2$ with TiOS as precursor. The highest emissions and energy demand correspond with titanium bis(ammonium lactate) (TiBALD) as precursor, which is a complex and expensive precursor, thus it requires organic compounds and an intensive process of production. However, the characterization of the $TiO_2$ nanoparticles synthesised with TiBALD shows the smallest size and narrowest distribution.

The first continuous synthesis of silver sulphide ($Ag_2S$) to the best of our knowledge is carried out in the present thesis. $Ag_2S$ nanoparticles are easily synthesised by the

only use of silver nitrate and thiourea at subcritical and supercritical conditions. The increase of temperature leads to smaller, non-agglomerated and more crystalline nanoparticles than subcritical conditions. Therefore $Ag_2S$ synthesised at 400 °C is used as lubricant additive in water and pure mineral oil. Tribological tests confirm the reduction of friction when $Ag_2S$ nanoparticles are used at 5 wt% content in water and mineral oil. The reduction of the coefficient of friction (COF) for the water-suspension of nanoparticles results in 9% with respect to the only use of water. The nano-lubricant of mineral oil and $Ag_2S$ nanoparticles decrease considerably the friction, reducing approximately 60%. The industrial production of nano-lubricant formed of mineral oil with 5 wt% $Ag_2S$ nanoparticles is also evaluated to determine the total GHG emissions. Results show that the emissions due to the industrial production of 1 kg of nano-lubricant correspond with 4.06 kg CO2-eq, being silver nitrate precursor ($AgNO_3$) the highest contributor (68%), due to the intensive production process of silver metal and the use of nitric acid. The industrial production of 1 kg of $Ag_2S$ nanoparticles correspond to a 68.60 kg $CO_2$-eq emission. Although this value could seem high, it represents a reduction up to 50% with respect to other industrial techniques to produce silver nanoparticles.

Ten metal sulfides nanomaterials (nano-sulfides) were dispersed in water and pure mineral oil at different weight loadings to study their tribological performance as potential nano-lubricant additives. Aqueous samples reduce the friction in all of the cases, with the exception of zinc sulfide (ZnS). ZnS increases lightly the COF with respect to pure water, due probably to agglomeration and poor crystallinity of the nanoparticles. The lowest COF values in water are shown by lead and copper sulfide (PbS and CuS) as well as molybdenum disulphide ($MoS_2$), which reduce the friction between 30-35%. These three nanomaterials, at 5 wt% in water, reach similar

performance to pure mineral oil (<0.3). The addition of nano-sulphides into mineral oil reduces up to 56-65% the COF. This magnificent decrease is above of average, encouraging their potential use as lubricant additives. Again PbS, CuS, $MoS_2$ and CdS correspond with the most favourable nanomaterials to decrease friction, although all of the COF range between 0.101 and 0.125. The industrial production of 1 kg of mineral oil with 5 wt% of $Ag_2S$, CuS, $MoS_2$ and Iron sulfide (FeS) is assessed to determine the total GHG emissions. These four nanoparticles involved a large variety precursors, reaction temperatures and synthesis configuration. Nano-lubricant forms with FeS nanoparticles shows the lowest emissions of $CO_2$ (1.66 kg $CO_2$-eq per kg), due mainly to its simple and low environmental burden precursor ($FeSO_4$). Although the production of CuS is carried out at the lowest temperature (300 °C), this likely reduction of the environmental impact is negated by the use of a nitrate salt ($Cu(NO_3)_2$), contributing with 2.02 kg $CO_2$-eq per kg nano-lubricant. Similarly, $Ag_2S$ results in higher emissions as previously it was mentioned, suggesting that sulfate salts compromise less emissions of $CO_2$. The industrial production of $MoS_2$ represents an alternative configuration, the total GHG emissions are higher than FeS and CuS (2.46 $CO_2$-eq per kg nano-lubricant), due to the use of acetic acid to precipitate the nanoparticles and sodium hydroxide to neutralize the wastewater.

## 8.2. Future work

### 8.2.1. Lithium iron phosphate nanoparticles

The production of LFP nanoparticles by CFHS synthesis has been studied in Chapter 4 for an industrial scale, offering clearly its potential as future emergent technique. In this case, the lack of information was mainly established in the calcination step,

therefore further research and development work should be carried out in order to design and generate more realistic data for an industrial calcination. This stage has been modelled to generate the basic data and to complete the LCA, but future work could determine, analyse and compare the scale-up of different alternatives of calcination stage; requirements of equipment, possible recycling of inert gases, inputs and outputs a complete assessment of an engineering process.

Other factors to be studied in the future include the optimisation of the lithiation process (which requires a longer residence time) which would increase the final energy capacity of the cathode material produced by a CFHS. Possibly, some of the operational parameters such as temperature, flow rates or residence time could influence the final capacity of the cathode material and their assessment technical and environmental supply valuable information for future LCAs of lithium ion batteries.

### 8.2.2. Titanium dioxide nanoparticles

Chapter 5 studied a large variety of operational conditions and parameters such as temperature, solvent or precursor. Future work in this case should be focus on the use of titania nanoparticles in emergent applications, completing the present assessment (cradle-to-gate) with a more extensive evaluation, including use and end-of-life. This future work clearly could determine the trade-off between the use of titanium oxysulfate (TiOS) and titanium bis(ammonium-lactate) (TiBALD) as precursors. The former shows the most favourable scenario to reduce the environmental impact, while that the latter one corresponds with the most expensive and unfavourable scenario as well as TiBALD leads the smallest and narrowest size-distribution.

### 8.2.3. Metal sulfide nanoparticles

Further research is necessary to determine the anti-wear effect and the lubricant mechanism of the nano-sulphides. The use of scanning electron microscopy (SEM), transmission electron microscopy (TEM) and a profilometer can contribute with significant information about the behaviour of the ten nanomaterials studied in Chapter 6 and 7.

The study of new synthesis alternatives should be carried out to reduce the emissions of $CO_2$ and to facilitate the industrial production of nano-sulphides. Firstly, it could be recommendable to find out other precursor choices that avoid the nitrate ions. It has been demonstrated that the use of nitric salts such as silver nitrate or copper nitrate lead higher environmental impact by the use of nitric acid during their production. By this, the synthesis of nano-sulphides with alternative metal salts that contain acetate or sulfate ions, it could mitigate the GHG emissions. Similarly, the substitution of thiourea by ammonium thiocyanate could lead an advantageous decrease of the environmental impact, since thiourea is produced by the heating of ammonium thiocyanate.

In order to easy the industrial production and to improve the stability of product, the use of surfactants, lubricants and capping agents in the CFHS could result favourable. After the reaction stage, the inlet of any of organic compounds could reduce the number of stages (sedimentation and evaporation) and the demand of energy by the incorporation of nanoparticles into the organic phase. Moreover the use of surfactants like oleic acid can help to prevent the agglomeration of nanoparticles and to improve dispersion, resulting in a more homogeneous and stable product (Peng et al., 2010, Chen and Liu, 2006, Gao et al., 2002).

## Chapter 8

The use of vegetable oil instead of mineral oil as lubricant base can contribute with a more respectful lubricant due to higher biodegradability (Luna et al., 2011) and no toxicity of vegetal liquid base in comparison with oil derivate base. In addition, vegetable oils molecules contain polar groups like $OH^-$ and COOH, which form physical absorption by Van der Waals force, reducing the friction (Zhang et al., 2015).

# References


ADSCHIRI, T., KANAZAWA, K. & ARAI, K. 1992a. Rapid and continuous hydrothermal crystallization of metal oxide particles in supercritical water. *Journal of the American Ceramic Society,* 75**,** 1019-1022.

ADSCHIRI, T., KANAZAWA, K. & ARAI, K. 1992b. Rapid and continuous hydrothermal synthesis of boehmite particles in subcritical and supercritical water. *Journal of the American Ceramic Society,* 75**,** 2615-2618.

ADSCHIRI, T., LEE, Y.-W., GOTO, M. & TAKAMI, S. 2011. Green materials synthesis with supercritical water. *Green Chemistry,* 13**,** 1380-1390.

AIMABLE, A., AYMES, D., BERNARD, F. & LE CRAS, F. 2009. Characteristics of $LiFePO_4$ obtained through a one step continuous hydrothermal synthesis process working in supercritical water. *Solid State Ionics,* 180**,** 861-866.

AKRAM, H., ACHAK, O., HAFFANE, S., ELMOUJAHID, C., ELMESBAHI, A., ELMESSOUDI, D., CHAFIK, T., BENSEMLALI, S. & ELMOUAKIBI, A. Comparison of synthesis routes of inorganic fullerene-like nano-additives for wind turbine lubrication: Application of Life Cycle Assessment approach. Renewable and Sustainable Energy Conference (IRSEC), 2014 International, 2014. IEEE, 788-790.

AKSOMAITYTE, G., POLIAKOFF, M. & LESTER, E. 2013. The production and formulation of silver nanoparticles using continuous hydrothermal synthesis. *Chemical engineering science,* 85**,** 2-10.

ALLEN, D. T. & SHONNARD, D. 2012. *Sustainable Engineering: Concepts, Design, and Case Studies*, Prentice Hall New York.

AMIENYO, D., GUJBA, H., STICHNOTHE, H. & AZAPAGIC, A. 2013. Life cycle environmental impacts of carbonated soft drinks. *The International Journal of Life Cycle Assessment,* 18**,** 77-92.

ARNOLD, G., GARCHE, J., HEMMER, R., STRÖBELE, S., VOGLER, C. & WOHLFAHRT-MEHRENS, M. 2003. Fine-particle lithium iron phosphate $LiFePO_4$ synthesized by a new low-cost aqueous precipitation technique. *Journal of Power Sources,* 119**,** 247-251.

AZAPAGIC, A. 2015. CCaLC sofware. http://www.ccalc.org.uk.

BAGHBANZADEH, M., GLASNOV, T. N. & KAPPE, C. O. 2013. Continuous-Flow Production of Photocatalytically Active Titanium Dioxide Nanocrystals and Its Application to the Photocatalytic Addition of N, N-Dimethylaniline to N-Methylmaleimide. *Journal of Flow Chemistry,* 3**,** 109-113.

BAKUNIN, V., SUSLOV, A. Y., KUZMINA, G., PARENAGO, O. & TOPCHIEV, A. 2004. Synthesis and application of inorganic nanoparticles as lubricant components–a review. *Journal of Nanoparticle Research,* 6**,** 273-284.

BALÁŽ, P., BOLDIŽÁROVÁ, E., GODOČI, E. & BRIANČIN, J. 2003. Mechanochemical route for sulphide nanoparticles preparation. *Materials Letters,* 57**,** 1585-1589.

BAR, H., BHUI, D. K., SAHOO, G. P., SARKAR, P., DE, S. P. & MISRA, A. 2009. Green synthesis of silver nanoparticles using latex of Jatropha curcas. *Colloids and surfaces A: Physicochemical and engineering aspects,* 339**,** 134-139.

BARKER, J., SAIDI, M. & SWOYER, J. 2003. Lithium iron (II) phospho-olivines prepared by a novel carbothermal reduction method. *Electrochemical and Solid-State Letters,* 6**,** A53-A55.

BAROCH, C., KACZMAREK, T., BARNES, W., GALLOWAY, L., MARK, W. & LEE, G. 1955. TITANIUM PLANT AT BOULDER CITY, NEV.: ITS DESIGN AND OPERATION. Bureau of Mines.

BARRETO, J. A., O'MALLEY, W., KUBEIL, M., GRAHAM, B., STEPHAN, H. & SPICCIA, L. 2011. Nanomaterials: applications in cancer imaging and therapy. *Advanced Materials,* 23.

## References


BAUMANN, H. & TILLMAN, A.-M. 2004. *The Hitch Hiker's Guide to LCA. An orientation in life cycle assessment methodology and application*, External organization.

BLANTON, T., MISTURE, S., DONTULA, N. & ZDZIESZYNSKI, S. 2011. In situ high-temperature X-ray diffraction characterization of silver sulfide, $Ag_2S$. *Powder Diffraction,* 26**,** 114-118.

BOBBA, S., DEORSOLA, F. A., BLENGINI, G. A. & FINO, D. 2016. LCA of tungsten disulphide ($WS_2$) nano-particles synthesis: state of art and from-cradle-to-gate LCA. *Journal of Cleaner Production,* 139**,** 1478-1484.

BOCQUET, J., CHHOR, K. & POMMIER, C. 1999. Barium titanate powders synthesis from solvothermal reaction and supercritical treatment. *Materials chemistry and physics,* 57**,** 273-280.

BODOARDO, S., GERBALDI, C., MELIGRANA, G., TUEL, A., ENZO, S. & PENAZZI, N. 2009. Optimisation of some parameters for the preparation of nanostructured $LiFePO_4$/C cathode. *Ionics,* 15**,** 19.

BRADLEY, D., HANCOCK, D. & WARDLAW, W. 1952a. 524. Titanium chloride alkoxides. *Journal of the Chemical Society (Resumed)***,** 2773-2778.

BRADLEY, D., MEHROTRA, R. & WARDLAW, W. 1952b. 376. Structural chemistry of the alkoxides. Part I. Amyloxides of silicon, titanium, and zirconium. *Journal of the Chemical Society (Resumed)***,** 2027-2032.

BRISSE, F. & HADDAD, M. 1977. Alkaline salts of oxalato titanate (IV) complexes. Part 1. Syntheses and characterizations. *Inorganica Chimica Acta,* 24**,** 173-177.

BRITAIN, G. 1979. Patents for inventions: abridgments of specifications, class 98, photography, periods 1839 through 1900. The Sources of modern photography. New York: Arno Press.

BRUNDTLAND, G. H. 1987. *Report of the World Commission on environment and development:" our common future."*, United Nations.

BÜCHNER, W. 1989. *Industrial inorganic chemistry*, VCH.

BUSECK, P., COWLEY, J. & EYRING, L. 1989. *High-Resolution Transmission Electron Microscopy: And Associated Techniques*, Oxford University Press.

CABANAS, A., LI, J., BLOOD, P., CHUDOBA, T., LOJKOWSKI, W., POLIAKOFF, M. & LESTER, E. 2007. Synthesis of nanoparticulate yttrium aluminum garnet in supercritical water–ethanol mixtures. *The Journal of supercritical fluids,* 40**,** 284-292.

CAO, G. 2004. *Nanostructures and nanomaterials: synthesis, properties and applications*, World Scientific.

CARAMAZANA-GONZALEZ, P., DUNNE, P. W., GIMENO-FABRA, M., ZILKA, M., TICHA, M., STIEBEROVA, B., FREIBERG, F., MCKECHNIE, J. & LESTER, E. 2017. Assessing the life cycle environmental impacts of titania nanoparticle production by continuous flow solvo/hydrothermal syntheses. *Green Chemistry,* 19**,** 1536-1547.

CARGNELLO, M., GORDON, T. R. & MURRAY, C. B. 2014. Solution-phase synthesis of titanium dioxide nanoparticles and nanocrystals. *Chem Rev,* 114**,** 9319-45.

CARP, O., HUISMAN, C. L. & RELLER, A. 2004. Photoinduced reactivity of titanium dioxide. *Progress in solid state chemistry,* 32**,** 33-177.

CATHALA, J. 1951. Le genie chimique: Historique de son développement—son objet et ses méthodes—programme de notre revue. *Chemical Engineering Science,* 1**,** 1-7.

CHAN, B. C. Y., WANG, X., LAM, L. K. W., GORDON, J. M., FEUERMANN, D., RASTON, C. L. & TONG CHUA, H. 2012. Light-driven high-temperature continuous-flow synthesis of TiO2 nano-anatase. *Chemical Engineering Journal,* 211-212**,** 195-199.

CHEN, J., VACCHIO, M. J., WANG, S., CHERNOVA, N., ZAVALIJ, P. Y. & WHITTINGHAM, M. S. 2008. The hydrothermal synthesis and

characterization of olivines and related compounds for electrochemical applications. *Solid State Ionics,* 178**,** 1676-1693.

CHEN, J. & WHITTINGHAM, M. S. 2006. Hydrothermal synthesis of lithium iron phosphate. *Electrochemistry Communications,* 8**,** 855-858.

CHEN, J., XU, L., LI, W. & GOU, X. 2005. α-$Fe_2O_3$ nanotubes in gas sensor and lithium-ion battery applications. *Advanced Materials,* 17**,** 582-586.

CHEN, M. & GAO, L. 2006. Synthesis of leaf-like $Ag_2S$ nanosheets by hydrothermal method in water–alcohol homogenous medium. *Materials Letters,* 60**,** 1059-1062.

CHEN, M., LIN, T., MA, C. Y. & WANG, X. Z. Population Balance Modelling and Experimental Study for Synthesis of $TiO_2$ Nanoparticles using Continuous Hydrothermal Process. Advanced Control of Chemical Processes, 2012. 609-613.

CHEN, S. & LIU, W. 2001. Characterization and antiwear ability of non-coated ZnS nanoparticles and DDP-coated ZnS nanoparticles. *Materials Research Bulletin,* 36**,** 137-143.

CHEN, S. & LIU, W. 2006. Oleic acid capped PbS nanoparticles: synthesis, characterization and tribological properties. *Materials Chemistry and Physics,* 98**,** 183-189.

CHEN, X. & MAO, S. S. 2007. Titanium dioxide nanomaterials: synthesis, properties, modifications, and applications. *Chem. Rev,* 107**,** 2891-2959.

CHERUVALLY, G. 2008. Introduction. *Materials Science Foundations (monograph series),* 38**,** 1-6.

CHHOWALLA, M. & AMARATUNGA, G. A. 2000. Thin films of fullerene-like $MoS_2$ nanoparticles with ultra-low friction and wear. *Nature,* 407**,** 164-167.

CHOI, D. & KUMTA, P. N. 2007. Surfactant based sol–gel approach to nanostructured $LiFePO_4$ for high rate Li-ion batteries. *Journal of Power Sources,* 163**,** 1064-1069.

CHUNG, S.-Y., BLOKING, J. T. & CHIANG, Y.-M. 2002. Electronically conductive phospho-olivines as lithium storage electrodes. *Nature materials,* 1**,** 123-128.

DAI, W., KHEIREDDIN, B., GAO, H. & LIANG, H. 2016. Roles of nanoparticles in oil lubrication. *Tribology International,* 102**,** 88-98.

DAMBOURNET, D., BELHAROUAK, I. & AMINE, K. 2009. Tailored Preparation Methods of $TiO_2$ Anatase, Rutile, Brookite: Mechanism of Formation and Electrochemical Properties†. *Chemistry of materials,* 22**,** 1173-1179.

DANGSHENG, X. 2001. Lubrication behavior of Ni–Cr-based alloys containing $MoS_2$ at high temperature. *Wear,* 251**,** 1094-1099.

DE BARROS, M., BOUCHET, J., RAOULT, I., LE MOGNE, T., MARTIN, J., KASRAI, M. & YAMADA, Y. 2003. Friction reduction by metal sulfides in boundary lubrication studied by XPS and XANES analyses. *Wear,* 254**,** 863-870.

DELACOURT, C., POIZOT, P. & MASQUELIER, C. 2006. Crystalline Nanometric $LiFePO_4$. Google Patents.

DENG, H., CHEN, C., PENG, Q. & LI, Y. 2006. Formation of transition-metal sulfide microspheres or microtubes. *Materials chemistry and physics,* 100**,** 224-229.

DEORSOLA, F. A., RUSSO, N., BLENGINI, G. A. & FINO, D. 2012. Synthesis, characterization and environmental assessment of nanosized $MoS_2$ particles for lubricants applications. *Chemical Engineering Journal,* 195**,** 1-6.

DEVARAJU, M. K. & HONMA, I. 2012. Hydrothermal and Solvothermal Process Towards Development of $LiMPO_4$ (M= Fe, Mn) Nanomaterials for Lithium-Ion Batteries. *Advanced Energy Materials,* 2**,** 284-297.

DIEBOLD, U. 2003. The surface science of titanium dioxide. *Surface science reports,* 48**,** 53-229.

## References


DING, Y., XU, B., GUO, R. & SHEN, M. 2005. The preparation of silver sulfide nanoparticles in lamellar liquid crystal and application to lubrication. *Materials research bulletin,* 40**,** 575-582.

DONG, L., CHU, Y., LIU, Y. & LI, L. 2008. Synthesis of faceted and cubic $Ag_2S$ nanocrystals in aqueous solutions. *Journal of colloid and interface science,* 317**,** 485-492.

DU, Y., YIN, Z., ZHU, J., HUANG, X., WU, X.-J., ZENG, Z., YAN, Q. & ZHANG, H. 2012. A general method for the large-scale synthesis of uniform ultrathin metal sulphide nanocrystals. *Nature communications,* 3**,** 1177.

DUAN, B. & LEI, H. 2001. The effect of particle size on the lubricating properties of colloidal polystyrene used as water based lubrication additive. *Wear,* 249**,** 528-532.

DUNNE, P. W., MUNN, A. S., STARKEY, C. L., HUDDLE, T. A. & LESTER, E. H. 2015a. Continuous-flow hydrothermal synthesis for the production of inorganic nanomaterials. *Phil. Trans. R. Soc. A,* 373**,** 20150015.

DUNNE, P. W., MUNN, A. S., STARKEY, C. L. & LESTER, E. H. 2015b. The sequential continuous-flow hydrothermal synthesis of molybdenum disulphide. *Chemical Communications,* 51**,** 4048-4050.

DUNNE, P. W., STARKEY, C. L., GIMENO-FABRA, M. & LESTER, E. H. 2014. The rapid size-and shape-controlled continuous hydrothermal synthesis of metal sulphide nanomaterials. *Nanoscale,* 6**,** 2406-2418.

EDELSTEIN, A. S. & CAMMARATRA, R. 1998. *Nanomaterials: synthesis, properties and applications*, CRC press.

EVANS, H. & KONNERT, J. 1976. Crystal structure refinement of covellite. *Am. Mineral,* 61**,** 996-1000.

FAN, C., LI, Q., CHEN, S., FAN, J., WEN, Z., ZENG, T., ZHANG, X. & HAN, S. 2016. Poly (vinylpylrrolidone) as Surfactant in the Sol–Gel Preparation of Lithium Iron Phospate/Carbon Cathodes for Lithium-Ion Batteries. *Energy Technology,* 4**,** 973-979.

FELDMAN, Y., FREY, G., HOMYONFER, M., LYAKHOVITSKAYA, V., MARGULIS, L., COHEN, H., HODES, G., HUTCHISON, J. & TENNE, R. 1996. Bulk synthesis of inorganic fullerene-like $MS_2$ (M= Mo, W) from the respective trioxides and the reaction mechanism. *Journal of the American Chemical Society,* 118**,** 5362-5367.

FORCE, E. R. 1991. *Geology of titanium-mineral deposits*, Geological Society of America.

FRANCESCO, F., RENZO, S. & GIUSEPPE, S. 1971. Process for the purification of titanium tetrachloride. Google Patents.

FRANGER, S., LE CRAS, F., BOURBON, C. & ROUAULT, H. 2003. Comparison between different $LiFePO_4$ synthesis routes and their influence on its physico-chemical properties. *Journal of Power Sources,* 119**,** 252-257.

FRANKS, A. 1987. NANOTECHNOLOGY. *Journal of Physics E-Scientific Instruments,* 20**,** 1442-1451.

GABBOTT, P. 2008. *Principles and applications of thermal analysis*, John Wiley & Sons.

GABERSCEK, M., DOMINKO, R. & JAMNIK, J. 2007. Is small particle size more important than carbon coating? An example study on $LiFePO_4$ cathodes. *Electrochemistry Communications,* 9**,** 2778-2783.

GAO, F., LU, Q. & KOMARNENI, S. 2005. Interface reaction for the self-assembly of silver nanocrystals under microwave-assisted solvothermal conditions. *Chemistry of materials,* 17**,** 856-860.

GAO, J., LI, Q., ZHAO, H., LI, L., LIU, C., GONG, Q. & QI, L. 2008. One-pot synthesis of uniform $Cu_2O$ and CuS hollow spheres and their optical limiting properties. *Chemistry of Materials,* 20**,** 6263-6269.

GAO, Y., CHEN, G., OLI, Y., ZHANG, Z. & XUE, Q. 2002. Study on tribological properties of oleic acid-modified $TiO_2$ nanoparticle in water. *Wear,* 252**,** 454-458.

## References


GAYA, U. I. & ABDULLAH, A. H. 2008. Heterogeneous photocatalytic degradation of organic contaminants over titanium dioxide: a review of fundamentals, progress and problems. *Journal of Photochemistry and Photobiology C: Photochemistry Reviews,* 9**,** 1-12.

GIMENO-FABRA, M., DUNNE, P., GRANT, D., GOODEN, P. & LESTER, E. 2013. Continuous flow synthesis of tungsten oxide ($WO_3$) nanoplates from tungsten (VI) ethoxide. *Chemical Engineering Journal,* 226**,** 22-29.

GIMENO-FABRA, M., MUNN, A. S., STEVENS, L. A., DRAGE, T. C., GRANT, D. M., KASHTIBAN, R. J., SLOAN, J., LESTER, E. & WALTON, R. I. 2012. Instant MOFs: continuous synthesis of metal–organic frameworks by rapid solvent mixing. *Chemical Communications,* 48**,** 10642-10644.

GREENWOOD, N. N. & EARNSHAW, A. 2012. *Chemistry of the Elements*, Elsevier.

GRUAR, R. I., TIGHE, C. J. & DARR, J. A. 2013. Scaling-up a confined jet reactor for the continuous hydrothermal manufacture of nanomaterials. *Industrial & Engineering Chemistry Research,* 52**,** 5270-5281.

GRUBB, G. F. & BAKSHI, B. R. 2011. Life cycle of titanium dioxide nanoparticle production. *Journal of Industrial Ecology,* 15**,** 81-95.

GUINÉE, J., GORRÉE, M., HEIJUNGS, R., HUPPES, G., KLEIJN, R., DE KONING, A., VAN OERS, L., WEGENER SLEESWIJK, A., SUH, S. & UDO DE HAES, H. 2001. Life cycle assessment; An operational guide to the ISO standards; Parts 1 and 2. *Ministry of housing, spatial planning and environment (VROM) and centre of environmental science (CML), Den Haag and Leiden, The Netherlands*.

GULZAR, M., MASJUKI, H., KALAM, M., VARMAN, M., ZULKIFLI, N., MUFTI, R. & ZAHID, R. 2016. Tribological performance of nanoparticles as lubricating oil additives. *Journal of Nanoparticle Research,* 18**,** 223.

HAINES, P. J. 2012. *Thermal methods of analysis: principles, applications and problems*, Springer Science & Business Media.

HASSAN, M. & ALI, A. 2008. Synthesis of nanostructured cadmium and zinc sulfides in aqueous solutions of hyperbranched polyethyleneimine. *Journal of Crystal Growth,* 310**,** 5252-5258.

HE, A., HUANG, S., YUN, J.-H., WU, H., JIANG, Z., STOKES, J., JIAO, S., WANG, L. & HUANG, H. 2017. Tribological Performance and Lubrication Mechanism of Alumina Nanoparticle Water-Based Suspensions in Ball-on-Three-Plate Testing. *Tribology Letters,* 65**,** 40.

HENCH, L. L. & WEST, J. K. 1990. The sol-gel process. *Chemical reviews,* 90**,** 33-72.

HIGUCHI, M., KATAYAMA, K., AZUMA, Y., YUKAWA, M. & SUHARA, M. 2003. Synthesis of $LiFePO_4$ cathode material by microwave processing. *Journal of Power Sources,* 119**,** 258-261.

HIRANI, H. 2016. *Fundamentals of Engineering Tribology with applications*, Cambridge University Press.

HOBBS, H., BRIDDON, S. & LESTER, E. 2009. The synthesis and fluorescent properties of nanoparticulate $ZrO_2$ doped with Eu using continuous hydrothermal synthesis. *Green Chemistry,* 11**,** 484-491.

HONDA, R. J., KEENE, V., DANIELS, L. & WALKER, S. L. 2014. Removal of $TiO_2$ nanoparticles during primary water treatment: role of coagulant type, dose, and nanoparticle concentration. *Environmental engineering science,* 31**,** 127-134.

HONG, S.-A., KIM, S. J., CHUNG, K. Y., CHUN, M.-S., LEE, B. G. & KIM, J. 2013a. Continuous synthesis of lithium iron phosphate ($LiFePO_4$) nanoparticles in supercritical water: effect of mixing tee. *The Journal of Supercritical Fluids,* 73**,** 70-79.

HONG, S.-A., KIM, S. J., CHUNG, K. Y., LEE, Y.-W., KIM, J. & SANG, B.-I. 2013b. Continuous synthesis of lithium iron phosphate nanoparticles in

## References


supercritical water: Effect of process parameters. *Chemical engineering journal,* 229**,** 313-323.

HONG, S.-A., KIM, S. J., KIM, J., CHUNG, K. Y., CHO, B.-W. & KANG, J. W. 2011a. Small capacity decay of lithium iron phosphate ($LiFePO_4$) synthesized continuously in supercritical water: comparison with solid-state method. *The Journal of Supercritical Fluids,* 55**,** 1027-1037.

HONG, S.-A., KIM, S. J., KIM, J., LEE, B. G., CHUNG, K. Y. & LEE, Y.-W. 2012. Carbon coating on lithium iron phosphate ($LiFePO_4$): Comparison between continuous supercritical hydrothermal method and solid-state method. *Chemical Engineering Journal,* 198-199**,** 318-326.

HONG, S.-A., NUGROHO, A., KIM, S. J., KIM, J., CHUNG, K. Y., CHO, B.-W. & KANG, J. W. 2011b. Continuous supercritical hydrothermal synthesis: lithium secondary ion battery applications. *Research on Chemical Intermediates,* 37**,** 429-440.

HORIBA, T. 2014. Lithium-ion battery systems. *Proceedings of the IEEE,* 102**,** 939-950.

HOWELL, D. 2008. Annual Progress Report for the Energy Storage Research and Development (Energy Efficiency and Renewable Energy Vehicle Technologies). *US Department of Energy*.

HU, S., CHEN, W., ZHOU, J., YIN, F., UCHAKER, E., ZHANG, Q. & CAO, G. 2014. Preparation of carbon coated $MoS_2$ flower-like nanostructure with self-assembled nanosheets as high-performance lithium-ion battery anodes. *Journal of Materials Chemistry A,* 2**,** 7862-7872.

HUANG, H., FAULKNER, T., BARKER, J. & SAIDI, M. 2009. Lithium metal phosphates, power and automotive applications. *Journal of Power Sources,* 189**,** 748-751.

IRIARTE, A., ALMEIDA, M. G. & VILLALOBOS, P. 2014. Carbon footprint of premium quality export bananas: Case study in Ecuador, the world's largest exporter. *Science of the Total Environment,* 472**,** 1082-1088.

ISO-14040 2006. 14040 (2006). *Environmental management - Life cycle assessment - Principles and framework*.

ISO-14044 2006. 14044 (2006). *Environmental management - Life cycle assessment - Requirements and guidelines*.

JACOBSON, A. R., MARTÍNEZ, C. E., SPAGNUOLO, M., MCBRIDE, M. B. & BAVEYE, P. 2005. Reduction of silver solubility by humic acid and thiol ligands during acanthite ($\beta$-$Ag_2S$) dissolution. *Environmental pollution,* 135**,** 1-9.

JANG, H. & TANIGUCHI, I. 2017. Influence of impregnated carbon on preparation and electrochemical properties of $Li_2FeP_2O_7$ composite synthesized by spray pyrolysis. *Journal of Alloys and Compounds,* 709**,** 557-565.

JCR 2002. Electricity Mix AC, 240 V to consumer (UK). *European Commission, Joint Research Center,* (ILCD).

JESWANI, H. K., SMITH, R. W. & AZAPAGIC, A. 2013. Energy from waste: carbon footprint of incineration and landfill biogas in the UK. *The International Journal of Life Cycle Assessment,* 18**,** 218-229.

JOHNSON, I. D., LÜBKE, M., WU, O. Y., MAKWANA, N. M., SMALES, G. J., ISLAM, H. U., DEDIGAMA, R. Y., GRUAR, R. I., TIGHE, C. J., SCANLON, D. O., CORÀA, F., BRETTC, D. J. L., SHEARINGC, P. R. & DARR, J. A. 2016. Pilot-scale continuous synthesis of a vanadium-doped $LiFePO_4$/C nanocomposite high-rate cathodes for lithium-ion batteries. *Journal of Power Sources,* 302**,** 410-418.

JOO, J., NA, H. B., YU, T., YU, J. H., KIM, Y. W., WU, F., ZHANG, J. Z. & HYEON, T. 2003. Generalized and facile synthesis of semiconducting metal sulfide nanocrystals. *Journal of the American Chemical Society,* 125**,** 11100-11105.

## References


JUGOVIĆ, D. & USKOKOVIĆ, D. 2009. A review of recent developments in the synthesis procedures of lithium iron phosphate powders. *Journal of Power Sources,* 190**,** 538-544.

JULIEN, C., ZAGHIB, K., MAUGER, A., MASSOT, M., AIT-SALAH, A., SELMANE, M. & GENDRON, F. 2006. Characterization of the carbon coating onto $LiFePO_4$ particles used in lithium batteries. *Journal of Applied Physics,* 100**,** 063511.

KABYEMELA, B. M., ADSCHIRI, T., MALALUAN, R. M. & ARAI, K. 1999. Glucose and fructose decomposition in subcritical and supercritical water: detailed reaction pathway, mechanisms, and kinetics. *Industrial & Engineering Chemistry Research,* 38**,** 2888-2895.

KAKIHANA, M., KOBAYASHI, M., TOMITA, K. & PETRYKIN, V. 2010. Application of water-soluble titanium complexes as precursors for synthesis of titanium-containing oxides via aqueous solution processes. *Bulletin of the Chemical Society of Japan,* 83**,** 1285-1308.

KALIN, M., KOGOVŠEK, J. & REMŠKAR, M. 2012. Mechanisms and improvements in the friction and wear behavior using $MoS_2$ nanotubes as potential oil additives. *Wear,* 280**,** 36-45.

KALPANA, K. & SELVARAJ, V. 2016. Thiourea assisted hydrothermal synthesis of $ZnS/CdS/Ag_2S$ nanocatalysts for photocatalytic degradation of Congo red under direct sunlight illumination. *RSC Advances,* 6**,** 4227-4236.

KANG, B. & CEDER, G. 2009. Battery materials for ultrafast charging and discharging. *Nature,* 458**,** 190-193.

KANG, X., WANG, B., ZHU, L. & ZHU, H. 2008. Synthesis and tribological property study of oleic acid-modified copper sulfide nanoparticles. *Wear,* 265**,** 150-154.

KATARI, V., DEVITT, T. W. & PARSONS, T. 1977. Industrial Process Profiles for Environmental Use: Chapter 26. Titanium Industry.

KAWASAKI, S.-I., XIUYI, Y., SUE, K., HAKUTA, Y., SUZUKI, A. & ARAI, K. 2009. Continuous supercritical hydrothermal synthesis of controlled size and highly crystalline anatase $TiO_2$ nanoparticles. *The Journal of Supercritical Fluids,* 50**,** 276-282.

KESSLER, V. G. 2013. Aqueous route to $TiO_2$-based nanomaterials using pH-neutral carboxylate precursors. *Journal of sol-gel science and technology,* 68**,** 464-470.

KLUGG, H. & ALEXANDER, L. 1974. *X-Ray Diffraction Procedures for Polycrystalline and Amorphous MaterialsWiley Interscience*, New York.

KOLTYPIN, M., AURBACH, D., NAZAR, L. & ELLIS, B. 2007. More on the performance of $LiFePO_4$ electrodes—the effect of synthesis route, solution composition, aging, and temperature. *Journal of Power Sources,* 174**,** 1241-1250.

KONAROVA, M. & TANIGUCHI, I. 2009. Preparation of carbon coated $LiFePO_4$ by a combination of spray pyrolysis with planetary ball-milling followed by heat treatment and their electrochemical properties. *Powder Technology,* 191**,** 111-116.

KONAROVA, M. & TANIGUCHI, I. 2010. Synthesis of carbon-coated $LiFePO_4$ nanoparticles with high rate performance in lithium secondary batteries. *Journal of Power Sources,* 195**,** 3661-3667.

KRALISCH, D., OTT, D. & GERICKE, D. 2015. Rules and benefits of Life Cycle Assessment in green chemical process and synthesis design: a tutorial review. *Green Chemistry,* 17**,** 123-145.

KUMARI, P., CHANDRAN, P. & KHAN, S. S. 2014. Synthesis and characterization of silver sulfide nanoparticles for photocatalytic and antimicrobial applications. *Journal of Photochemistry and Photobiology B: Biology,* 141**,** 235-240.

## References


LEE, J. & TEJA, A. S. 2005. Characteristics of lithium iron phosphate ($LiFePO_4$) particles synthesized in subcritical and supercritical water. *The Journal of supercritical fluids,* 35**,** 83-90.

LEE, J. & TEJA, A. S. 2006. Synthesis of $LiFePO_4$ micro and nanoparticles in supercritical water. *Materials Letters,* 60**,** 2105-2109.

LESTER, E., AKSOMAITYTE, G., LI, J., GOMEZ, S., GONZALEZ-GONZALEZ, J. & POLIAKOFF, M. 2012. Controlled continuous hydrothermal synthesis of cobalt oxide ($Co_3O_4$) nanoparticles. *Progress in Crystal Growth and Characterization of Materials,* 58**,** 3-13.

LESTER, E. & AZZOPARDI, B. 2004. Counter Current Mixing Device. *Patent CA 2597480 C - US 7566436 B2*.

LESTER, E., BLOOD, P., DENYER, J., GIDDINGS, D., AZZOPARDI, B. & POLIAKOFF, M. 2006. Reaction engineering: The supercritical water hydrothermal synthesis of nano-particles. *The Journal of Supercritical Fluids,* 37**,** 209-214.

LESTER, E., TANG, S. V., KHLOBYSTOV, A., ROSE, V. L., BUTTERY, L. & ROBERTS, C. J. 2013. Producing nanotubes of biocompatible hydroxyapatite by continuous hydrothermal synthesis. *CrystEngComm,* 15**,** 3256-3260.

LESTER, E. H. & AZZOPARDI, B. J. 2009. Counter current mixing reactor. Google Patents.

LEVARD, C., HOTZE, E. M., LOWRY, G. V. & BROWN JR, G. E. 2012. Environmental transformations of silver nanoparticles: impact on stability and toxicity. *Environmental science & technology,* 46**,** 6900-6914.

LEWIS, A. E. 2010. Review of metal sulphide precipitation. *Hydrometallurgy,* 104**,** 222-234.

LI, D. P., ZHENG, Z., LEI, Y., YANG, F. L., GE, S. X., ZHANG, Y. D., HUANG, B. J., GAO, Y. H., WONG, K. W. & LAU, W. M. 2011. From Nanoplates to Microtubes and Microrods: A Surfactant-Free Rolling Mechanism for Facile Fabrication and Morphology Evolution of $Ag_2S$ Films. *Chemistry–A European Journal,* 17**,** 7694-7700.

LI, Q., MAHENDRA, S., LYON, D. Y., BRUNET, L., LIGA, M. V., LI, D. & ALVAREZ, P. J. 2008. Antimicrobial nanomaterials for water disinfection and microbial control: potential applications and implications. *Water research,* 42**,** 4591-4602.

LI, X. L., GE, J. P. & LI, Y. D. 2004. Atmospheric Pressure Chemical Vapor Deposition: An Alternative Route to Large-Scale $MoS_2$ and $WS_2$ Inorganic Fullerene-like Nanostructures and Nanoflowers. *Chemistry-A European Journal,* 10**,** 6163-6171.

LIANG, G., WANG, L., OU, X., ZHAO, X. & XU, S. 2008. Lithium iron phosphate with high-rate capability synthesized through hydrothermal reaction in glucose solution. *Journal of Power Sources,* 184**,** 538-542.

LIANG, Y., SU, J., XI, B., YU, Y., JI, D., SUN, Y., CUI, C. & ZHU, J. 2017. Life cycle assessment of lithium-ion batteries for greenhouse gas emissions. *Resources, Conservation and Recycling,* 117**,** 285-293.

LIM, W. P., ZHANG, Z., LOW, H. Y. & CHIN, W. S. 2004. Preparation of $Ag_2S$ nanocrystals of predictable shape and size. *Angewandte Chemie,* 116**,** 5803-5807.

LIU, W.-T. 2006. Nanoparticles and their biological and environmental applications. *Journal of Bioscience and bioengineering,* 102**,** 1-7.

LIU, Y. & CAO, C. 2010. Enhanced electrochemical performance of nano-sized $LiFePO_4$/C synthesized by an ultrasonic-assisted co-precipitation method. *Electrochimica Acta,* 55**,** 4694-4699.

LU, Q., GAO, F. & ZHAO, D. 2002. Creation of a Unique Self-Supported Pattern of Radially Aligned Semiconductor $Ag_2S$ Nanorods. *Angewandte Chemie International Edition,* 41**,** 1932-1934.

## References


LUNA, F. M. T., ROCHA, B. S., ROLA, E. M., ALBUQUERQUE, M. C., AZEVEDO, D. C. & CAVALCANTE, C. L. 2011. Assessment of biodegradability and oxidation stability of mineral, vegetable and synthetic oil samples. *Industrial Crops and Products,* 33**,** 579-583.

LUZ, S. M., CALDEIRA-PIRES, A. & FERRÃO, P. M. 2010. Environmental benefits of substituting talc by sugarcane bagasse fibers as reinforcement in polypropylene composites: Ecodesign and LCA as strategy for automotive components. *Resources, Conservation and Recycling,* 54**,** 1135-1144.

MA, D., HU, X., ZHOU, H., ZHANG, J. & QIAN, Y. 2007. Shape-controlled synthesis and formation mechanism of nanoparticles-assembled $Ag_2S$ nanorods and nanotubes. *Journal of crystal growth,* 304**,** 163-168.

MACWAN, D., DAVE, P. N. & CHATURVEDI, S. 2011. A review on nano-$TiO_2$ sol–gel type syntheses and its applications. *Journal of Materials Science,* 46**,** 3669-3686.

MAJEAU-BETTEZ, G., HAWKINS, T. R. & STROMMAN, A. H. 2011. Life cycle environmental assessment of lithium-ion and nickel metal hydride batteries for plug-in hybrid and battery electric vehicles. *Environ Sci Technol,* 45**,** 4548-54.

MAKWANA, N. M., TIGHE, C. J., GRUAR, R. I., MCMILLAN, P. F. & DARR, J. A. 2016. Pilot plant scale continuous hydrothermal synthesis of nano-titania; effect of size on photocatalytic activity. *Materials Science in Semiconductor Processing,* 42**,** 131-137.

MALINGER, K. A., MAGUER, A., THOREL, A., GAUNAND, A. & HOCHEPIED, J.-F. 2011. Crystallization of anatase nanoparticles from amorphous precipitate by a continuous hydrothermal process. *Chemical engineering journal,* 174**,** 445-451.

MARCUS, Y. 2012. Supercritical Water. A Green Solvent: Properties and Uses.: Wiley & Sons, New Jersey.

MERTSCHENK, B., BECK, F. & BAUER, W. 1995. Thiourea and thiourea derivatives. *Ullmann's Encyclopedia of Industrial Chemistry*.

MEWS, A., EYCHMÜLLER, A., GIERSIG, M., SCHOOSS, D. & WELLER, H. 1994. Preparation, characterization, and photophysics of the quantum dot quantum well system cadmium sulfide/mercury sulfide/cadmium sulfide. *The Journal of Physical Chemistry,* 98**,** 934-941.

MIDDLEMAS, S., FANG, Z. Z. & FAN, P. 2013. A new method for production of titanium dioxide pigment. *Hydrometallurgy,* 131**,** 107-113.

MIDDLEMAS, S., FANG, Z. Z. & FAN, P. 2015. Life cycle assessment comparison of emerging and traditional Titanium dioxide manufacturing processes. *Journal of Cleaner Production,* 89**,** 137-147.

MO, Z., LIU, P., GUO, R., DENG, Z., ZHAO, Y. & SUN, Y. 2012. Graphene Sheets/$Ag_2S$ nanocomposites: synthesis and their application in supercapacitor materials. *Materials Letters,* 68**,** 416-418.

MUNN, A. S., DUNNE, P. W., TANG, S. V. & LESTER, E. H. 2015. Large-scale continuous hydrothermal production and activation of ZIF-8. *Chem Commun (Camb),* 51**,** 12811-4.

MURUGAN, A. V., MURALIGANTH, T. & MANTHIRAM, A. 2008. Comparison of microwave assisted solvothermal and hydrothermal syntheses of $LiFePO_4$/C nanocomposite cathodes for lithium ion batteries. *The Journal of Physical Chemistry C,* 112**,** 14665-14671.

NANOMILE 2016. *Nanosafety Cluster Compendium,* http://nanomile.eu-vri.eu/filehandler.ashx?file=15553.

NAVARRO, E., BAUN, A., BEHRA, R., HARTMANN, N. B., FILSER, J., MIAO, A.-J., QUIGG, A., SANTSCHI, P. H. & SIGG, L. 2008. Environmental behavior and ecotoxicity of engineered nanoparticles to algae, plants, and fungi. *Ecotoxicology,* 17**,** 372-386.

NAZRI, G.-A. & PISTOIA, G. 2008. *Lithium batteries: science and technology*, Springer Science & Business Media.

## References


NELLES, J. 1940. Preparation of titanium alcoholates and phenolates. Google Patents.

NI, J., ZHOU, H., CHEN, J. & ZHANG, X. 2005. $LiFePO_4$ doped with ions prepared by co-precipitation method. *Materials letters,* 59**,** 2361-2365.

NI, Y., GE, X., LIU, H., XU, X. & ZHANG, Z. 2001. γ-Irradiation preparation of CdS nano-particles and their formation mechanism in non-water system. *Radiation Physics and Chemistry,* 61**,** 61-64.

NI, Y., WEI, X., HONG, J. & MA, X. 2007. Hydrothermal preparation of PbS crystals and shape evolution. *Materials research bulletin,* 42**,** 17-26.

NIEDERBERGER, M. & GARNWEITNER, G. 2006. Organic reaction pathways in the nonaqueous synthesis of metal oxide nanoparticles. *Chemistry-A European Journal,* 12**,** 7282-7302.

NIELSEN, P., NIELSEN, A., WEIDEMA, B., DALGAARD, R. & HALBERG, N. 2003. LCA food data base. *Representative inventory for resource use and environmental impact of Danish farms and food products. Available on-line at* http://www.lcafood.dk.

NIU, X., LIU, S., XING, R., WANG, X., ZHANG, B., CHEN, J. & YANG, L. 2007. Synthesis of single-crystalline silver sulfide nanowires by diffusion in porous anodic aluminium oxide template. *Materials Letters,* 61**,** 5098-5101.

OHYA, T., ITO, M., YAMADA, K., BAN, T., OHYA, Y. & TAKAHASHI, Y. 2004. Aqueous titanate sols from Ti alkoxide-α-hydroxycarboxylic acid system and preparation of titania films from the sols. *Journal of sol-gel science and technology,* 30**,** 71-81.

OKU, T. 2014. *Structure Analysis of Advanced Nanomaterials: Nanoworld by High-resolution Electron Microscopy*, Walter de Gruyter GmbH & Co KG.

PADHI, A., NANJUNDASWAMY, K., MASQUELIER, C., OKADA, S. & GOODENOUGH, J. 1997a. Effect of structure on the $Fe^{3+}/Fe^{2+}$ redox couple in iron phosphates. *Journal of the Electrochemical Society,* 144**,** 1609-1613.

PADHI, A. K., NANJUNDASWAMY, K. & GOODENOUGH, J. 1997b. Phospho-olivines as positive-electrode materials for rechargeable lithium batteries. *Journal of the electrochemical society,* 144**,** 1188-1194.

PANKHURST, Q. A., CONNOLLY, J., JONES, S. & DOBSON, J. 2003. Applications of magnetic nanoparticles in biomedicine. *Journal of physics D: Applied physics,* 36**,** R167.

PENG, D.-X., CHEN, C.-H., KANG, Y., CHANG, Y.-P. & CHANG, S.-Y. 2010. Size effects of $SiO_2$ nanoparticles as oil additives on tribology of lubricant. *Industrial Lubrication and Tribology,* 62**,** 111-120.

PENG, X., MENG, G., ZHANG, J., WANG, X., ZHAO, L., WANG, Y. & ZHANG, L. 2002. Electrochemical fabrication of ordered $Ag_2S$ nanowire arrays. *Materials Research Bulletin,* 37**,** 1369-1375.

PENNYCOOK, S. J. & NELLIST, P. D. 2011. *Scanning transmission electron microscopy: imaging and analysis*, Springer Science & Business Media.

PIGHINI, C., AYMES, D., MILLOT, N. & SAVIOT, L. 2007. Low-frequency Raman characterization of size-controlled anatase $TiO_2$ nanopowders prepared by continuous hydrothermal syntheses. *Journal of Nanoparticle Research,* 9**,** 309-315.

PINI, M., ROSA, R., NERI, P., BONDIOLI, F. & FERRARI, A. M. 2015. Environmental assessment of a bottom-up hydrolytic synthesis of $TiO_2$ nanoparticles. *Green Chemistry,* 17**,** 518-531.

POURZAHEDI, L. & ECKELMAN, M. J. 2015. Comparative life cycle assessment of silver nanoparticle synthesis routes. *Environmental Science: Nano,* 2**,** 361-369.

QIAN, X.-F., YIN, J., HUANG, J.-C., YANG, Y.-F., GUO, X.-X. & ZHU, Z.-K. 2001. The preparation and characterization of PVA/$Ag_2S$ nanocomposite. *Materials Chemistry and Physics,* 68**,** 95-97.

## References


RAMACHANDRAN, V. S. & BEAUDOIN, J. J. 2000. *Handbook of analytical techniques in concrete science and technology: principles, techniques and applications*, Elsevier.

RAMAIAH, K. S. 1999. Electrical properties of In doped CdS thin films. *Journal of Materials Science: Materials in Electronics,* 10**,** 291-294.

RAPOPORT, L., BILIK, Y., FELDMAN, Y., HOMYONFER, M., COHEN, S. & TENNE, R. 1997. Hollow nanoparticles of $WS_2$ as potential solid-state lubricants. *Nature,* 387**,** 791-3.

RATTE, H. T. 1999. Bioaccumulation and toxicity of silver compounds: a review. *Environmental Toxicology and Chemistry,* 18**,** 89-108.

RAVEENDRAN, P., FU, J. & WALLEN, S. L. 2003. Completely "green" synthesis and stabilization of metal nanoparticles. *Journal of the American Chemical Society,* 125**,** 13940-13941.

RAVET, N., CHOUINARD, Y., MAGNAN, J., BESNER, S., GAUTHIER, M. & ARMAND, M. 2001. Electroactivity of natural and synthetic triphylite. *Journal of Power Sources,* 97**,** 503-507.

RECK, E. & RICHARDS, M. 1999. $TiO_2$ manufacture and life cycle analysis. *Pigment & Resin Technology,* 28**,** 149-157.

REISFELD, R. 2002. Nanosized semiconductor particles in glasses prepared by the sol–gel method: their optical properties and potential uses. *Journal of Alloys and Compounds,* 341**,** 56-61.

SADOVNIKOV, S., GUSEV, A. & REMPEL, A. 2015. Artificial silver sulfide $Ag_2S$: Crystal structure and particle size in deposited powders. *Superlattices and Microstructures,* 83**,** 35-47.

SAGADE, A. A. & SHARMA, R. 2008. Copper sulphide ($Cu_xS$) as an ammonia gas sensor working at room temperature. *Sensors and Actuators B: Chemical,* 133**,** 135-143.

SALAH, A. A., MAUGER, A., ZAGHIB, K., GOODENOUGH, J., RAVET, N., GAUTHIER, M., GENDRON, F. & JULIEN, C. 2006. Reduction $Fe^{3+}$ of impurities in $LiFePO_4$ from pyrolysis of organic precursor used for carbon deposition. *Journal of the Electrochemical Society,* 153**,** A1692-A1701.

SEBENIK, R. F., BURKIN, A. R., DORFLER, R. R., LAFERTY, J. M., LEICHTFRIED, G., MEYER-GRÜNOW, H., MITCHELL, P. C. H., VUKASOVICH, M. S., CHURCH, D. A., VAN RIPER, G. G., GILLILAND, J. C. & THIELKE, S. A. 2000. Molybdenum and Molybdenum Compounds. *Ullmann's Encyclopedia of Industrial Chemistry.* Wiley-VCH Verlag GmbH & Co. KGaA.

ŞENGÜL, H., THEIS, T. L. & GHOSH, S. 2008. Toward sustainable nanoproducts. *Journal of Industrial Ecology,* 12**,** 329-359.

SENTHILKUMAAR, S. & SELVI, R. T. 2008. Synthesis and characterization of one dimensional ZnS nanorods. *Synthesis and Reactivity in Inorganic, Metal-Organic, and Nano-Metal Chemistry,* 38**,** 710-715.

SEPEUR, S. 2008. *Nanotechnology: technical basics and applications*, Vincentz Network GmbH & Co KG.

SHEN, G., CHEN, D., TANG, K., LIU, X., HUANG, L. & QIAN, Y. 2003. General synthesis of metal sulfides nanocrystallines via a simple polyol route. *Journal of Solid State Chemistry,* 173**,** 232-235.

SHYMAN-PROJECT, T. 2015. *SHYMAN Project FP7-NMP4-LA-2012-280983,* http://www.shyman.eu/project.php

SIERRA-PALLARES, J., HUDDLE, T., GARCÍA-SERNA, J., ALONSO, E., MATO, F., SHVETS, I., LUEBBEN, O., COCERO, M. J. & LESTER, E. 2016. Understanding bottom-up continuous hydrothermal synthesis of nanoparticles using empirical measurement and computational simulation. *Nano Research,* 9**,** 3377-3387.

SLOTTE, M., METHA, G. & ZEVENHOVEN, R. 2015. Life cycle indicator comparison of copper, silver, zinc and aluminum nanoparticle production through electric arc evaporation or chemical reduction. *International Journal of Energy and Environmental Engineering,* 6**,** 233-243.

## References


STACHOWIAK, G. & BATCHELOR, A. W. 2004. *Experimental methods in tribology*, Elsevier.

STIEBEROVA, B., ZILKA, M., TICHA, M., FREIBERG, F., CARAMAZANA-GONZALEZ, P., MCKECHNIE, J. & LESTER, E. 2017. Application of ZnO nanoparticles in a self-cleaning coating on a metal panel: an assessment of environmental benefits. *ACS Sustainable Chemistry & Engineering,* 5**,** 2493-2500.

SULLIVAN, J. M., WILLIARD, J. W., WHITE, D. L. & KIM, Y. K. 1983. Production of oxalic acid via the nitric acid oxidation of hardwood (red oak) sawdust. *Industrial & engineering chemistry product research and development,* 22**,** 699-709.

SUN, P., ZHANG, W., HU, X., YUAN, L. & HUANG, Y. 2014. Synthesis of hierarchical $MoS_2$ and its electrochemical performance as an anode material for lithium-ion batteries. *Journal of Materials Chemistry A,* 2**,** 3498-3504.

SURYANARAYANA, C. 2001. Mechanical alloying and milling. *Progress in materials science,* 46**,** 1-184.

TANG, W. & CAMERON, D. 1996. Electroluminescent zinc sulphide devices produced by sol-gel processing. *Thin Solid Films,* 280**,** 221-226.

TANG, Z. & LI, S. 2014. A review of recent developments of friction modifiers for liquid lubricants (2007–present). *Current opinion in solid state and materials science,* 18**,** 119-139.

TANIGUCHI, I. 2005. Physical and Electrochemical Properties of Spherical Nanostructured $LiCr_xMn_{2-x}O_4$ Particles Synthesized by Ultrasonic Spray Pyrolysis. *Industrial & engineering chemistry research,* 44**,** 6560-6565.

TEVET, O., VON-HUTH, P., POPOVITZ-BIRO, R., ROSENTSVEIG, R., WAGNER, H. D. & TENNE, R. 2011. Friction mechanism of individual multilayered nanoparticles. *Proceedings of the National Academy of Sciences,* 108**,** 19901-19906.

THOMPSON, R. 1995. *Industrial inorganic chemicals: production and uses*, Royal Society of Chemistry.

THOMPSON, R. & GROUP, C. S. I. C. 1977. *The Modern inorganic chemicals industry: the proceedings of a symposium organised by the Inorganic Chemicals Group of the Industrial Division of the Chemical Society, London, March 31st - April 1st, 1977*, Chemical Society.

TIAN, S., LOU, S. & ZHOU, S. 2014. Monoclinic α-$Ag_2S$ hollow nanospheres: Promising candidates for ethanol gas sensors at room-temperature. *Materials Letters,* 137**,** 382-384.

TICHÁ, M., ŽILKA, M., STIEBEROVÁ, B. & FREIBERG, F. 2016. Life cycle assessment comparison of photocatalytic coating and air purifier. *Integrated environmental assessment and management,* 12**,** 478-485.

TOFT, L. L., AARUP, D. F., BREMHOLM, M., HALD, P. & IVERSEN, B. B. 2009. Comparison of T-piece and concentric mixing systems for continuous flow synthesis of anatase nanoparticles in supercritical isopropanol/water. *Journal of Solid State Chemistry,* 182**,** 491-495.

TOPRAKCI, O., TOPRAKCI, H. A., JI, L. & ZHANG, X. 2010. Fabrication and electrochemical characteristics of $LiFePO_4$ powders for lithium-ion batteries. *KONA Powder and Particle Journal,* 28**,** 50-73.

TRENGOVE, L. 1972. William Gregor (1761–1817) discoverer of titanium. *Annals of Science,* 29**,** 361-395.

TRINDADE, T., O'BRIEN, P. & PICKETT, N. L. 2001. Nanocrystalline semiconductors: synthesis, properties, and perspectives. *Chemistry of Materials,* 13**,** 3843-3858.

TSANG, M., PHILIPPOT, G., AYMONIER, C. & SONNEMANN, G. 2016. Anticipatory life-cycle assessment of supercritical fluid synthesis of barium strontium titanate nanoparticles. *Green Chemistry,* 18**,** 4924-4933.

## References


TSUZUKI, T. & MCCORMICK, P. G. 1999. Mechanochemical synthesis of metal sulphide nanoparticles. *Nanostructured Materials,* 12**,** 75-78.

TSUZUKI, T. & MCCORMICK, P. G. 2004. Mechanochemical synthesis of nanoparticles. *Journal of materials science,* 39**,** 5143-5146.

VAN DE VELDE, G., HARKEMA, S. & GELLINGS, P. 1974. The crystal and molecular structure of ammonium titanyl oxalate. *Inorganica Chimica Acta,* 11**,** 243-252.

VANDERZEE, C. E. & WESTRUM, E. F. 1970. Heat capacities and thermodynamic properties of ammonium and potassium thiocyanates from 5 to 340 K. *The Journal of Chemical Thermodynamics,* 2**,** 417-429.

VAUGHAN, D. J. 2006. *Sulfide mineralogy and geochemistry*, Mineralogical Society of America.

VAUGHAN, D. J. & CRAIG, J. R. 1978. *Mineral chemistry of metal sulfides*, Cambridge University Press.

VIGNESHWARAN, N., NACHANE, R., BALASUBRAMANYA, R. & VARADARAJAN, P. 2006. A novel one-pot 'green'synthesis of stable silver nanoparticles using soluble starch. *Carbohydrate research,* 341**,** 2012-2018.

VINCE, F., AOUSTIN, E., BRÉANT, P. & MARECHAL, F. 2008. LCA tool for the environmental evaluation of potable water production. *Desalination,* 220**,** 37-56.

WALLACE, B. 2005. *Becoming part of the solution: the engineer's guide to sustainable development*, ASCE Publications.

WANG, C., ZHANG, X., QIAN, X., WANG, W. & QIAN, Y. 1998. Ultrafine powder of silver sulfide semiconductor prepared in alcohol solution. *Materials research bulletin,* 33**,** 1083-1086.

WANG, J. & SUN, X. 2012. Understanding and recent development of carbon coating on $LiFePO_4$ cathode materials for lithium-ion batteries. *Energy & Environmental Science,* 5**,** 5163-5185.

WANG, L., CHEN, L., LUO, T. & QIAN, Y. 2006. A hydrothermal method to prepare the spherical ZnS and flower-like CdS microcrystallites. *Materials Letters,* 60**,** 3627-3630.

WANG, Q., TANG, S. V. Y., LESTER, E. & O'HARE, D. 2013. Synthesis of ultrafine layered double hydroxide (LDHs) nanoplates using a continuous-flow hydrothermal reactor. *Nanoscale,* 5**,** 114-117.

WANG, Y., LI, C., ZHANG, Y., LI, B., YANG, M., ZHANG, X., GUO, S. & LIU, G. 2016. Experimental evaluation of the lubrication properties of the wheel/workpiece interface in MQL grinding with different nanofluids. *Tribology International,* 99**,** 198-210.

WEBER, T., PRINS, R. & VAN SANTEN, R. A. 2013. *Transition metal sulphides: chemistry and catalysis*, Springer Science & Business Media.

WEEKS, M. E. 1933. The discovery of the elements. Chronology. *J. Chem. Educ,* 10**,** 223.

WEGNER, K., SCHIMMOELLER, B., THIEBAUT, B., FERNANDEZ, C. & RAO, T. N. 2011. Pilot plants for industrial nanoparticle production by flame spray pyrolysis. *KONA Powder and Particle Journal,* 29**,** 251-265.

WEIDEMA, B. P., BAUER, C., HISCHIER, R., MUTEL, C., NEMECEK, T., REINHARD, J., VADENBO, C. & WERNET, G. 2013. Overview and methodology: Data quality guideline for the ecoinvent database version 3. Swiss Centre for Life Cycle Inventories.

WEN, X., WANG, S., XIE, Y., LI, X.-Y. & YANG, S. 2005. Low-temperature synthesis of single crystalline $Ag_2S$ nanowires on silver substrates. *The Journal of Physical Chemistry B,* 109**,** 10100-10106.

WENLI, Y., YAPING, Z. & QUNLI, R. 2009. Rapid and continuous production of $LiFePO_4$/C nanoparticles in super heated water. *Chinese Journal of Chemical Engineering,* 17**,** 171-174.

WU, B., LI, N. & REN, Y. 2011. *$LiFePO_4$ cathode material*, INTECH Open Access Publisher.

## References


WU, H., ZHAO, J., XIA, W., CHENG, X., HE, A., YUN, J. H., WANG, L., HUANG, H., JIAO, S. & HUANG, L. 2017. A study of the tribological behaviour of $TiO_2$ nano-additive water-based lubricants. *Tribology International,* 109**,** 398-408.

WU, M., PAN, X., QIAN, X., YIN, J. & ZHU, Z. 2004. Solution-phase synthesis of $Ag_2S$ hollow and concave nanocubes. *Inorganic Chemistry Communications,* 7**,** 359-362.

WU, Z.-S., REN, W., WEN, L., GAO, L., ZHAO, J., CHEN, Z., ZHOU, G., LI, F. & CHENG, H.-M. 2010. Graphene anchored with $Co_3O_4$ nanoparticles as anode of lithium ion batteries with enhanced reversible capacity and cyclic performance. *ACS nano,* 4**,** 3187-3194.

WUEBBLES, D. J. & EDMONDS, J. A. 1991. *Primer on Greeenhouse Gases*, CRC Press.

XIA, Q., CHEN, X., ZHAO, K. & LIU, J. 2008. Synthesis and characterizations of polycrystalline walnut-like CdS nanoparticle by solvothermal method with PVP as stabilizer. *Materials Chemistry and Physics,* 111**,** 98-105.

XIANG, J., CAO, H., WU, Q., ZHANG, S., ZHANG, X. & WATT, A. A. 2008. L-cysteine-assisted synthesis and optical properties of $Ag_2S$ nanospheres. *The Journal of Physical Chemistry C,* 112**,** 3580-3584.

XING, R., LIU, S. & TIAN, S. 2011. Microwave-assisted hydrothermal synthesis of biocompatible silver sulfide nanoworms. *Journal of Nanoparticle Research,* 13**,** 4847-4854.

XU, B., QIAN, D., WANG, Z. & MENG, Y. S. 2012. Recent progress in cathode materials research for advanced lithium ion batteries. *Materials Science and Engineering: R: Reports,* 73**,** 51-65.

XU, C., LEE, J. & TEJA, A. S. 2008. Continuous hydrothermal synthesis of lithium iron phosphate particles in subcritical and supercritical water. *The Journal of Supercritical Fluids,* 44**,** 92-97.

XU, C., ZHANG, Z. & YE, Q. 2004. A novel facile method to metal sulfide (metal= Cd, Ag, Hg) nano-crystallite. *Materials Letters,* 58**,** 1671-1676.

YAMADA, A., CHUNG, S.-C. & HINOKUMA, K. 2001. Optimized $LiFePO_4$ for lithium battery cathodes. *Journal of the electrochemical society,* 148**,** A224-A229.

YAN, S., WANG, H., ZHANG, Y., LI, S. & XIAO, Z. 2008. A simple route to large-scale synthesis of silver sulfide nanowires. *Journal of Non-Crystalline Solids,* 354**,** 5559-5562.

YAN, S., ZHANG, Y., ZHANG, Y. & XIAO, Z. 2009. Synthesis of silver sulfide nanowires in ethylene glycol through a sacrificial templating route. *Inorganic Materials,* 45**,** 193-197.

YANG, S., ZAVALIJ, P. Y. & WHITTINGHAM, M. S. 2001. Hydrothermal synthesis of lithium iron phosphate cathodes. *Electrochemistry Communications,* 3**,** 505-508.

YANG, S., ZHOU, X., ZHANG, J. & LIU, Z. 2010. Morphology-controlled solvothermal synthesis of $LiFePO_4$ as a cathode material for lithium-ion batteries. *Journal of Materials Chemistry,* 20**,** 8086-8091.

YANG, W., XIE, T., JIANG, T. & WANG, D. 2013. Facile preparation of $Ag_2S$ nanoparticles with broad photoelectric response region. *Colloids and Surfaces A: Physicochemical and Engineering Aspects,* 433**,** 55-58.

YASIN, A., GUO, F. & DEMOPOULOS, G. P. 2016. Continuous-reactor, pH-controlled synthesis of multifunctional mesoporous nanocrystalline anatase aggregates. *Chemical Engineering Journal,* 287**,** 398-409.

YAZDANI, B., XU, F., AHMAD, I., HOU, X., XIA, Y. & ZHU, Y. 2015. Tribological performance of Graphene/Carbon nanotube hybrid reinforced $Al_2O_3$ composites. *Scientific reports,* 5**,** 11579.

YU, C., LENG, M., LIU, M., YU, Y., LIU, D. & WANG, C. 2012. Synthesis of normal and flattened rhombic dodecahedral $Ag_2S$ particles. *CrystEngComm,* 14**,** 3772-3777.

## References


YU, Y., WANG, D., HUANG, K., WANG, X., LIANG, Y., SUN, W., CHEN, B. & CHEN, S. 2014. Assessment of cathode active materials from the perspective of integrating environmental impact with electrochemical performance. *Journal of Cleaner Production,* 82**,** 213-220.

YUAN, L.-X., WANG, Z.-H., ZHANG, W.-X., HU, X.-L., CHEN, J.-T., HUANG, Y.-H. & GOODENOUGH, J. B. 2011. Development and challenges of $LiFePO_4$ cathode material for lithium-ion batteries. *Energy & Environmental Science,* 4**,** 269-284.

ZACKRISSON, M., AVELLÁN, L. & ORLENIUS, J. 2010. Life cycle assessment of lithium-ion batteries for plug-in hybrid electric vehicles–Critical issues. *Journal of Cleaner Production,* 18**,** 1519-1529.

ZAGHIB, K., SHIM, J., GUERFI, A., CHAREST, P. & STRIEBEL, K. 2005. Effect of carbon source as additives in $LiFePO_4$ as positive electrode for lithium-ion batteries. *Electrochemical and Solid-State Letters,* 8**,** A207-A210.

ZHANG, J. & RICHARDSON, H. W. 2000. Copper compounds. *Ullmann's Encyclopedia of Industrial Chemistry*.

ZHANG, L.-J., SHEN, X.-C., LIANG, H., GUO, S. & LIANG, Z.-H. 2010. Hot-injection synthesis of highly luminescent and monodisperse CdS nanocrystals using thioacetamide and cadmium source with proper reactivity. *Journal of colloid and interface science,* 342**,** 236-242.

ZHANG, W.-J. 2011. Structure and performance of $LiFePO_4$ cathode materials: a review. *Journal of Power Sources,* 196**,** 2962-2970.

ZHANG, Y., HUANG, B., LI, P., WANG, X. & ZHANG, Y. 2013. Tribological performance of CuS–ZnO nanocomposite film: The effect of CuS doping. *Tribology International,* 58**,** 7-11.

ZHANG, Y., LI, C., JIA, D., ZHANG, D. & ZHANG, X. 2015. Experimental evaluation of $MoS_2$ nanoparticles in jet MQL grinding with different types of vegetable oil as base oil. *Journal of Cleaner Production,* 87**,** 930-940.

ZHANG, Z., BROWN, S., GOODALL, J. B., WENG, X., THOMPSON, K., GONG, K., KELLICI, S., CLARK, R. J., EVANS, J. R. & DARR, J. A. 2009. Direct continuous hydrothermal synthesis of high surface area nanosized titania. *Journal of Alloys and Compounds,* 476**,** 451-456.

ZHAO, J., HE, Y., WANG, Y., WANG, W., YAN, L. & LUO, J. 2016. An investigation on the tribological properties of multilayer graphene and $MoS_2$ nanosheets as additives used in hydraulic applications. *Tribology International,* 97**,** 14-20.

ZHAO, Q. & BAHADUR, S. 1998. A study of the modification of the friction and wear behavior of polyphenylene sulfide by particulate $Ag_2S$ and PbTe fillers. *Wear,* 217**,** 62-72.

ZHOU, Z.-Y., TIAN, N., LI, J.-T., BROADWELL, I. & SUN, S.-G. 2011. Nanomaterials of high surface energy with exceptional properties in catalysis and energy storage. *Chemical Society Reviews,* 40**,** 4167-4185.

ZHU, Y., FAN, D. & SHEN, W. 2008. Chemical conversion synthesis and optical properties of metal sulfide hollow microspheres. *Langmuir,* 24**,** 11131-11136.

ZHUANG, Z., PENG, Q., ZHANG, B. & LI, Y. 2008. Controllable synthesis of $Cu_2S$ nanocrystals and their assembly into a superlattice. *Journal of the American Chemical Society,* 130**,** 10482-10483.

# Appendix

## Laboratory scale simulation

Figure A.1 corresponds with the Aspen HYSYS simulation of the lithium iron phosphate (LFP) nanoparticles synthesis described by Hong et al. (2013b). The modelling of this synthesis was carried out to determine the electrical consumptions of the equipment (pumps and heater), cooling and evaporation stages. Table A.1 describes the material and energy inputs and outputs of the simulation process in Aspen, while Table A.2 corresponds with the Life cycle inventory (LCI) and greenhouse gas (GHG) emissions to produce 1 kg of LFP nanoparticles.

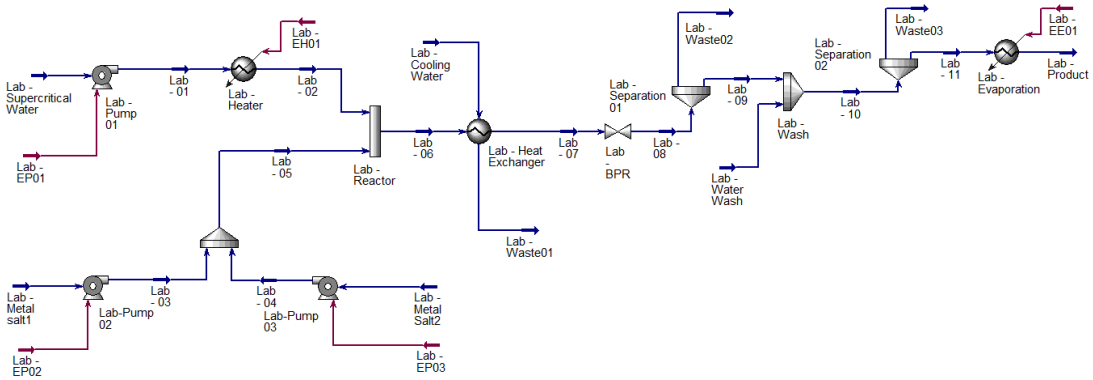



Figure A.1: Aspen HYSYS simulation of laboratory synthesis of LFP nanoparticles.

## Appendix

Table A.1. Inputs and outputs of the Aspen HYSYS simulation for the production of LFP nanoparticles by continuous-flow hydrothermal synthesis at laboratory scale.

| | Stream - Unit | Items | Units | Quantity | Comments |
|---|---|---|---|---|---|
| Inputs | Supercritical Water | $H_2O$ | g $h^{-1}$ | 540.00 | Deionised water |
| | Metal Salt1 | $H_2O$ | g $h^{-1}$ | 102.00 | Deionised water |
| | | $FeSO_4$ | g $h^{-1}$ | 0.47 | - |
| | | $H_3PO_4$ | g $h^{-1}$ | 0.30 | - |
| | Metal Salt2 | $H_2O$ | g $h^{-1}$ | 102.00 | Deionised water |
| | | LiOH | g $h^{-1}$ | 0.22 | - |
| | Pump 01 | Electrical energy | kJ $h^{-1}$ | 17.73 | Efficiency 75% |
| | Pump 02 | Electrical energy | kJ $h^{-1}$ | 3.35 | Efficiency 75% |
| | Pump 03 | Electrical energy | kJ $h^{-1}$ | 3.35 | Efficiency 75% |
| | Heater | Electrical energy | kJ $h^{-1}$ | 1864.40 | Minimum heat to increase the temperature (540 °C) |
| | Cooling Water | $H_2O$ | g $h^{-1}$ | 17015.11 | Inlet Tap water at 15 °C - Outlet 40 °C |
| | Water Wash | $H_2O$ | g $h^{-1}$ | 37.20 | Deionised water |
| | Evaporation | Electrical energy | kJ $h^{-1}$ | 96.47 | Minimum heat to evaporate the water content |
| Outputs | Waste01 | $H_2O$ | g $h^{-1}$ | 17015.11 | - |
| | Waste02 | $H_2O$ | g $h^{-1}$ | 706.80 | - |
| | Waste03 | $H_2O$ | g $h^{-1}$ | 37.20 | - |
| | Product | $LiFePO_4$ | g $h^{-1}$ | 0.46 | - |

**Appendix**

Table A.2. Life cycle inventory and greenhouse gas emissions for the synthesis of 1 kg of LFP nanoparticles at laboratory scale.

| | Categories | Items | Units | Quantity | $CO_2$ eq per kg or MJ | Database - Source | Total $CO_2$ eq per kg LFP |
|---|---|---|---|---|---|---|---|
| Raw Materials | Lithium Hydroxide | LiOH | kg | 0.48 | 2.43 | Ecoinvent data V2.2 (2010) | 1.16 |
| | Deionized Water | $H_2O$ | kg | 1703.45 | 8.52E-03 | ILCD, Europe (2005) | 14.52 |
| | Cooling Water | Tap Water | kg | 37102.33 | 3.40E-04 | Water UK (2010) | 12.61 |
| | Iron Sulfate | $FeSO_4$ | kg | 1.01 | 0.17 | Ecoinvent data V2.2 (2010) | 0.17 |
| | Phosphoric Acid $_{85\ wt\%}$ | $H_3PO_4$ | kg | 0.77 | 1.42 | Ecoinvent data V2.2 (2010) | 1.09 |
| Production Stages | Pumping | Electrical energy | MJ | 53.28 | 0.19 | ILCD, Europe (2005) | 9.90 |
| | Heating & Cooling | Electrical energy | MJ | 4065.42 | 0.19 | ILCD, Europe (2005) | 755.76 |
| | Washing & Evaporation | Electrical energy | MJ | 210.35 | 0.19 | ILCD, Europe (2005) | 39.10 |
| | Water Treatment | Wastewater | kg | 38727.13 | 7.00E-04 | Water UK (2010) | 27.10 |

## Appendix

### Pilot scale simulation

Figure A.2 represents simulation in Aspen HYSYS of the LFP nanoparticles synthesis described by Johnson et al. (2016). Pilot scale was modelled to determine the energy and material inputs of heating, cooling and drying stages. Table A.3 describes all of these inputs and outputs of the simulation process in Aspen HYSYS. Table A.4 corresponds with the LCI and GHG emission to produce 1 kg of LFP nanoparticles at the pilot plant scale.

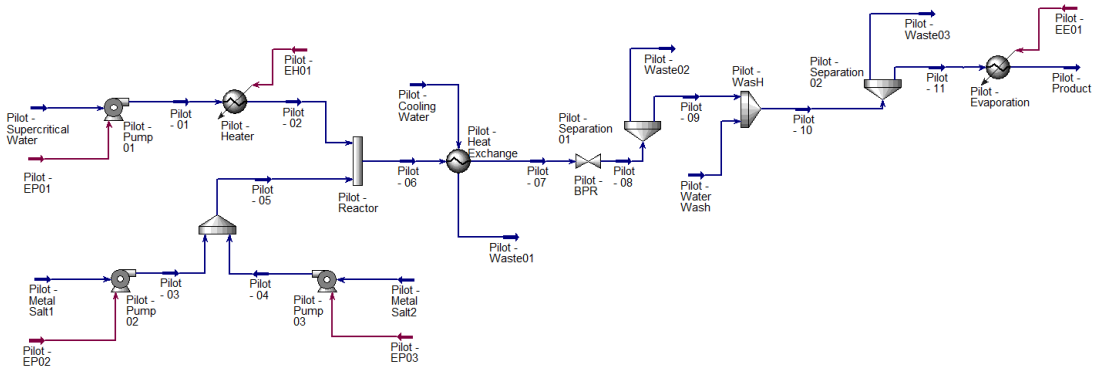



Figure A.2: Aspen HYSYS simulation of pilot scale for the production of LFP nanoparticles.

## Appendix

Table A.3. Inputs and outputs of the Aspen HYSYS simulation for the production of LFP nanoparticles by continuous-flow hydrothermal synthesis at laboratory scale.

| | Stream - Unit | Items | Units | Quantity | Comments |
|---|---|---|---|---|---|
| Inputs | Supercritical Water | $H_2O$ | kg $h^{-1}$ | 24.00 | Deionised water |
| | Metal Salt1 | $H_2O$ | kg $h^{-1}$ | 12.00 | Deionised water |
| | | $FeSO_4$ | g $h^{-1}$ | 455.72 | - |
| | | $H_3PO_4$ | g $h^{-1}$ | 441.00 | - |
| | | Fructose | g $h^{-1}$ | 1891.68 | - |
| | Metal Salt2 | $H_2O$ | kg $h^{-1}$ | 12.00 | Deionised water |
| | | LiOH | g $h^{-1}$ | 247.88 | - |
| | Pump 01 | Electrical energy | kJ $h^{-1}$ | 759.54 | Efficiency 75% |
| | Pump 02 | Electrical energy | kJ $h^{-1}$ | 379.77 | Efficiency 75% |
| | Pump 03 | Electrical energy | kJ $h^{-1}$ | 379.77 | Efficiency 75% |
| | Heater | Electrical energy | kJ $h^{-1}$ | 74230.72 | Minimum heat to increase the temperature (540 °C) |
| | Cooling Water | $H_2O$ | kg $h^{-1}$ | 660.79 | Inlet Tap water at 15 °C - Outlet 40 °C |
| | Water Wash | $H_2O$ | kg $h^{-1}$ | 2.40 | Tap Water |
| | Evaporation | Electrical energy | kJ $h^{-1}$ | 6223.65 | Minimum heat to evaporate the water content |
| Outputs | Waste01 | $H_2O$ | kg $h^{-1}$ | 660.79 | - |
| | Waste02 | $H_2O$ | kg $h^{-1}$ | 45.60 | - |
| | Waste03 | $H_2O$ | kg $h^{-1}$ | 2.40 | - |
| | Product | $LiFePO_4$ | kg $h^{-1}$ | 0.45 | - |

**Appendix**

Table A.4. Life cycle inventory and greenhouse gas emissions for the synthesis of 1 kg of LFP nanoparticles at pilot scale.

| | Categories | Items | Units | Quantity | $CO_2$ eq per kg or MJ | Database - Source | Total $CO_2$ eq per kg LFP |
|---|---|---|---|---|---|---|---|
| Raw Materials | Lithium Hydroxide | LiOH | kg | 0.55 | 2.43 | Ecoinvent data V2.2 (2010) | 1.33 |
| | Deionized Water | $H_2O$ | kg | 111.78 | 8.52E-03 | ILCD, Europe (2005) | 0.95 |
| | Cooling Water | Tap Water | kg | 1469.70 | 3.40E-04 | Water UK (2010) | 0.50 |
| | Iron Sulfate | $FeSO_4$ | kg | 1.01 | 0.17 | Ecoinvent data V2.2 (2010) | 0.17 |
| | Phosphoric Acid $_{85\ wt\%}$ | $H_3PO_4$ | kg | 1.15 | 1.42 | Ecoinvent data V2.2 (2010) | 1.63 |
| Production Stages | Pumping | Electrical energy | MJ | 3.38 | 0.19 | ILCD, Europe (2005) | 0.63 |
| | Heating & Cooling | Electrical energy | MJ | 165.10 | 0.19 | ILCD, Europe (2005) | 30.70 |
| | Washing & Evaporation | Electrical energy | MJ | 13.84 | 0.19 | ILCD, Europe (2005) | 2.57 |
| | Water Treatment | Wastewater | kg | 1579.44 | 7.00E-04 | Water UK (2010) | 1.11 |

## Appendix

### Evaporation and calcination stages for the industrial production

These stages were simulated to determine the mass and energy inputs according to literature review Hong et al. (2013b). Figure A.3 represents the simulation in Aspen HYSYS of the evaporation stage, which determines the minimum energy to dry the concentrated suspension at the industrial scenario. Figure A.4 corresponds with the process flow diagram of the calcination step, which uses a furnace to increase the temperature of the inert gases. Also, Table A.5 and A.6 describe all of the requirements used to dry and calcine 1 kg of LFP nanoparticles and the greenhouse gas emissions (GHG) per kg of LFP nanoparticles.

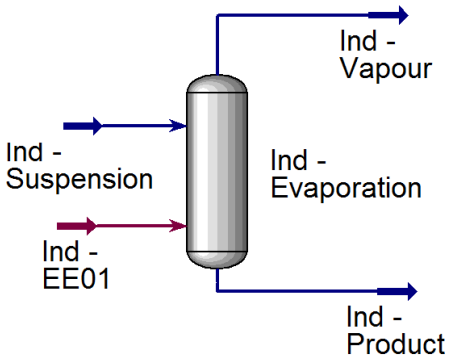



Figure A.3: Aspen HYSYS simulation of the evaporation stage for the industrial production.

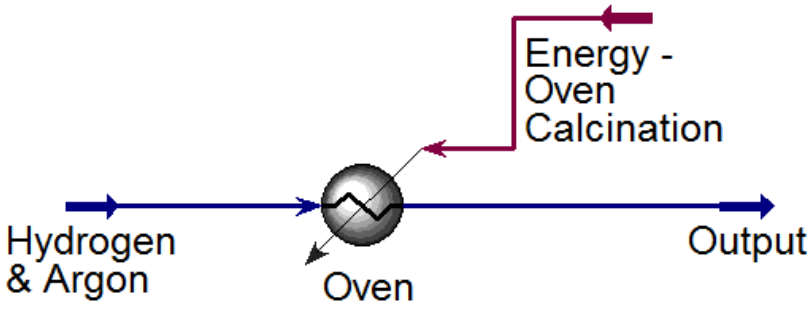



Figure A.4: Aspen HYSYS simulation of the calcination stage.

## Appendix

Table A.5. Life cycle inventory and total greenhouse gas emissions to dry 1 kg of LFP nanoparticles for the industrial scale of the continuous-flow hydrothermal synthesis.

| Items | Units | Quantity | $CO_2$ eq per MJ | Source | Total kg $CO_2$-eq/kg LFP |
|---|---|---|---|---|---|
| Suspension Inlet | Kg of $H_2O$ | 4.00 | - | - | - |
| Natural gas burned in a boiler | MJ | 10.40 | 6.82E-02 | Ecoinvent data V2.2 (2010) | 0.71 |

Table A.6. Life cycle inventory and total greenhouse gas emissions to calcine 1 kg of C-LFP for the laboratory, pilot and industrial scale of the continuous-flow hydrothermal synthesis.

| Items | Units | Quantity | $CO_2$ eq per kg or MJ | Source | Total kg $CO_2$-eq/kg C-LFP |
|---|---|---|---|---|---|
| $H_2O$ | kg | 0.33 | 8.52E-03 | ILCD, Europe (2005) | 2.77E-03 |
| Sucrose | kg | 0.07 | 0.60 | British Sugar, UK (2008) | 0.04 |
| Argon | kg | 23.40 | 0.27 | Ecoinvent data V2.2 (2010) | 6.40 |
| Hydrogen | kg | 0.06 | 0.92 | Ecoinvent data V2.2 (2010) | 0.06 |
| Electrical energy | MJ | 7.60 | 0.19 | ILCD, Europe (2005) | 1.41 |

## Appendix

### Titanium oxysulfate production

Ilmenite mineral and sulfuric acid are mixed in a digester to under heating (130 ºC). After digestion, liquid phased is cooled down (water and cooling system) up to 10-15 ºC to precipitate iron sulfate ($FeSO_4$) from the solution of titanium oxysulfate (TiOS). Figure A.5 shows the process flow diagram from Aspen simulate, which was used to estimate material and energy inputs of the TiOS production in a batch system. Also, table A.7 defines the assumptions and main streams of the simulation in Aspen HYSYS.

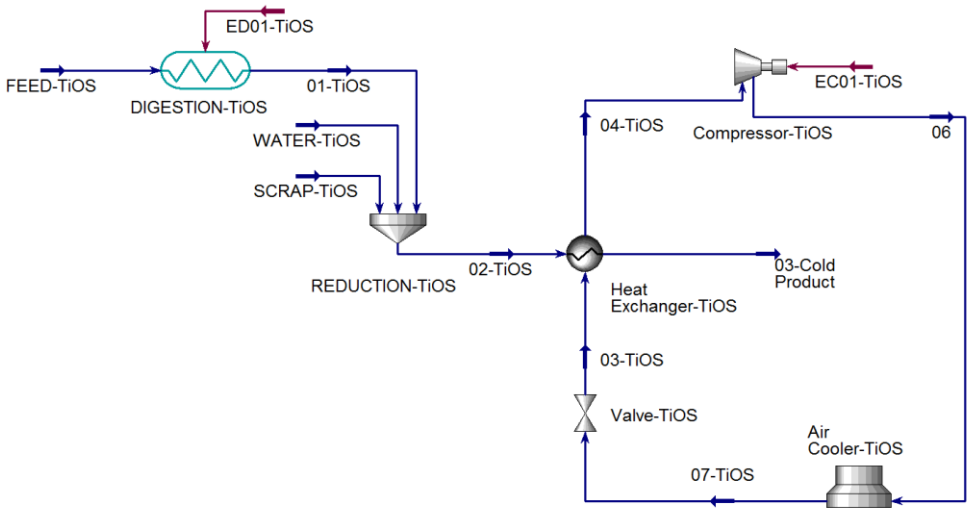



Figure A.5: Aspen HYSYS simulation of the titanium oxysulfate production.

## Appendix

Table A.7. Inputs and outputs for the production of 1 kg of TiOS precursor (15 %wt.) in Aspen HYSYS simulation.

| | Stream - Unit | Items | Units | Quantity | Comments |
|---|---|---|---|---|---|
| Inputs | Feed-TiOS | $H_2SO_{4\ 95\%wt.}$ | kg | 0.14 | - |
| | | Ilmenite | kg | 0.30 | 55% $TiO_2$ |
| | Water-TiOS | $H_2O$ | kg | 0.83 | Deionised water |
| | Scrap-TiOS | Fe | kg | 0.01 | - |
| | ED01-TiOS | Energy, natural gas | MJ | 0.05 | Minimum heat to increase the temperature (130 °C) |
| | EC01-TiOS | Electrical energy | MJ | 1.91E-02 | Efficiency 75%, compressor with Refrig - 717 |
| | Air cooler - TiOS | Electrical energy | MJ | 1.68E-03 | Air inlet 25 °C – Air outlet 35°C Fan speed 60 rpm |
| Outputs | 03 - Cold Product | $FeSO_4$ | kg | 1.84 | Precipitation |
| | | $TiOSO_4$ | kg | 1.00 | 15 %wt. |

## Appendix

### Titanium tetrachloride production

Coal, rutile mineral and chlorine are mixed in a fluidized reactor, which operates in steady state at high temperature (900 ºC). The temperature is maintained by the exothermic reaction between the reagents, operating the system in steady state. After the chlorination, solids and impurities are precipitated. Finally, the gas stream is cooled down to precipitate more impurities (metal chlorides). Finally the product is distillate to increase the purity. Figure A.6 represents simulation in Aspen, which was carried out to determine material and energy inputs of the titanium tetrachloride ($TiCl_4$) production. Also, table A.8 defines the main streams of the simulation in Aspen HYSYS.

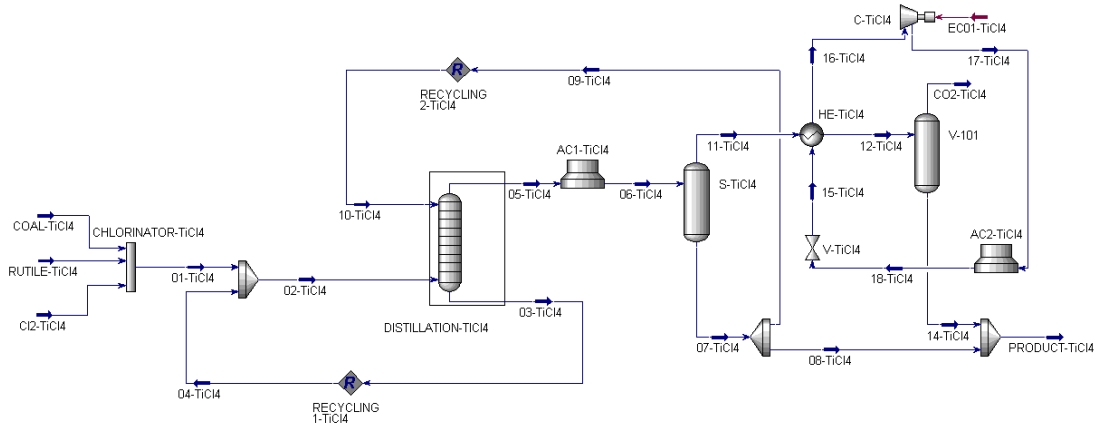



Figure A.6: Aspen HYSYS simulation of the titanium tetrachloride production.

## Appendix

Table A.8. Inputs and outputs for the production of 1 kg of TiCl4 precursor in Aspen HYSYS simulation.

| | Stream - Unit | Items | Units | Quantity | Comments |
|---|---|---|---|---|---|
| Inputs | Cl2 – TiCl4 | $TiCl_4$ | kg | 0.75 | - |
| | Rutile – TiCl4 | Rutile mineral | kg | 0.43 | 97.34 % $TiO_2$ |
| | Coal – TiCl4 | Coal | kg | 0.10 | - |
| | EC01 – TiCl4 | Electrical energy | MJ | 3.40E-03 | Efficiency 75%, compressor with Refrig - 717 |
| | AC1 – TiCl4 | Energy, natural gas | MJ | 0.02 | Air inlet 25 °C – Air outlet 35°C Fan speed 60 rpm |
| | AC2 – TiCl4 | Electrical energy | MJ | 2.87E-04 | Air inlet 25 °C – Air outlet 35°C Fan speed 60 rpm |
| Outputs | CO2 – TiCl4 | $CO_2$ | kg | 85.71 | - |
| | Product – TiCl4 | $TiCl_4$ | kg | 1.00 | 99.83 %wt. |

## Appendix

### Distillation of benzene

The production of titanium isopropoxide requires the use of benzene to precipitate ammonium chloride. After this stage the benzene is recovered by distillation. Figure A.7 represents simulation in Aspen, which was carried out to determine energy requirements during the distillation stage. Also, table A.9 defines the main streams of the simulation in Aspen HYSYS.

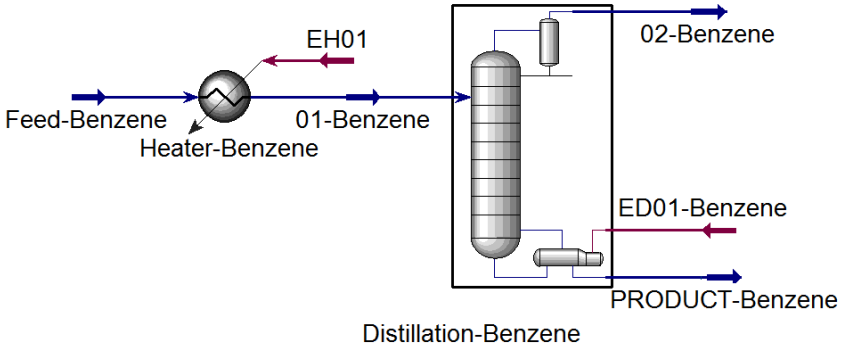



Figure A.7: Aspen HYSYS simulation of distillation of benzene and isopropanol.

Table A.9. Information about the distillation of benzene and isopropanol in Aspen HYSYS simulation.

| | Stream - Unit | Items | Units | Quantity | Comments |
|---|---|---|---|---|---|
| Inputs | Feed – Benzene | Benzene | kg $h^{-1}$ | 148.74 | - |
| | | Isopropanol | kg $h^{-1}$ | 20.50 | - |
| | EH01 | Energy, natural gas | MJ $h^{-1}$ | 90.05 | Inlet 25 ºC – Outlet 80 ºC |
| | ED01 – Benzene | Energy, natural gas | MJ $h^{-1}$ | 21.61 | - |
| Outputs | 02 – Benzene | Benzene and isopropanol | kg $h^{-1}$ | 44.25 | To be recycled |
| | Product – Benzene | Benzene | kg $h^{-1}$ | 124.98 | 95 %wt. |

## Appendix

### Distillation of isopropanol

The production of titanium bis(ammonium lactato) dihydroxide (TiBALD) requires the use of isopropanol (IPA) to precipitate the precursor. After this stage the IPA is recovered by distillation. Figure A.8 represents simulation in Aspen, which was carried out to determine energy requirements during the distillation stage. Also, table A.10 defines the main streams of the simulation in Aspen HYSYS.

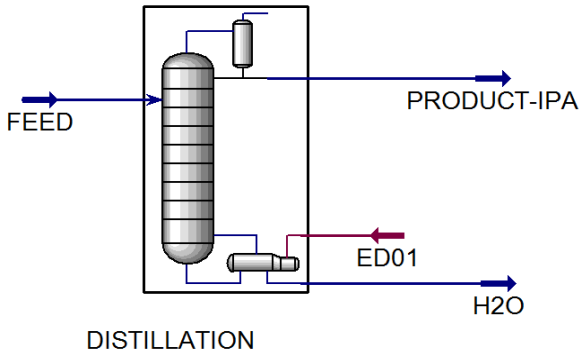



Figure A.8: Aspen HYSYS simulation of distillation of isopropanol and water.

Table A.10. Information about the distillation of isopropanol and water in Aspen HYSYS simulation.

| | Stream - Unit | Items | Units | Quantity | Comments |
|---|---|---|---|---|---|
| Inputs | Feed | Isopropanol | kg $h^{-1}$ | 8.20 | - |
| | | Water | kg $h^{-1}$ | 6.57 | - |
| | ED01 | Energy, natural gas | MJ $h^{-1}$ | 18.36 | - |
| Outputs | $H_2O$ | $H_2O$ | kg $h^{-1}$ | 5.94 | 90 %wt. |
| | Product – IPA | IPA | kg $h^{-1}$ | 8.83 | 86.10 %wt. |

## Appendix

### Distillation of ethanol

The production of potassium titanium oxide oxalate dehydrate (PTOOD) requires the use of ethanol to precipitate the metal salt precursor. After this stage the ethanol is recovered by distillation. Figure A.9 represents simulation in Aspen, which was carried out to determine energy requirements during the distillation stage. Also, table A.11 defines the main streams of the simulation in Aspen HYSYS.

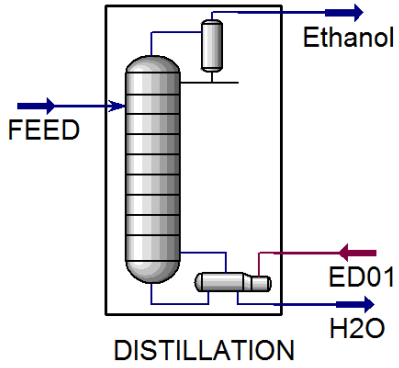



Figure A.9: Aspen HYSYS simulation of distillation of ethanol and water.

Table A.11. Information about the distillation of ethanol and water in Aspen HYSYS simulation.

| | Stream - Unit | Items | Units | Quantity | Comments |
|---|---|---|---|---|---|
| Inputs | Feed | Ethanol | kg $h^{-1}$ | 74.84 | - |
| | | Water | kg $h^{-1}$ | 88.82 | - |
| | ED01 | Energy, natural gas | MJ $h^{-1}$ | 219.56 | - |
| Outputs | $H_2O$ | $H_2O$ | kg $h^{-1}$ | 82.19 | 99.96 %wt. |
| | Ethanol | Ethanol | kg $h^{-1}$ | 77.47 | 91.40 %wt. |

## Appendix

### Evaporation of nano-sulfide suspensions for the industrial production

Suspension of nano-sufides were simulated in Aspen HYSYS to determine the minimum energy to evaporate the water content. Figure A.10 represents the simulation of the evaporation stage for the industrial scenario. Table A.12 describes the process flow diagram of Aspen simulation to dry 1 kg of nanoparticles and the greenhouse gas emissions (GHG) per kg of nano-sulfides.

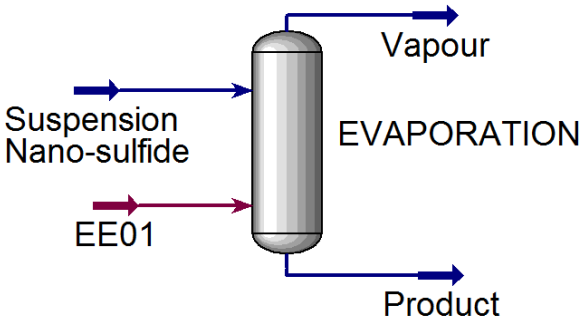



Figure A.10: Aspen HYSYS simulation of the evaporation stage for the industrial production of nano-sulfides.

## Appendix

Table A.12. Life cycle inventory and total greenhouse gas emissions to dry 1 kg of nano-sulfides for the industrial scale of the continuous-flow hydrothermal synthesis.

| | Items | Units | Quantity | $CO_2$ eq per MJ | Source | Total kg $CO_2$-eq/kg nano-sulfide |
|---|---|---|---|---|---|---|
| CuS 300B | Suspension Inlet | Kg of $H_2O$ | 13.21 | - | - | - |
| | Natural gas burned in a boiler | MJ | 34.26 | 6.82E-02 | Ecoinvent data V2.2 (2010) | 2.34 |
| FeS 400A&B | Suspension Inlet | Kg of $H_2O$ | 14.37 | - | - | - |
| | Natural gas burned in a boiler | MJ | 37.26 | 6.82E-02 | Ecoinvent data V2.2 (2010) | 2.54 |
| $Ag_2S$ 400B | Suspension Inlet | Kg of $H_2O$ | 10.20 | - | - | - |
| | Natural gas burned in a boiler | MJ | 26.44 | 6.82E-02 | Ecoinvent data V2.2 (2010) | 1.80 |
| $MoS_2$ | Suspension Inlet | Kg of $H_2O$ | 10.52 | - | - | - |
| | Natural gas burned in a boiler | MJ | 26.71 | 6.82E-02 | Ecoinvent data V2.2 (2010) | 1.82 |